Cyclodextrin Based Multivalent Glycoprobes for Targeting, Imaging and Drug Delivery

A Thesis
Submitted in partial fulfillment of the requirements
of the degree of
Doctor of Philosophy

By
Harikrishna Bavireddi
ID: 20113134

Under the Guidance of
Dr. Raghavendra Kikkeri

Indian Institute of Science Education and Research, Pune

Dedicated to

My Family and Teachers

CERTIFICATE

This is to certify that the work incorporated in this thesis entitled **"Cyclodextrin Based Multivalent Glycoprobes for Targeting, Imaging and Drug Delivery"** submitted by Harikrishna Bavireddi carried out by candidate at Indian Institute of Science Education and Research(IISER), Pune, under my supervision. The work presented here or any part of it has not been included in any other thesis submitted previously for the award of any degree or diploma from any other University or institution.

Date:

Dr. Raghavendra V. Kikkeri
(Research Supervisor)
Associate Professor, IISER, Pune
Pune-411008, India.

Declaration

I hereby declare that the thesis entitled**"Cyclodextrin Based Multivalent Glycoprobes for Targeting, Imaging and Drug Delivery"** submitted for Doctor of Philosophy in Chemistry at Indian Institute of Science Education and Research (IISER), Pune, has not been submitted by me to any other University or Institution. This work presented here was carried out at the, Indian Institute of Science Education and Research, Pune, India ubder the supervision of Dr. Raghavendra V. Kikkeri.

Date:

Harikrishna Bavireddi
ID- 20113134
(Senior Research Fellow)
Department of Chemistry, IISER
Pune- 411008, India.

Acknowledgments

The past six years has become one of the most important and memorable chapters in my life. This, in many ways, is the beginning, not the end, of my journey. Looking back, there are so many people that deserve my heartfelt gratitude. First, of all I would like to express my heartfelt sincere profound thanks to my supervisor Dr. Raghavendra V. Kikkeri in bringing me in field of glycobiology and pursuing good knowledge of interdisciplinary research. As a Ph.D student it gives me a great pleasure to express my deep sense of gratitude to my research supervisor for all his advice, guidance, support and encouragement in chemistry and its relevance in biological systems. His energy and tireless enthusiasm and passion for science have been an inspiration for me in the past six years and will always be in me years to come. I cannot think of a better advisor who can give me such freedom to pursue science and foster me to become independent thinker.

I thank our Director, Prof. K. N. Ganesh for giving excellent research platform, financial support and facilities that I have been fortunate with during my research here Indian Institute of Science Education and Research, Pune. Besides I gained many novel ideas and enthuse regarding how to become a great researcher at initial stage. A special vote of thanks would be for Dr. Nirmalya Ballav and Dr. Pankaj Poddar for their valuable suggestion during research advisory committee (RAC) meeting. I am also thankful for CSIR, India for my 5 year research fellowship. I am thankful to all the chemistry faculties IISER-Pune for their support. Also my work wouldn't be possible without help from our collaborators Prof. AjitVarki and Dr. Bernd Lepenies. I also thank to all administrative staff of our department.

The research becomes interesting and fruitful due to wonderful lab mates around me. I am fortunate to have an excellent blend of talented and hardworking lab mates who can rise in any occasion in their own different way, in addition being supportive and helpful. My special thanks to Dr. Raghavendra, Sivakoti, Dr. Rohan, Dr. Preeti, Madhuri, Catherin, Phani, Chetan, Balamurugan, Suraj, Prashant, Akhil and Sandhya for their generous support. I would also thankful to all B.S.-M.S. students of RK group for cooperation and their active participation in group tour and joyful moments. Further, I thank to my friends for sharing many personal problems and thoughts. And I also acknowledge my uncle Anjaneyulu for helping me personally and financially during CSIR coaching tenure.

This thesis remains incomplete without mentioning the motivation blessings and love of my family. There are no better words to express my heartfelt gratitude for their unconditional love, gracious understanding and life time support.

Finally, I pray to almighty Lord ‘Hanuma’ whose blessings made me able to complete the research work and submit this thesis for Ph. D degree.

Harikrishna Bavireddi

Contents

Index	**i-iv**
Abbreviations	**v-x**
Abstract of Thesis	**xi-xii**
Publications	**xiii**

Chapter 1: Multivalent Cyclodextrin Synthesis

Abstract	**2**
1.1. Introduction	**3-4**
1.2. Cyclodextrins	**4-5**
1.3. Developements in cyclodextrin based multivalent systems	**5**
1.3.1. Polyglycosylated-*β*-Cyclodextrin for Investigating Carbohydrate - Carbohydrate Interactions	**5**
1.3.1.1. Introduction	**5**
1.3.1.2. Synthesis	**5-6**
1.3.1.3. Application	**7-8**
1.3.1.4. Conclusions	**8**
1.3.2. Fuzzy Logics Based Analysis of CPI and CCIs Recognition	**9**
1.3.2.1. Introduction	**9**
1.3.2.2. Synthesis	**9-10**
1.3.2.3. Application	**10-12**
1.3.2.4. Conclusions	**12-13**
1.3.3. Lactose-GM_3 Interaction as Drug Delivery Vehicles	**13**
1.3.3.1. Introduction	**13**
1.3.3.2. Synthesis	**14**
1.3.3.3. Application	**14-16**
1.3.3.4. Conclusions	**16**
1.3.4. Carbohydrate-functionalized Cyclodextrin Conjugated Collagen Model Peptides	**16**

1.3.4.1. Introduction **16**
1.3.4.2. Synthesis **17-18**
1.3.4.3. Application **18**
1.3.4.4. Conclusions **18**
1.3.5. Immobilization of Multivalent Cyclodextrin on Gold Surfaces for Sensing Proteins and Macrophages **18**
1.3.5.1. Introduction **18-19**
1.3.5.2. Synthesis **19-21**
1.3.5.3. Application **21-23**
1.3.5.4. Conclusions **23**
1.4. Factors influence in carbohydrate protein interactions **24**
1.4.1. Symmetry **24**
1.4.2. Shape **24**
1.5. References **26-31**

Chapter 2: Understanding Carbohydrate-Protein Interactions using Homologous Supramolecular Chiral Ru(II)-Glyconanoclusters.

Abstract **33**
2.1. Introduction **34-36**
2.2. Results and discussion **36**
2.2.1. Synthesis of Ru(II) complexes **36-38**
2.2.2. Circular dichroism (CD) spectroscopy of Ru(II) complexes **38-39**
2.2.3. NMR study of Ru(II) complexes **39**
2.2.4. HPLC profile of Ru(II) complexes **39-40**
2.2.5. Synthesis of *β*-Cyclodextrin derivatives **40-41**
2.2.6. Host-Guest formation **41-42**
2.2.7. Mass spectrometric analysis of supramolecular complexes **42-44**
2.2.8. NMR study of supramolecular complexes **44-45**
2.2.9. Circular dichroism (CD) spectroscopy of supramolecular complexes **45-46**
2.2.10. DFT calculations of Ru(II) complexes **46**
2.2.11. Uv-visible and fluorescence spectra of MGDS **46-47**
2.2.12. ITC profile of MGDs **48**

2.2.13. SEM images of MGDs **48-49**
2.2.14. Binding affinity to C-type lectin receptor-Fc fusion proteins **50-52**
2.2.15. STD NMR of MGDs **52-53**
2.2.16. Cell viability assay of MGDs **54**
2.2.17. Confocal laser scanning microscopy (CLSM) studies of MGDs **54-56**
2.2.18. Fluorescence activated cell sorting (FACS) Analysis of MGDs **57**
2.2.19. Co-localization of MGDs **58**
2.2.20. Pathway blocking study of MGDs **58-59**
2.2.21. *In vivo* liver bio distribution and sequestration of MGDs **59-61**
2.3. Conclusions **62**
2.4. Experimental section **62-83**
2.5. References **83-87**
2.6. Appendix I: characterization data of synthesized compounds **87-98**

Chapter 3: Supramolecular Metalloglycodendrimers Selectively Modulate Lectin Binding and Delivery of Ru(II) Complex into Mammalian Cells.

Abstract **100**
3.1. Introduction **101-102**
3.2. Results and discussion **102**
3.2.1. Synthesis of diadamantyl Ru(II) Complex **102-103**
3.2.2. Host-guest formation **103**
3.2.3. NMR study of supramolecular complexes **104**
3.2.4. Uv-visible spectra and fluorescence spectra **104-105**
3.2.5. ITC profile of MGDs **105-106**
3.2.6. Binding affinity of Ru(II) complexes **106**
3.2.7. Cell viability assay **107-108**
3.2.8. Confocal laser scanning microscopy images **108-109**
3.2.9. Co-localization **109-110**
3.2.10. Mechanistic studies **110**
3.3. Conclusions **110-111**
3.4. Experimental section **111-116**
3.5. References **116-118**

3.6. Appendix I: Characterization data of synthesized compounds 118-121

Chapter 4: Glyco-Cyclodextrin Capped Quantum Dots: Synthesis, Cytotoxicity and Optical Detection of Carbohydrate-Protein Interactions.

Abstract 123
4.1. Introduction 124-125
4.2. Results and discussion 125
4.2.1. Host-guest assembly of glyco-QD complexes 125-126
4.2.2. TEM images of glyco-QD complexes 126
4.2.3. UV-visible and fluorescence spectra 127
4.2.4. FT-IR spectroscopic studies 127-128
4.2.5. ^{1}H-NOESY spectra 128-129
4.2.6. Binding affinity of modified quantum dots 129-131
4.2.7. Cell viability assay 131-132
4.2.8. FACS analysis 133
4.2.9. Confocal laser scanning microscopy (CLSM) studies 133-134
4.3. Conclusions 134
4.4. Experimental section 134-136
4.5. References 136-137
4.6. Appendix I: Characterization data of synthesized compounds 137-138

Abbreviations

abs = Absorption

ABTS = 2, 2'-azidobis(3-ethyl-benzo-thiazoline-6-sulfonic acid) diammonium salt

Ac = acetyl

AcOH = Acetic acid

AcSH = Thioacetic acid

AFM = Atomic force microscopy

AIBN = Azobisisobutyronitrile

ALT = Alanine aminotransferase

Ar = Argon

AST = Aspartate aminotransferase

ATP = Adenosine triphosphate

$BF_3.ET_2O$ = Boron trifluoride diethyl etherate

BL = Boolean logic

Boc = tert-Butyloxycarbonyl

Br = Bromine

bs = broad singlet

BSA = Bovine serum albumine

byp = bipyridine

$CaCl_2$ = Calcium chloride

Calc'd = Calculated

CD = Circular dichroism

CD_3OD = Deuterated methanol

$CDCl_3$ = Deuterated chloroform

CH_3 = methyl

CH_3CN = Acetonitrile

$CHCl_3$ = Chloroform

CHO = Chinese hamster ovary

CHOP = Nuclear transcription factor C/EBP homologous protein

CLR= C-type lectin receptor

cm = Centimeter

ConA = Concanavalin A

CrO_3 = Chromium trioxide

Cs_2CO_3 = Caesium carbonate

D_2O = Deuterium oxide

DCM = Dichloromethane

DC-SIGN = Dendritic cells Specific Intercellular adhesion molecule-3-Grabbing Non-integrin

deg = Degree

DFT = Density functional theory

DIC = N,N'-Diisopropylcarbodiimide

DIPEA = Diisopropylethylamine

DMAP = *N*,*N*-dimethylaminopyridine

DMEM = Dulbecco's modified eagle's medium

DMF = *N*,*N*'-Dimethylformamide

DMSO = Dimethyl sulfoxide

DNA = Deoxyribonucleic acid

dppz = dipyrido[3,2-**a**:2′,3′-**c**]phenazine

ECD = Electronic circular dichroism

EDC = 1-Ethyl-3-(3-Dimethylaminopropyl)carbodiimide

ELISA = Enzyme linked immunosorbent assay

em = Emission

eq. = equivalents

ER = Endoplasmic reticulum

ESI = Electrospray ionisation

ET = Electron transfer

et al. = and others (*et alii*)

Et_3N = Triethylamine

EtOAc = Ethylacetate

EtOH = Ethanol

FBS = Fetal bovine serum

FL = Fuzzy logic

FRET = Fluorescence resonance energy transfer

Gal = Galactose

Gg3 = Gangliotriaosylceramide

GlcNAc = *N*-acetylglucosamine

Gly = Glycine

GM1 = Monosialosetetrahexoseganglioside

GM3 = Monosialodihexosylganglioside

GNA = Galantus nivilis agglutinin

H = Hydrogen

H_2O_2 = Hydrogen peroxide

H_2SO_4 = Sulfuric acid

HEPES = (4-(2-hydroxyethyl)-1-piperazineethanesulfonic acid)

HNO_3 = Nirtic acid

HOBT = Hydroxybenzotriazole

HPLC = high-performance liquid chromatography

HRMS = High resolution mass spectroscopy

HRP = Horseradish peroxidase

Hyp = Hydroxyproline

IC_{50} = Inhibitory concentration

ICD = Induced circular dichroism

ICP-MS = Induced couple clasmon mass spectrometry

ITC = Isothermal titration calorimetry

J = Coupling constant

K = Formation constant

KSCN = Potassium isocyanate

LC = Ligand centered

m/z = Mass to charge ratio

MALDI = Matrix-assisted laser desorption ionization

Man = Mannose

MeOH = Methanol

$MgSO_4$ = Magnesium sulfate

MHz = Mega hertz

mL = Mille liter

MLCT = Metal to ligand charge transfer

mM = Millimolar

MS = Mass spectroscopy

MT = Mitochondria tracker

MTT = 3-(4, 5-dimethylthiazol-2-yl)-2, 5-diphenyltetrazolium bromide

Mw = Molecular weight

Na = Sodium

NaCl = Sodium chloride

$NaIO_4$ = Sodium periodate

NaN_3 = Sodium azide

NaOH = Sodium hydroxide

NaOMe = Sodium methoxide

ng = Nano gram

nm = Nano meter

NMR = Nuclear magnetic resonance

NOESY = Nuclear overhauser effect spectroscopy

PBS = Phosphate buffered saline

Phe = Phenylalanine

Phen = phenanthroline

PNA = Peanut agglutinin

ppm = parts per million

Pro = Proline

Py = Pyridine

q = Quadrate

QCM = Quartz crystal microbalance

QD = Quantum dots

r.t. = room temperature

R_f = Retardation factor

RNA = Ribonucleic acid

$RuCl_3$ = Ruthenium trichloride

s = Singlet

SD = Standard deviation

SDS = Sodium dodecyl sulfate

SEM = Scanning electron microscope

$SOCl_2$ = Thionyl chloride

SPR = Surface Plasmon resonance

STD = Saturation transfer difference

t = triplet

TEM = Transmission electron microscopy

TFA = Trifluoroacetic acid

THF = Tetrahydrofuran

TLC = Thin layer chromatography

TOF = Time of flight

TOPO = Trioctylphosphine oxide

Zn = Zinc

β-CD = Beta cyclodextrin

δ = chemical shift

μM = Micromolar

Φ = Quantum yield

Abstract

Designing multivalent template structures have immense importance not only to amplify the carbohydrate-protein interactions but also from the perspective of translational chemistry. Significant progress has been achieved in this regard using glyco-nanoparticles, glycodendrimers and glycopolymers. However, other important issues regarding the preparation of multivalent carbohydrates are related to the orientation, spacing and local concentration of the carbohydrates with respect to external stimuli. Therefore, it is important to form a general scaffold which are facile, robust, presents tunable symmetry and exhibit optical and electrochemical properties to develop a direct probing system. Inspired by the large number of supramolecular assembly of adamantyl/β-cyclodextrin associated complexes, I explored poly-glycosyl β-cyclodextrin probes in the synthesis next generation diagnostic, biosensing and imaging tools. In the following chapters, I have investigated the role of different carbohydrate constructs-from cyclodextrin scaffods-and their application in targeting, imaging, and drug delivery.

Chapter 1 summarizes different strategies for preparing cyclodextrin based multivalent probes probes and their major applications in biosensing, imaging, and other biological or medical applications. To address fundamental aspects of cyclodextrin-based interactions that were developed in the Kikkeri group, different types of cyclodextrin based systems ranging from photoswitchable glycodendrimers to glycopeptides structures in order to fine tune the spatial and the topology structures of the carbohydrate ligands required in such systems.

Chapter 2 demonstrates the inherent chirality of glycodendrimers as one of the promising factors to generate different spatial carbohydrate micro-environments to modulate the specific carbohydrate-protein interactions. By exploiting the host-guest strategy and chiral Ru(II) complexes (Δ and Λ) and mannose capped β-cyclodextrin (β-CD), we generated a library of homologous metallo-glycodendrimers (MGDs) of size 50-70 nm. These nanoclusters can enantioselectively bind to specific C-type lectins and displayed selectivity in cellular uptake. We also discovered their potential clathrin-mediated endocytotic pathway in DC-SIGN and SIGNR3-transfected cell lines. Finally, *in vivo* biodistribution and sequestration of MGDs was determined to decipher the role of chirality mediated spatial arrangement in carbohydrate-mediated interactions.

Chapter 3 deals with the synthesized Ru(II)-bis sugar capped β-cyclodextrin derivatives to demonstrate selective controlled delivery of metal complex into cancer cells. Cell viability assay and imaging studies revealed that hepta glycosylated-CD capped Ru(II) complexes

exhibited cytotoxic activities in cancer cells with IC_{50} values close to other Ru(II) complexes. The death inducer was found to accumulate favourable to the endoplasmic reticulum (ER) and induced ER stress in cells**.** The upregulation of CHOP and**,** caspase-3 and 12 disturbed the ER morphology initiating apoptosis pathway.

Chapter 4 reports the synthesis of glyco-quantum dots using sonochemical procedure. The high sugar density on QDs resulted in selective colloidal aggregation with ConcanavalinA (ConA), Galanthus nivalis lectin (GNA) and Peanut agglutinin (PNA) lectins. Subsequently, *in-vitro* studies indicated that *β*-CD modification of QDs had good cell viability of human hepatocellular carcinoma cell line (HepG2) cells. Finally, flow cytometry and confocal imaging studies revealed that *β*-CDgal capped QDs undergo preferential binding with HepG2 cells compared to *β*CD capped QDs. These results clearly demonstrate that *β*-CD capped QDs could be a promising candidate for further carbohydrate based biomedical applications.

Publications

1. Sivakoti Sangabathuni, Raghavendra Vasudeva Murthy, Madhuri Gade, **Harikrishna Bavireddi,** Mahesh V Sonar, Krishna N Ganesh, Raghavendra Kikkeri, "Phenotypic Cell Migration Triggered By Combinatorial Specific Glyco-Collagen Peptides"-**manuscript under preparation.**
2. Rohan Yadav, Preeti Madhukar Chaudhary, Balamurugan Subramani, **Harikrishna Bavireddi,** Suraj Toraskar, Sivakoti Sangabathuni, Raghavendra Kikkeri, "Maping the Sialylated-quantum dots Toxicity, Biodistribution, and sequestration in Zebrafish and mouse model"-**manuscript submitted.**
3. **Harikrishna Bavireddi,** Raghavendra Vasudeva Murthy, Madhuri Gade, Sivakoti Sangabathuni, Preeti Madhukar Chaudhary, Catherine Alex, Bernd Lepenies, Raghavendra Kikkeri, "Deciphering Carbohydrate-Protein Interactions using Homologous Supramolecular Chiral Ru(II)-Glyconanoclusters" *Nanoscale* **2016**, DOI: 10.1039/C6NR06431K.
4. **Harikrishna Bavireddi**, Raghavendra Vasudeva Murthy, Madhuri Gade, Sivakoti Sangabathuni, Raghavendra Kikkeri, "Supramolecular Metallo-glycodendrimers Selectively Modulate Lectin Binding and Delivery of Ru(II) Complex into Mammalian Cells" *Org.Biomol.Chem.* **2016**, *14*, 10816.
5. Madhuri Gade, Puneet Khandelwal, Sivakoti Sangabathuni, **Harikrishna Bavireddi,** Raghavendra Vasudeva Murthy, Pankaj Poddar, Raghavendra Kikkeri, "Immobilization of Multivalent Glycoprobes on Gold Surfaces For Sensing Proteins and Macrophages" *Analyst* **2016**, *141*, 2250.
6. Raghavendra Vasudeva Murthy[#], Harikrishna Bavireddi[#], Madhuri Gade, Raghavendra Kikkeri, "Exploiting the Lactose-GM_3 Interaction for Drug Delivery" *ChemMedChem* 2015, *10*, 792. (# Equal contribution)
7. **Harikrishna Bavireddi,** Priya Bharate, Raghavendra Kikkeri, "Use of Boolean and Fuzzy Logics in Lactose by Glycoclusters Research" *Chem. Commun*. **2013**, *49*, 9185.
8. **Harikrishna Bavireddi**, Priya Bharate, Raghavendra Kikkeri, "Probing Carbohydrate-Carbohydrate Interactions by Photoswitchable Supramolecular Glycoclusters" *Chem. Commun.* **2013**, *49*, 3988.
9. Harikrishna Bavireddi, Raghavendra Kikkeri, "Glyco-*β*-cyclodextrin Capped Quantum Dots: Synthesis, Cytotoxicity and Optical Detection of Carbohydrate-protein Interactions" *Analyst* **2012**, *137*, 5123.

CHAPTER 1

Multivalent Cyclodextrin Synthesis

Abstract

To address fundamental aspects of carbohydrate-based interactions, Kikkeri and other groups developed cyclodextrin based multivalent systems and functionalize them various templates ranging from, photochromic groups, peptides, metal complexes, dendrimers and surfaces to fine tune the spatial and the topology structures of the carbohydrate ligands required for external stimuli.

Chapter 1 briefly introduces the work on cyclodextrin based different probes developed by Kikkeri group and its potential application in the areas of biosensing, imaging, and therapeutics.

1.1. Introduction

Lectins are specific carbohydrate-binding or carbohydrate cross-linking proteins. The interactions between lectins and sugars are involved in a large number of biological processes, such as cell adhesion and migration, phagocytosis, cell differentiation and apoptosis,[1-4] Over the past 120 years, numerous lectins have been isolated from plants, microorganisms, fungi, animals and viruses.[5-7] Lectins have been used as tools for the detection, isolation and characterization of various glycoproteins and for the clinical diagnosis of carcinoma and leukemia.[8,9] Despite the prevalence of lectin in biological systems, the binding between an individual lectin and monovalent carbohydrate are quite weak and not particularly specific.[10,11] Nature provides strong and specific responses by carbohydrate multivalency. In multivalent interactions, multiple copies of the ligand and receptors sequentially or simultaneously bind and significantly increase binding affinity for a meaningful and biologically relevant recognition processes.[12,13] A host of glycoclusters have been prepared and explored in different applications. It has been shown that multivalent mannose glycoclusters inhibited HIV infection.[14,15] Multivalent glycoclusters have also been shown to function against bacterial toxins[16,17] and against bacterial adhesion to human cells.[18-20] Multivalent glycoconjugates are also being used for stimulation of immune system.[21- 23] Similarly, several glycoclusters have been used as a potential target for drug development, gene delivery and diagnostic tools.[24-27] Hence there is a need for new multivalent probe to study carbohydrate-protein interactions in order to unravel the finer details of these interactions.

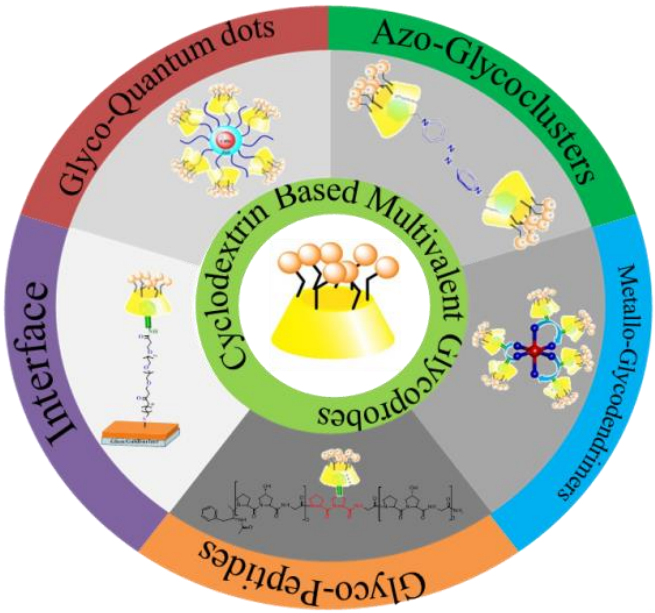

Figure 1: Cyclodextrin applications.

Recently, Kikkeri laboratory has contributed to that field by focusing part of its work on the development of cyclodextrin-based multivalent structures and in the investigation of their applications for biosensing, imaging, and drug development (**Fig. 1**).

This introductory chapter discusses the strategies developed by Kikkeri group in preparing cyclodextrin based multivalent carbohydrate probes with platforms ranging from photochromic groups, glycopeptides, surfaces and their major applications to understand carbohydrate-protein and carbohydrate-carbohydrate interactions.

1.2. Cyclodextrins

Cyclodextrins are a family of compounds formed from a cyclic array of α-(l,4)-linked glucose monomers (**Fig. 2**). The most common members of the family, in the order of decreasing availability, are three types of cyclodextrins: β-cyclodextrin**,** α-cyclodextrin**,** and γ-cyclodextrin**,** macrocycles containing 7, 6 and 8 glucose units respectively. The cyclodextrin families are generally synthesised through degradation of starch by the enzyme glucosyltransferase. This gives rise to a variety of cyclic and acyclic dextrin forms, from which α-, β- or γ-cyclodextrins can be selectively extracted.

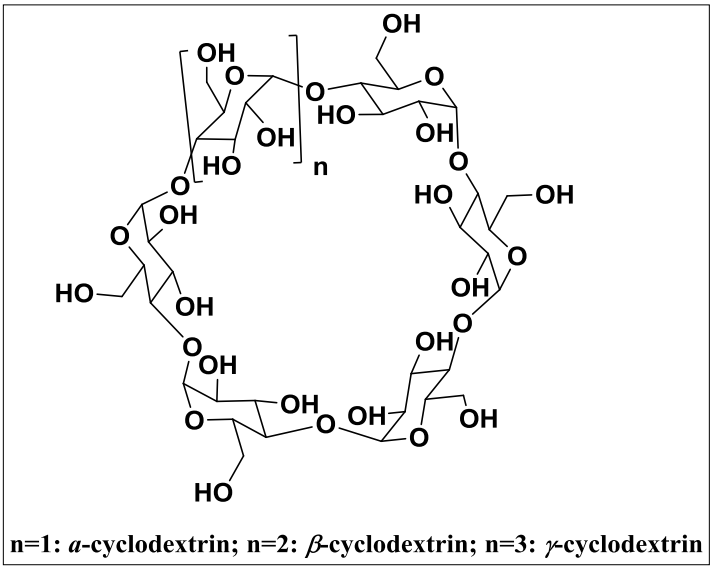

Figure 2: Structure of Cyclodextrins.

The conformation of the glucose subunits in cyclodextrins gives rise to a structure resembling a 'molecular bucket.' Each glucose subunit contains a primary hydroxyl-group on the 6th position, and two secondary hydroxyl groups on the 2nd and 3rd positions. The cyclic compounds form a hollow truncated cone shape with the primary (6-) hydroxyls located on

the narrow face of the torus and the secondary (2- and 3-) hydroxyls at the wider face. The non-bonding electrons of the glycosidic oxygens are directed into the centre of the cavity formed, as are the 3- and 5- hydrogen atoms. This gives the molecule a hydrophobic cavity capable to form host-guest complexes with a variety of guest hydrophobic molecules (e.g. adamantane, phenyl, aliphatic chains, etc.).[28] cyclodextrin derivatives have been used for drug delivery and sensing as well as developing carbohydrate-selective systems. We focus on the application of CDs in supramolecular chemistry with particular attention on CDs as glycocluster scaffolds.

1.3. Developements in cyclodextrin based multivalent systems

1.3.1. Polyglycosylated-*β*-Cyclodextrin for Investigating Carbohydrate-Carbohydrate Interactions.

1.3.1.1. Introduction

Ever since the discovery of the phenomenon of carbohydrate-carbohydrate interactions (CCIs) by Hakomori *et al*,[29-33] speculation has arisen regarding the factors important for such recognitions. Today, there are considerable synthetic models showing that multivalent presentation of carbohydrate and the role of Ca^{2+} ion are important factors for CCIs.[34] In spite of all the research in this field, the binding affinity and differentiation of inter- and intra-molecular CCIs is still unexplored. We used photo-switchable glycoclusters for systematic investigation of the CCIs with Ca^{2+} ions using isothermal titration calorimetry (ITC) technique. We have demonstrated that by using the photo-tuneable glycocluster a straight-forward and relatively fast access to different sugar densities through self-assembly and tuning of intra-to intermolecular CCIs was observed.

1.3.1.2. Synthesis

The synthesis of the lactose substituted *β*-cyclodextrin **8** was started with peracetylated lactose **3**, followed by treatment of bromoethanol with $BF_3 \cdot Et_2O$ and thiocyanate to yield the thiocyanate–lactose derivative. The thiocyanate was reduced by Zn-AcOH to the corresponding thiol **5** and reacted with 6-hepta iodinated *β*-cyclodextrin **7** in the presence of Cs_2CO_3 to yield lactose-substituted *β*-cyclodextrin, which was finally treated with base yielding compound **8**.

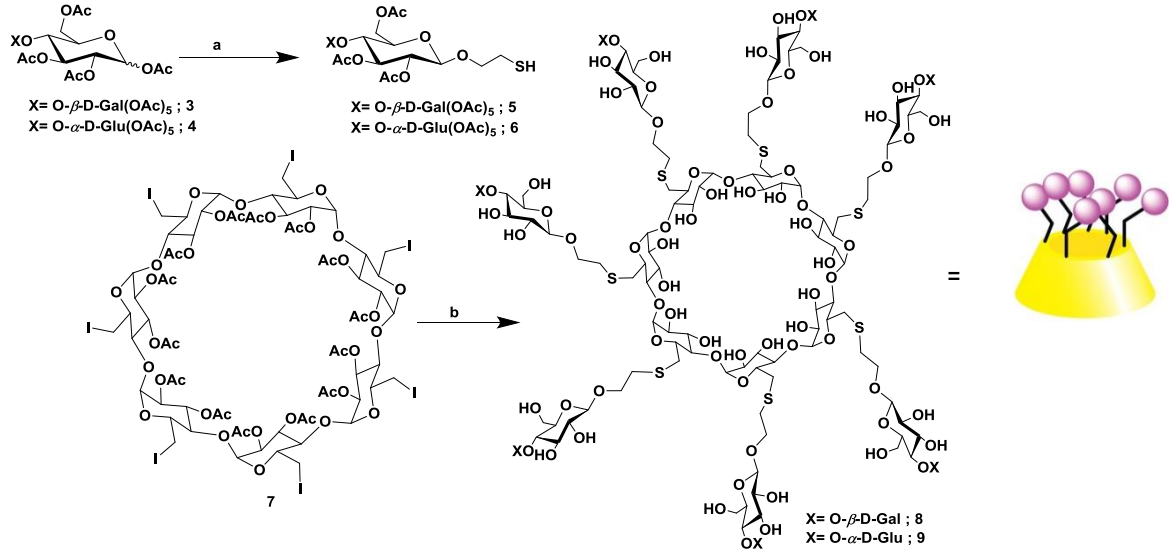

Scheme 1: Synthesis of cyclodextrin derivatives; (a) Bromoethanol/$BF_3 \cdot Et_2O$ (46-47%); KSCN/DMF (74-89%); Zn/AcOH (84-91%); (b) $CsCO_3$/DMF (39-46%); NaOMe-MeOH (43%).

The photochromic molecule **11** was obtained as a brown solid by reacting benzyl bromide and 4, 4′-azo-pyridine in acetonitrile for 24 hours.

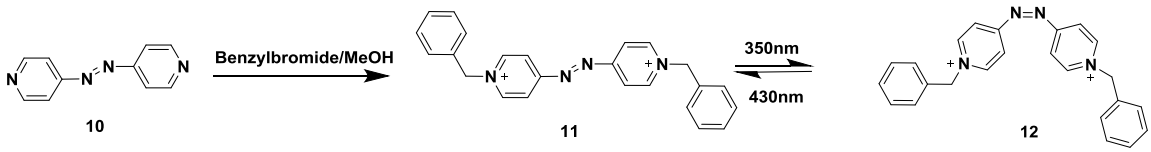

Scheme 2: Synthesis of azo derivatives.

β-cyclodextrin complexes with **8** and **11** were prepared by mixing stoichiometric amounts these compounds.

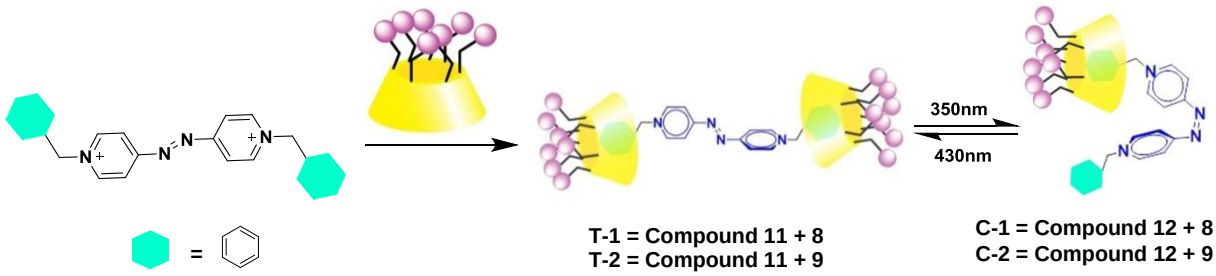

Scheme 3: Synthesis of supramolecular complexes (**T-1** to **T-2** and **C-1** to **C-2**).

1.3.1.3. Application

In order to gain insight into the binding affinity and thermodynamics of the interaction between glycoclusters and different cations (Na^+, K^+, Ca^{2+}) we used isothermal calorimetry (ITC). The metal ions were titrated into the glycoclusters in the calorimeter cells. Upon binding of glycoclusters to Ca^{2+} heat is released, yielding a typical titration isotherm. Based on the qualitative assessment, the Ca^{2+} binding isotherm was fitted to a binding model containing one set of binding sites. The values of formation constants (K) and thermodynamic parameters determined using ITC are summarized in Table 1, where 'N' represents the number of carbohydrate groups on the glycoclusters that are available for binding with metal ions. In the case of **8**, the best fit was obtained using an N value of 4 and a K value of 57.9 ± 4.7 M^{-1}. It shows that there might be 4 lactose units coordinated to Ca^{2+}. Thus, the result demonstrates that only a subset of the available ligands of **8** participated in Ca^{2+} mediated CCIs and may involve intramolecular CCIs. To demonstrate the specificity of Ca^{2+} and **8** binding, we performed an ITC experiment of **8** with Na^+ and K^+. As expected, highly disordered enthalpy changes were observed, indicating that no CCIs exist in the presence of Na^+ or K^+ ions.

Table 1: Thermodynamic parameters of *cis-trans* isomers measured with isothermal titration calorimetry (ITC); N = 1/n.

Ligand	n	~N	Binding constant (M^{-1})	ΔH (Kcal/mol) 10^6	ΔS (cal/mol/deg) 10^3
lac-*β*-CD	0.28	4	57.9 ± 4.7	-1.73±0.02	-5.80
T-1	0.047	21	115 ± 23.0	-3.43 ± 0.81	-11.5
C-1	0.0051	196	276 ± 39.7	-3.71 ± 0.2	-12. 4

With **T-1**, the best fit was obtained with one set of sites model using N = 21, indicating five-fold more lactose units involved in CCIs compared to **8**. However, the binding affinity varies by as much as two-fold (115 ± 23 M^{-1}) from **8** to **T-1** (**Table 1**). This may be attributed to the fact that the inherent sugar density of **T-1** propagates intra-to-intermolecular CCIs. A similar experiment with Na^+ and K^+ ions resulted in disordered enthalpy changes, indicating no binding between **T-1** and alkali metal ions. In the case of **C-1**, an N value of 196 and a K value of 276 ± 39.7 M^{-1} were obtained (**Table 1**). The formation constant increased approximately three fold more compared to the nine-fold increase in the binding sites with respect to **T-1**. A reason for this low binding affinity with respect to the number of binding

sites is due to the increase in inter-CCIs. Overall, the above results show that the intra-CCIs can be quantified by using a few sugar substituted glycoclusters **8**, whereas high sugar density results in a combination of inter and intra-CCIs and it is difficult to isolate inter-CCIs. Significantly, the formation constant of glycoclusters-Ca^{2+} interactions can be compared to other weak host-guest models.[35,36] In addition, the standard enthalpies of formation (ΔH) are negative in all cases indicating that the association is exothermic in the order **C-1** > **T-1** > **8**. These trends appear to be general and are shown by carbohydrate-protein models.[37]

To gain deeper insight into the nature of CCIs, we conducted AFM measurements. We have found that compound **8** with Ca^{2+} did not show any aggregation, an observation that refers to the possibility of intramolecular CCIs, whereas, **T-1** in the presence of Ca^{2+} ions showed aggregates of size 200 nm and ~1 μm, respectively. The sizes of the small aggregates represent intra-CCIs as their size is approximately the same as that of **T-1**, whereas the large aggregations showed integration of several small aggregates, representing inter-CCIs. Furthermore, **C-1** showed random aggregations. This may be due to the combination of intra and intermolecular CCIs. The above approach was further tested with maltose analogs (**9**, **C-2** and **T-2**). The ITC curves show slightly weaker formation constants compared to lactose analogs. These results suggest that the glucose sugar moiety of maltose weakens the Ca^{2+} ions binding to some extent. Finally, to verify the quality and sensitivity of the photoisomerization process, the platform was subjected to three cycles of cis–trans isomerisation and the resultant sample was subjected to Ca^{2+} mediated CCIs. The system exhibits excellent reproducibility.

1.3.1.4. Conclusions

We have synthesized lactose or maltose appended *β*-cyclodextrin, and complexes with the photo-switchable compound **11** were prepared. It was found that the complex not only tunes the sugar topology, but also exhibits specific calcium mediated CCIs. Furthermore, we have demonstrated that sugar topology and density can tune the intra vs. intermolecular CCIs. A drawback of the current system is the relatively small changes in the CCIs measured for **C-1** and **T-1**, **C-2** and **T-2**. We believe that better results might be obtained with more complex glycans, such as gangliosides, Le^X-Le^X, GM_3-Gg_3 and sulphated *β*-D-GlcNAc(3S)-(1→3)-α-L-Fuc models.[38,39] We are currently investigating these aspects.

1.3.2. Fuzzy Logics Based Analysis of Carbohydrate-Protein Interaction (CPI) and Carbohydrate-Carbohydrate Interactions (CCIs) Recognition.

1.3.2.1. Introduction

Several techniques have been developed to analyze CPIs and CCIs, such as surface plasmon resonance (SPR), microarray, quartz crystal microbalance (QCM), enzyme-linked immonosorbent assay (ELISA).[40-46] All these methods require expensive instruments, laborous experimentations and extensive technical expertise. Recently, Boolean logic (BL)[47-61] was used for real-time and straightforward analysis of CPIs to select best scaffolds for specific interaction and also for sensing processes.[62-65] The BL model is simple and very effective in differentiating true and false interactions, it is not adequate for describing fine tuned systems and degrees of truthfulness.

Fuzzy logic system (FLS) is a superset of BL extended to characterize partial true values between completely true (1) and completely false (0). It is one of the automatic fine-tuning control systems that can handle several middle steps and define degrees of truth. It stems from the notion that human reasoning and decision making is too complex to be precisely defined. We have applied these BL and FL for optimization of CPIs mediated by Ca^{2+} ions, with emphasis on the multivalent ionic interactions between lactose, appended on a cyclodextrin skeleton, and peanut agglutinin (PNA) lectin. We have compared the two methods and concluded that the logic operation of FL is more appropriate for analyzing CPI, than BL.

1.3.2.2. Synthesis

Compound **15** was prepared by reacting the dichloride of ferrocene dicarboxylic acid, prepared by reaction with oxalyl chloride, and adamantyl 2′-amino-*β*-alanine amide. (**Scheme 4**)

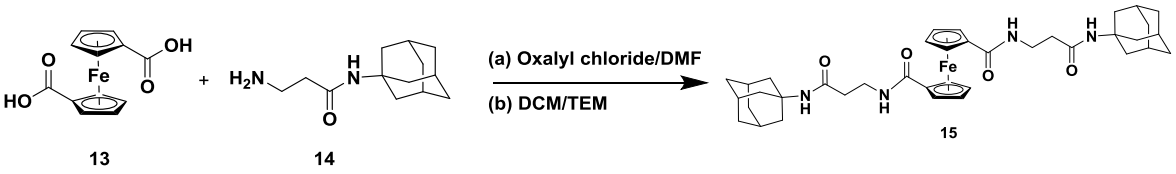

13 14 15

Scheme 4: Synthesis of ferrocene derivative.

The experimental setup was based on a newly synthesized lactose-modified *β*-cylodextrin (**8**) and the two glycodendrimers (**T-1** and 1**6**), which were prepared by exploiting the tendency of adamantane and benzene to form stable complexes with *β*-cylodextrin and its derivatives used as the 'host' in complexes **T-1** and **16** with compounds **11** and **15**, respectively, used as the 'guests' (**Scheme 5**). The syntheses of compounds **11** and **T-1** were described above (**Section 1.3.2**). Complexes **T-1** and **16** having azo and ferrocene guest molecules respectively.

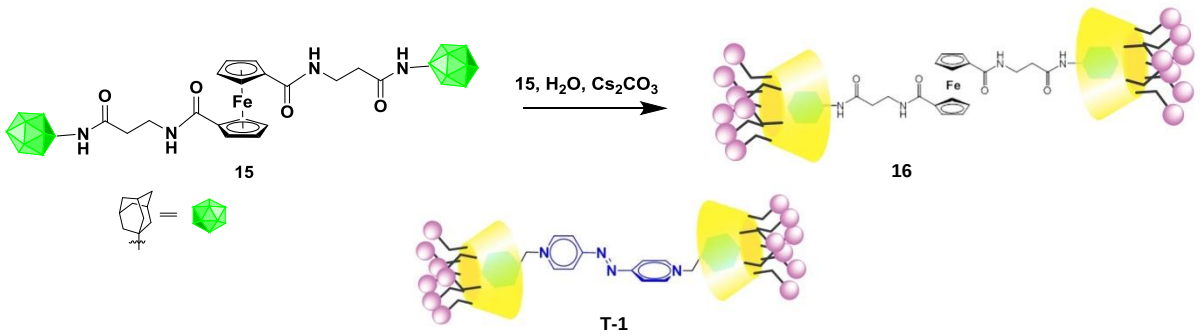

Scheme 5: Structures of lactose glycodendrimers.

1.3.2.3. Application

For demonstrating the use of the operation AND gate in Boolean logic, PNA lectin and Ca^{2+} ions, separately or in a mixture, were titrated with the glycoclusters **T-1** and the process was followed by ITC. The binding processes are accompanied with release of heat and typical isotherms were recorded. With complex **T-1**, best fit was obtained for 'N' ≈ 21 and ≈232 for Ca^{2+} and PNA, respectively. Since the CCIs are weak, addition of Ca^{2+} ions resulted in weak binding affinity (115 M^{-1}).

(a)

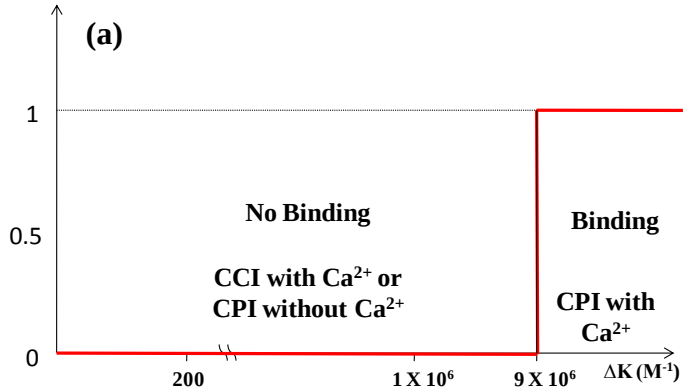

(b)

(Ca^{2+}, lectin)	T-1 (BL)	16 (BL)
(0,0)	0	0
(1,0)	0	0
(0,1)	0.35	0.28
(1,1)	1	1

Figure 3: (a) Boolean logic: If binding affinity ≥ 9 x 10^6 $M^{-1,}$ it is a specific CPI (1 or true) and if binding affinity ≤ 9 x$10^{6,}$ it is not a specific CPI (0 or false) ; **(b)** Truth table.

For PNA lectin interactions, a significant increase in binding affinity of **T-1** as compared to CCIs (3.18 x 10^6 M^{-1}) was observed. In the presence of both, Ca^{2+} ions and PNA lectin, the binding affinity was increased, 'N' value ≈334, indicating that Ca^{2+} ions not only assist lectin amino acids in positioning for achieving maximum binding, but also induce inter/intra CCIs and increase the number of binding sites. By setting the binding affinity of CPIs in presence of Ca^{2+} ions as the threshold level (red line **Fig 3a**), **T-1** exhibited the behavior of AND logic; in the presence of a single input signal ((1.0) and (0.1)), **T-1** displayed low output or no binding at all (0) while with both inputs high (1, 1) the output is high and represents binding (1). The truth table is presented in Figure 3b. The major limiting feature of BL is that the values 0 and 1 are mutually exclusive and it is not possible to define a transition from one state to the other, i.e., 'non-binding' to 'binding', by considering a single value. This limitation is overcome by using the fuzzy logic systems (FLS) for presentation.

(a)

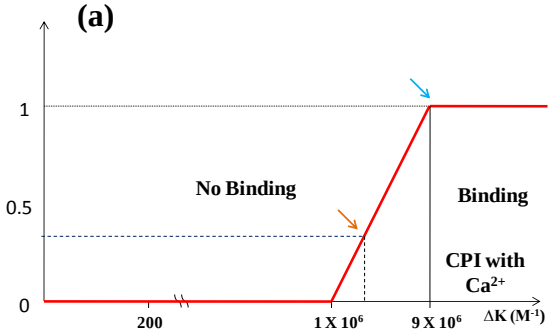

(b)

(Ca^{2+}, lectin)	**T-1 (FL)**	**16 (FL)**
(0,0)	0	0
(1,0)	0	0
(0,1)	0.35	0.28
(1,1)	1	1

Figure 4: (a) Fuzzy logic of strong binding; **(b)** Truth table.

FLS can be defined as the nonlinear mapping of an input data set to a scalar output data. The parameters obtained from the ITC measurements, which reflect the degree of interaction were used for the construction of a fuzzy subset. They have degrees of membership between 0 and 1. A subset of 'strong binding', defined in the following way, was used as the 'rule base'. Strong binding (x) = {0, if $\Delta K \leq 1 \times 10^6$ M^{-1}; 0-1 if $1 \times 10^6 < \Delta K \leq 9 \times 10^6$ M^{-1}, 1 if $\Delta K \geq 9 \times 10^6$ M^{-1}} Based on this definition we have built the truth table (**Fig. 4b**) from which we conclude that PNA lectin binding to **T-1** is a '35% strong binding'. Similarly, from the experiment with **16** we received 0.28, which is also 'strong binding'.

From the above presentation it seems clear what does the statement 'degree of strong binding' mean. In order to interpret 'weak', 'medium' and 'strong' binding affinities in fuzzy linguistic terms, we have performed a set of operations (union, intersection and complement). 'Intersection' and 'union' are defined as minimum and maximum of two interactions and 'complement' is defined as the negation of specific interaction. Using these operations, Fuzzy

(a)

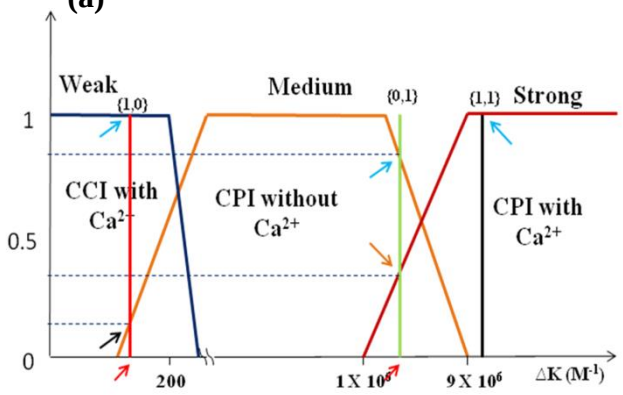

(b)

(Ca^{2+}, lectin)	T-1 (FL)	16 (FL)
(0,0)	0	0
(1,0)	0; 0.11 (SM); 1.0 (TW)	0; 0.2 (SM); 1.0 (TW)
(0,1)	0; 0.35 (SS); 0.74 (FM)	0; 0.5 (SS); 0.64 (FM)
(1,1)	1 (S)	1 (S)

Figure 5: (a) FLS rules: $\Delta K \leq 250\ M^{-1}$ - weak interaction, $100 \leq \Delta K \leq 9\ X10^6\ M^{-1}$ - medium interaction and for $\Delta K \geq 1X10^6\ M^{-1}$ - strong binding; SM (slightly medium); TW (true weak); SS (slightly strong); FM (fairly medium); FW (fairly weak); **(b)** Truth table.

sets (weak, medium and strong binding) are constructed in which 'weak binding' is defined for systems of binding affinity (x) = {1 (FL) or 0 (BL), if (ΔK) $\leq 200\ M^{-1}$ and gradient binding (0 - 1) (FW) between $200 \geq \Delta K \leq 250\ M^{-1}$}. 'Medium binding' affinity is defined as (y) = {0 - 1, if $100 \geq \Delta K \leq 250\ M^{-1}$ (SM) or $1\ X10^6 \geq \Delta K \leq 9X10^6\ M^{-1}$(FM); 1, if $250 \geq \Delta K \leq 1X10^6\ M^{-1}$} finally, 'strong binding' as: (z) ={0-1, if $1X10^6 \geq \Delta K \leq 9X10^6\ M^{-1}$; 1, if $\Delta K \geq 9X10^6\ M^{-1}$}. The FLS that characterizes specific CPIs of **T-1** are presented in Figure 5a. The red vertical line represents Ca^{2+} binding of **T-1** ({1, 0}) with binding affinity 115 M^{-1} and three degrees of interaction. The red arrow pointing the zero may be interpreted as 'no-binding' or low output (0) (as in BL). The black arrow (pointing to 0.11) may be described as 'slightly medium (SM) binding' and light blue arrow (pointing to 1.0) - 'true weak (TW) binding'. In general, Ca^{2+} ions mediated interactions can be considered as real values, ranging from 0 to 1, with three degrees of weak interactions. Similarly, PNA lectin interactions with **T-1** (green vertical line) displayed three degrees of medium interaction. The red arrow indicates 'no-binding' and black arrow (pointing to 0.35) may be described as 'slightly strong (SS) binding'. Light blue arrow at 0.74, indicates 'fairly medium (FM) binding'. Similarly, the black line ({1, 1}) represents 'strong binding' or output 1. Similarly, the experiment with **16** showed three degrees of interactions.

1.3.2.4. Conclusions

We introduced the use of the two logic systems, FLS and BL, for presenting carbohydrate-protein interactions in glycoclusters composed of multivalent *β*-cyclodextrin appended with

lactose molecules and peanut agglutinin lectin. We compared between the two logic systems, emphasized and demonstrated the preference of FLS over BL, which described only the two states 1 and 0. FLS provides a real-time analytical tool for exploring these systems, and is adequate for presenting transitions from one state to the other, namely from 'non-binding' to 'binding' states. Degrees of interactions between the glycoclusters and PNA lectin, with and without calcium Ca^{2+} ions, were used as the linguistic variables for the fuzzy logic sets. The association constants, between these parameters, measured by ITC, were the output.

1.3.3. Lactose-GM_3 Interaction as Drug Delivery Vehicles.

1.3.3.1 Introduction

Controlled drug delivery at its proposed sites has potential therapeutic advantages, including reduced side effects, minimum dosage and maximum treatment effect.[66] This can be achieved by either exploiting specific interactions on cell surfaces or creating an artificial interaction.[67] Much of the effort to address the needs of the cell surface interactions are directed towards the protein-protein interactions and protein-carbohydrate interactions. To further expand the targets, several groups have considered membrane-bound receptors, ion channels and enzymes such as kinases and proteases.[68] Despite having so many selective and sensitive receptors on the cell surfaces, cross reactivity and homologous activity of the receptors prompt the discovery of new strategies or alternative pathways to deliver drugs efficiently. Herein, for the first time we have proven the potential application of carbohydrate-carbohydrate interactions (CCIs) in the drug delivery process.

Le^X-Le^X carbohydrate interaction plays an important role in embryogenesis.[69] The GM_3-Gg_3 interaction is involved in the cell-cell adhesion between lymphoma and melanoma cells,[70] and this interaction was recently reported to trigger signal transduction.[71] Gal-SO_3Gal interaction was reported to participate in the formation of compacted myelin sheaths.[72] Despite the novel biological functions, the direct application of the CCIs have not been reported. Because the binding interaction between C-C is rather weak and multivalent display is crucial for interactions.[73] Recently, we and others have investigated the application of *β*-cyclodextrin (*β*-CD) to interrogate the CCIs.[29-31] The advantage of the *β*-cyclodextrin scaffold is its facile mode to synthetically incorporate sugar in a multivalent display and also to express the hydrophobic guest cavity to host several drugs and biologically active molecules.[32] Here, we have aimed at taking the advantage of lactose-capped *β*-CD having

hosted doxorubicin (Dox) as a drug delivery system. As a prototype, we have used in this study the GM_3-lactose model to demonstrate this delivery process.

1.3.3.2. Synthesis

The inclusion complexes were prepared by mixing equimolar **8** (*β*-CD-Lac)/ **9** (*β*-CD-Mal)/ *β*-CD with doxorubicin and sonicated for 20 min, using water as the solvent, yielding **D-1** to **D-3**.

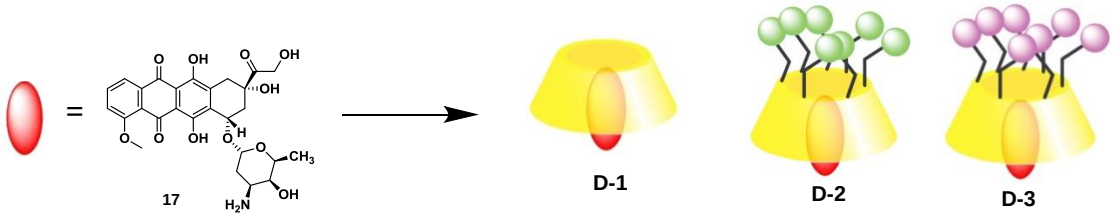

Scheme 5: Schematic representation of supramolecular complexes **D-1 to 3**: **(a)** Dox/water.

Inclusion complexation of doxorubicin and dendrimer was verified by ^{1}H NOESY experiments and FT-IR. An equimolar mixture of **9** and doxorubicin displayed the clear Nuclear Overhauser Effect (NOE) correction between aromatic region H-1, H-2 and H-3 of doxorubicin (~7.25, 7.57 ppm) and *β*-CD of **C-1** indicating the inclusion of doxorubicin into *β*-CD. The stoichiometry of the host-guest complex was established by isothermal titration experiments.

1.3.3.3. Application

Having completed the synthesis and characterization of the host-guest complexes, we proceeded to evaluate the *in vitro* toxicity of CCIs mediated drug delivery in B16 cell line by measuring the cell viability assay using MTT (2-(4, 5-dimethylthiazol-2-yl)-2,5-diphenyl tetrazolium bromide) at 24 h and 48h post-incubation. We selected B16 melanoma cell line as it expresses exceptionally high levels of GM_3.[33] At 24 h **D-1, D-2,** and **D-3** showed cell death with IC_{50} between 21-23 μM compared to free Dox with IC_{50} = 12 ± 1 μM. Interestingly, at 48 h, **D-3** induced B16 cell death having IC_{50} = 0.7 ± 0.3 μM compared to IC_{50} = 0.1± 0.14 μM for free **Dox**. **D-3** induced 90 ± 3% cell death compared to 87 ± 3% cell death induced by free Dox at 30 μM concentration. On the other hand, **D-1**and **D-2** demonstrated IC_{50} between 16 to 18 μM by inducing 61-68% cell death at 30 μM concentration. It is evident from the above data that the **D-3** is more effective at 48 h compared to 24 h *via* CCIs. As expected, free **Dox** induced toxicity very quickly uptake through diffusion, whereas, CD capped **Dox**

showed lower efficacy than free drug. Moreover, the specific CCIs might regulate the specific delivery at particular time periods (after 48 h), and has proved their efficacy as novel cancer chemotherapy agents.

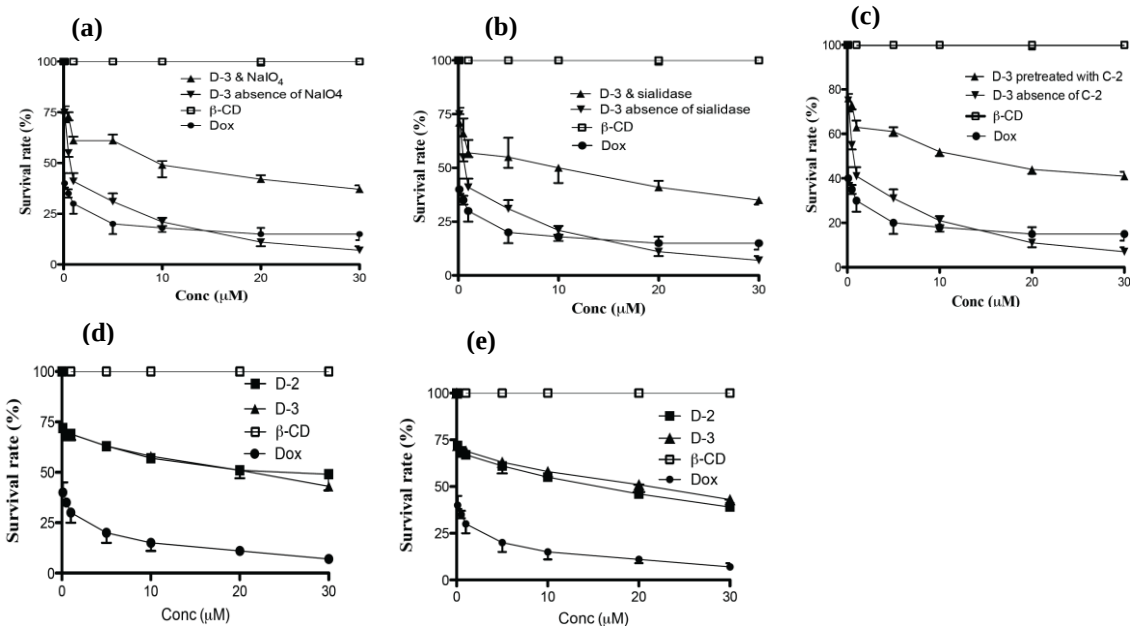

Figure 6: Cytotoxicity assay in B16 cells pre-treated with **(a)** 0.1 mM sodium periodate and 1 mM of sodium borohydrates; **(b)** sialidase enzyme (10 µl of 1µg/ml) from *vibrio vulnificus*; **(c) 8** (0.1 mM); for 2 h before performing the experiments. After treatment, the cells were incubated with *β*-CD, D-3 or Dox alone with 1 mM of $CaCl_2$ for 48h. **(d)** Cytotoxicity assay in THP-1 cells and **(e)** NIH-3T3 treated with D-2 or D-3 and 1 mM of $CaCl_2$ for 48h. Cytotoxicity was determined by using an MTT assay. Data are given as mean ± SEM (n = 3).

We further investigated the CCIs mechanism of cellular internalization of these CD capped **Dox** by performing MTT assay with sialidase, periodate and excess of lactose treated cells. B16 cells were grown in 96-well plates, and were treated with 0.1 mM sodium periodate at 4^oC for 30 mins followed by incubation with 1 mM sodium borohydrate for 30 min at RT. These treated cells were washed with PBS and incubated in a fresh media with **Dox** loaded CD derivatives for 48 h. MTT assay revealed that **D-3 (**$NaIO_4$ treated cells) induced 60 ± 3 % cell death compared to 82 ± 3% cell death by free **Dox** (**Fig. 6a**), indicating the absence of CCIs for specific uptake. To support this hypothesis, we repeated the same experiment with sialidase treated B16 cell lines and we got similar observations (**Fig. 6b**). To further rationalize CCIs, we carried out the competitive assay, where B16 cells were incubated with **8** (0.1 mM) followed by **Dox** and **D-3**. As expected, **D-3** (presence of **8)** showed nearly 48 % cell death compared to 82% in the absence of **8** (**Fig. 6c**). Finally, we carried out drug

delivery process with THP-1 and NIH-3T3 cell lines, which has (2-6) sialic acid glycans and very low level of GM_3 glycans.[74] The MTT revealed almost identical cell death of **D-2** and **D-3** (53 ± 4 %) compared to 84% cell death by free **Dox** after 48 h (**Fig. 6d & 6e**).

1.3.3.4. Conclusions

We have successfully developed a simple and a versatile platform to prepare drug delivery system by applying GM_3-lactose mediated interaction. We demonstrated that the complex **D-3** transport doxorubicin *via* specific carbohydrate-carbohydrate interactions. This was confirmed by MTT assay and FACS measurement. Moreover, **D-3** drug delivery is more effective in B16 cells compared THP-1 or sialidase or $NaIO_4$ treated B16 cells. We believe that better results might be obtained with full length GM_3 glycan and with higher order of multivalent systems.

1.3.4. Carbohydrate-functionalized Cyclodextrin Conjugated Collagen Model Peptides.

1.3.4.1. Introduction

Protein glycosylation is a post-translational process responsible for more than 50% of protein modifications in nature. Attaching glycans to proteins results in a dramatic increase in the bioavailability, stability and solubility of proteins.[75] For example mucin, a heavily glycosylated protein serves as a lubricant in cell signaling overcoming the chemical barriers on epithelial tissues.[76] The glycosylation pattern of histo-blood group antigens is critical for blood coagulation. Numerous immune functions, anti-freezing and chaperone activity of proteins are all related to glycosylation patterns.[77-79]

Cellular glycosylation commonly presents in the form of either *N*- or *O*-glycosides. Biosynthesis of glycoproteins is not a genetically coded process and often yield heterogeneous mixtures of proteins that differ in glycosylation pattern. It is difficult to predict or direct the pattern of glycosylation in proteins. Recently, *de novo* designed and synthesized peptides were shown to appropriately mimick protein structures for understanding the post-translational modifications.[80-83] Glycopeptides modified at specific positions are good probes to study the function of the native protein. Such synthetic approaches have been used to prepare tumor associated MUC-1 conjugated to immune stimulating components for the production of immunogenic vaccines.[84,85] Short coiled-coil model and amyloid peptides were employed to study the role of glycosylation and phosphorylation.[89,90] A number of different

covalent modifications have been used to improve the biological relevance of collagen peptide.[91-100]

We have shown a non-covalent glyco-complexation of collagen peptide and its ability to probe glyco-protein interactions.

1.3.4.2 Synthesis

The synthesis of peptides CP [**Col-1**, AcHN-Phe-(Pro-Hyp-Gly)$_6$-NH$_2$] and ACP [**Col-2,** AcNH-Phe-(Pro-Hyp-Gly)$_2$-(Pro-**Z**-Gly)-(Pro-Hyp-Gly)$_3$-NH$_2$ with **Z** = 4-amido-adamantoyl proline**)**] were done using the Fmoc solid phase peptide synthesis on Rink amide resin.[101,102]

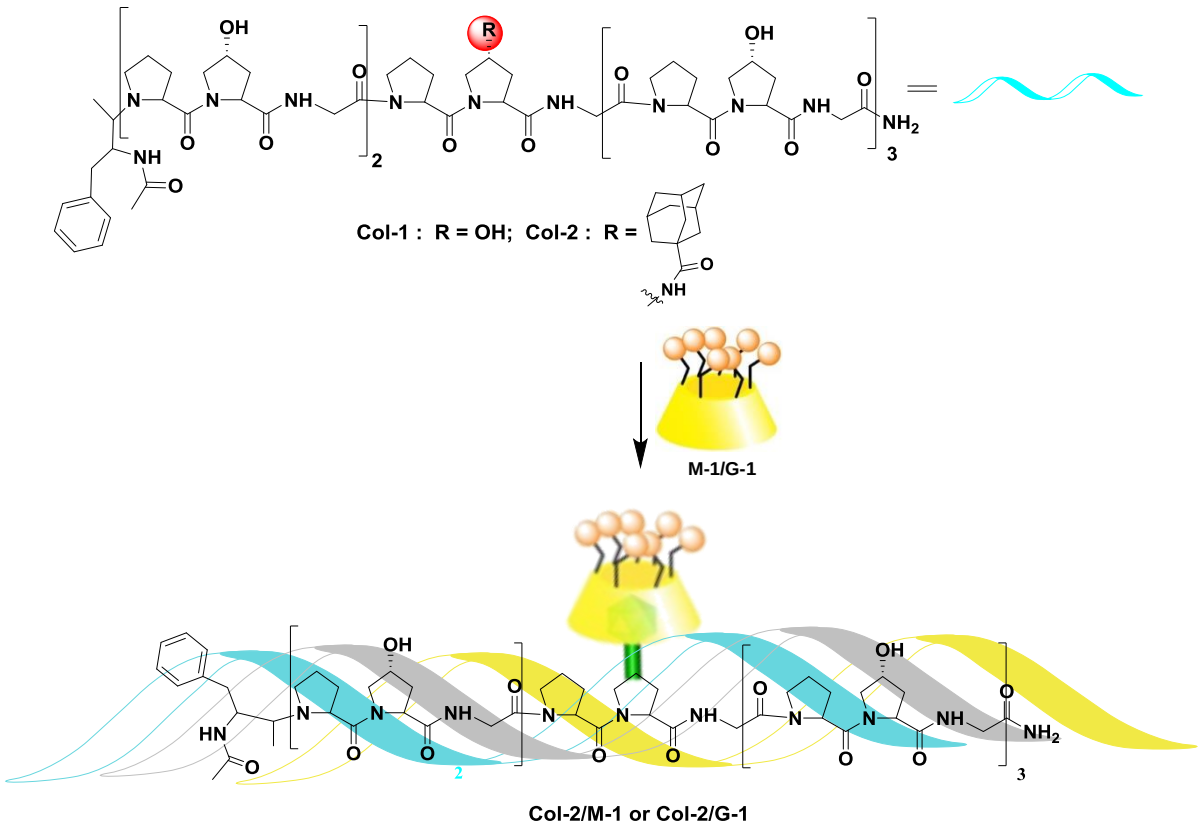

Scheme 6: Synthesis of glycopeptides.

The peptides after cleavage from the resin were purified by preparative HPLC and characterized by MALDI-TOF. The *β*-cyclodextrin complexes of **Col-2** were assembled by mixing stoichiometric amounts of (**G-1**/**M-1)**[103-105] and **Col-2**. The formation of the 1:1 complexes (**Col-2**/**M-1**) was proven by western blot assay using both primary (anti-collagen II) and secondary (anti-rabbit-HRP) antibodies.[106,107]

Circular Dichroism (CD) spectra of **Col-2 (**pH 7.2) revealed a positive band between 220 and 230 nm and a negative band between 200 and 210 nm. The ratio of positive to negative band ($R_{p/n}$) increased rapidly from 0.075 to 0.104 with the increase in the concentration of **Col-2** till saturation at 150 μM and remained nearly constant thereafter. Both these features are similar to that of CP (**Col-1**) and characteristic of collagen triplexes. This indicates that the 4-adamantoyl group though bulky does not inhibit the formation of the triple helical structures.

1.3.4.3. Application

The potential application for mannose-conjugate **Col-2/M-1** was illustrated by its interaction with α-mannose specific lectin (ConA). The complexation was followed by isothermal calorimetric titration (ITC) of glyco-conjugate with the protein. The binding isotherms fitted to a 1:1 binding model and the affinities determined from isothermal data indicated a 10 fold increase in binding of **Col-2/M-1** with Con A ($5.3x10^4$ M^{-1}) compared to that of **M-1** with Con A ($4.1x10^3$ M^{-1}).

1.3.4.3. Conclusions

In summary, a new concept for anchoring multivalent sugar residues through host-guest interactions employing cyclodextrin-adamantyl collagen peptide construct is reported. This is demonstrated to be useful to assemble specific carbohydrate-protein complexes. It is expected that this strategy will contribute to the development and tuning of collagen peptide conjugates to recognise specific receptors for potential biomedical applications, such as tissue engineering and prevention of cancer metastasis.

1.3.5. Immobilization of Multivalent Cyclodextrin on Gold Surfaces For Sensing Proteins and Macrophages.

1.3.5.1. Introduction

Controlled surface decoration of carbohydrates through precise reactions hold an enormous promise for advances in microarray, biosensors and nanotechnology. Among the myriad of technologies that has been developed to immobilize carbohydrates on a solid support; covalent binding is the most prominent method. In contrast to covalent attachment, non-covalent adsorption is a straightforward method to immobilize biomolecules on surfaces.

Among them, host-guest interactions, such as those of cyclodextrin (CD) systems, have proven to be important for constructing patterned surfaces.[108-110] The advantage of host-guest method is that they can provide structural versatility and also functional modulation. Several examples have been reported about the use of CDs for fabricating the surfaces,[111] however, multivalent carbohydrate surfaces formed by direct self-assembly of CDs on adamantane surfaces have not been described till date. We have reported a novel way to construct glyco-surface triggered by direct self-assembly of CD-based host-guest interactions. In brief, host-guest conjugation on gold surfaces was achieved by immobilizing PEGylated adamantyl linker in a straightforward self-assembly process, followed by non-covalent interaction of *β*-cyclodextrin derivatives. The formation of host-guest complex on gold substrate was determined from contact angle measurement, ellipsometry and AFM imaging techniques. Combination of surface plasmon resonance (SPR) and gold coated photolithography were applied to demonstrate specific carbohydrate-protein interactions. The main benefits of this approach include simplicity and multivalent carbohydrate-protein interaction, which is essential to tune the selectivity and sensitivity of the specific biomolecular interaction.

1.3.5.2. Synthesis

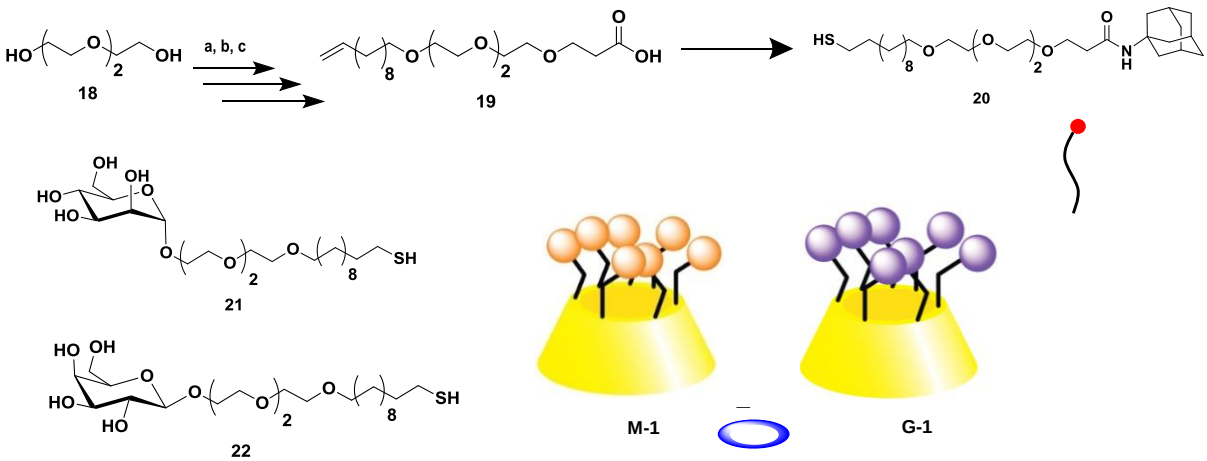

Scheme 7: Synthetic route to **20**: (a) 11-bromoundec-1-ane/NaH/THF; (b) t-butylacrylate/KO^{t}Bu/THF; (c) NaOH; (d) Adamantanyl-NH_2/EDC/HOBT/DIPEA/DMF; (e) AIBN/AcSH/1,4-dioxane followed by NaOMe/MeOH.

The adamantyl derivative (the linker, **20**) was prepared in several steps, starting from conjugation of triethylene glycol with 11-bromoundec-1-ene, followed by reaction with *t*-

butyl acrylate to yield compound **19**. After hydrolysis with NaOH the carboxylic acid was obtained and coupling with adamantane amine, yielded adamantyl derivative. The compound was treated with thioacetic acid and azo isobutyronitrile (AIBN), followed by deacetylation with NaOMe to yield compound **20**. And the monovalent mannose- and galactose-modified linkers **(21** and **22**) were synthesized by using slightly modified procedure to that reported in the literature.[112]

The formation of host-guest complex on gold substrate was determined from contact angle measurement, ellipsometry and AFM imaging techniques. Combination of surface plasmon resonance (SPR) and gold coated photolithography were applied to demonstrate specific carbohydrate-protein interactions. The main benefits of this approach include simplicity and multivalent carbohydrate-protein interaction, which is essential to tune the selectivity and sensitivity of the specific biomolecular interaction.

Robust adamantyl-based monolayers were formed by covalent assembly of the linker **20** on gold coated glass slides. Freshly gold sputtered glass substrates were fully immersed in a degassed ethanol solution of linker **20**. Subsequently, the functionalized substrates were rinsed with ethanol to remove physisorbed materials. The new monolayers were characterized by a combination of aqueous contact angles, atomic force microscopy (AFM), ellispometry and XPS. AFM images of bare gold surfaces were relatively homogeneous, with nodules. Whereas, monolayers grown on gold coated glass slides showed essentially rough surface. The root mean square surface roughness R was 0.12 nm.

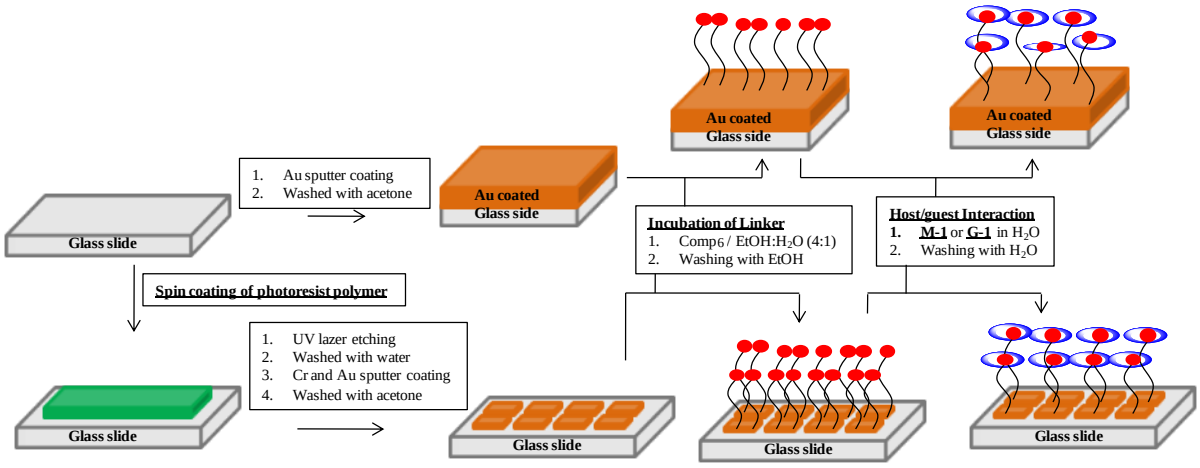

Figure 7: Schematic illustration of gold coated/microimprited glass substrate prepration and glyco-functionalization.

The glyco-dendrimer monolayers were prepared by host-guest interaction between β-CD derivatives on adamantyl SAM on gold substrates. Freshly prepared adamantyl monolayers were immersed in **M-1** solution. Subsequently, the functionalized substrates were rinsed with deionized water to remove physisorbed materials. The contact angle of **20/M-1** complex revealed that the concentration of **20** decides maximum host-guest complexes on the gold surface. In our experiment, the best concurrence was obtained by using an optimum concentration of linker **20** monolayer and **M-1**, indicating that the best host-guest interactions is possible only if there is enough distance between two adamantyl units, which is consistent with Park et al report.[113] The ellipsometric measurements showed that the film thickness was incresed to 2.7 nm, which is 1.4 nm more than adamantane layer and somewhat close to the thinkness of β-CD. Finally, the formation of host-guest complexes was further confirmed by AFM measurement. The surface morphology and the root mean-square roughness were increased from 0.12 to 0.19 nm. Similar results were also obtained with **20/G-1** functionalization.

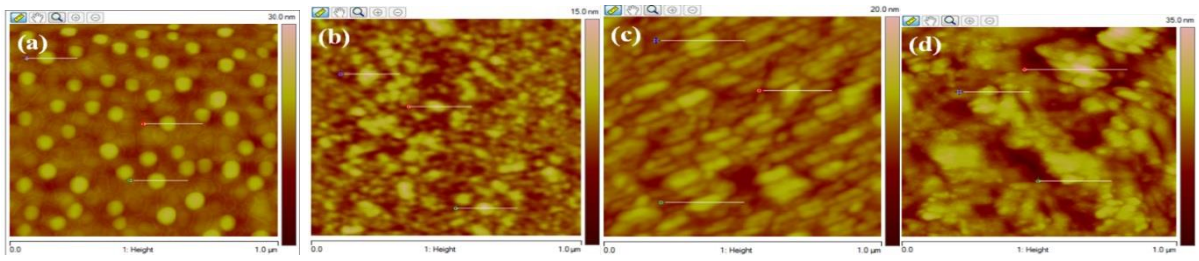

Figure 8: AFM images measured in air on the surfaces of **(a)** bare Au, **(b)** Comp **20** coated Au substrate, **(c) 20**/**M-1**coated Au substrate and **(d) 20**/**M-1**/**conA** coated Au substrate.

1.3.5.3. Application

ConA lectin was immobilized by immerising the **M-1** coated slides in ConA solution. The slides were washed with water and used as such for ellipsometry measurment, which showed a very strong increase in the thinkness. The large increases in the hight are typical for the protein immobilization on the gold substrate.

To understand the influence of multivalent carbohydrate on lectin binding, surface plasmon resonance (SPR) studies have been performed. Both monovalent substrate (**21 & 22**) and multivalent (**M-1**/**20** & **G-1**/**20)** were immobilizied on polycarboxylated CM5 sensor chip using step-by-step assembly of ethylene diamine by amino coupling chemistry and sulfo-GMBS reaction to form a surface with maleimide function that can be used to attach thio-

ligands. Adamantyl functionalized CM5 chips were treated with **M-1** or **G-1** resulting in host-guest glyco-clusters. The kinetic analysis was carried out based on a 1:1 interaction model. The SPR analyses of **M-2** and **M-1**/**20** with different concentration of ConA indicated that both association and dissociation of multivalent mannose cluster was 100 fold stronger than monovalent **20** probe (**Fig. 9**). Similar experiment with **G-1**/**20** and **G-1** showed no binding, as expected. Based on these results, it has been concluded that spatial arrangement of mannose bearing CD tune the sensitivity of carbohydrate-protein interactions compared to monovalent mannose ligand.

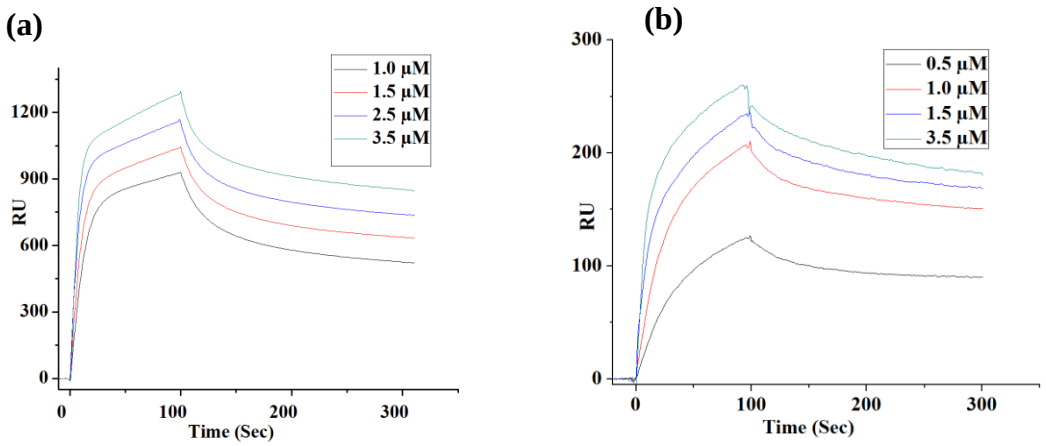

Figure 9: SPR sensograms of different concentration of ConA to **(a) 20**; **(b) 20/M-1**

After establishing selective and sensitive carbohydrate-protein interactions, the potential application of multivalent carbohydrate interactions was illustrated by the specific adhesion of macrophages on sugar patternized surfaces. Macrophages have been reported to show C-type lectin receptors, such as DC-SIGN or murine DC-SIGN homologues which recognize high-mannose glycans.[114] Thus, sugar rich surfaces profile a model platform for high-throughput screening of glycan-cell interactions. In this study, we used photoresist lithography technique to produce well-defined patterns of host-guest glycoprobes. Uniform homologous gold pattern surfaces were made on glass surfaces by spin coating of photoresist polymer, which was exposed to UV lazer to patternize the surfaces. The polymer etched glass areas were washed several times with deionized water to remove loosely bound polymer and coated with chromium (50 nm) and subsequent gold (100 nm) using sputter coating technique. Finally, the surfaces were washed with acetone to remove the photoresist polymers yielded gold patternized surfaces (**Fig. 10**). The self-assembled monolayer of host-guest

complexes were prepared by treating adamantyl linker **20** (0.02 M) followed by cyclodextrin analoges (**M-1** or **G-1** 10 μM). The contact angles of Comp **20**, **M-1** and **G-1** modified surfaces were consistent with gold coated glass slide experiments.

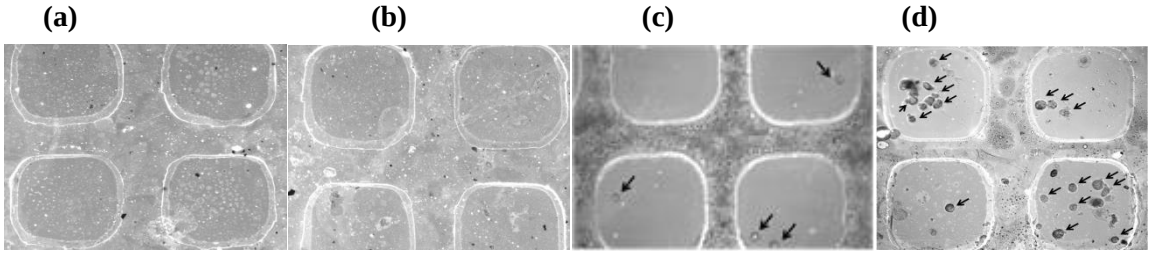

Figure 10: Representative images of macrophage attachment on **(a)** bare gold **(b)** Comp **20**, **(c) M-2** and (d) **20/M-1**, after 1 h incubation. Scale bar length is 50 mm. Arrows indicate macrophage sequestered to gold coated lithographic plate.

Similarly, gold coated micropattern surfaces were also functionalized with monovalent sugar **M-2** to compare the multivalent binding assay.

After preparing the glyco-patternized surfaces, slides were exposed to known amount of cells. After 60 min incubation, slides were washed with PBS and taken as such for bright microscopic imaging and counting. **20/M-1** coated slides showed maximum number of cells and some of them even clustered and started elongating on glass slides. Similar experiments with comp **20,** and **M-2** coated surfaces showed only few cells attached on the surfaces.

1.3.5.4. Conclusions

We have developed a novel technique for immobilizing multivalent carbohydrates on surfaces that is based on self-assembly-driven host-guest interaction between *β*-CD and adamantyl molecules. This approach is simple, sensitive, and applicable for the study of carbohydrate-protein and carbohydrate-cells interaction using surface bound sugars. This innovative strategy enables to explore the significance of spatial arrangements of sugars on the surfaces on the interaction with lectins and to probe the role of uniform monovalent sugar *vs* multivalent sugar immobilization. It can also be utilized as a platform for building more-complex biological functional and biomedical devices.

1.4. Factors influence in carbohydrate protein intractions.

1.4.1. Symmetry

One of the important considerations for designing multivalent probes is symmetry of the multivalent probes**.** For instance, C5-symmetrical glycoconjugates that orient five Gb3 trisaccharide can neutralize the pentameric Shiga toxin via a specific and multivalent interaction. Similarly, a multivalent C3-symmetrical ganglioside GM3 trisaccharide is a potent inhibitor of hemagglutin protein of influenza virus. Seeberger et al. reported the synthesis of fullerene C5-symmetric of Gb3 trisaccharide and demonstrated it potential application to inhibit the shiga toxin more selectively compare to linear polymers.[115,116] Nishimura et al. reported the synthesis of C3 symmetrical cyclic glycopeptide (GM3) to target influenza virus (**Fig. 11**).[117]

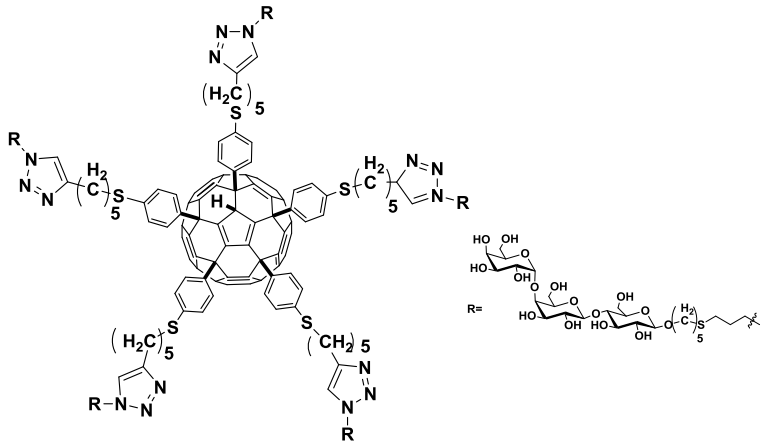

Figure 11: C5-symmetrical arrangement of Gb3 trisacchride.

1.4.2. Shape

Another consideration for designing multivalent probes is shape of the multivalent probes**.** To address the importance of the shape of the multivalent probes, kikkeri et al shown the synthesis of glyco-gold nanoparticles of three different shapes and their applications in bacterial aggregations and infection. More specifically, they compared the behavior of nanospheres, nanorods and nanostars with mannose and galactose conjugations. The mechanism of aggregation revealed that the large number of surface interaction of rod shaped mannose-AuNPs with E.coli ORN 178 compared with spherical and star-shaped AuNPs.

Moreover, such sensitive binding can be used for effective inhibition of bacterial infection of cells (**Fig. 12**).[118]

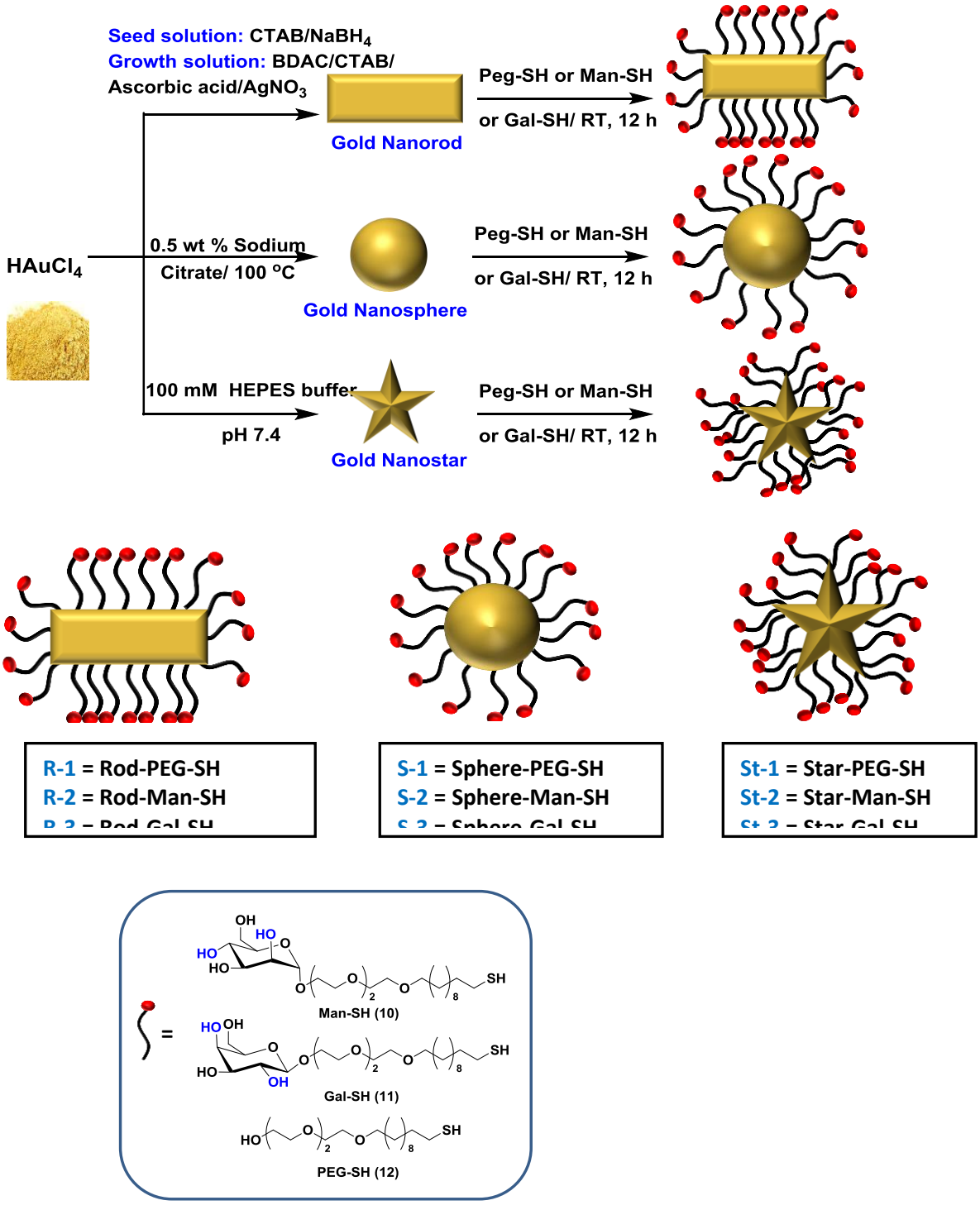

Scheme 12: Synthesis of gold nanoparticles and glyco-goldnanoparticles (G-AuNPs)

1.5. References

1. D. B. Werz, P. H. Seeberger, *Nat. Rev*., 2005, **4**, 751.
2. T. Angata, A. Varki, *Chem. Rev*., 2002, **102**, 439.
3. A. Varki, R. Cummins, J. Esko, H. Freeze, G. Hart, J. Marth (Eds.), Essentials of Glycobiology. Consortium of Glycobiology, La Jolla, California, Cold Spring Harbor Laboratory Press, Cold Spring Harbor, NY 1999.
4. M. L. Hecht, P. Stallforth, D. Varon Silva, A. Adibekian, P. H. Seeberger, *Curr. Opin. Chem. Biol*., 2009, **13**, 354.
5. R. Loris, T. Hamelryck, J. Bouckaert, L. Wyns, *Biochim. Biophys. Acta*, 1998, **1383**, 9.
6. D. C. Kilpatrick, *Biochim. Biophys. Acta*, 2002, **1572**, 187.
7. J. Bouckaert, J. Berglund, M. Schembri, E. De Genst, L. Cools, M. Wuhrer, C.-S. Hung, J. Pinkner, R. Släettegård, A. Zavialov, D. Choudhury, S. Langermann, S. J. Hultgren, L. Wyns, P. Klemm, S. Oscarson, S. D. Knight and H. De Greve, *Mol. Microbiol*., 2005, **55**, 441.
8. Z. Zuo, H. Fan, X. Wang, W. Zhou, L. Li, Springer Plus, 2012, **13**, 1.
9. B. Liu, H. J. Bian, J. K. Bao, *Cancer Lett*., 2010, **287**, 1.
10. R. Liang, L. Yan, J. Loebach, M. Ge, Y. Uozumi, L. Sekanina, N.Horan, J. Gildersleeve, C. Thompson, A. Smith, *Science*, 1996, **274**, 1520.
11. R. Liang, J. Loebach, N. Horan, M. Ge, C. Thompson, L. Yan, D. Kahne, *Proc. Natl. Acad. Sci. U.S.A*., 1997, **94**, 10554.
12. Petite and Sweet Glyco-Nanotechnology as a Bridge to New Medicines, ed. X. Huang and J. J. Barchi Jr., ACS Chem. Soc. Rev. 2012 Symposium Series, American Chemical Society, Washington, DC, 2011.
13. O. Renaudet, N. Spinelli (Eds.), Synthesis and Biological Applications of Glycoconjugates, Bentham Science Publishers Ltd. 2011.
14. S. K. Wang, P. H. Liang, R. D. Astronomo, T. L. Hsu, S. L. Hsieh, D. R. Burton, C. H. Wong, *Proc. Natl. Acad. Sci. U.S.A*., 2008, **105**, 3690.
15. O. Martinez-Avila, K. Hijazi, M. Marradi, C. Clavel, C. Campion, C. Kelly, S. Penadés, *Chem. Eur. J*., 2009, **15**, 9874.
16. Z. Zhang, E. A. Merritt, M. Ahn, C. Roach, Z. Hou, C. L. Verlinde, W. G. Hol, E. Fan, *J. Am. Chem. Soc*., 2002, **124**, 12991.

17. A. V. Pukin, B. C. Jacobs, A. P. Tio-Gillen, M. Gilbert, H. P. Endtz, A. van Belkum, G. M. Visser, H. Zuilhof, *Glycobiology*, 2011, **21**, 1642.

18. C. Heidecke, T. K. Lindhorst, *Chem. Eur. J*., 2007, **13**, 9056.

19. A. Bernardi, A. Checchia, P. Brocca, S. Sonnino, F. Zuccotto, *J. Am. Chem. Soc*., 1999, **121**, 2032.

20. C. Chemani, A. Imberty, S. de Bentzmann, M. Pierre, M. Wimmerova, B. P. Guery, K. Faure, *Infect. Immun*., 2009, **77**, 2065.

21. F. Peri, M. Piazza, *Biotechnol. Adv*., 2012, **30**, 251.

22. M. Piazza, C. Rossini, S. Della Fiorentina, C. Pozzi, F. Comelli, I. Bettoni, P. Fusi, B. Costa, F. Peri, *J. Med. Chem*., 2009, **52**, 1209.

23. M. Piazza, M. Colombo, I. Zanoni, F. Granucci, P. Tortora, J. Weiss, T. Gioannini, D. Prosperi, F. Peri, *Angew. Chem., Int. Ed*., 2011, **50**, 622.

24. P. H. Seeberger, D. B. Werz, *Nat. Rev. Drug. Discov*., 2005, **4**, 751.

25. R. Pejchal, K. J. Doores, L. M. Walker, R. Khayat, P. S. Huang, S. K. Wang, R. L. Stanfield, J. P. Julien, A. Ramos, M. Crispin, R. Depetris, U. Katpally, A. Marozsan, A. Cupo, S. Maloveste, Y. Liu, R. McBride, Y. Ito, R. W. Sanders, C. Ogohara, J. C. Paulson, T. Feizi, C. N. Scanlan, C. H. Wong, J. P. Moore, W. C. Olson, A. B. Ward, P. Poignard, W. R. Schief, D. R. Burton, I. A. Wilson, *Science*, 2011, **334**, 1097.

26. S. Boonyarattanakalin, X. Liu, M. Michieletti, B. Lepenies, P. H. Seeberger, *J. Am. Chem. Soc*., 2008, **130**, 16791.

27. A. Imberty, Y. M. Chabre, R. Roy, *Chem. Eur. J*., 2008, **14**, 7490.

28. M-X. Zhao, H-F. Huang, Q. Xia, L-N. Ji, Z-W. Mao, *J. Mater. Chem.* 2011, **21**, 10290.

29. H. Bavireddi, P. Bharate, R. Kikkeri, *Chem. Commun*., 2013, **49**, 3988.

30. S. Hakomori, *Glycoconjugate J*., 2000, **17**, 143.

31. S. Yu, N. Kojima, S. Hakomori, S. Kudo, S. Inoue, Y. Inoue, *Proc. Natl. Acad. Sci. U.S.A.*, 2002, **99**, 2854.

32. S. Hakomori, K. Handa, FEBS Lett., 2002, **531**, 88.

33. I. Bucior, M. M. Burger, *Glycoconjugate J*., 2004, **21**, 111.

34. B. Lorenz, L. Álvarez de Cienfuegos, M. Oelkers, E. Kriemen, C. Brand, M. Stephan, E. Sunnick, D. Yüksel, V. Kalsani, K. Kumar, D. B. Werz, A. Janshoff, *J. Am. Chem. Soc*., 2012, **134**, 3326.

35. L. J. Waters, S. Bedford, G. M. B. Parkes, J. C. Mitchell, *Thermochimica Acta*, 2010, **511**, 102.

36. V. J. Smith, N. M. Rougier, R. H. de Rossi, M. R. Caira, E. I. Buján, M. A. Fernandez, S. A. Bourne, *Carbohydrate Research*, 2009, **344**, 2388.

37. X. Wang, E. Matei, A. Gronenborn, O. Ramstrőm, M. Yan, *Anal. Chem*., 2012, **84**, 4248.

38. K. Matsuura, H. Kitakouji, R. Oda, Y. Morimoto, H. Asano, H. Ishida, M. Kiso, K. Kitajima, K. Kobayashi, *Langmuir*, 2002, **18**, 6940.

39. K. Matsuura, R. Oda, H. Kitakouji, M. Kiso, K. Kitajima, K. Kobayashi, *Biomacromolecules*, 2004, **5**, 937.

40. S. Andrè, Z. Pei, H-C. Siebert, O. Ramström, H-J. Gabius, *Bioorg. Med. Chem*., 2006, **18**, 6314.

41. X. Wang, E. Matei, A. M. Gronenborn, O. Ramström, M. Yan, *Anal. Chem*., 2012, **84**, 4248.

42. O. Norberg, L. Deng, T. Aastrup. M. Yan, O. Ramström. *Anal. Chem*., 2011, **83**, 1000.

43. T. Horlacher, P. H. Seeberger, *Chem. Soc. Rev*., 2008, **37**, 1414.

44. J. L. de Paz, P. H. Seeberger, *Methods. Mol. Biol*., 2012, **808**, 1.

45. E. M. Munoz, J. Correa, R. Riguera, E. Fernandez-Megia. *J. Am. Chem. Soc*., 2013, **135**, 5966.

46. E. M. Munoz, J. Correa, E. Fernandez-Megia, R. Riguera. *J. Am. Chem. Soc*., 2009, **131**, 17765.

47. A. P. de Silva, H. Q. N. Gunaratne, C. P. A. McCoy, *Nature*, 1993, **364**, 42.

48. A. Credit, V. Balzani, S. J. Langford, J. F. Stoddart, *J. Am. Chem. Soc.*, 1997, **119**, 2679.

49. A. P. de Silva, N. D. McClenaghan, *Chem. Eur. J*., 2002, **8**, 4935.

50. D. Margulies, G. Melman, C. E. Felder, R. Arad-Yellin, A. Shanzer, *J. Am. Chem. Soc*., 2004, **126**, 15400.

51. D. Margulies, G. Melman, A. Shanzer, *Nat. Mater*., 2005, **4**, 768.

52. G. de Ruiter, L. Motiei, J. Chowdhury, N. Oded, M. E. van der Boom, *Angew. Chem. Int. Ed*., 2010, **49**, 4780.

53. G. de Ruiter, E. Tartakovsky, N. Oded, M.E. van der Boom, *Angew. Chem. Int. Ed.*, 2010, **49**, 169.

54. T. Gupta, M. E. van der Boom, *Angew. Chem. Int. Ed.*, 2008, **47**, 5322.

55. P. Ceroni, G. Bergamini, V. Balzani, *Angew. Chem.*, 2009, **121**, 8668.

56. B. Rout, L. Unger, G. Harmony, M. E. Iron, and D. Margulies, *Angew. Chem. Int. Ed*., 2012, **51**, 12477.

57. Z. Li, M. A. Rosenbaum, A. Venkataraman, T. K. Tam, E. Katz, L. T. Angenent, *Chem. Commun*., 2011, **47**, 3060.

58. M. A. Arugula, D. Saffarini, E. Katz, Z. He, *Chem. Commun.*, 2012, **48**, 10174.

59. M. Zhou, Y. Du, C. G. Chen, B. L. Li, D. Wen, S. J. Dong, E. K. Wang, *J. Am. Chem. Soc*., 2010, **132**, 2172.

60. T. K. Tam, G. Strack, M. Pita, E. Katz, *J. Am. Chem. Soc*., 2009, **131**, 11670.

61. L. Amir, T. K. Tam, M. Pita, M. M. Meijler, L. Alfonta, E. Katz, *J. Am. Chem. Soc*., 2009, **131**, 826.

62. R. Kikkeri, D. Grünstein, P. H. Seeberger, *J. Am. Chem. Soc*., 2010, **132**, 10230.

63. M. Elstner, K. Weisshart, K. Mullen, A. Schiller, *J. Am. Chem. Soc*., 2012, **134**, 8098.

64. W. Shi, X. Ji, M. Wei, D. G. Evans, X. Duan, *Langmuir*, 2012, **28**, 7119.

65. B. K. Gorityala, Z. Lu, M. L. Leow, J. Ma, X. W, Liu, *J. Am. Chem. Soc*., 2012, **134**, 15229.

66. Z. Ge, S. Liu, *Chem. Soc. Rev*., 2013, **42**, 7289.

67. J. C. Rogers, S. Kornfeld, *Biochem. Biophys. Res. Commun*., 1971, **45**, 622.

68. M. R. Arkin, J. A. Wells, *Drug Discovery*, 2004, **3**, 301.

69. A. D. Strosberg, *Expert Review of Proteomics*, 2004, **1**, 141.

70. A. Whitty, G. Kumaravel, *Nat. Chem. Biol*., 2006, **2**, 112.

71. M. Monsigny, A.-C. Roche, P. Midoux, R. Mayer, *Adv. Drug. Deliv. Rev*., 1994, **14**, 1.

72. M. S. Wadhwa, K. G. Rice, *J. Drug. Targeting*, 1995, **3**, 111.

73. G. J. L. Bernardes, R. Kikkeri, M. Maglinao, P. Laurino, M. Collot, S. Y. Hong, B. Lepenies, P. H. Seeberger, *Org. Bio. Chem*., 2010, **8**, 4987.

74. I. Eggenst, B. Fenderson, T. Toyokuni, D. Dean, M. Stroud, S. Hakomori, *J. Biol. Chem*., 1989, **264**, 9476.

75. R. Apweiler, H. Hermjakob, N. Sharon, *Biochim. Biophys. Acta*, 1999, **1473**, 4.

76. S. van der Post, D. B. Subramani, M. Backstrom, M. E. Johnsson, M. B. Vester-Christensen, U. Mandel, E. P. Bennett, H. Clausen, G. Dahlen, A. Sroka, J. Potempa, G. C. Hansson, *J. Biol. Chem.*, 2013, **288**, 14636.

77. A. Varki, *Glycobiology*, 1993, **2**, 97.

78. C. R. Bertozzi, L. L. Kiessling, *Science*, 2001, **291**, 2357.

79. J. Lukasiewicz, T. Niedziela, W. Jachymek, L. Kenne, C. Lugowski, *Glycobiology*, 2006, **16**, 113.

80. B. J. Davis, *Chem. Rev.*, 2002, **102**, 579.

81. D. P. Gamblin, E. M. Scanlan, B. J. Davis, *Chem. Rev.*, 2009, **109**, 131.

82. Y. Yuan, J. Chen, Q. Wan, Z. Tan, G. Chen, C. Kan, S. J. Danishefsky, *J. Am. Chem. Soc.*, 2009, **131**, 5432.

83. Z. Tan, S. Shang, T. Halkina, Y. Yuan, S. J. Danishefsky, *J. Am. Chem. Soc.*, 2009, **131**, 5424.

84. P. Nagorny, B. Fasching, X. Li, G. Chen, B. Aussedat, S. J. Danishefsky, *J. Am. Chem. Soc.*, 2009, **131**, 5792.

85. P. Wang, J. Zhu, Y. Yuan, S. J. Danishefsky, *J. Am. Chem. Soc*., 2009, **131**, 16669.

86. N. Gaidzik, U. Westerlind, H. Kunz, *Chem Soc. Rev*., 2013, **21**, 4421.

87. H. Cai, Z. H. Huang, L. Shi, Z. Y. Sun, Y. F. Zhao, H. Kunz, Y. M. Li, *Angew. Chem. Int. Ed*., 2012, **13**, 1719.

88. K. Baumann, D. Kowalczyk, H. Kunz, *Angew. Chem. Int. Ed*., 2008, **47**, 3445.

89. J. A. Falenski, U. I. Gerling, B. Koksch, *Bioorg. Med. Chem*., 2010, **18**, 3703.

90. M. Broncel, J. A. Falenski, S. C. Wagner, C. P. Hackenberger, B. Koksch, *Chem. Eur. J*., 2010, **16**, 7881.

91. K. L. Gorres, R. T. Raines, *Crit. Rev. Biochem. Mol. Biol*., 2010, **45**, 106.

92. F. W. Kotch, I. A. Guzei, R. T. Raines, *J. Am. Chem. Soc*., 2008, **130**, 2952.

93. R. S. Erdmann, H. Wennemers, *Angew. Chem. Int. Ed*., 2011, **50**, 6835.

94. M. M. Pires, D. E. Przybyla, J. Chmielewski, *Angew. Chem. Int. Ed*., 2009, **48**, 7813.

95. L. E. R. O'Leary, J. A. Fallax, E. L. Bakota, M. K. Kang. J. D. Hartgerink. *Nat. Chem*., 2011, **3**, 821.

96. C. M. Yamazaki, I. Nakase, H. Endo, S. Kishimoto, Y. Mashiyama, R. Masuda, S. Futaki, T. Koide, *Angew. Chem. Int. Ed*., 2013, **52**, 1.

97. J. Kwak, A. De Capua, E. Locardi, M. Goodman, *J. Am. Chem. Soc*., 2002, **124**, 14085.

98. X. Wu, M. E. Levenston, E. L. Chaikof, *Biomaterials*, 2006, **30**, 5315.

99. M. V. Sonar, K. N. Ganesh, *Org. Lett*., 2010, **12**, 5390.

100. M. Nanda, K. N. Ganesh, *J. Org. Chem*., 2012, **77**, 4131.

101. I. R. Babu, K. N. Ganesh, *J. Am. Chem. Soc.*, 2001, **123**, 2079-2080.

102. M. Umashankara, I. R. Babu, K. N. Ganesh, *Chem. Commun.*, 2003, 2606.

103. H. Bavireddi, R. Kikkeri, *Analyst*, 2012, **137**, 5123.

104. H. Bavireddi, P. Bharate, R. Kikkeri, *Chem. Commun*., 2013, **49**, 9185.

105. D. Grünstein, M. Naglinao, R. Kikkeri, M. Collot, K. Barylyuk, B. Lepenies, F. Kamena, R. Zenobi, P. H. Seeberger, *J. Am. Chem. Soc.*, 2011, **133**, 13957.

106. H-J, Barrach, C. O. Chichester, *US5541295A*, 1996.

107. H-J, Barrach, C. O. Chichester, *PCT patent*, 1998, WO1994018563A1.

108. A. Gonzalez-Campo, S-H. Hsu, L. Puig, J. Huskens, D. N. Reinhoudt, A. H. Velders. *J. Am. Chem. Soc*., 2010, **132**, 11434.

109. L. Yang, A. Gomez-Casado, J. F. Young, H. D. Nguyen, J. Cabanas-Danes, J. Huskens, L. Brunsveld, P. Jonkheijm, *J. Am. Chem. Soc*., 2012, **134**, 19199.

110. C. A. Nijhuis, J. K. Sinha, G. Wittstock, J. Huskens, B. J. Ravoo, D. N. Reinhoudt, *Langmuir*, 2006, **22**, 9770.

111. V. Mahalingam, S. Onclin, M. Peter, B. J. Ravoo, J. Huskens, D. N. Reinhoudt, *Langmuir*, 2004, **20**, 11756.

112. G. Bellapadrona, A. B. Tesler, D. Grünstein, L. H. Hossain, R. Kikkeri, P. H. Seeberger, A. Vaskevich, I. Rubinstein, *Anal. Chem*., 2012, **84**, 232.

113. J. H. Park, S. Hwang, J. Kwak, *ACS Nano*, 2010, **4**, 3949.

114. S. I. Gringhuis, J. den Dunnen, M. Litjens, M. van der Vlist, T. B. H. Geijtenbeek, *Nature Immunol*., 2009, **10**, 1081.

115. P.I. Kitov, J. M. Sadowska, G. Mulvey, G. D. Armstrong, H. Ling, N. S. Pannu, R. J. Read, D. R. Bundle, *Nature*, 2000, **403**, 669.

116. H. Isobe, K. Cho, N. Solin, D. B. Werz, P. H. Seeberger, E. Nakamura, *Org. Lett.*, 2007, **9**, 4611.

117. T. Ohta, N. Miura, N. Fujitani, F. Nakajima, K. Niikura, R. Sadamoto, C. T. Guo, T. Suzuki, Y. Suzuki, K. Monde, S. Nishimura, *Angew. Chem. Int. Ed.*, 2003, **42**, 5186.

118. P. M. Chaudhary,[#] S. Sangabathuni,[#] R. V. Murthy, A. Paul, H. V. Thulasiram, R. Kikkeri, *Chem. Commun*., 2015, **51**, 15669. ([#] = equal contribution).

CHAPTER 2

Understanding Carbohydrate-Protein Interactions using Homologous Supramolecular Chiral Ru(II)-Glyconanoclusters

Abstract

Multivalent glycodendrimers make a promising tool to tackle the basic and translational research in the field of carbohydrate-mediated interactions. Despite advances in glycodendrimers and glycopolymers, the multivalent probes available to date are still far from being ideal biological mimics. This work, demonstrates the inherent chirality of glycodendrimers as one of the promising factors to generate different spatial carbohydrate micro-environments to modulate the specific carbohydrate-protein interactions. By exploiting the host-guest strategy and chiral Ru(II) complexes (Δ and Λ) and mannose capped *β*-cyclodextrin (*β*-CD), we generated a library of homologous metallo-glycodendrimers (MGDs) of size 50-70 nm. These nanoclusters can enantioselectively bind to specific C-type lectins and displayed selectivity in cellular uptake. We also discovered their potential clathrin-mediated endocytotic pathway in DC-SIGN and SIGNR3-transfected cell lines. Finally, *in vivo* biodistribution and sequestration of MGDs was determined to decipher the role of chirality mediated spatial arrangement in carbohydrate-mediated interactions.

2.1. Introduction

Carbohydrate-protein interactions (CPIs) are the most common biological events at cell surfaces.[1,2] A significant body of data has indicated that multivalency is a critical step to increase CPIs binding avidity. Therefore, glycopeptides,[2,3] glycopolymers,[4-6] glycodendrimers[7-14] and supramolecular complexes[15-17] have been synthesized to target and image CPIs.

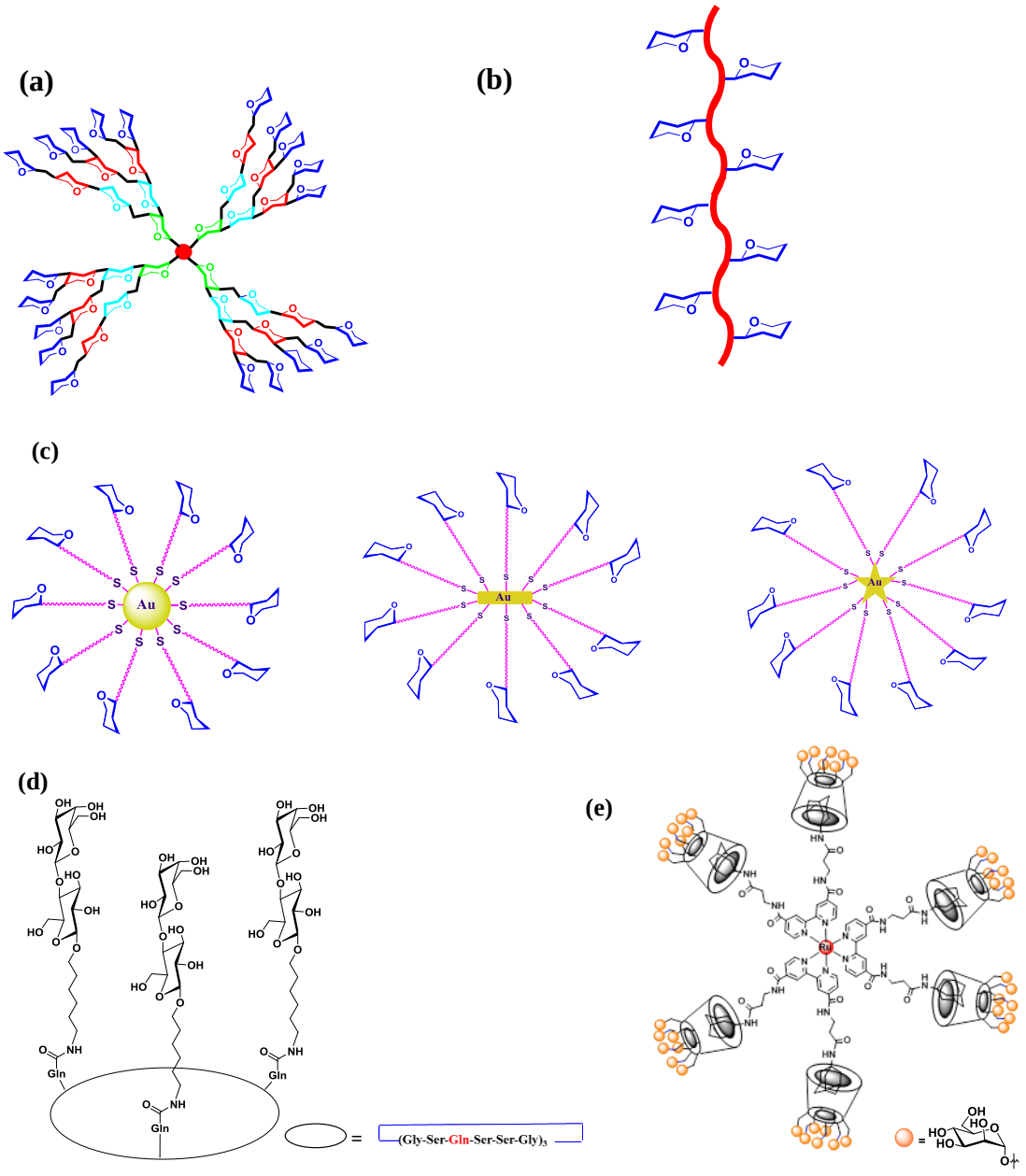

Figure 1: Different approaches to study carbohydrate-protein interactions. **(a)** Glycodendrimenrs; **(b)** Glycopolymers; **(c)** Glyconanoparticles; **(d)** Glycopeptides; **(e)** Supramolecular Complexes.

Yet, these multivalent glycodendrimers are still far away from mimicking the natural CPIs perfectly, which are far more selective and sensitive. Hence, multivalent probes have been designed with additional parameters, where inherent properties of the dendrimers such as symmetry, size and shape have been altered to increase binding avidity. For example, C_5-symmetric GM1 ganglioside and C_3-symmetric GM3 ganglioside inhibited cholera toxin binding and influenza virus hemagglutination selectively.[18,19] Mannosylated rod-shaped gold nanoparticles (AuNPs) exhibited sensitive and selective cellular uptake and inhibition of bacterial infections compared to spherical and star-AuNPs counterparts.[20,21] Hetero-glycopolymers[22] and Janus glycodendrimers[23-27] were synthesized to decipher the importance of spatial arrangements in CPIs. Alternatively, chirality in the dendrimers can also induce defined spatial arrangements.[28-30]

Studying how the particular chirality at the glycodendrimers translates its information to the final CPIs is crucial, because usually just one enantiomer of the molecule is biologically active, while the other one may exhibit side effects. Owing to the critical role of chirality in biological interactions, glycoclustures and hydrogels carrying different enantiomers of amino acids and carbohydrates have been synthesized to alter lectin binding affinity and cellular recognition.[31-34] In order to rationalize the enantiomeric effect on carbohydrate-protein interactions, it is essential to examine chirality at different positions of the glycodendrimers, their spatial arrangement, and lectin and cellular interactions.

With the aim of designing glycodendrimers with multiple chiral centers, we synthesized Ru(II) glycodendrimers *via* host-guest strategy. Previously, the Seeberger laboratory has introduced the host-guest strategy to synthesize racemic Ru(II)-glycodendrimers by mixing the Ru(II)-adamantyl dendrimers and sugar appended β-cyclodextrins.[35] These MGDs offer a simple supramolecular approach to simulate the natural multivalent display of sugars. They provide stereogenic centers at their core (Δ & Λ), C_3-symmetry and also optical and electrochemical properties for direct detection of their specific recognition.[36,37] The effect of chirality was further rationalized by incorporating additional chiral centers close to the mannose units on β-CD derivatives to modulate the binding affinity. Overall, we synthesized two distinct series of MGDs, the first group of the supramolecular complexes contain racemic Ru(II)-adamantyl derivative (**Ru-1**) decorated with β-CD (**C-A**) or mannosylated β-CD derivatives (**C-B** to **C-D**) resulted in MGDs (**M-1A** to **M-1D**). The second group of molecules bearing chiral Ru(II)-adamantyl derivatives (**Ru-2** and **Ru-3**) hosted β-CD derivatives resulted in MGDs (**M-2A** to **M-2D** or **M-3A** to **M-3D**). The stability, enantiopurity, spatial arrangement of sugars and topology of the complexes were

characterized. Lectin inhibition assay of the MGDs was performed using selected C-type lectins. Finally, the optical properties of the Ru(II) complexes were exploited to track cell uptake *in-vitro* and *in-vivo*.

2.2. Results and discussion

2.2.1. Synthesis of chiral (Δ & Λ) and racemic Ru(II) complexes

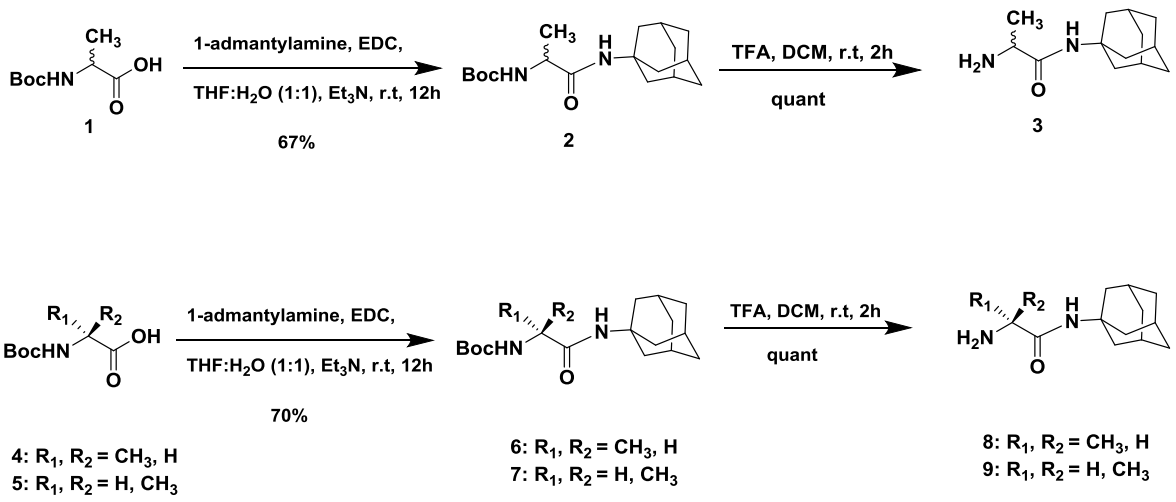

Scheme 1: Synthesis of adamantine derivatives.

The Bipyridine ligand **12** was prepared via convergent synthesis by using Boc protected DL-alanine and 4,4[1] Bipyridine dicarboxylic acid. **2** was synthesised by coupling of 1-admantylamine with Boc protected DL-alanine in presence of water soluble coupling reagent *N*-ethyl-*N*'-(diethylaminopropyl)-carbodiimide (EDC) and triethyl amine (Et_3N), followed by deprotection of Boc protecting group by using trifluoro acetic acid (TFA) (**Scheme 1**).

Parllely bipyridine carboxylic **11** acid was synthesised by oxidising the 4,4[1] dimethyl bipyridine with chromium trioxide (CrO_3) in presence of sulphuric acid (H_2SO_4) then carboxylic acids were converted into acid chlorides using thionyl chloride ($SOCl_2$) at refluxing temparature followed by coupling with **3** to afford lgand **12** (**Scheme 2**).

Same synthetic stratergy has been used for the synthesis of other two ligands (**Scheme 2**).

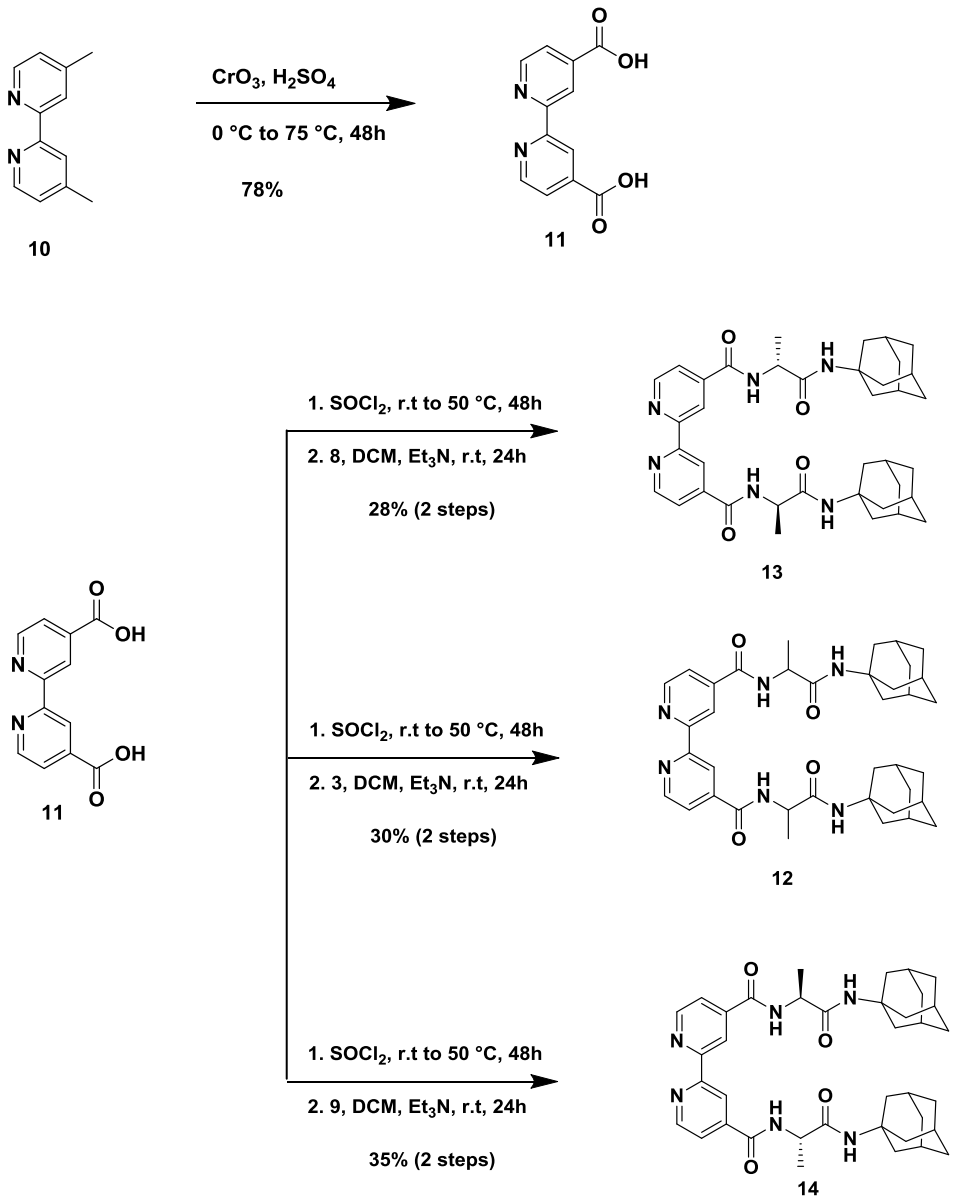

Scheme 2: Synthesis of bipyridine ligands.

Chiral (Δ & Λ) and Racemic Ru(II) complexes were obtained by refluxing $RuCl_3.3H_2O$ with bipyridine ligands in presence of ethanol for 12h. The usage of ligand **12** resulted in non-chiral Ru(II) complex; ligand **13** resulted in Delta (Δ)-Ru(II) complex and ligand **14** resulted in Lambda (Λ)- Ru(II) complex (**Scheme 3**).

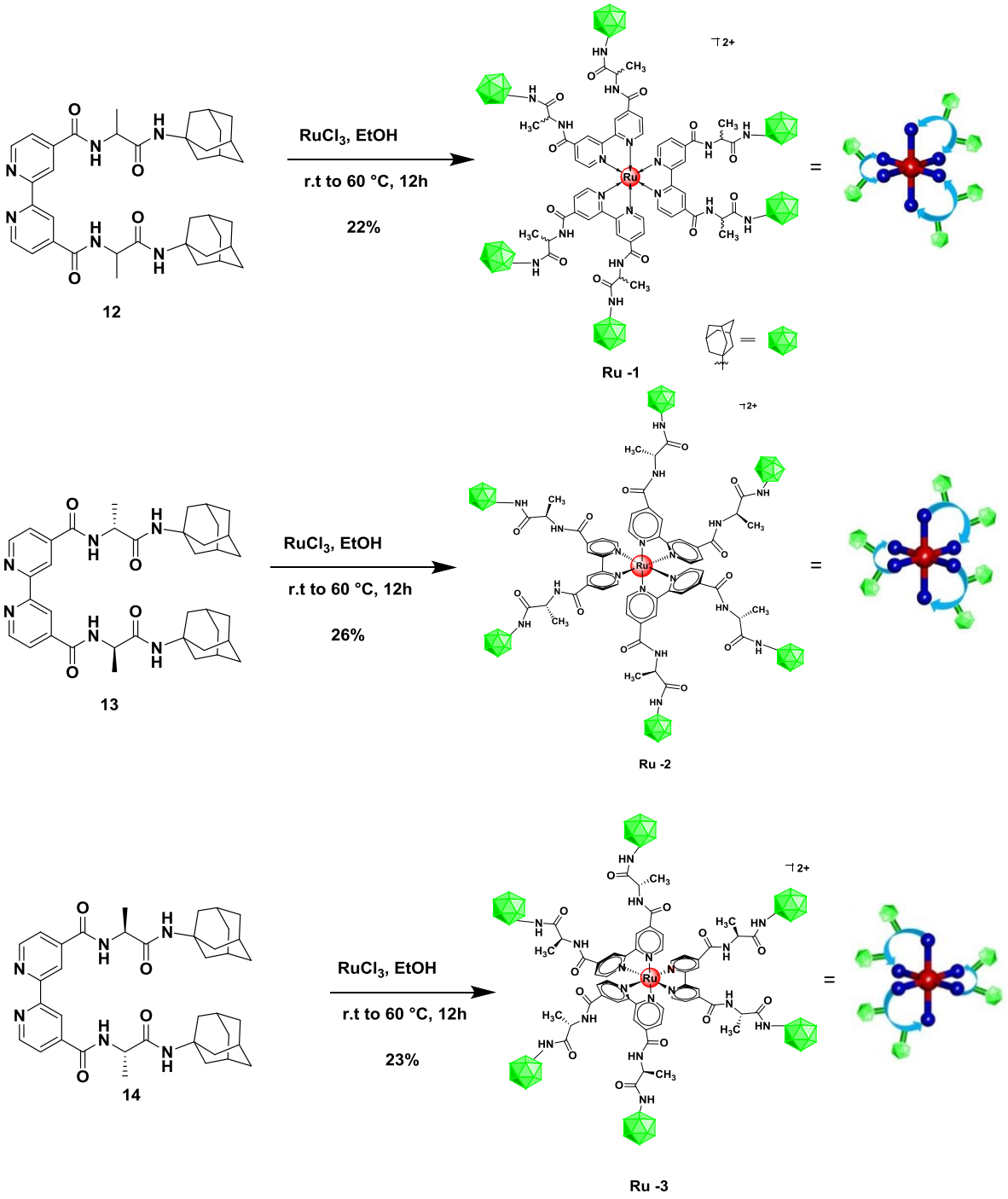

Scheme 3: Synthesis of chiral and non Ru(II) complexes.

2.2.2. Circular dichroism spectroscopy (CD) of Ru(II) complexes

The structures and stereochemistry of chiral and rec-Ru(II) complexes were corroborated by circular dichroism (CD). CD spectra of **Ru-2** and **Ru-3** revealed opposite signals as expected from the two enantiomers. The absolute configurations Δ (delta, negative sign) and Λ (lambda, positive sign) were assigned according to the sign of the MLCT transition at λ=480 nm (**Fig. 2**). **Ru-1** displayed neutral signal at the MLCT region.

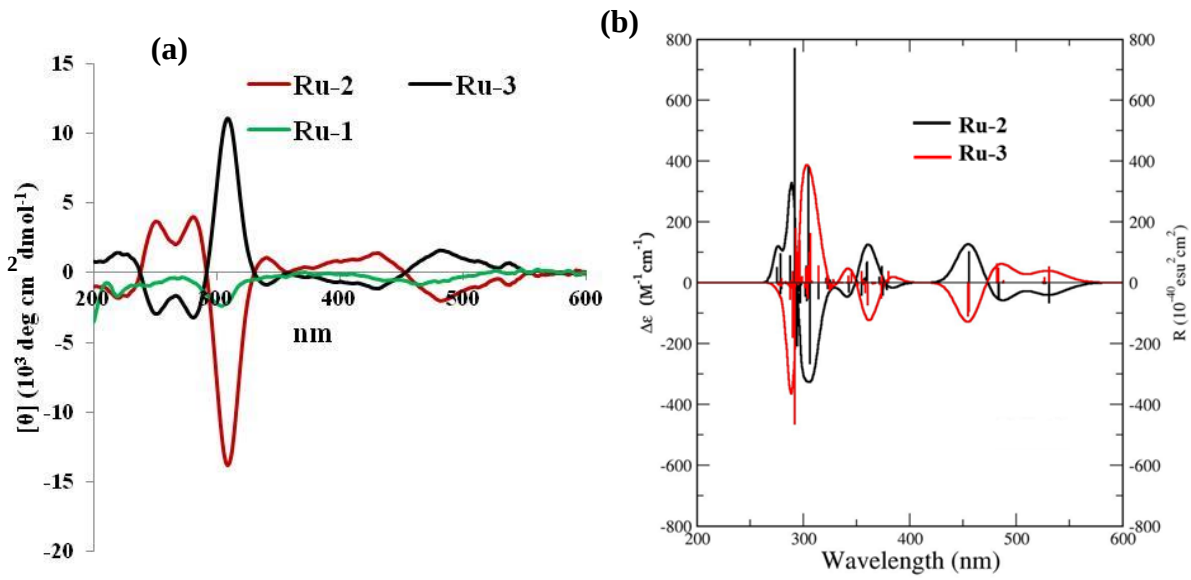

Figure 2: (a) CD profile of Ru(II) complexes in water at 25 °C. **(b)** Computed ECD (electronic circular dichroism) spectra of **Ru-2** and **Ru-3** in methanol (0.20 ev Gaussian broadening).

2.2.3. NMR study of Ru(II) complexes

The enantiopurity of the complexes was confirmed by the ^{1}H-NMR spectra. Ru(II) complexes revealed a set of two bipyridine signals, corresponding to Δ and Λ-isomers. The diasteromeric ratio of **Ru-1** was 50:50, indicating a racemic mixture of the complex, whereas **Ru-2** and **Ru-3** displayed 90:10 (**Fig. 3**).

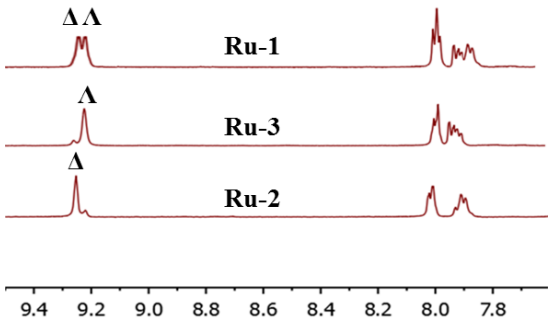

Figure 3: ^{1}H NMR spectra of bipyridyl protons of the **Ru-1** to **Ru-3** in CD_3OD.

2.2.4. HPLC profile of Ru(II) complexes

Chiral column HPLC further confirmed the purity of the complexes (**Fig. 4**).[38-40] The enantiopurity of **Ru-1** to **Ru-3** was quantified by HPLC (Waters 600 equipped with 2998-Photodiode array detector, PDA) using a Daicel chiralpak-AS-H Analytical column (250 ×

4.6 mm) and the following method: Solvent- 10% MeOH in MeCN for 25 min. Flow rate - 1 mL/min monitored at λ = 254 nm.

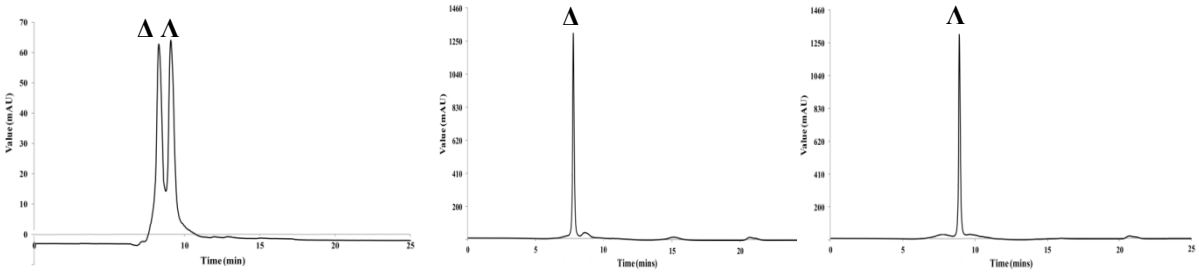

Figure 4: HPLC profiles of Ru(II) complexes.

2.2.5. Synthesis of *β*-cyclodextrin derivatives

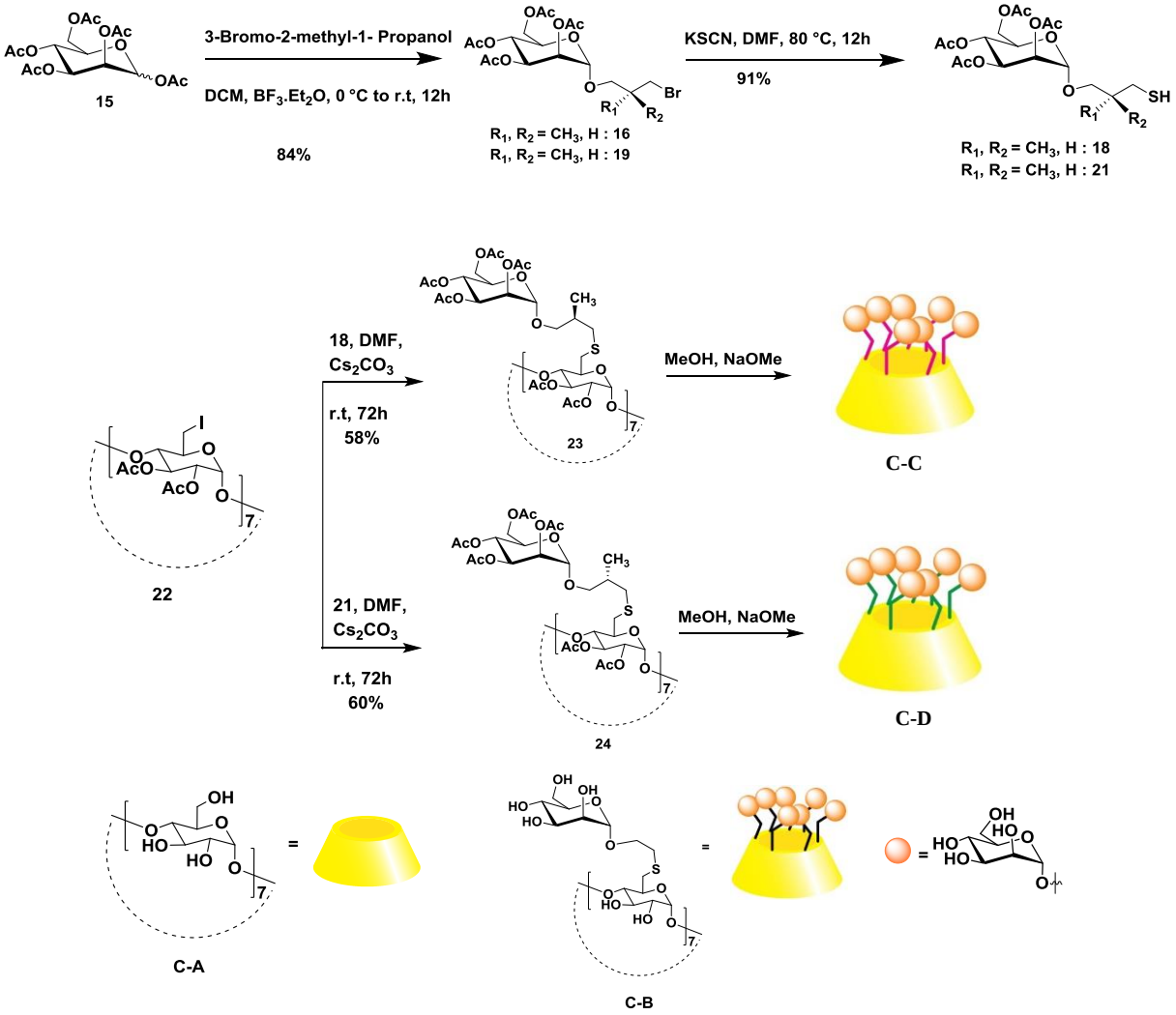

Scheme 4: Synthesis cyclodextrin derivatives.

The synthesis of the Mannose substituted *β*-cyclodextrin **C-C** has started with peracetylated Mannose **15**, followed by treatment of 3-bromo-2-methyl-1-propanol with $BF_3{\cdot}Et_2O$ and thiocyanate to yield the thiocyanate- Mannose derivative **17**. The thiocyanate was reduced by Zn/AcOH to the corresponding thiol **18** and reacted with 6-hepta iodinated *β*-cyclodextrin **22** in the presence of Cs_2CO_3 to yield Mannose-substituted *β*-cyclodextrin, which was finally treated with base yielding compound **C-C** (**Scheme 4**).

Similar synthetic strategy has been used for the synthesis of **C-B** and **C-D**.

2.2.6. Host-Guest formation

Ru(II) complexes (**Ru-1** to **Ru-3**) having a linked adamantyl core were complexed with *β*-cyclodextrin (*β*-CD) derivatives by mixing stoichiometric amounts (1:6) of (**C-A** to **C-D**) to yield a library of metallo-glycodendrimers (**M-1A** to **M-3D**).

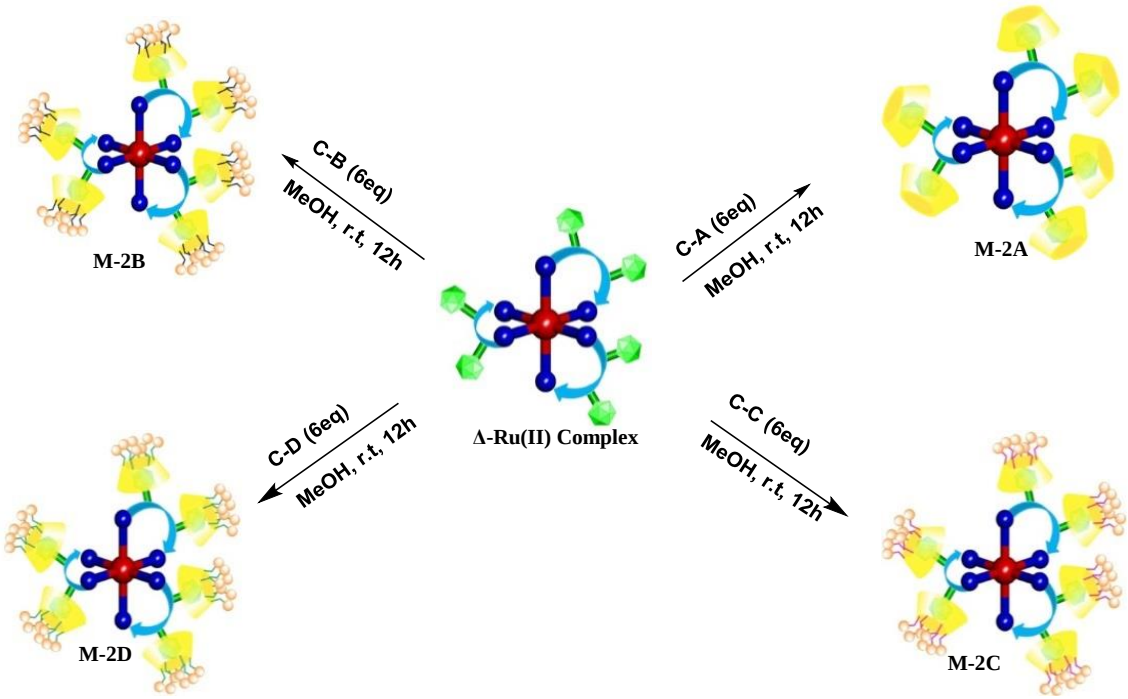

Scheme 5: Synthesis of metallo-glycodendrimers.

The complexes of Ru(II**)** series **1** to **3** were soluble in methanol. After mixing them with stoichiometric amounts of native *β*-CD (**C-A**), cyclodextrin derivatives (**C-B** to **C-D**) were found to be soluble in water.

Series of metallo-glycodendrimers (**M-1A** to **M-3D**) have been synthesised similarly (**Table 1**, **Fig. 5**).

Table 1: Metallo-glycodendrimers from **M-1A** to **M-3D.**

Sr.No	Ru-1	Ru-2	Ru-3
C-A (*β*-CD)	M-1A	M-2A	M-3A
C-B (*β*-CD man)	M-1B	M-2B	M-3B
C-C (*β*-CD man (R))	M-1C	M-2C	M-3C
C-D (*β*-CD man (S))	M-1D	M-2D	M-3D

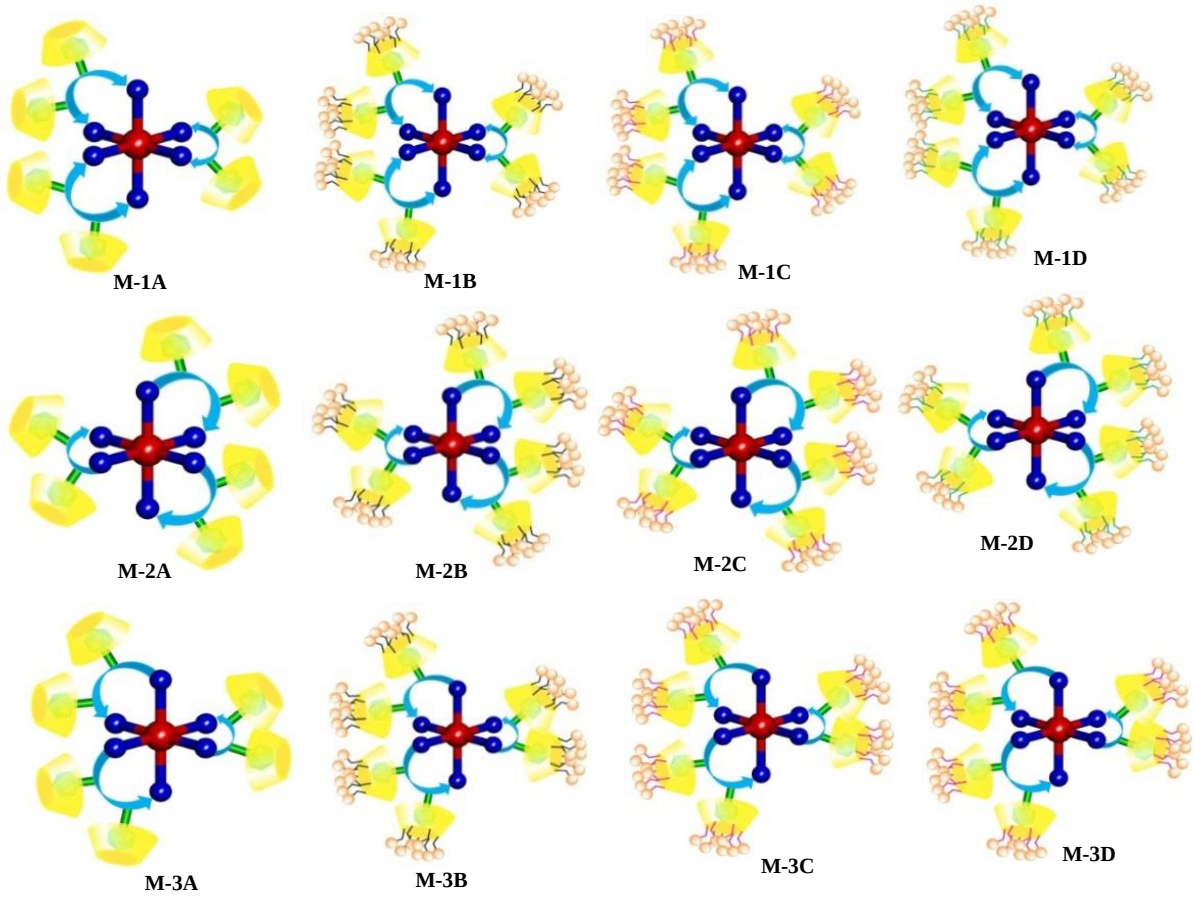

Figure 5: Systamatic representation of metallo-glycodendrimers.

2.2.7. Mass spectrometric analysis of supramolecular complexes

The different complexes were analysed by mass spectrometry to determine their molecular mass[35,41] and the stoichiometry of the host and guest in the supramolecular assemblies. The positive ion mass spectrum of the fully assembled complex clearly indicates the presence of a hexa charged ion [**M-2A**+2Na+2H]$^{6+}$ with m/z = 1485 (**Fig. 6**). Other peaks at m/z 1944 [**Ru-2** with 5(**C-A**) +2Na]$^{4+}$and m/z 1660 [**Ru-2** with 4(**C-A**) + 2Na] $^{4+}$ fully match to penta-

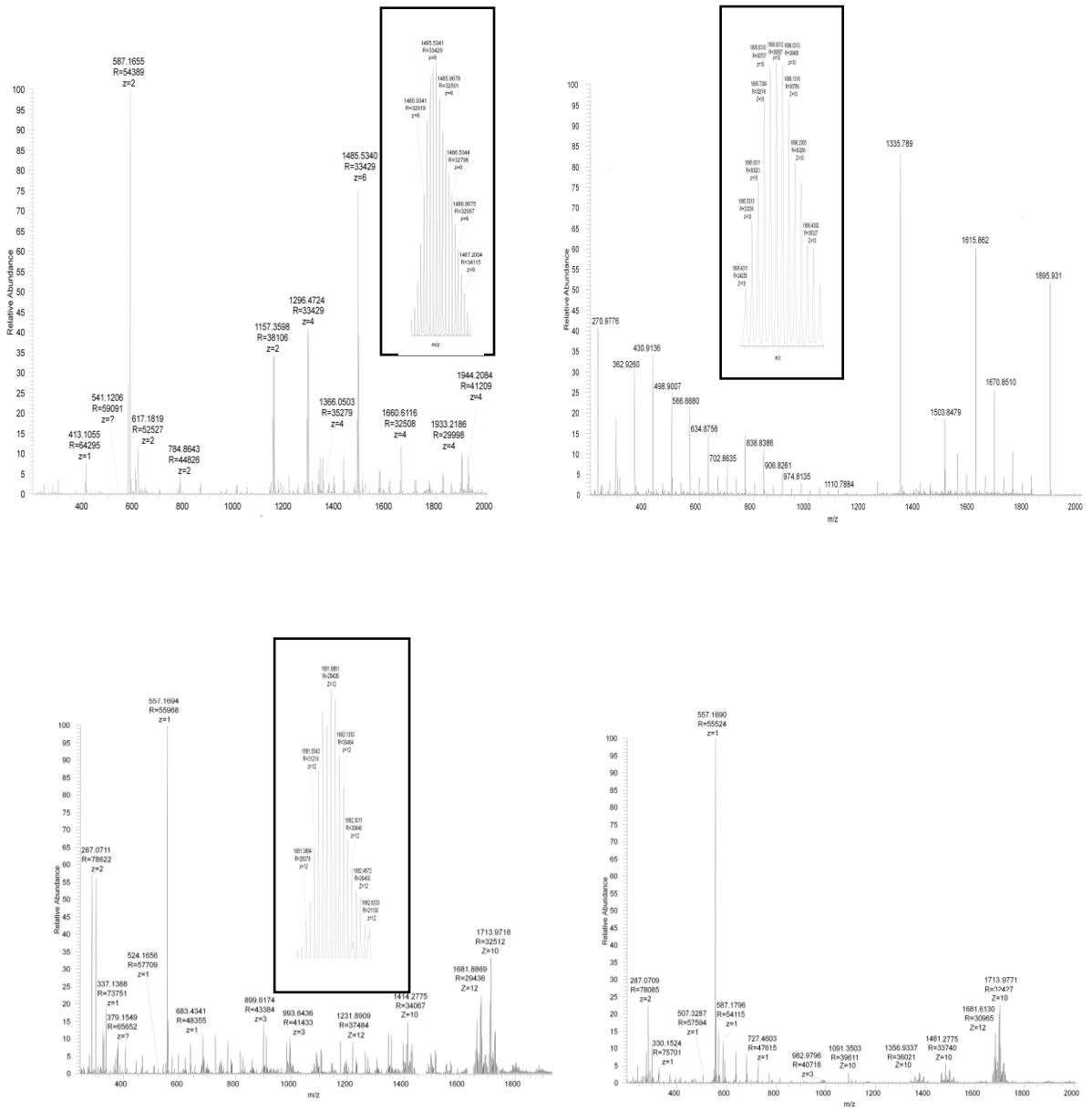

Figure 6: (a) ESI-MS of **M-2A** peaks corresponds to 1485.5340 [**M-2A** + 2Na +2H]$^{6+}$, 1296.4724 [**Ru-2** with 5(**C-1**) + 2Na+2H]$^{6+}$; 1933.2186 [**Ru-2** with 5(**C-1**) + 2H]$^{4+}$; 1944.2086 [**Ru-2** with 5(**C-1**) +2Na]$^{4+}$; 1660.6161 [**Ru-2** with 4(**C-1**) + 2Na] $^{4+}$; 1366.033 [**Ru-2** with 3(**C-1**) + 2H]$^{4+}$; 1377.0237 [**Ru-2** with 3(**C-1**)+2Na]$^{4+}$. **(b)** ESI-MS of **M-2B** peaks corresponds to 1895.931 [**M-2B** + 4Na +4H]$^{10+}$, 1615.8622 [**Ru-2** with 5(**C-2**) +4Na+4H]$^{10+}$; 1335.789 [**Ru-2** with 5(**C-2**) + 4H + 4Na]$^{10+}$. **(c)** ESI-MS of **M-2C** marked peaks corresponds to 1681.8961 [**M-2C** + 6Na +4H]$^{12+}$, 1713.9718 [**Ru-2** with 5(**C-3**) +4Na+4H]$^{10+}$; 1414.2775 [**Ru-2** with 4(**C-3**) + 4H + 4Na]$^{10+}$. **(d)** ESI-MS of **M-2D** marked peak corresponds to 1681.8961 [**M-2D** + 6Na +4H]$^{12+}$, 1713.9718 [**Ru-2** with 5(**C-3**) +4Na+4H]$^{10+}$.

and tetra-substituted complexes. The data for **M-2B** [m/z 1681[**M-2B** + 6Na+ 4H]$^{12+}$ (**Fig. 6**) established the formation of assemblies of **Ru-2** and *β*-CD derivatives via anchoring of the adamantyl moieties in *β*-CD cavities forming host-guest complexes.

2.2.8. NMR study of the supramolecular complexes

To confirm that the host-guest assemblies are anchored by adamantyl and cyclodextrin group, Nuclear Overhauser effect spectroscopy (NOESY) experiments was employed. Cross peaks arising from the proximity of the adamantyl and cyclodextrin groups *via* NOESY analysis of solutions of **M-1A** to **M-3D** in D_2O were observed. The cross peaks indicate strong interactions between H_3 and H_5 of CD with all adamantly protons (H_a, H_b and H_c) throughout

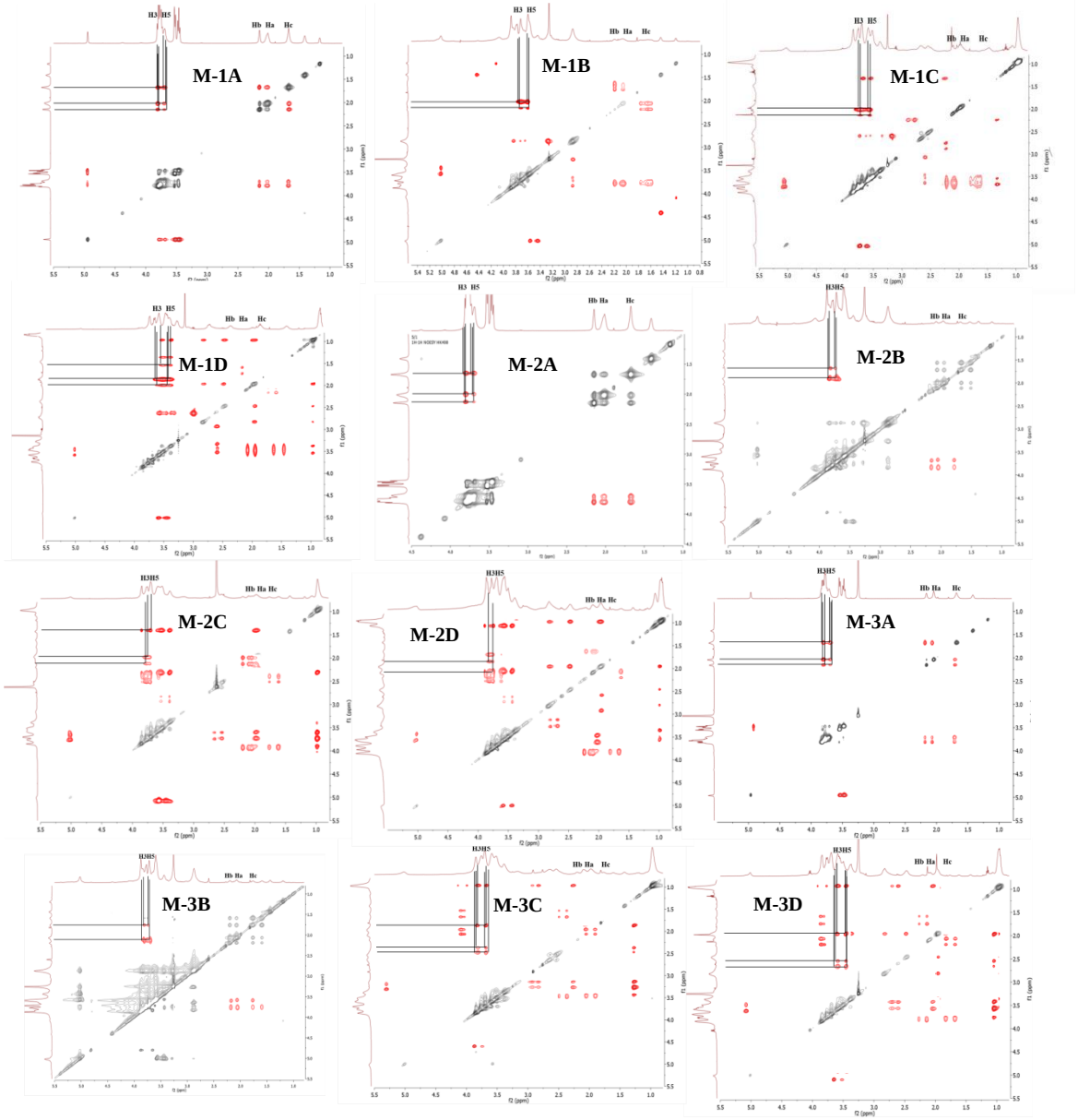

Figure 7: NOESY spectra of metallo-glycodendrimers.

the **M-1A, M-2A** and **M-3A** complexes, confirming that the adamantly group penetrated completely into the CD cores. Whereas H_2 and H_4 of CD are localized outside the CD cavity and do not interact with adamantly group. However, in case of **M-1B** to **M-1D** or **M-2B** to **M-2D** or **M-3B** to **M-3D**, due to the very complex ^{1}H NMR between 4.2 and 3.6 ppm, it was difficult to identify the H_3 and H_5 of **C-B** to **C-D** and assign changes after supramolecular assembly. Instead, we focused our attention on the protons of the adamantyl moiety and observed a strong NOE interaction with protons from the **C-B** to **C-D** region. Overall, the results from the NOESY experiments clearly indicate that the inner cyclodextrin derivatives protons are in close proximity to the adamantyl moieties, confirming the presence of fully assembled complexes in the **M-1A** to **M-3D** complexes (**Fig. 7**).

2.2.9. Circular dichroism spectroscopy of supramolecular complexes

Proof for the structural arrangement of the host-guest complexes in solution was established by the induced circular dichroism (ICD) method,[42,43] which has been extensively used to study the host-guest complexes in solution. Chirality transformation from metal complexes (**Ru-1** to **Ru-3**) to the chiral host *β*-CD derivatives (**C-B** to **C-D**) was established by comparing the Cotton effect.

The CD spectra of **C-B** displayed a strong positive Cotton effect at λ = 222 nm with a cross over at λ = 238 nm, **C-C** and **C-D** exhibited a biphasic CD signal with a positive signal at λ = 222 nm and a negative signal at λ = 240 and 248 nm, respectively (**Fig. 8a**).

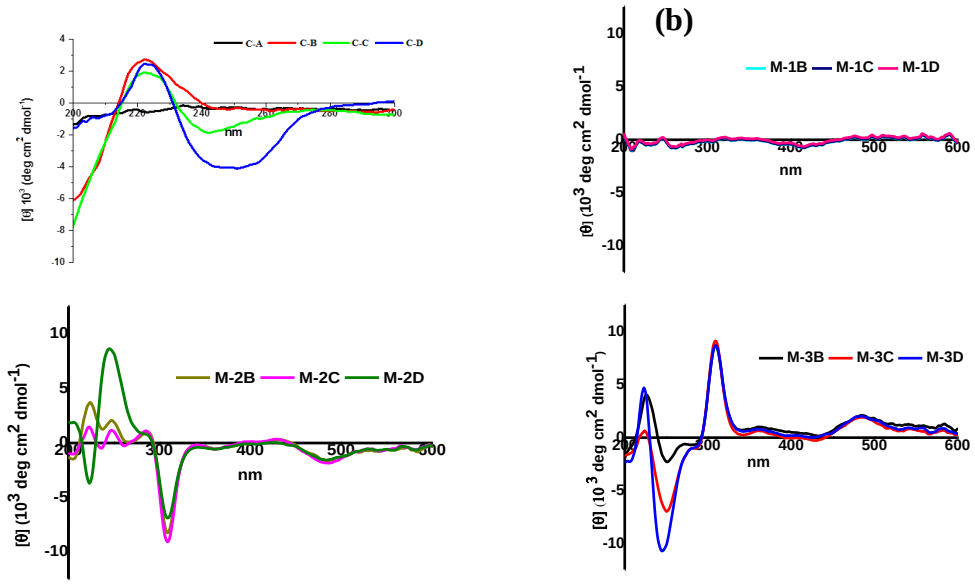

Figure 8: Circular dichroism spectra. **(a) C-A** to **C-D; (b) M-1B** to **M-1D**; **(c) M-2B** to **M-2D**; **(d) M-3B** to **M-3D**.

We also compared the CD spectra of the different host-guest complexes. Interestingly, we found that the CD profile of **M-1B**, **M-1C** and **M-1D** displayed a similar Cotton effect as observed in the case of *β*-CD derivatives (**Fig. 8b**), which indicates that the racemic **Ru-1** complex has no impact on the chirality. In contrast, the CD profiles of **M-2B** to **M-2D** exhibited an identical negative Cotton effect at MLCT and LC region (λ = 300-600 nm) and strong response of a positive Cotton effect at λ = 200-260 nm (positive signal λ = 222 nm and a negative signal at λ ~ 250 nm), indicating that the Δ-form of **Ru-2** has a strong impact on positive chirality around sugar region (**Fig. 8c**). Complexes **M-3B**, **M-3C** and **M-3D** displayed a strong negative Cotton effect in the region 200-260 nm (**Fig. 8d**), indicating that Λ- and Δ-forms of the Ru(II) complexes transfer its chirality to the *β*-CD derivatives *via* host-guest interactions.

2.2.10. DFT calculations of Ru(II) complexes

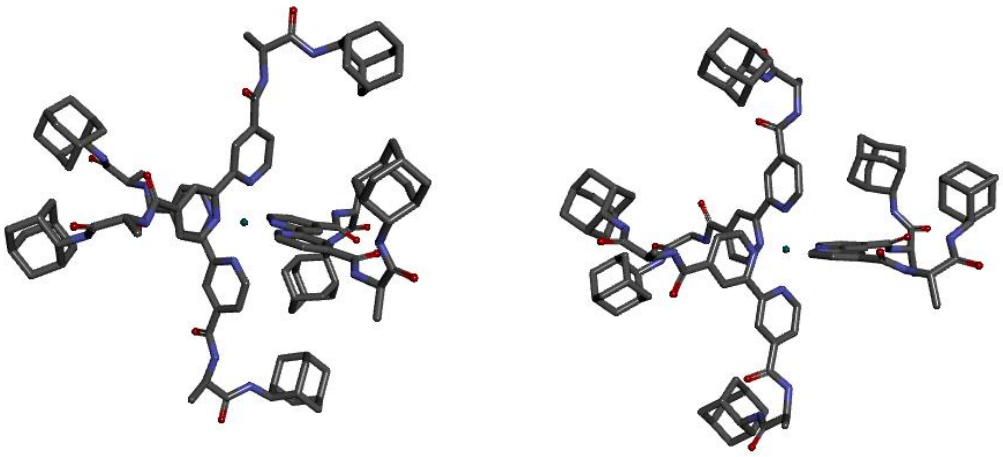

Figure 10: DFT minimum energy structures of the complexes. Optimized structure of Delta **(a)** & Lambda **(b)** Ru(II) complexes. The blue, red, grey and greenish violet spheres represent N, O, C, and Ru atoms respectively. All the Ru-N bond lengths are equidistant with 2.09 Å.

The DFT calculations of **Ru-2** and **Ru-3** displayed quite opposite adamantyl orientation (**Fig. 10**) resulting in two distinct chiralities through host-guest interactions.

2.2.11. Uv-visible and fluorescence spectra of MGDs

The molar absorption coefficient ε is measured at MLCT band, where the metal complexes displayed maximum absorption of light.

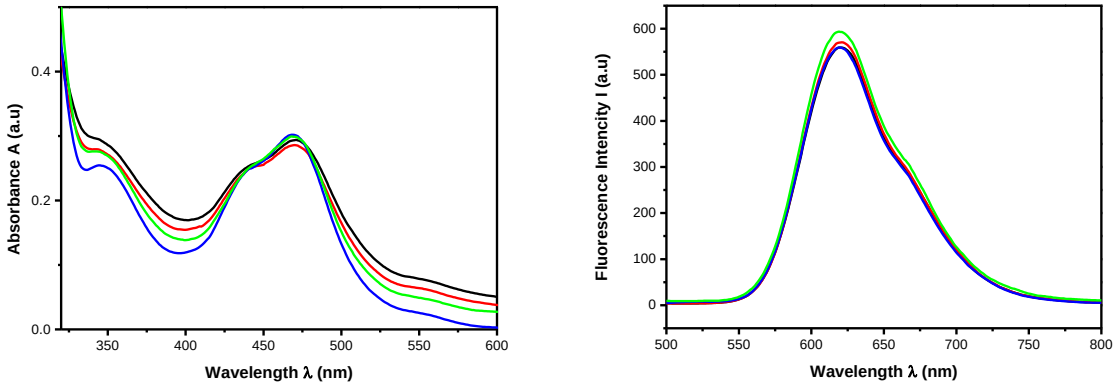

Figure 11: (a) Uv-visible and **(b)** fluorescence spectra of MGDs.

Table 2: Photophysical data of ruthenium complexes in methanol (**Ru-1** to **Ru-3**), **MGDs** in water.

Complex name	λ^{abs}_{max} [nm]	$\varepsilon^{abs}_{\lambda max}$[L.M^{-1}.cm^{-1}]	λ^{em}_{max} [nm]	Φ
Ru-1	461	6231	632	0.38
Ru-2	461	6346	635	0.41
Ru-3	462	6511	635	0.38
M-3A	469.7	181	620.5	0.71
M-3B	470.6	175	620.0	0.7
M-3C	468.9	187	620.4	0.72
M-3D	469.2	181	618.8	0.68

The relative fluorescence quantum yields were determined by measuring the fluorescence of a reference chromophore (in this case, Rhodamine) with known quantum yield and the quantum yield was calculated by below equation.

$$\Phi = \Phi_{ref} \times \frac{c[mol \cdot L^{-1}]}{c_{ref}[mol \cdot L^{-1}]} \times \frac{S_{ref}}{S}$$

Where ϕ_{ref} = 0.31, Table 2 illustrate that the host-guest complexation increase the quantum yield of the complexes by encapsulating the Ru(II) core.

2.2.12. ITC profile of MGDs

In order to gain an insight into the binding affinity, thermodynamics and stoichiometry of the **M-2A** and **M-2B**, we performed isothermal calorimetry (ITC) (**Fig. 12**).

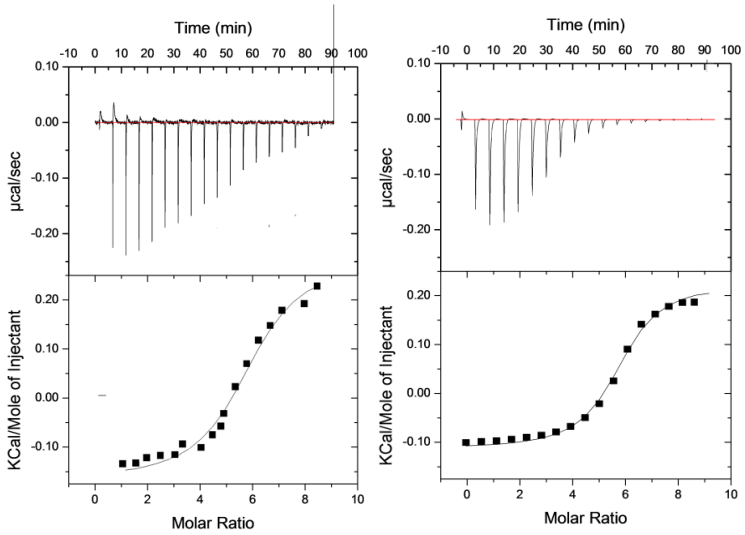

Figure 12: ITC profile for **Ru-2** in the presence of **C-A (a)** and **C-B (b)** at 298 K in DMSO. The top panels represent the energy (µcal/s) enquired to maintain isothermal conditions with respect to the reference cells and the lower panels represent the heat evolved from each injection per mole of metal ions versus the molar ratio of conc. of **Ru-2** = 0.001 mM in water and **C-A** and **C-B** solution = 2.5 mM in water.

Table 3: Thermodynamic parameters measured with isothermal titration calorimetry.

MGDs	n	Binding constant (M^{-1})	ΔH (Kcal/mol)	ΔS (cal/mol/deg)
M-2A	0.18	$3.64X\ 10^4$	-1.04± 0.12	$-3.12\ X\ 10^3$
M-2B	0.17	$2.12\ X\ 10^4$	-2.01 ± 0.42	$-4.33\ X\ 10^3$

2.2.13. SEM Images of MGDs

Finally, morphology of the MGDs was established by SEM images of the complexes. As seen in SEM images, the self-assembly of MGDs resulted in globular morphology with slight difference in their sizes (**Fig. 13**).

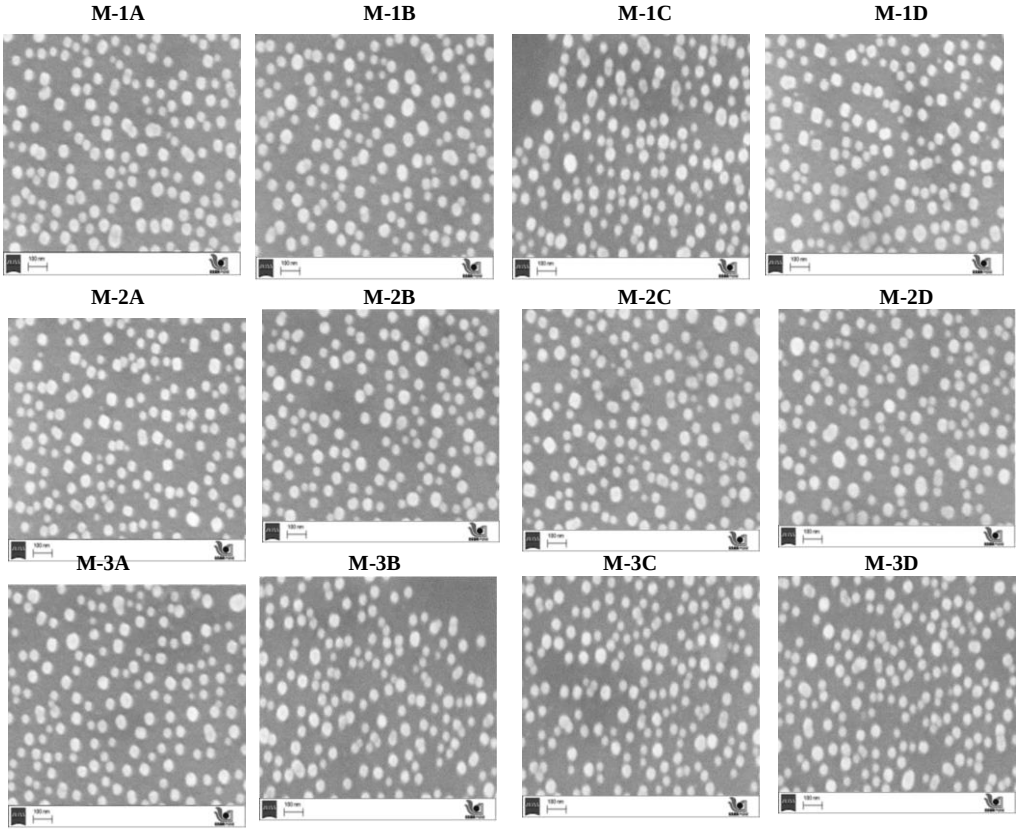

Figure 13: SEM images of MGDs.

Table 4: Sizes of the MGDs quantified by SEM images.

MGDs	Diameter[nm]
M-1A	55 ± 12
M-1B	59 ± 9
M-1C	59 ± 9
M-1D	61 ± 12
M-2A	57 ± 8
M-2B	61 ± 12
M-2C	58 ± 11
M-2D	58 ± 9
M-3A	57 ± 11
M-3B	59± 14
M-3C	59 ± 11
M-3D	62 ± 9

In summary, the homologous MGDs showed similar topology but differed in their chiral microenvironments, which is expected to have a major impact on carbohydrate-mediated interactions.

2.2.14. Binding affinity to C-type lectin receptor-Fc fusion proteins

To address the biological relevance of MGDs, their binding affinity to mannose-specific C-type lectin receptor (CLR)-Fc fusion proteins (h-DC-SIGN-Fc, m-SIGNR3-Fc), Dectin-1-Fc and plant lectins (ConA and PNA)[44-46] was examined.

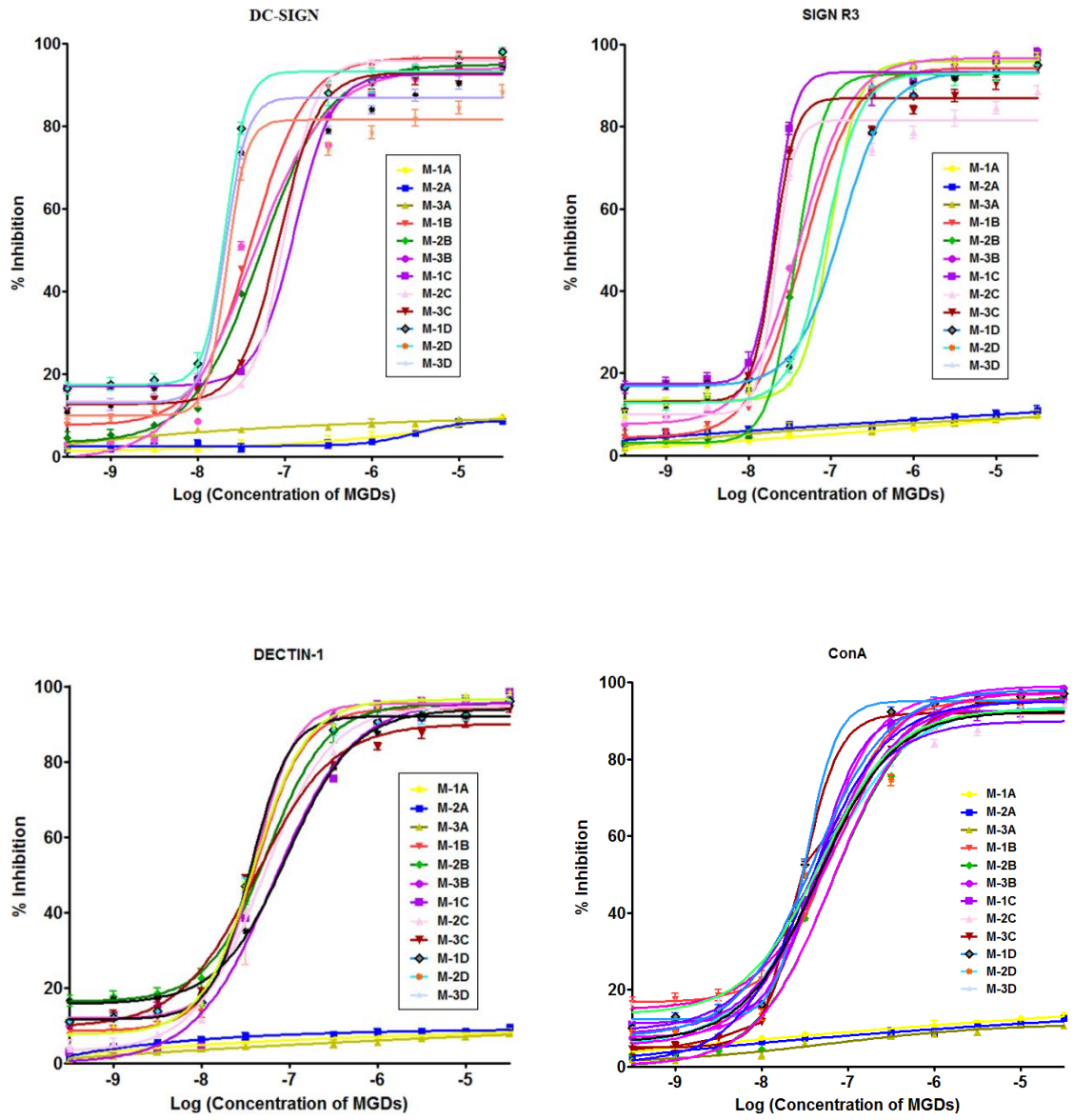

Figure 16a: The binding affinity between MGDs and C-type lectins and ConA. Data represents mean ± SD, n = 3.

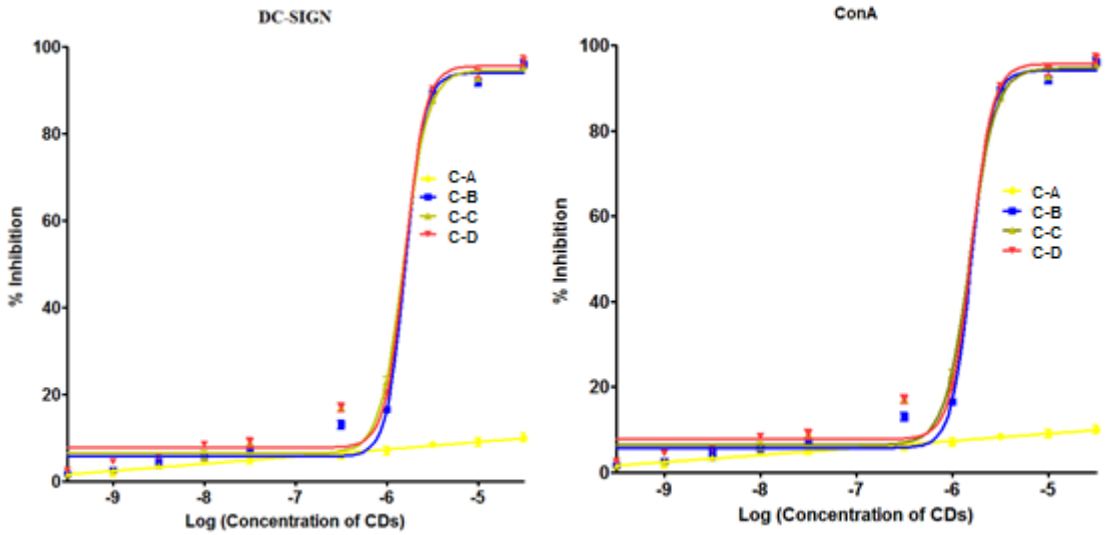

Figure 16b: The binding affinity between cyclodextrin derlivatives and C-type lectins and ConA. Data represents mean ± SD, n = 3.

To this end, CLR-Fc fusion proteins were used in which the extracellular part of the respective CLR containing the carbohydrate recognition domain was fused to the Fc fragment of human IgG_1 molecules leading to dimeric presentation of the lectins.[47] CLR-Fc fusion proteins have proven useful to identify carbohydrate ligands of CLRs and to analyze receptor/ligand interactions in numerous studies.[48-50] We performed inhibition studies for the binding of these lectins to mannose-BSA in the presence of MGDs and quantitative binding avidity was measured as IC_{50} value. As expected, all mannose-MGDs exhibited strong inhibition compared to *β*-CD capped MGDs (**M-1A**, **M-2A** and **M-3A**) and *β*-CD derivatives (**C-A** to **C-D**) (**Fig. 16a & 16b**).

Among the mannose-MGDs, we observed two distinct types of binding affinity. DC-SIGN-Fc and SIGNR3-Fc showed a unique binding pattern, where Δ-mannose MGD (**M-2B** to **M-2D**) showed nearly 4-5 fold strong inhibition effect compared to Λ-MGD (**M-3B** to **M-3D**). In contrast, ConA and Dectin-1-Fc showed approximately 1.5 fold binding difference between Δ & Λ-complexes and nearly 10-fold difference compared to DC-SIGN-Fc (**Table.5 & Fig. 16a**) and no binding to PNA lectin. The probable reason for the highest binding avidity may be attributed to the preferred specific spatial arrangement of MGDs, which triggered high binding affinity.[51] The clear distinction in the binding pattern between DC-SIGN and other mannose binding proteins confirms that DC-SIGN has a broader specificity compared to ConA or Dectin-1 lectins.[52-54] Furthermore, the disparity in the inherent chirality (Δ vs Λ) of

the complexes resulted in the opposite chiral micro-environment with distinct spatial arrangement of the MGDs to fine tune the lectin sensitivity.

Table 5: Binding affinity of the compounds to h-DC-SIGN-Fc, m-SIGNR3-Fc and m-Dectin-1-Fc. Data represents mean ± SD, n = 3. **M1A**, **M-2A** and **M-3A** displayed out of range binding affinity.

Comp	DC-SIGN ($X 10^{-7}$)	SIGN R3 ($X 10^{-7}$)	DECTIN-1 ($X 10^{-6}$)	ConA ($X 10^{-6}$)	PNA
M-1B	0.41 ± 0.02	0.45± 0.01	0.42± 0.01	0.69± 0.06	-
M-2B	0.2± 0.03	0.21± 0.03	0.65± 0.02	0.65± 0.01	-
M-3B	1.3± 0.08	1.4± 0.03	0.66± 0.02	0.51± 0.02	-
M-1C	0.47± 0.01	0.37± 0.05	0.55± 0.03	0.52± 0.04	-
M-2C	0.21± 0.03	0.25± 0.01	0.48± 0.05	0.39± 0.03	-
M-3C	1.01± 0.01	0.9± 0.06	0.48± 0.04	0.36± 0.03	-
M-1D	0.39± 0.01	0.42± 0.02	0.42± 0.06	0.39± 0.08	-
M-2D	0.24± 0.04	0.22± 0.06	0.41± 0.01	0.45± 0.07	-
M-3D	0.86± 0.01	0.99± 0.02	0.41± 0.03	0.48± 0.03	-

2.2.15. STD NMR of MGDs

Finally, to confirm the selectivity and sensitivity of the binding, we performed ^{1}H-STD NMR[55] of DC-SIGN-Fc and Dectin-1-Fc with **M-2C** complexes. STD effects confirmed that the main contact areas of MGDs to lectins are protons from mannose and methyl group of the linker respectively. The comparison of STD-NMR at different saturation time clearly showed that **M-2C** showed significant binding affinity to DC-SIGN-Fc compared to **M-1C** and **M-3C**. This clearly illustrates that the spatial arrangement due to inherent chirality indeed markedly influenced the binding affinity (**Fig. 17 & 18**).

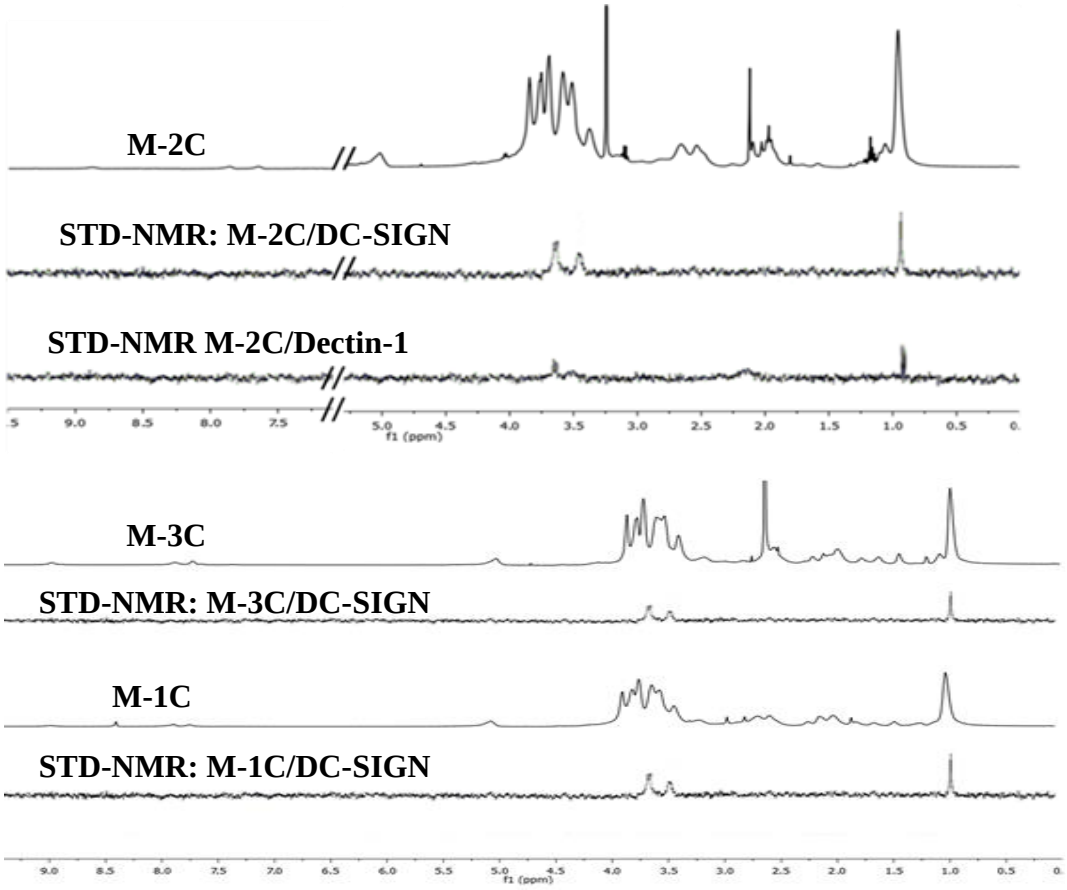

Figure 17: STD-NMRs of **M-2C** in the presence of DC-SIGN and Dectin-1; (b) STD-NMR of **M-3C** and **M-1C** in the presence of DC-SIGN.

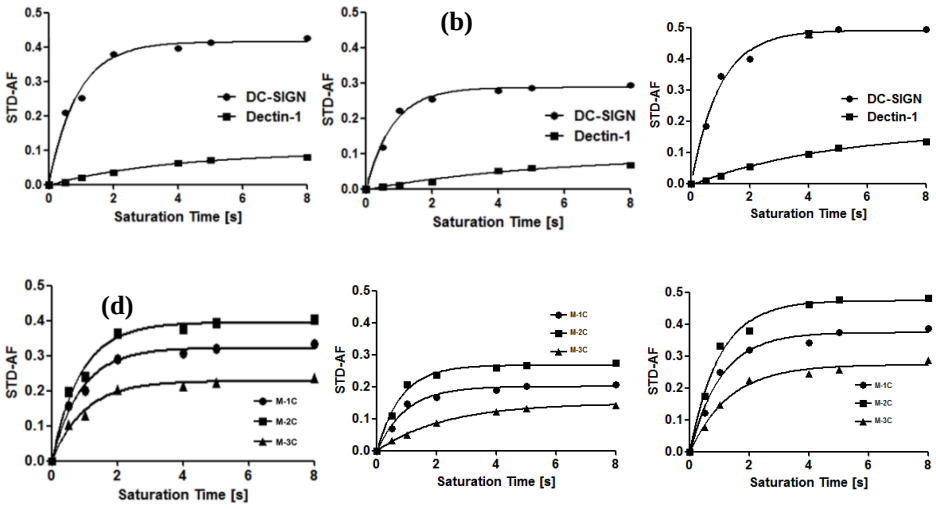

Figure 18: STD-amplification factor of (a) **M-2C** at proton peak at 3.68 ppm; (b) 3.53 ppm; (c) 0.98 ppm in the presence of DC-SIGN and Dectin-1; STD-amplification factor of **M-1C**, **M-2C** and **M-3C** at (d) 3.68 ppm; (e) 3.53 ppm; (f) 0.98 ppm in the presence of DC-SIGN.

2.2.16. Cell viability assay of MGDs

As an initial screen, the toxicity of host-guest complexes in HeLa and NIH-3T3 cells (**Fig. 19**) were evaluated. The rationale for choosing these cell lines was based on the fact that HeLa cells express mannose receptors. The concentration-dependent toxicity assay in both cells showed that up to 15 µM concentrations of the complexes could be used without significant toxicity.

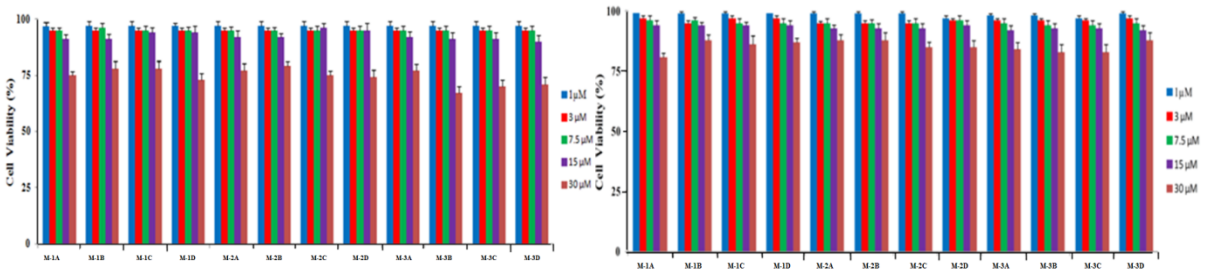

Figure 19: MTT assay of metallo-glycodendrimers (**M-1A** to **M-3D**) in HeLa **(a)** and NIH-3T3 **(b)** after 24 h.

Hence, 15 µM concentration of the MGDs was fixed for the following in vitro studies.

2.2.17. Confocal laser scanning microscopy (CLSM) studies

The cellular internalization of MGDs was investigated by treating the complexes with DC-SIGN transfected HeLa and SIGNR3-CHO cell lines respectively, while knockdown HeLa and CHO-K1 cells were used as negative control (**Fig. 22 & 25**).

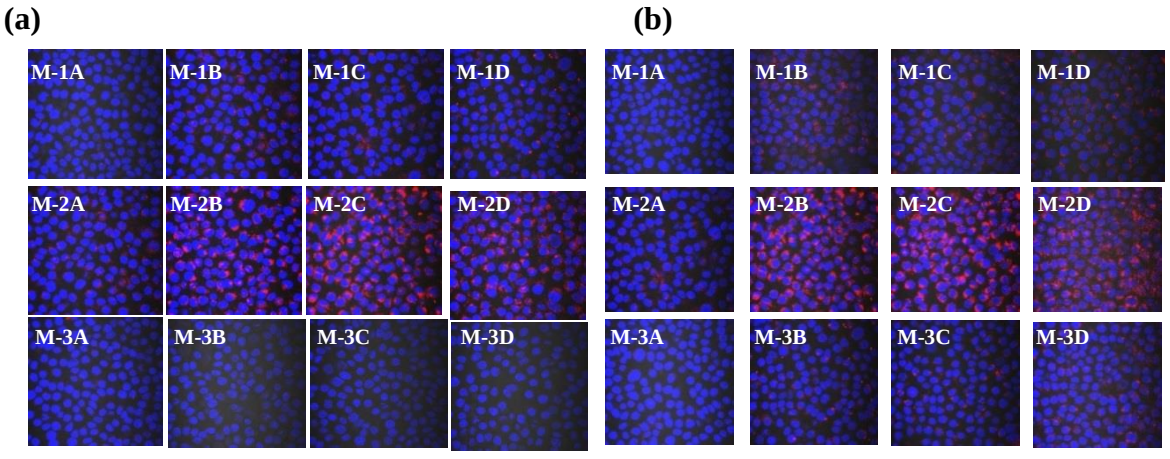

Figure 21: Confocal laser scanning microscopy images of metallo-glycodendrimers internalization into DC-SIGN-transfected HeLa cells after 6 h **(a)**, 24h **(b)**. Nucleus compartment was stained with Hoechst 33342 (blue). Scale bar = 30µm.

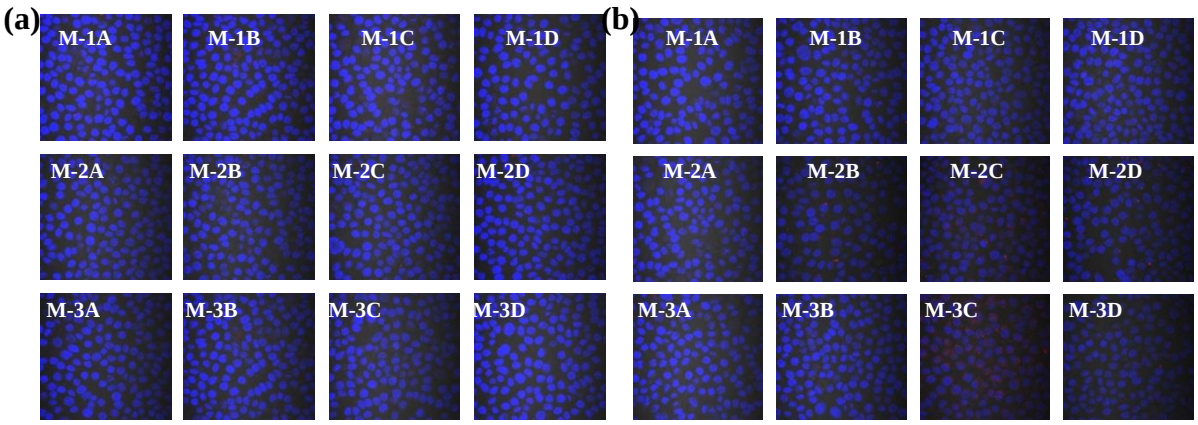

Figure 22: Confocal laser scanning microscopy images of metallo-glycodendrimers internalization into DC-SIGN-knockdown HeLa cells after 6 h **(a)**, 24h **(b)**. Nucleus compartment was stained with Hoechst 33342 (blue). Scale bar = 30µm.

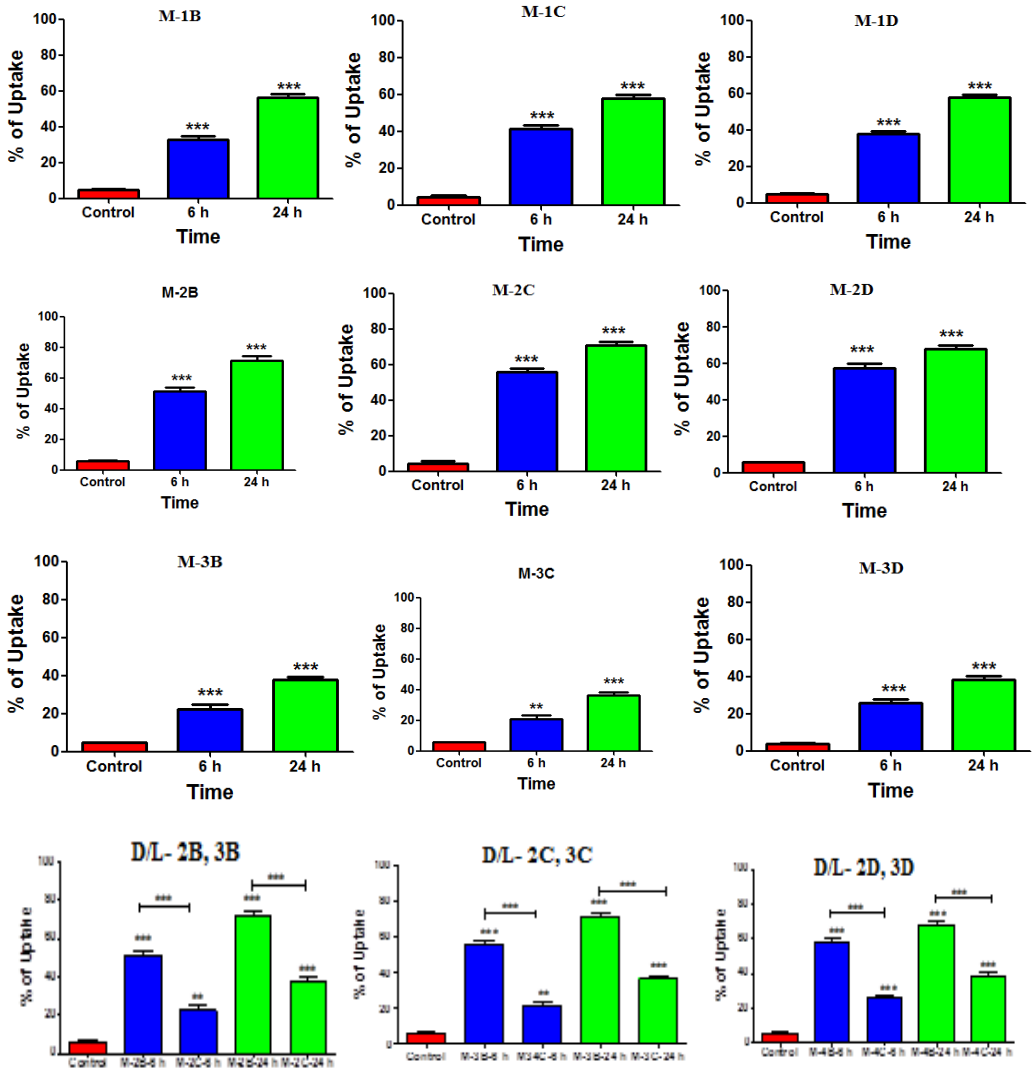

Figure 23: Statistical analysis of FACS data. Data are presented as mean ± SD for three independent experiments (***P<0.001, **P<0.01 *P<0.05 and n.s = not significant).

The optical properties of MGDs were used to analyze the internalization process. As expected, all mannose coated MGDs entered DC-SIGN-HeLa and SIGNR3-CHO cells (**Fig. 21 & 24**). However, the intrinsic chirality of the complexes generated a different rate of uptake. Remarkably, Δ -complexes (**M-2B**, **M-2C** & **M-2D**) showed disparity in uptake efficiency as compared to Λ-complexes (**M-3B**, **M-3C** & **M-3D**) and also with racemic complexes (**M-1B, M-1C** & **M-1D**). The uptake efficiency of Δ-complexes was nearly 2-fold higher after 6 h compared to other MGDs. This trend continued even after 24 h incubation, indicating that a small difference in chirality-mediated spatial arrangement had a major impact on cell uptake. Similarly, SIGNR3-CHO cells also exhibited disparity in chirality-mediated uptake.

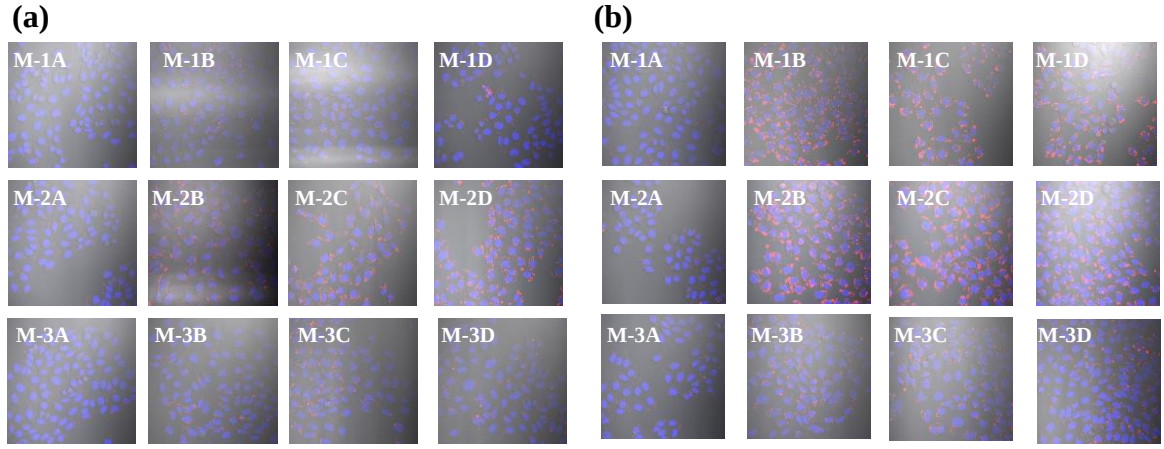

Figure 24: Confocal laser scanning microscopy images of metallo-glycodendrimers internalization into SIGNR3-transfected-CHO cells after 6 h **(a)**, 24h **(b)**. Nucleus compartment was stained with Hoechst 33342 (blue). Scale bar = 30µm.

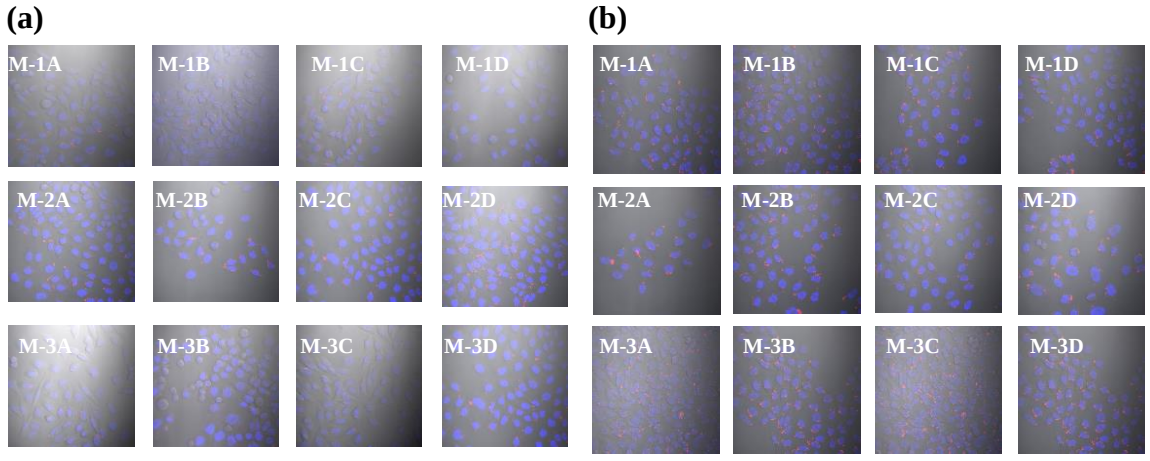

Figure 25: Confocal laser scanning microscopy images of metallo-glycodendrimers internalization into CHO-K1 cells after 6 h **(a)**, 24h **(b).** Nucleus compartment was stained with Hoechst 33342 (blue). Scale bar= 30µm.

2.2.18. FACS Analysis

To uncover the rate of uptake of different MGDs, flow cytometric analysis was carried out after 6 h and 24 h respectively (**Fig. 26**). After 6 h, DC-SIGN-HeLa cells displayed 52-58% uptake of **M-2B** to **M-2D** compared to 36-41% uptake of **M-1B** to **M-1D** and 21-26% uptake of **M-3B** to **M-3D**. A similar trend was observed after 24 h of incubation revealing the role of inherent chirality in carbohydrate-mediated uptake (**Fig. 26**).

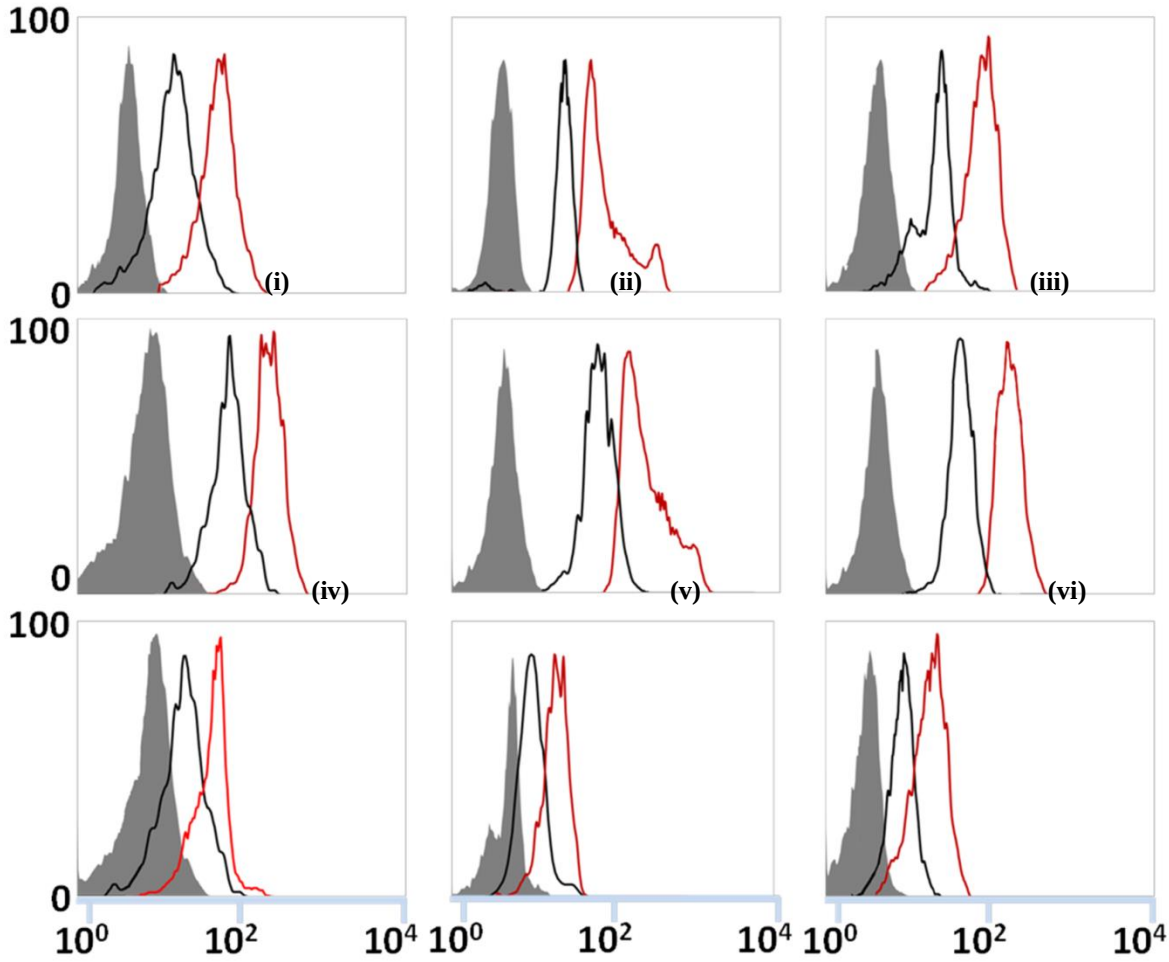

Figure 26: Flow cytometry analysis of DC-SIGN-HeLa cell uptake of different MGDs after 6 h and 24 h respectively: (i) **M-1B**: 6 h (36 % uptake) and 24 h (57 % uptake); (ii) **M-1C**: 6 h (41% uptake) and 24 h (58% uptake); (iii) **M-1D**: 6 h (38% uptake) and 24 h (58% uptake); (iv) **M-2B**: 6 h (52% uptake) and 24 h (72% uptake); (v) **M-2C**: 6 h (56% uptake) and 24 h (71% uptake); (vi) **M-2D**: 6 h (58% uptake) and 24 h (68% uptake); (vii) **M-3B**: 6 h (22% uptake) and 24 h (37% uptake); (viii) **M-3C**: 6 h (21% uptake) and 24 h (36% uptake); (ix) **M-3D**: 6 h (26% uptake) and 24 h (38% uptake); (shaded region) cells without MGDs, (black line region) cell treated with MGDs for 6 h and (red line region) cells with MGDs for 24 h.

2.2.19. Co-localization

The co-localization experiments of these complexes showed that they sequestered in both endoplasmic reticulum (ER) and mitochondrial region (**Fig. 27**).

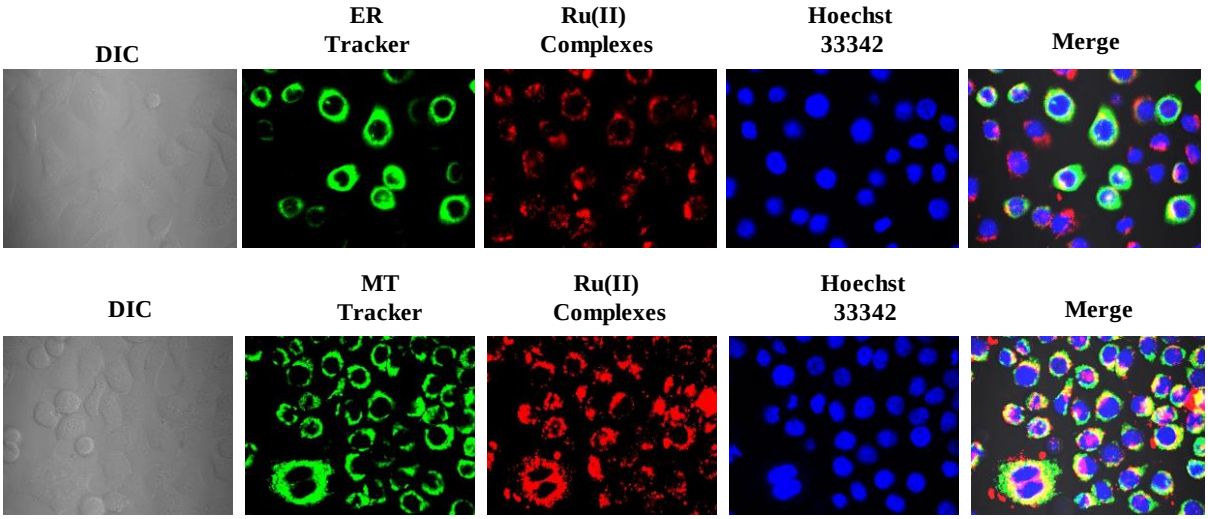

Figure 27: Confocal laser scanning microscopy images of metallo-glycodendrimer (**M-2C**) colocalization in DC-SIGN-HeLa cells in presence of ER and MT trackers. Nucleus compartment was stained with Hoechst 33342 (blue). Scale bar = 30µm.

2.2.20. Pathway blocking study of MGDs

To analyze the mechanism of endocytosis, we first evaluated its energy-dependent pathway. To this end, we incubated the DC-SIGN-HeLa cells with NaN_3 for 30 mins to deplete ATP, followed by treatment with **M-2C** for 6 h. We observed a strong decrease in cellular uptake of MGDs, confirming that active endocytic pathway plays an important role in the uptake. To analyze the contribution of dynamin-dependent uptake, dynasore hydrate was added. Blockade of dynamin function inhibited the internalization of **M-2C**, indicating that the internalization followed the conventional route of clathrin or caveolae dependent pathway.[56] As a next step, we studied the effect of methyl-*β*-cyclodextrin (m-*β*-CD, inhibitor of caveolae-mediated endocytosis), chlorpromazine and sucrose (inhibitor of clathrin-mediated endocytosis). As shown in figure 4, cells that were pre-treated with clathrin inhibitor showed a considerable reduction in internalization, whereas m-*β*-CD pre-treatment of cells exhibited a minor inhibition effect. These findings indicate that **M-2C** was internalized *via* energy-dependent, clathrin pathway (**Fig. 28**). The uptake of **M-2C** in SIGNR3-CHO cells followed the same endocytic pathway (**Fig. 29**).

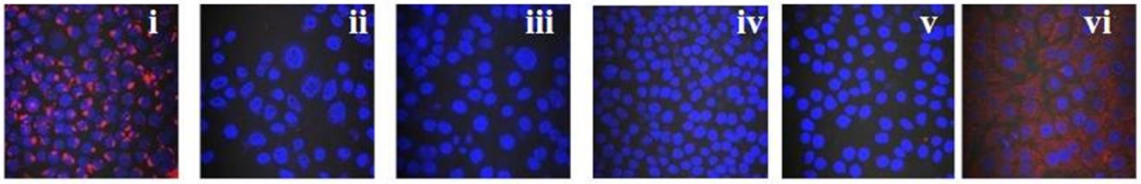

Figure 28: Confocal microscopy images of HeLa cells in presence of different endocytic pathway inhibitors: (i) M-2C; (ii) NaN_3; (iii) Dynasore Hydrate; (iv) Chlorpromazine; (v) Sucrose; (vi) m-β-CD (n=3).

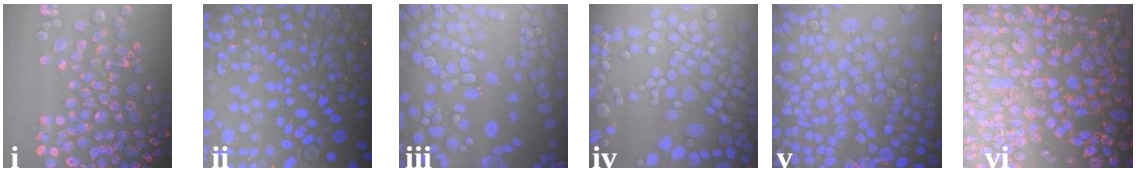

Figure 29: Confocal laser scanning microscopy images of SIGNR3-CHO cells in presence of different endocytic pathway inhibitors: (i) M-2C; (ii) NaN_3; (iii) Dynasore Hydrate; (iv) Chlorpromazine; (v) Sucrose; (vi) m-β-CD (n=3).

2.2.21. *In vivo* liver bio-distribution and sequestration of metallo-glycodendrimers

Based on the *in vitro* screening experiments, we examined the characteristics of mannose coated metallo-glycodendrimers and their racemic counterparts regarding toxicity, plasma clearance and specific sequestration in wild-type mice. Determination of body weight is a useful method for studying the toxicity effect of the MGDs. Hence, MGDs (**M-1C**, **M-2C** and **M-3C** 50 µM) were injected i.v into mice and the fluctuation in body weight was monitored over a period of 50 days. Body weight of the control and MGDs injected mice were approximately identical, illustrating that the MGDs had no side effect on body weight (**Fig. 30a**). Further, serological tests of liver function by measuring the alanine aminotransferase (ALT) and aspartate aminotransferase (AST) levels at different time intervals also revealed similar results in treated mice and control mice suggesting no significant toxicity of MGDs (**Fig. 30b**). Finally, plasma clearance and sequestration of MGDs were quantified by measuring the Ru(II) concentration by ICP-MS (**Fig. 32**), followed by analyzing the bio distribution of MGDs at different time intervals in liver, kidney, heart, brain and spleen (**Fig. 31**). Once again, Δ-complexes were more active than Λ-complexes and sequestered in liver (**Fig 31 & Fig 33**).[57] Overall, our study shows that the

development of chiral MGDs represents an important step forward in tuning the spatial arrangement of carbohydrates for specific lectin targeting as demonstrated here for selected lectins and CLR-Fc fusion proteins.

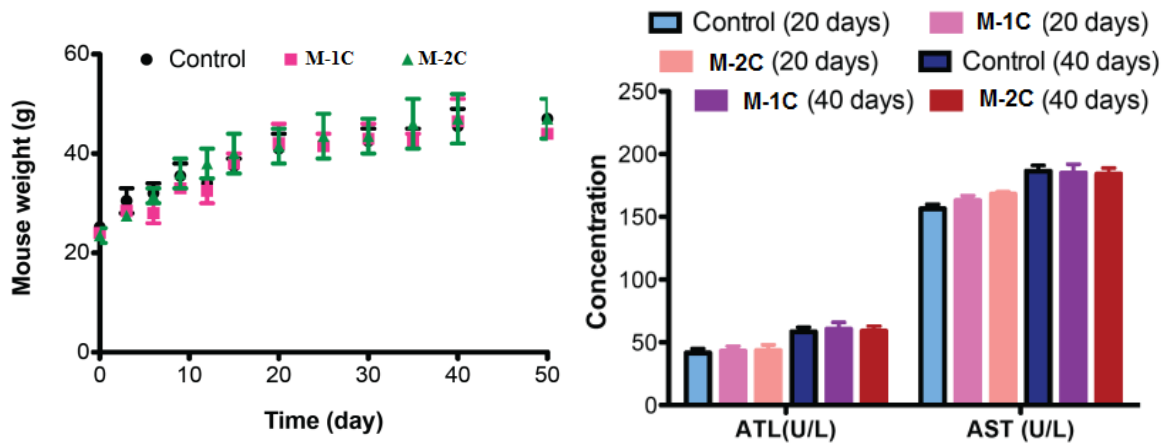

Figure 30: (a) Change in the body-weight of the mice injected with the MGDs. Data represents mean ± SD, n = 3. **(b)** Serological test results obtained from mice injected with MGDs for 20 and 40 days.

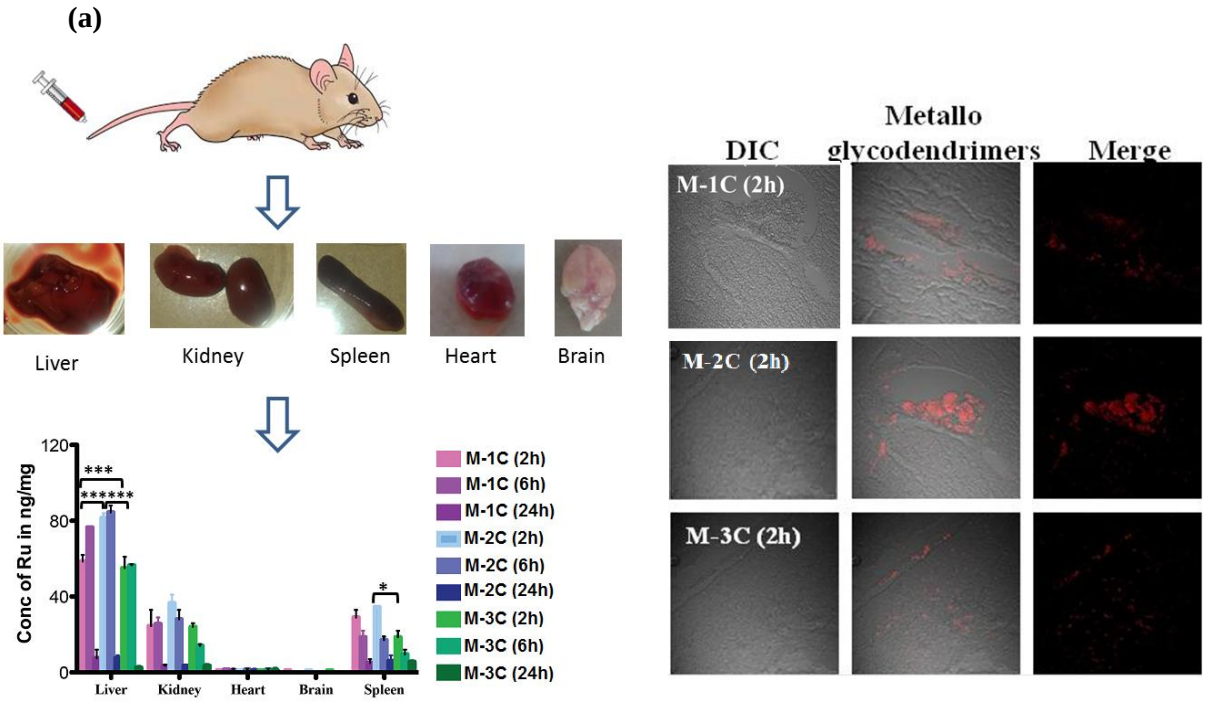

Figure 31: (a) Bio distribution of MGDs in mouse model; The amount of Ru metal per mg of the tissue was determined by ICP-MS. Data are presented as mean ± SD for each group (***P<0.001, *P<0.05); **(b)** Paraffin sections of the liver after Ru(II) complex sequestration as visualized by confocal microscopy (n=3).

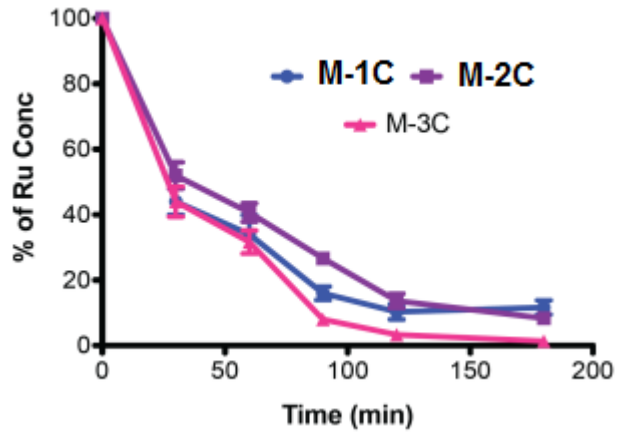

Figure 32: Blood clearance profile of MGDs after i. v injection in mice at different time intervals. Data represent mean ± SD, n = 3.

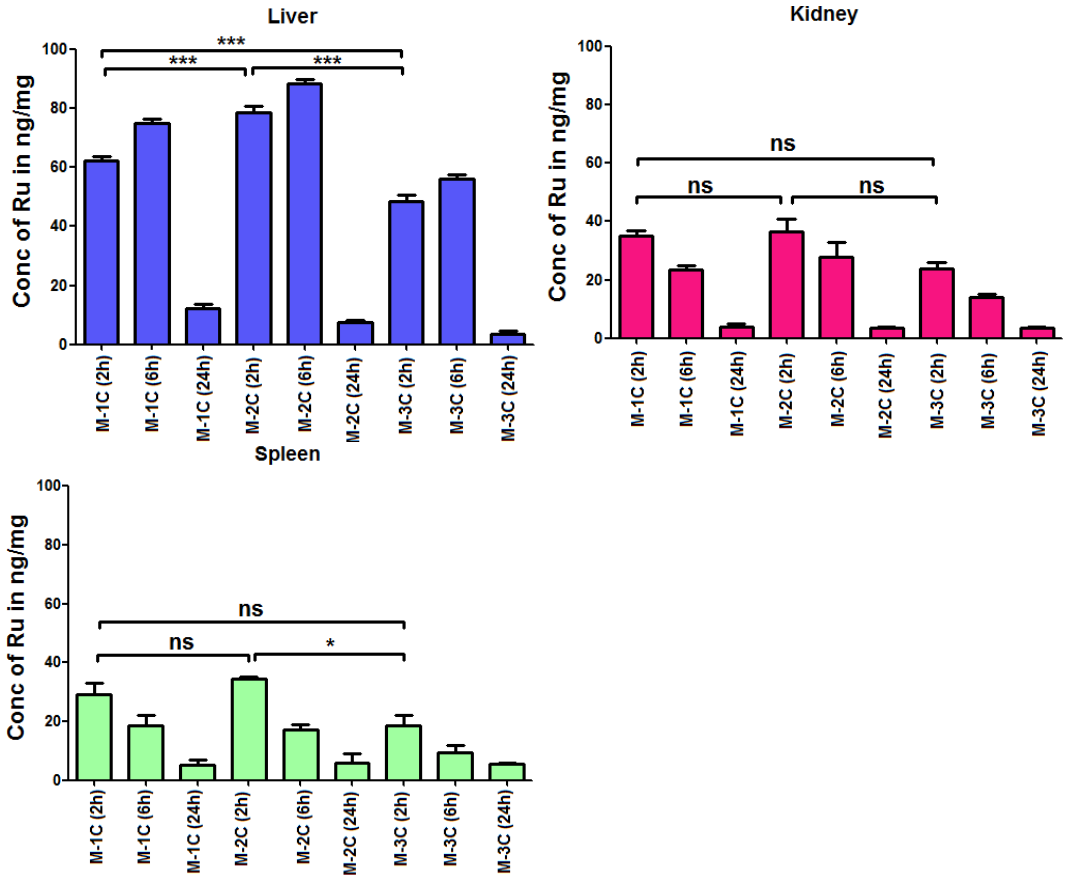

Figure 33: Biodistribution of MGDs in mouse model; The amount of Ru metal per mg of the tissue was determined by ICP-MS. Data are presented as mean ± SD for each group (***P<0.001, *P<0.05).

2.3. Conclusion

In conclusion, a library of Ru(II) complexes attached to glycodendrimers *via* chiral linkers were prepared and their binding to selected lectins and C-type lectin receptor-Fc fusion proteins, cell penetration and *in vivo* bio-distribution were studied. The interrelationship between carbohydrate-protein interactions and the spatial arrangement of carbohydrates generated by multiple chiral centers in a glycodendrimer were examined. Our results highlight that small changes in chirality of the compounds had a major impact on selected CPIs.

2.4. Experimental part

General Information

All chemicals were reagent grade and used as supplied except where noted. Analytical thin layer chromatography (TLC) was performed on Merck silica gel 60 F254 plates (0.25 mmol). Compounds were visualized by UV irradiation or dipping the plate in CAM/ninhydrin solution followed by heating. Column chromatography was carried out using force flow of the indicated solvent on Fluka Kieselgel 60 (230–400 mesh). ^{1}H and ^{13}C NMR spectra were recorded on Jeol 400 MHz, Bruker 600 MHz with cryo probe using residual solvent signals as an internal reference ($CDCl_3$ δ_H 7.26 ppm, δ_C 77.3 ppm and CD_3OD δ_H 3.31 ppm, δ_C 49.0 ppm). The chemical shifts (δ) are reported in ppm and coupling constants (*J*) in Hz. UV-visible measurements were performed with Evolution 300 UV-visible spectrophotometer (Thermo Fisher Scientific, USA). Circular Dichroism measurements were performed with J-815 CD spectro-polarimeter (Jasco, Japan). Each CD profile is an average of five independent scans of the same sample collected at a scan speed of 30 nm min^{-1}. Fluorescence spectra were recorded in FluoroMax-4 spectrofluorometer (Horiba Scientific, U.S.A.), 8 well microscopic plates were subjected to fluorescence imaging using CLSM (Zeiss LSM 710). BSA-Mannose was purchased from vector laboratory.

Mass Spectrometry Study

Metallo-glycodendrimers (**M-2A** to **M-2D**) were dissolved in ultrapure water to give final concentration of 10-100 μM. In order to keep the non-covalent complexes intact during the ionization process a native-ESI technique was employed.

Circular Dichroism spectroscopy

The CD spectra of the MGDs were recorded at 25°C. CD data are given as normal ellipticity from the normalisation of ellipticity [θ]. To facilitate analysis of uncertainties, each set of

spectra were measured using at least three individually prepared solutions and the spectra are the result of 5 accumulations. Quartz cells with a path length of 0.2 cm were used to ensure volume 0.2 ml (400 μM). Water was used as blank and the samples were equilibrated for at least 10 hours before the measurement. The parameters of the measurements are as follows:

Resolution:	1 nm	Band width:	1.0 nm
Sensitivity:	100 mdeg	Response:	1 sec
Speed :	100 nm/min	Accumulation:	5

DFT calculation

The DFT calculations were performed with the Gaussian 09 rev-D suite of program.[58] We have employed B3LYP[59,60] exchange hybrid functional, SDD[61] basis set for the Ruthenium atom and 6-31G[62] basis set for all the other atoms. Δ/Λ Ru(II) $(bipy)_3$ geometries are considered from Cambride Crystolographic MB data [CCDC No 166368][63,64] then D and L-alanine were substituted at 4, 4'-position of the bipyridine ligand, followed by adamantly group. We have employed IEFPCM implicit solvation model (methanol) for to describe solvent effect.[65] When the minimum energy structures of **Ru-2** and **Ru-3** were compared, the adamantyl group of **Ru-2** adopted quite opposite arrangement compared to **Ru-3**, particularly the amide bond of the adamantyl groups are projecting antiparallel to the bipyridine axis. Overall, two distinct chirality of the Ru(II) complexes resulted two different spatial arrangement of the adamantyl group, which eventually results with two different spatial arrangement of the host-guest complexes. Further, computed CD spectra of the complexes are closely resembles to Figure10.

Corroboration of the complexes structure by Isothermal calorimetry titration

In order to gain an insight into the binding affinity, thermodynamics and stoichiometry of the **M-2A** and **M-2B**, we performed isothermal calorimetry (ITC). The **C-A** and **C-B** were titrated into the **Ru-2** in the calorimeter cells. Upon forming complex between *β*-CD derivatives and **Ru-2** heat is released, yielding a typical titration isotherm. Based on the qualitative assessment, **Ru-2** binding isotherm was fitted to a binding model. The values of formation constants (K) and thermodynamic parameters determined by ITC are summarized in Table 3, where 'N' represents the number of **Ru-2** on the *β*-CD that are available for binding.

General procedure for the production of the CLR-Fc library

The general procedure for the production of the mouse CLR-Fc fusion protein library has been described previously (Maglinao et al., *J. Control. Release* 2014, 10, 175, 36-42). The following primers were used for PCR amplification of cDNA fragments encoding the extracellular part of the respective C-type lectin receptor (CLR):

DC-SIGN	DC-SIGN-f	5'-GAATTCGTCCAAGGTCCCCAGCTCCAT-3'
	DC-SIGN-r	5'-CCATGGACGCAGGAGGGGGGTTTGGGGT-3'
SIGNR3	SIGNR3-f	5'-GAATTCCATGCAACTGAAGGCTGAAG-3'
	SIGNR3-r	5'-AGATCTTTTGGTGGTGCATGATGAGG-3'
Dectin-1	Dectin-1-f	5'-GAATTCTTCAGGGAGAAATCCAGAGG-3'
	Dectin-1-r	5'-AGATCTTGAAGAAGTATTGCAGATTTGGTT-3'

The cDNA fragments were cloned into the pDrive cloning vector (Qiagen) and further ligated into the pFuse-hIgG1-Fc expression vector (InvivoGen). Next, the CLR-Fc encoding vectors were transiently transfected using the FreeStyle Max CHO-S Expression System (Life Technologies). The cell supernatant containing the CLR-Fc fusion proteins was collected and the CLR-Fc fusion proteins were purified using HiTrap Protein G HP columns (GE Healthcare). Identity and purity of the CLR-Fc fusion proteins were confirmed by SDS-PAGE with subsequent Coomassie stain as well as Western Blot. Concentration determination was performed using the Micro BCA Protein Assay Kit (Thermo Scientific).

Binding affinity

96-well ELISA plates were treated with immobilized mannose-BSA (1 mg/ml) as reference ligand and incubated with h-DC-SIGN/m-SIGNR3/m-Dectin-1/HRP-ConA/HRP-PNA (5 µg/ml) in the presence of different MGDs (10^{-3} to 10^{-8} mg) in varying concentrations in HEPES buffer (pH 7.2 containging 0.15 M NaCl and 20 mM $CaCl_2$). After incubation for 2 h, anti-human IgG HRP was added to quantify the binding of lectin and quantified by a HRP-catalysed color reaction using 2, 2'-azinobis(3-ethyl-benzo-thiazoline-6-sulfonic acid) diammonium salt (ABTS) as substrate. From these curves the concentration that reduces the binding of labeled lectin to the microtiter plates by 50% (IC_{50} values) were determined as a means of potency of the synthesized inhibitors.

STD-NMR

STD NMR samples were prepared in 20 mM TRIS-d_{11} (pD = 8.0), 150 mM NaCl, 4 mM $CaCl_2$ in H_2O on Bruker 400 MHz spectrometer equipped with water as internal control. In all the STD NMR, samples containing 0.1 mM ligand and 10 µg/0.5 ml of DC-SIGN or Dectin-1 were used. On-resonance irradiation was set to 0.0 ppm, and off resonance irradiations was set to 0.8 ppm, A 35 ms T1ρ spin-lock filter and a W5 watergate for solvent suppression were applied. A total of 1024 scans were collected with saturation pulse of 50 ms duration and 1 ms interpulse delay with strength of 10dB. STD build-up curse were recorded at saturation time of 0.5, 1, 2, 4 and 8 s.

For **M-2C** the most intense STD signals were observed at δ 3.68, 3.52 and 0.98 ppm, Which might be corresponds to mannose and methyl group of the linker between the mannose and *β*-cyclodextrin. However, further interpretation of the exact proton of mannose involved in the binding was hampered due to the overall lap of cyclodextrin sugar moieties. Consequently, the signal of methyl group was set as a reference with 50% STD effect. Intensities of 3.68 and 3.52 ppm were quantified, which turned out to be 39% and 28% respectively.

In order to evaluate the binding affinity, STD spectra was collected at five different saturation time. The STD-amplification facto was determined by equation 1, where I_{off} corresponds to intensity of signal in off-resonance and I_{sat} corresponds to intensity of signal in on-resonance spectra. [L] and [P] corresponds to concentration of the ligand and receptor respectively.[66]

$$\text{STD-AF} = (I_{off}-I_{sat})/I_{off} \text{ X } [L]/[P] \qquad \text{Equation-1}$$

Cell viability assay

HeLa and NIH-3T3 (1×10^5 cells/well) were seeded in 96-well microtiter plate and incubated overnight in a 5% CO_2 incubator at 37 °C for attachment. Cells were then treated with metallo-glycodendrimers in different concentrations (1, 3, 7.5, 15, 30µM) for 24 h. The medium was removed and 20 µL of MTT reagent (5 mg/mL) and 100 µL of fresh medium was added to each well and incubated for 4 h at 37 °C. Formazan crystals were then solubilized in 100 µL of the solubilization buffer (10% SDS in 0.01 M HCl) and incubated overnight. Absorbance was measured with spectrophotometer at 550 nm. The percent cell viability was calculated considering the untreated cells as 100% viability.

Confocal laser scanning microscopy (CLSM) studies

Cellular internalization

Cell line	Growth Media
DC-SIGN-HeLa	Cells were grown at 37 °C in 5% CO_2 atmosphere in DMEM medium containing 10% fetal bovine serum and 0.1% streptomycin
SINGR3-CHO Or CHO-K1	Cells were grown at 37 °C in 5% CO_2 atmosphere in RPMI-40 medium containing 10% fetal bovine serum and 0.1% streptomycin

Transfected Hela/CHO (1 $\times 10^6$ cells/well) was seeded on an eight well chambered cover glass and incubated overnight in a 5% CO_2 incubator at 37 °C for attachment. Cells were then first washed with PBS and then treated with **Ru-1** to **3** or MGDs (at a concentration 15 μM) for 6 h and 24 h respectively (in case of HepG2 and MDA-MB-231 cells, MGDs were treated for 6 h and 24 h respectively). Cells were then washed with PBS and fresh medium was added. Then cells were subjected to fluorescence imaging using a CLSM (Zeiss LSM 710).

Co-localization

DC-SIGN-HeLa cells (1 $\times 10^6$ cells/well) were seeded on an 8 well chambered cover glass (Sigma Aldrich) and incubated overnight in a 5% CO_2 incubator at 37 °C for attachment. Cells were then treated with **M-2C (**15 μM) for 24 h. Cells were then washed twice with PBS (pH = 7.4) and treated with MitoTracker green CMXROS at a concentration of 200 nM in PBS and incubated in dark at 37 °C for 30 min. Similarly, ER-tracker green at a concentration of 500 nM in DMSO and incubated in dark for 30 min. The cells were treated with Hoechst 33342 (10 μL of 2 μg/mL solution) to stain nuclei for 30 mins, washed 3 times with PBS buffer. The fluorescence of Hoechst 33342, FITC complexes and red tracker were excited with an argon laser at 405 nm 450 nm and 600 nm respectively, and the emission was collected through 403–452 nm, 500-530 nm and 600-630 nm filters respectively.

FACS analysis

DC-SIGN-HeLa cells (2 × 10^6 cells/well) were incubated in 6-well plates overnight for attachment and then treated with **M-1B** to **M-3B**, **M-1C** to **M-3C** and **M-1D** to **M-3D** (15

μM) for 6 h and 24 h. After the treatment, media was removed and cells were trypsinized and washed twice with PBS by means of centrifugation at 750 rpm for 4 min. Cell pellet was then resuspended in 500 μL of incubation buffer at 25 °C for 15 min. Cells were then passed through cell strainer to get uniform cell suspension and analyzed using BD FACS Calibur to detect uptake. Statistical comparisons were done using the Student *t* test or one-way ANOVA. The $p < 0.05$ is considered to be statistical significance.

Cellular uptake mechanism

For all these experiments, DC-SIGN transfected HeLa or SIGNR3-transfected CHO cells were grown in 8-well chamber cover glass (1×10^6 cells/well) and treated with the specific inhibitor for 30 min followed by **M-2C** (15 μM) for 6 h at 37 °C. For energy dependent study, cells were incubated for 30 min with NaN_3 (50 mM). For dynamin-mediated uptake (clathrin and caveolae-mediated uptake) cells were treated with dynasore Hydrate (50 μM). For clathrin mediated uptake studies chlorpromazine (25 μM) were added. For caveolae mediated uptake, cells were treated with methylated-*β*-cyclodextrin (10 mM). After 6 h of **M-2C** treatment, cells were washed to remove unbound materials, cells were fixed and imaged.

***In vivo* experiments**

Adult male C57/BL/6 mice (4-6 week old) were housed individually in a climate-controlled room (25-27ºC and 60% relative humidity) under 12-12 h light/dark cycle with ad libitum access to food and drinking water except during the test period. The surgical procedures were performed in accordance with Institutional Animal Ethical Committee regulation, set up by CPCSEA, Govt. of India. All experiments were performed in INTOX quality toxicological services, Pune.

Body weight analysis

Mice (n=3) were anaesthetized with ketamine and i.v MGDs were injected (**M-1C**, **M-2C** and **M-3C** 50 μM) . Body weights of the mice in both groups were recorded for next 50 days. Blood samples from control and MGDs mice were collected after 20 and 40 days and two important hepatic damage indicators, alanine aminotransferase and aspartate aminotransferase level were measured.

ICP-MS quantification

Mice (n = 3 per MGDs) were anaesthetized with ketamine (2.0 mg/mouse) and received 50 μM (**M-1C, M-2C** and **M-3C**), following 2 h, 6 h and 24 h interval and liver, spleen, heart,

brain and lungs were dissected. The dissected organs were digested in 3 ml of acidic conc. HNO_3 and H_2O_2 (30-32%) 1:1 ratio at 60℃ for 12 h using heating blocks. Samples were homogenized every hour using a vortex mixer. After complete digestion, samples were transferred to a 15 ml conical tube, diluted to a final volume of 10 ml with ultra trace analysis water. Then, all samples were filtered through 0.45 µm syringe filters and transferred to sampling tubes. Ruthenium concentration was determined by ICP-MS.

Another set of mice (n=3 per MGDs) were anaesthetized with ketamine (2.0 mg/mouse) and received 50 µM (**M-1C, M-2C** and **M-3C**) each *via* tail vein injection (total volume 100 µL). Afterwards, 50 µL PBS were injected to flush the tail vein. 1 h after the injection, mice were sacrificed and livers were harvested *via* the portal vein with 4% paraformaldehyde (PFA). Organs were processed through series of xylene and ethanol fixation before preparing the paraplast block. 10 µm thickness sections were collected on PLL coated plates and sequestration of Ru(II) into liver was analyzed by confocal fluorescence microscopy using a CLSM (Zeiss LSM 710) microscope. The excitation wavelength was 450 nm; detection wavelength was 600/650 nm. The objective magnification used for the analysis of each liver section was 25 and 40x. Ru(II) sequestration in the liver was measured by counting the number of Ru(II) complexes using the imageJ software**.**

Blood sample analysis

Mice (n =3) were anaesthetized with ketamine and received 50 µM of (**M-1C, M-2C** and **M-3C**). After 0, 30, 60, 90, 120 and 180 mins. Mice were sacrificed and 0.5 ml of blood was drawn. Collected blood samples were digested with 500 µl of 70% nitric acid, followed by heating at 90°C for 30 min. Then each digested samples were diluted to 6 ml with Millipore water. The concentration of QDs in the blood samples was determined by ICP-MS (Thermo-Fisher Scientific, Germany) by quantifying the ruthenium concentration. Finally, the concentration of cadmium was converted into ng/mg.

Synthesis of Ru(II) complexes.

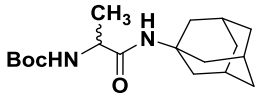

1

Tert-butyl ((R,S)-1-((3S,5S,7S)-adamantan-1-ylamino)-1-oxopropan-2-yl)carbamate (1). 1-Adamantylamine (1.0 g, 6.62 mmol) and Boc-DL-alanine (1.4 g, 7.2 mmol) were dissolved in CH_2Cl_2 (60 mL) at r.t. DIC (1.0 g, 7.94 mmol) was then added, followed by the addition of DIPEA (2.1 g, 16.5mmol). The reaction mixture was stirred at r.t for 12 h. The product was then extracted with EtOAc (70 mL) and the organic layer was washed with H_2O (2×50 mL). The resulting organic layer was then dried over $MgSO_4$, filtered, concentrated and the crude was purified by flash column chromatography (silica gel, CH_2Cl_2:MeOH = 19:1) and dried under *high vacuo* to give the final product **1** (1.5 g, 71%) as a white foam. R_f = 0.72 (CH_2Cl_2:MeOH = 19:1): ^{1}H NMR ($CDCl_3$, 400 MHz): δ_H: 5.77 (s, 1H), 5.11 (s, 1H), 4.03 (s, 1H), 2.09 (s, 3H), 2.00 (s, 6H), 1.69 (s, 6H), 1.47 (s, 9H), 1.33 (d, *J* = 4 Hz, 3H); ^{13}C NMR ($CDCl_3$, 100 MHz): δ_C: 171.80, 155.63, 79.86, 51.81, 50.54, 41.54, 36.37, 29.44, 28.39, 18.49; HRMS: (m/z) calculated for $C_{18}H_{30}N_2O_3[M+H]^+$ = 323.2334; found = 323.2336.

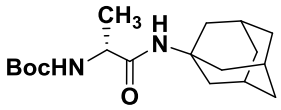

4

Tert-butyl ((R)-1-((3S,5S,7S)-adamantan-1-ylamino)-1-oxopropan-2-yl)carbamate (4). 1-Adamantylamine (1.0 g, 6.62 mmol) and Boc-L-alanine (1.4 g, 7.2 mmol) were dissolved in CH_2Cl_2 (60 mL) at r.t. DIC (1.0 g, 7.94 mmol) was then added, followed by the addition of of DIPEA (2.1 g, 16.5 mmol). The reaction mixture was stirred at r.t. for 12 h. The product was then extracted with EtOAc (70 mL) and the organic layer was washed with H_2O (2×50 mL). The resulting organic layer was then dried over $MgSO_4$, filtered, concentrated, and the crude was purified by flash column chromatography (silica gel, CH_2Cl_2:MeOH = 19:1) and dried under *high vacuo* to give the final product **4** (1.7 g, 80.9%) as a white foam. R_f = 0.72 (CH_2Cl_2:MeOH = 19:1): ^{1}H NMR ($CDCl_3$, 400 MHz): δ_H: 5.77 (s, 1H), 5.01 (s, 1H), 4.03 (s, 1H), 2.09 (s, 3H), 2.00 (s, 6H), 1.69 (s, 6H), 1.47 (s, 9H), 1.33 (d, *J* = 4 Hz, 3H); ^{13}C NMR ($CDCl_3$, 100 MHz): δ_C: 171.80, 155.63, 79.86, 51.81, 50.54, 41.54, 36.37, 29.44, 28.39, 18.49; HRMS: (m/z) calculated for $C_{18}H_{30}N_2O_3[M+H]^+$ = 323.2334; found = 323.2336.

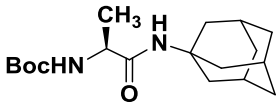

5

Tert-butyl ((S)-1-((3R,5R,7R)-adamantan-1-ylamino)-1-oxopropan-2-yl)carbamate (5). 1-Adamantylamine (1.0 g, 6.62 mmol) and Boc-D-alanine (1.4 g, 7.2 mmol) were dissolved in CH_2Cl_2 (60 mL) at r.t. DIC (1.0 g, 7.94 mmol) was then added, followed by the addition of DIPEA (2.1 g, 16.5mmol). The reaction mixture was stirred at r.t for 12 h. The product was then extracted with EtOAc (70 mL) and the organic layer was washed with H_2O (2×50 mL). The resulting organic layer was then dried over $MgSO_4$, filtered, concentrated and the crude was purified by flash column chromatography (silica gel, CH_2Cl_2:MeOH = 19:1) and dried under *high vacuo* to give the final product **5** (1.4 g, 66.6%) as a white foam. R_f = 0.72 (CH_2Cl_2:MeOH = 19:1): ^{1}H NMR ($CDCl_3$, 400 MHz): δ_H: 5.92 (s, 1H), 5.18 (s, 1H), 4.03 (s, 1H), 2.05 (s, 3H), 1.97 (s, 6H), 1.66 (s, 6H), 1.43 (s, 9H), 1.30 (d, *J* = 8 Hz, 3H); ^{13}C NMR ($CDCl_3$,100 MHz): δ_C: 71.79, 155.62, 79.86, 51.81, 50.53, 41.54, 36.36, 29.43, 29.39, 18.48; HRMS: (m/z) calculated for $C_{18}H_{30}N_2O_3[M+H]^+$ = 323.2334; found = 323.2339.

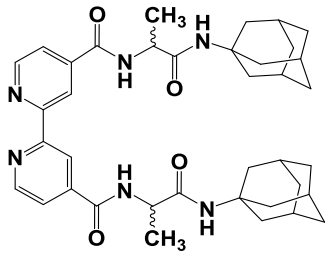

12

N^4,$N^{4'}$-bis((R, S)-1-((3S, 5S, 7S)-adamantan-1-ylamino)-1-oxopropan-2-yl)- [2,2'-bipyridine]-4,4'-dicarboxamide (12). Under an Ar atmosphere, 2,2'-bipyridine-4,4'-dicarboxylic acid (100 mg, 1.23 mmol) and $SOCl_2$ (5.0 mL, 42.6 mmol) were mixed together at r.t. to give a white suspension. The reaction mixture was then heated under reflux over 2 days at 60 °C to give a clear green solution. Excess of $SOCl_2$ was removed by vacuum distillation at 70 °C and the crude was dried under *high vacuo* to give 2,2'-bipyridine-4,4'-dicarbonyl dichloride as a green solid which was then dissolved in dry CH_2Cl_2 (5 mL) under N_2 atmosphere, followed by the addition of adamantyl derivative **3** (340 mg, 4.6 mmol). The resulting mixture was then treated dropwise with Et_3N to reach pH = 8. The solution was stirred over 1 day at r.t. The solvent was then removed under reduced pressure and the

residue was then purified by flash column chromatography (silica gel, CH_2Cl_2:MeOH = 19:1 to 9:1), and dried under *high vacuo* to give **12** (100 mg, 37%) as a white solid. R_f = 0.45 (CH_2Cl_2:MeOH = 9:1): ^{1}H NMR ($CDCl_3$, 400 MHz) δ_H: 9.02 (s, 2H), 8.68 (d, *J* = 4 Hz, 2H), 8.44 (s, 2H), 7.75 (d, *J* = 4 Hz, 2H), 6.59 (s, 2H), 4.80 (q, *J* = 2 Hz, 2H), 2.02 (s, 6H), 1.99 (s, 12H), 1.63 (s, 12H), 1.53 (d, *J* = 4 Hz, 6H); ^{13}C NMR ($CDCl_3$, 100 MHz): δ_C: 172.12, 164.82, 156.66, 150.21, 141.71, 121.69, 118.54, 52.32, 50.44, 41.49, 36.31, 29.42, 18.80; HRMS: (m/z) calculated for $C_{38}H_{49}N_6O_4[M+H]^+$ = 653.3815; found = 653.3812.

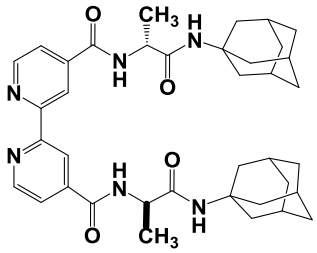

13

N^4,$N^{4'}$-bis((R)-1-((3S,5S,7S)-adamantan-1-ylamino)-1-oxopropan-2-yl)-[2,2'-bipyridine]-4,4'-dicarboxamide (13). Under an Ar atmosphere, 2,2'-bipyridine-4,4'-dicarboxylic acid (100 mg, 1.23 mmol) and $SOCl_2$ (5.0 mL, 42.6 mmol) were mixed together at r.t. to give a white suspension. The reaction mixture was then heated under reflux over 2 days at 60 °C to give a clear green solution. Excess of $SOCl_2$ was removed by vacuum distillation at 70 °C and the crude was dried under *high vacuo* to give 2,2'-bipyridine-4,4'-dicarbonyl dichloride as a green solid which was then dissolved in dry CH_2Cl_2 (5 mL) under N_2 atmosphere, followed by the addition of adamantyl derivative **8** (340 mg, 4.6 mmol). The resulting mixture was then treated dropwise with Et_3N to reach pH = 8. The solution was stirred over 1 day at r.t. The solvent was then removed under reduced pressure and the residue was then purified by flash column chromatography (silica gel, CH_2Cl_2:MeOH = 19:1 to 9:1), and dried under *high vacuo* to give **13** (78mg, 29%) as a white solid. R_f = 0.45 (CH_2Cl_2:MeOH = 9:1): ^{1}H NMR ($CDCl_3$, 400 MHz): δ_H: 8.90 (s, 2H), 8.68 (d, *J* = 4 Hz, 2H), 8.44 (s, 2H), 7.75 (d, *J* = 4 Hz, 2H), 6.59 (s, 2H), 4.80 (q, *J* = 2 Hz, 2H), 2.02 (s, 6H), 1.99 (s, 12H), 1.63 (s, 12H), 1.53 (d, *J* = 4 Hz, 6H); ^{13}C NMR ($CDCl_3$, 100 MHz): δ_C: 172.21, 163.97, 157.02, 149.81, 141.92, 121.09, 118.75, 51.89, 50.34, 40.92, 36.28, 29.42, 18.78; HRMS: (m/z) calculated for $C_{38}H_{49}N_6O_4[M+H]^+$ = 653.3815; found = 653.3809.

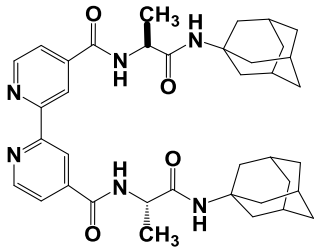

14

N^4,$N^{4'}$-bis((S)-1-((3S,5S,7S)-adamantan-1-ylamino)-1-oxopropan-2-yl)-[2,2'-bipyridine]-4,4'-dicarboxamide (14). Under an Ar atmosphere, 2,2'-bipyridine-4,4'-dicarboxylic acid (100 mg, 1.23 mmol) and $SOCl_2$ (5.0 mL, 42.6 mmol) were mixed together at r.t. to give a white suspension. The reaction mixture was then heated under reflux over 2 days at 60 °C to give a clear green solution. Excess of $SOCl_2$ was removed by vacuum distillation at 70 °C and the crude was dried under *high vacuo* to give 2,2'-bipyridine-4,4'-dicarbonyl dichloride as a green solid which was then dissolved in dry CH_2Cl_2 (5 mL) under N_2 atmosphere, followed by the addition of adamantyl derivative **9** (340 mg, 4.6 mmol). The resulting mixture was then treated dropwise with Et_3N to reach pH = 8. The solution was stirred over 1 day at r.t. The solvent was then removed under reduced pressure and the residue was then purified by flash column chromatography (silica gel, CH_2Cl_2:MeOH = 19:1 to 9:1), and dried under *high vacuo* to give **14** (110 mg, 41%) as a white solid. R_f = 0.45 (CH_2Cl_2:MeOH = 9:1): ^{1}H NMR ($CDCl_3$, 400 MHz): δ_H: 8.76 (s, 2H), 8.70 (d, *J* = 4 Hz, 2H), 8.44 (s, 2H), 7.74 (d, *J* = 4 Hz, 2H), 6.46 (s, 2H), 4.78 (q, *J* = 8 Hz, 2H), 2.03 (s, 6H), 1.98 (s, 12H), 1.63 (s, 12H), 1.54 (d, *J* = 8 Hz, 6H); ^{13}C NMR ($CDCl_3$, 100 MHz): δ_C: 172.41, 164.87, 156.74, 150.30, 141.66, 121.74, 118.71, 52.37, 50.58, 41.51, 36.37, 29.47, 18.85; HRMS: (m/z) calculated for $C_{38}H_{49}N_6O_4$ $[M+H]^+$ = 653.3815; found = 653.3781.

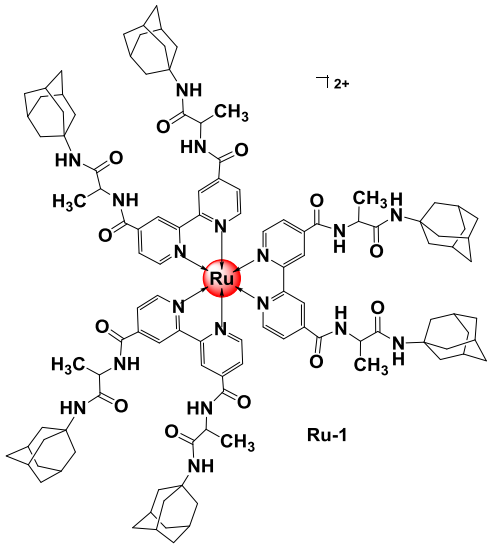

Ru-1

Rec-Ru-hexaadamantyl (Ru-1):

Ligand **12** (120 mg, 180.0 mol) and $RuCl_3.3H_2O$ (11 mg, 40.0 mol) were dissolved in EtOH (20 mL) at r.t. The reaction mixture was heated at 60 °C for 4 h. The solvent was then removed under reduced pressure and the residue was then purified by flash column chromatography (silica gel, CH_2Cl_2:MeOH = 85:15) to afford the product **Ru-1** (30mg, 35%) as a red solid. R_f = 0.40 (CH_2Cl_2:MeOH = 85:15): ^{1}H NMR (CD_3OD, 400 MHz): δ_H: 9.25-9.24 (d, 6H, *J* = 4 Hz), 8.01-7.97 (m, 6H), 7.93-7.88 (m, 6H), 4.54 (q, *J* = 8 Hz, 6Hz), 2.03 (bs, 54H), 1.70 (bs, 36H), 1.47 (d, *J* = 8 Hz, 18H); ^{13}C NMR (CD_3OD, 100 MHz): δ_C: 172.31, 163.81, 157.35, 152.15, 143.11, 125.60, 122.61, 51.69, 50.44, 40.92, 36.11, 29.50, 21.01; HRMS: (m/z) calculated for $C_{114}H_{144}N_{18}O_{12}Ru[M]^{2+}$ = 2059.0255; found $[M/2]^{2+}$ = 1029.5142.

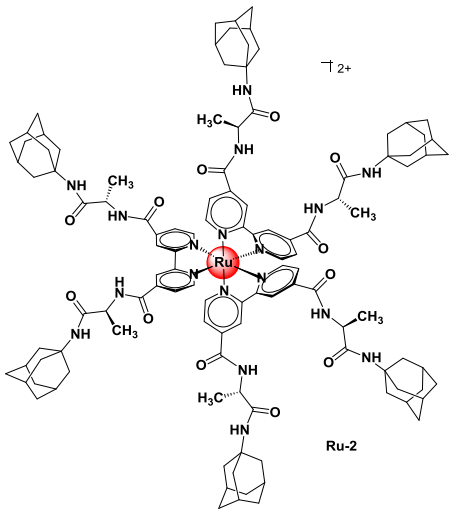

Δ-Ru-hexaadamantyl (Ru-2): Ligand **13** (120 mg, 180.0 mol) and $RuCl_3.3H_2O$ (11 mg, 40.0 mol) were dissolved in EtOH (20 mL) at r.t. The reaction mixture was heated at 60 °C for 4 h. The solvent was then removed under reduced pressure and the residue was then purified by flash column chromatography (silica gel, CH_2Cl_2:MeOH = 85:15) to afford the product **Ru-2** (24mg, 28%) as a red solid. R_f = 0.40 (CH_2Cl_2:MeOH = 85:15): ^{1}H NMR (CD_3OD, 400 MHz): δ_H: 9.24 (s, 6H), 8.01-7.99 (m, 6H), 7.92-7.88 (m, 6H), 4.54 (q, *J* = 8 Hz, 6Hz), 2.05 (bs, 54H), 1.72 (bs, 36H), 1.47 (d, *J* = 8 Hz, 18H); ^{13}C NMR (CD_3OD, 100 MHz): δ_C: 172.29, 163.90, 157.27, 152.10, 143.18, 125.59, 122.59, 51.70, 50.44, 40.88, 36.05, 29.50, 20.96; HRMS: (m/z) calculated for $C_{114}H_{144}N_{18}O_{12}Ru$ $[M]^{2+}$ = 2059.0255; found $[M/2]^{2+}$ = 1029.5153.

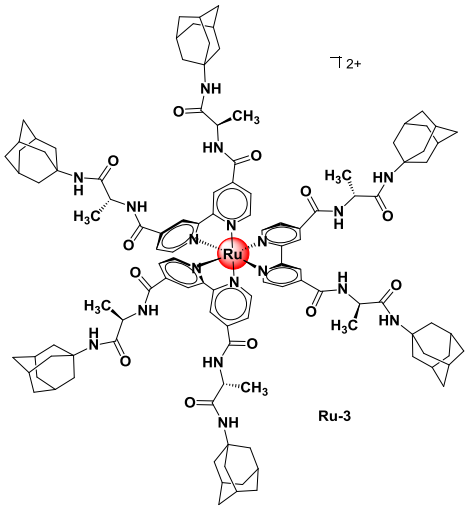

Λ-Ru-hexaadamantyl (Ru-3): Ligand **14** (120 mg, 180.0 mol) and $RuCl_3.3H_2O$ (11 mg, 40.0 mol) were dissolved in EtOH (20 mL) at r.t. The reaction mixture was heated at 60 °C for 4 h. The solvent was then removed under reduced pressure and the residue was then purified by flash column chromatography (silica gel, CH_2Cl_2:MeOH = 85:15) to afford the product **Ru-3** (21mg, 24%) as a red solid. R_f = 0.40 (CH_2Cl_2:MeOH = 85:15): ^{1}H NMR (CD_3OD, 400 MHz): δ_H: 9.25 (s, 6H), 7.99-7.95 (m, 6H), 7.93-7.89 (m, 6H), 4.53 (q, 6H), 2.02 (s, 54H), 1.69 (s, 36H), 1.48 (d, *J* = 8 Hz, 18H); ^{13}C NMR (CD_3OD, 100 MHz): δ_C: 172.37, 163.85, 157.33, 152.21, 143.13, 125.65, 122.65, 51.68, 50.51, 40.92, 36.12, 29.56, 21.04; HRMS: (m/z) calculated for $C_{114}H_{144}N_{18}O_{12}Ru[M]^{2+}$ = 2059.0255; found $[M/2]^{2+}$ = 1029.4882.

Synthesis of *β*-cyclodextrin derivatives.

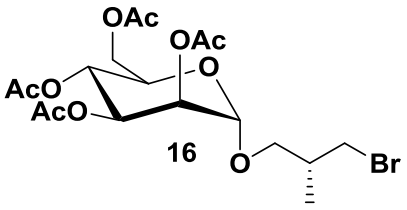

(2R,3R,4S,5S,6S)-2-(acetoxymethyl)-6-((R)-3-bromo-2-methylpropoxy)tetrahydro-2H-pyran-3,4,5-triyl triacetate (16). Peracetylated Mannose **15** (0.5 g, 1.28 mmol) and (*R*)-(−)-3-Bromo-2-methyl-1-propanol (0.40 mL, 3.84 mmol) were dissolved in CH_2Cl_2 (10 mL) and maintained 0°C. To the reaction mixture $BF_3.Et_2O$ (0.62 mL, 5.12 mmol) was added slowly for 30 min and stirred overnight at r.t. Completion of reaction was monitored by TLC. After completion, the reaction mixture was diluted with 20 mL CH_2Cl_2 and washed with $NaHCO_3$

(2 X 20 mL) and brine (2 X 20 mL). Organic layer was dried over anhydrous Na_2SO_4 and concentrated under reduced pressure to give crude product, which was purified by flash column chromatography (silica gel, Petroleum ether:EtOAc = 50:50) to afford the product **16** (0.51 g, 84%) as a white solid. $[\alpha]^D_{25}$ +52 (c 0.1%, $CHCl_3$): R_f = 0.50 (Petroleum ether:EtOAc = 50:50): ^{1}H NMR ($CDCl_3$, 400 MHz): δ_H: 5.27 (m, 1H), 5.25-5.22 (m, 2H), 4.79 (d, *J* = 1.37 Hz, 1H), 4.28-4.23 (m, 1H), 4.11 (dd, *J* = 2.29, 2.29 Hz, 1H), 3.99-3.95 (m, 1H), 3.73-3.69 (m, 1H), 3.44 (dd, *J* = 2.75, 1.83 Hz, 2H), 3.40-3.35 (m, 1H), 2.13 (s, 3H), 2.11-2.09 (m, 1H), 2.08 (s, 3H), 2.02 (s, 3H), 1.97 (s, 3H), 1.05 (d, *J* = 6.87 Hz, 3H); ^{13}C NMR ($CDCl_3$, 100 MHz): δ_C: 170.48, 169.90, 169.80, 169.63, 97.78, 70.40, 69.33, 69.06, 68.63, 65.99, 62.37, 37.04, 35.12, 20.80, 20.68, 20.64, 20.61, 15.88; HRMS: (m/z) calculated for $C_{18}H_{27}NaBrO_{10}[M+Na]^+$ = 505.0685; found = 505.0681.

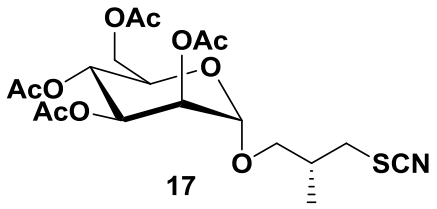

17

(2R,3R,4S,5S,6S)-2-(acetoxymethyl)-6-((R)-2-methyl-3-thiocyanatopropoxy)tetrahydro-2H-pyran-3,4,5-triyl triacetate (17). Glycosylated sugar derivative **16** (0.4 g, 0.85 mmol) was dissolved in DMF (10 mL). Then potassium thiocyanate (0.33 g, 3.42 mmol) was added and stirred at 80 °C for 12 hr. The reaction mixture was diluted with 100 ml ethyl acetate and washed several times with water. The organic layer was dried over anhydrous Na_2SO_4 and concentrated under reduced pressure to give crude product, which was purified by flash column chromatography (silica gel, Petroleum ether:EtOAc = 75:25) to afford the product **17** (0.35 g, 91%) as a white solid. $[\alpha]^D_{25}$ +66(c 0.1%, $CHCl_3$): R_f = 0.7 (Petroleum ether:EtOAc = 75:25): ^{1}H NMR: ($CDCl_3$, 400 MHz): δ_H: 5.26 (m, 1H), 5.25-5.22 (m, 2H), 4.79 (d, *J* = 1.37 Hz, 1H), 4.28-4.23 (m, 1H), 4.12-4.07 (m, 1H), 3.94-3.89 (m, 1H), 3.79-3.76 (m, 1H), 3.39-3.35 (m, 1H), 3.10-3.06 (m, 1H), 2.97-2.92 (m, 1H), 2.26-2.20 (m, 1H), 2.14 (s, 3H), 2.08 (s, 3H), 2.03 (s, 3H), 1.97 (s, 3H), 1.13 (d, *J* = 6.87 Hz, 3H) ; ^{13}C NMR ($CDCl_3$, 100 MHz): δ_C: 170.70, 170.11, 170.03, 169.80, 112.44, 98.08, 70.66, 69.29, 69.03, 68.92, 66.06, 62.54, 37.62, 34.14, 20.95, 20.84, 20.78, 20.76, 15.99; HRMS: (m/z) calculated for $C_{19}H_{27}NaSO_{10}[M+Na]^+$ = 484.1253; found = 484.1248.

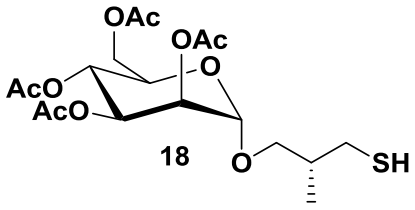

(2R,3R,4S,5S,6S)-2-(acetoxymethyl)-6-((R)-3-mercapto-2-methylpropoxy)tetrahydro-2H-pyran-3,4,5-triyl triacetate (18). Peracetylated thiocyanate-sugar derivative **17** (0.2 g, 0.43 mmol) was dissolved in glacial acetic acid (30 mL). Then Zn dust (0.17 g, 2.6 mmol) was added and refluxed at 80 °C for 4 h. The compound was filtered to remove zinc dust. The organic layer was quenched with water (50 mL). Then product was extracted with EtOAc (3 X 50 mL) and dried over anhydrous Na_2SO_4. Organic layer was concentrated under reduced pressure to give product **18** (0.14, 72%) as a syrup. This was further used for next reaction without purification. $[\alpha]^{D}_{25}$ +44 (c 0.1%, CHCl3): ^{1}H NMR ($CDCl_3$, 400 MHz): δ_H: 5.29-5.27 (m, 1H), 5.25-5.22 (m, 2H), 4.78 (d, *J* = 1.83 Hz, 1H), 4.28-4.24 (m, 1H), 4.12 (dd, *J* = 2.75, 2.29 Hz, 1H), 3.98-3.94 (m, 1H), 3.68-3.65 (m, 1H), 3.40-3.36 (m, 1H), 2.64-2.57 (m, 1H), 2.55-2.48 (m, 1H), 2.14 (s, 3H), 2.09 (s, 3H), 2.03 (s, 3H), 1.98 (s, 3H), 1.96-1.90 (m, 1H), 1.59 (bs, 1H), 1.01 (d, *J* = 6.87 Hz, 3H) ; ^{13}C NMR ($CDCl_3$, 100 MHz): δ_C: 170.76, 170.20, 170.02, 169.85, 97.91, 71.23, 69.59, 69.17, 68.68, 66.20, 62.57, 36.12, 27.98, 20.99, 20.85, 20.80, 20.78, 16.05; HRMS: (m/z) calculated for $C_{18}H_{28}NaSO_{10}[M+Na]^+$ = 459.1301; found = 459.1306.

Synthesis of sugar substituted *β*-cyclodextrin (23).

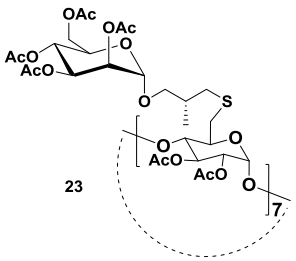

Per-acetylated 6'-Iodo- β-cyclodextrin **22** (0.1 g, 0.04 mmol) and the per-acetylated thio-sugar **18** (0.22 g, 0.52 mmol) was dissolved in DMF (10 mL) and added Cs_2CO_3 (0.17 g, 0.52 mmol) stirred at r.t. for 72 h. The reaction mixture was diluted with 100 ml EtOAc and washed several times with water. The organic layer was dried over anhydrous Na_2SO_4 and concentrated under reduced pressure to give crude product, which was purified by flash

column chromatography (silica gel, CH_2Cl_2:MeOH = 93:7) to afford the product **23** (0.1, 58%) as a white solid. $[\alpha]^D_{25}$ +60.8 (c 0.1%, CHCl3): R_f = 0.40 (CH_2Cl_2:MeOH = 93:7): ^{1}H NMR ($CDCl_3$, 400 MHz): δ_H: 5.30-5.21 (m, 25H), 5.11 (bm, 7H), 4.99-4.88 (m, 7H), 4.83-4.74 (m, 14H), 4.30 (dd, *J* = 4.12, 4.85 Hz, 7H), 4.15-4.07 (m, 14H), 3.95-3.72 (m, 14H), 3.63-3.52 (m, 7H), 3.44-3.31 (m, 7H), 3.24-2.88 (m, 14H), 2.84-2.59 (m, 7H), 2.56-2.41 (m, 7H), 2.12-1.94 (m, 133H), 1.04 (d, *J* = 6.87 Hz, 21H) ; ^{13}C NMR ($CDCl_3$, 100 MHz): δ_C:170.68, 170.01, 169.88, 169.83, 169.59, 169.49, 114.12, 97.86, 97.00, 72.24, 72.07, 71.84, 69.52, 69.23, 68.61, 66.05, 62.39, 37.83, 34.13, 33.87, 31.98, 31.68, 29.73, 29.67, 29.55, 29.41, 29.20, 28.99, 22.74, 20.92, 20.82, 20.77, 20.72, 14.17; HRMS: (m/z) calculated for $C_{198}H_{284}NaS_7O_{110}$ $[M+Na]^+$ = 4645.4674; found $[M+2Na/2]^+$ = 2345.0986.

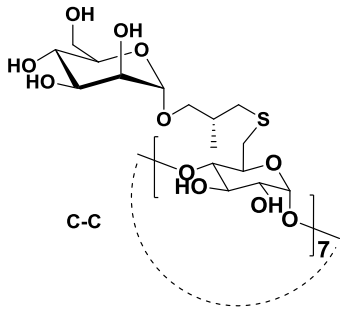

Deacetylation of Per-glycosylated *β*-cyclodextrin derivatives (C-C). The sugar-substituted *β*-cyclodextrin (0.06 g, 0.012 mmol) was dissolved in MeOH (10 mL). Then NaOMe (35 mg, 0.64 mmol) was added and stirred for 2h at r.t. The mixture was neutralized with amberlite–IR120H$^+$ resin, filtered and concentrated *in vacuo* to afford the final compound **C-C** (0.02, 51%) as a white solid. $[\alpha]^D_{25}$ + 138 (c 0.1%, CHCl3): ^{1}H NMR ($CDCl_3$, 400 MHz): δ_H: 5.04 (bs, 7H), 4.76-4.75 (m, 7H), 3.86-3.80 (m, 14H), 3.77-3.70 (m, 28H), 3.61-3.44 (m, 34H), 3.42-3.28 (m, 14H), 3.23-3.11 (m, 7H), 2.88-2.63(m, 12H), 2.58-2.48 (m, 7H), 2.01-1.88 (m, 7H), 0.97 (bs, 21H) ; ^{13}C NMR ($CDCl_3$, 100 MHz): δ_C: 102.17, 101.91, 101.30, 99.97, 73.47, 72.75, 72.24, 71.77 71.44, 71.19, 70.69, 70.48, 69.94, 69.73, 66.80, 66.63, 60.86, 62.44, 60.86, 37.02, 33.49, 29.82, 29.22, 16.36, 15.76; HRMS: (m/z) calculated for $C_{114}H_{200}NaS_7O_{68}$[M+Na]$^+$ = 2881.0237; found $[M+2Na/2]^+$ = 1463.9823.

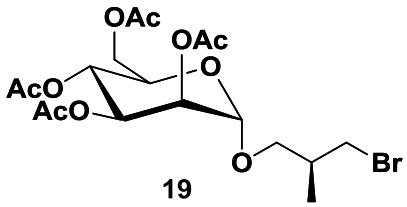

19

(2R,3R,4S,5S,6S)-2-(acetoxymethyl)-6-((S)-3-bromo-2-methylpropoxy)tetrahydro-2H-pyran-3,4,5-triyl triacetate (19). Per-acetylated sugar **15** (0.6 g, 1.53 mmol) was dissolved in CH_2Cl_2 (10 mL). Then (S)-(+)-3-Bromo-2-methyl-1-propanol (0.49 mL, 4.61 mmol) was added. Then $BF_3.Et_2O$ (0.8 mL, 6.12 mmol) and at 0 ^oC for 1h and the reaction mixture was allowed to stir at room temperature for 12 h. Completion of reaction was monitored by TLC. After completion, the reaction mixture was neutralized with triethylamine, followed by extraction with ethylacetate:water (1:1) mixture. Organic layer was dried over anhydrous Na_2SO_4 and concentrated under reduced pressure to give crude product, which was purified by flash column chromatography (silica gel, Petroleum ether/EtOAc = 50:50) to afford the product **19** (0.67 g, 91%) as a white solid. $[\alpha]^D_{25}$ +48.4 (c 0.1%, CHCl3): R_f = 0.50 (Petroleum ether:EtOAc = 50:50): ^1H NMR ($CDCl_3$, 400 MHz): δ_H: 5.26-5.23 (m, 2H), 5.21-5.19 (m, 1H), 4.77 (d, *J* = 1.37 Hz, 1H), 4.26-4.21 (m, 1H), 4.11-4.06 (m,1H), 4.01-3.97 (m, 1H), 3.69-3.64 (m, 1H), 3.58-3.52 (m, 1H), 3.42-3.39 (m, 1H), 3.33-3.29 (m, 1H), 2.12-2.11 (m, 4H), 2.06 (s, 3H), 2.01 (s, 3H), 1.95 (s, 3H), 1.00 (d, *J* = 6.87 Hz, 3H) ; ^{13}C NMR ($CDCl_3$, 100 MHz): δ_C: 170.56, 169.99, 169.85, 169.69, 97.58, 70.20, 69.41, 69.11, 68.68, 65.89, 62.33, 37.73, 34.60, 20.86, 20.73, 20.70, 20.66, 15.68; HRMS: (m/z) calculated for $C_{18}H_{27}NaBrO_{10}[M+Na]^+$ = 507.0665; found = 507.0667.

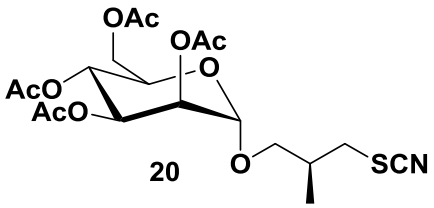

20

(2R,3R,4S,5S,6S)-2-(acetoxymethyl)-6-((S)-2-methyl-3-thiocyanatopropoxy)tetrahydro-2H-pyran-3,4,5-triyl triacetate (20). Glycosylated sugar derivative **19** (0.5 g, 1.02 mmol) was dissolved in DMF (10 mL). Then potassium thiocyanate (0.4 g, 4.08 mmol) was added and stirred at 80^oC for 12 h. The reaction mixture was diluted with 100 ml EtOAC and washed several times with water. The organic layer was dried over anhydrous Na_2SO_4 and concentrated under reduced pressure to give crude product, which was purified by flash

column chromatography (silica gel, Petroleum ether:EtOAc = 75:25) to afford the product **20** (0.44 g, 93%) as a white solid. $[\alpha]^{D}_{25}$ + 26 (c 0.1%, CHCl3): R_f = 0.75 (Petroleum ether:EtOAc = 75:25): ^{1}H NMR ($CDCl_3$, 400 MHz) δ_H: 5.28-5.25 (m, 2H), 5.23-5.21 (m, 1H), 4.79 (d, *J* = 1.37 Hz, 1H), 4.28-4.24 (m, 1H), 4.12 (dd, *J* = 2.75, 2.75 Hz, 1H), 3.95-3.90 (m, 1H), 3.71-3.67 (m, 1H), 3.51-3.47 (m, 1H), 3.10-3.05 (m, 1H), 2.98-2.93 (m, 1H), 2.29-2.23 (m, 1H), 2.14 (s, 3H), 2.09 (s, 3H), 2.03 (s, 3H), 1.98 (s, 3H), 1.15 (d, *J* = 7.33 Hz, 3H) ; ^{13}C NMR ($CDCl_3$, 100 MHz): δ_C:170.70, 170.15, 170.03, 169.82, 112.44, 97.78, 70.39, 69.34, 69.06, 68.92, 66.01, 62.55, 37.46, 34.06, 20.96, 20.84, 20.79, 20.7616.24; HRMS: (m/z) = calculated for $C_{19}H_{27}NaSO_{10}[M+Na]^+$ = 484.1253; found = 484.1262.

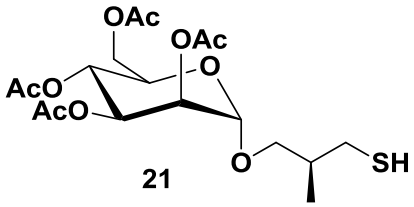

21

(2R,3R,4S,5S,6S)-2-(acetoxymethyl)-6-((S)-3-mercapto-2-methylpropoxy)tetrahydro-2H-pyran-3,4,5-triyl triacetate (21). Peracetylated thiocyanate-sugar derivative **20** (0.35 g, 0.75 mmol) was dissolved in glacial acetic acid (30 mL). Then Zn dust (0.3 g, 4.55 mmol) was added and refluxed at 70 ^{o}C for 4 h. The compound was filtered to remove zinc dust. The organic layer was quenched with water (50 mL). Then product was extracted with EtOAc (3 X 50 mL) and dried over anhydrous Na_2SO_4. Organic layer was concentrated under reduced pressure to give crude product. Organic layer was concentrated under reduced pressure to give product **21** (0.22 g, 69%) as a syrup. This was further used for next reaction without purification. $[\alpha]^{D}_{25}$ + 70 (c 0.1%, CHCl3): ^{1}H NMR ($CDCl_3$, 400 MHz): δ_H: 5.23-5.29 (m, 2H), 5.23-5.22 (m, 1H), 4.78 (d, *J* = 1.37 Hz, 1H), 4.27-4.23 (m, 1H), 4.12 (dd, *J* = 1.83 Hz, 1H), 3.98-3.95 (m, 1H), 3.70-3.66 (m, 1H), 3.37-3.33 (m, 1H), 2.66-2.59 (m, 1H), 2.57-2.50 (m, 1H), 2.14 (s, 3H), 2.09 (s, 3H), 2.03 (s, 3H), 1.98-1.97 (m, 4H), 1.23 (s, 1H), 1.00 (d, *J* = 6.87 Hz, 3H) ; ^{13}C NMR ($CDCl_3$, 100 MHz): δ_C: 170.75, 170.20, 170.01, 169.86, 97.75, 71.08, 69.60, 69.19, 68.72, 66.17, 62.56, 35.74, 29.77, 27.98, 20.98, 20.85, 20.80, 20.77, 15.84; HRMS: (m/z) calculated for $C_{18}H_{28}NaSO_{10}[M+Na]^+$ = 459.1301; found = 459.1294.

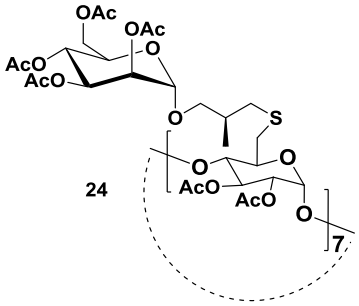

Synthesis of sugar substituted *β*-cyclodextrin (24). Per-acetylated 6'-Iodo-*β*-cyclodextrin **22** (0.15 g, 0.06 mmol) and the per-acetylated thio-sugar **21** (0.34 g, 0.78 mmol) in DMF (10 mL) was dissolved and Cs_2CO_3 (0.25 g, 0.78 mmol) added, stirred at room temperature for 72 h. The reaction mixture was diluted with 100 ml EtOAc and washed several times with water. The organic layer was dried over anhydrous Na_2SO_4 and concentrated under reduced pressure to give crude product, which was purified by flash column chromatography (silica gel, CH_2Cl_2:MeOH = 93:7) to afford the product **24** (0.16 g, 60%) as a white solid. $[\alpha]^{D}_{25}$ +66.4 (c 0.1%, CHCl3): R_f = 0.40 (CH_2Cl_2:MeOH = 93:7): ^{1}H NMR ($CDCl_3$, 400 MHz) δ_H: 5.28-5.21 (m, 32H), 5.12 (d, *J* = 3.66 Hz, 7H), 4.84-4.75 (m, 14H), 4.30 (dd, *J* = 4.58 Hz, 7H), 4.15-4.07 (m, 14H), 3.96-3.91(m, 14H), 3.67-3.63 (m, 7H), 3.41-3.37 (m, 7H), 3.10-32.95 (m, 14H), 2.76-2.71 (m, 7H), 2.60-2.55 (m, 7H), 2.12 (s, 21H), 2.08 (s, 21H), 2.06-1.99 (m, 79H), 1.94 (s, 12H), 1.05 (d, J = 6.7 Hz, 21H); ^{13}C NMR ($CDCl_3$, 100 MHz): δ_C: 170.68, 170.00, 169.86, 169.83, 169.40, 115.83, 114.12, 97.78, 96.94, 72.01, 71.85, 71.71, 71.67, 71.17, 70.62, 70.42, 69.49, 69.26, 68.61, 66.00, 62.37, 37.66, 34.09, 33.87, 33.48, 31.97, 31.67, 29.73, 29.66, 29.55, 29.40, 29.20, 28.99, 22.74, 20.91, 20.81, 20.76, 20.71; HRMS (m/z) calculated for $C_{198}H_{284}NaS_7O_{110}[M+Na]^+$ = 4645.4674; found: $[M+2Na/2]^+$ = 2345.9976.

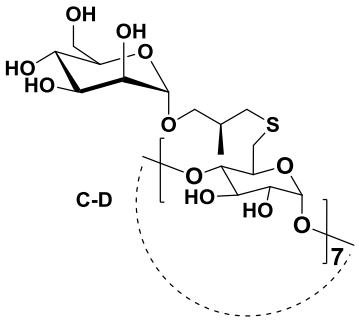

Deacetylation of Per-glycosylated *β*-cyclodextrin derivatives (C-D). The sugar-substituted *β*-cyclodextrin **24** (0.12 g, 0.025 mmol) was dissolved in MeOH (10 mL). Then NaOMe (68

mg, 1.26 mmol) was added and stirred for 2h at r.t. The mixture was neutralized with amberlite–IR120H$^+$ resin, filtered and concentrated *in vacuo* to afford the final compound **C-D** (0.03 g, 47%) as a white solid. $[\alpha]^D_{25}$ + 104.8 (c 0.1%, CHCl3): ^{1}H NMR ($CDCl_3$, 400 MHz): δ_H: 5.15 (bs, 7H), 4.93-4.87 (m, 7H), 4.00-3.98 (m, 14H), 3.94-3.89 (m, 14H), 3.85-3.78 (m, 14H), 3.72-3.63 (m, 34H), 3.56-3.51 (m, 12H), 3.38-3.32 (m, 7H), 3.00-2.96 (m, 14H), 2.67-2.52 (m, 7H), 2.14-2.00 (m, 7H), 1.09 (d, *J* = 6.6 Hz, 21H) ; ^{13}C NMR ($CDCl_3$, 100 MHz): δ_C: 99.90, 99.73, 72.99, 72.92, 72.86, 70.81, 70.69, 70.09, 70.01, 66.71, 66.64, 60.93, 60.86, 37.07, 29.81, 29.75, 29.72, 17.09, 16.77, 16.71; HRMS (m/z) calculated for $C_{114}H_{200}NaS_7O_{68}[M+Na]^+$ = 2881.0237; found:$[M+2Na/2]^+$ = 1463.9801.

Formation of host-guest complexes.

Ruthenium Complexes with Native *β*-Cyclodextrin (M-1A, M-2A, M-3A).

To a solution of Ruthenium complex **(Ru-1/2/3)** (3.0 mg. 1.4 µmol) in MeOH (3 mL) was added native *β*-CD (10.0 mg, 9.1 mol) and the reaction mixture was kept at r.t. for 12 h. The solvent was then removed under reduced pressure and dried under *high vacuo*. The product was then dissolved in H_2O (4 mL) and lyophilized to afford the product **M-1A** or **M-2A** or **M-3A** as a red solid.

M-1A: ^{1}H NMR (600 MHz, D_2O) δ_H: 8.96 (d, 6H), 7.84-7.79 (m, 6H), 7.68-7.63 (m, 6H), 3.81-3.69 (m, 266), 3.53-3.45 (m, 172), 2.15 (bs, 18H), 2.01 (bs, 36H), 1.67 (bs, 36H), 1.41 (bs, 18H).

M-2A: ^{1}H NMR (600 MHz, D_2O) δ_H: 8.96 (s, 6H), 7.87-7.78 (s, 6H), 7.68-7.63 (s, 6H), 3.81-3.69 (m, 266), 3.53-3.45 (m, 172), 2.15 (bs, 18H), 2.01 (bs, 36H), 1.67 (bs, 36H), 1.41 (bs, 18H).

M-3A: ^{1}H NMR (600 MHz, D_2O) δ_H: 8.96 (s, 6H), 7.88-7.81 (s, 6H), 7.69-7.63 (s, 6H), 3.82-3.71 (m, 266H), 3.55-3.46 (m, 172H), 2.16 (bs, 18H), 2.04 (bs, 36H), 1.68 (bs, 36H), 1.42 (bs, 18H).

Ruthenium Complexes with chiral *β*-Cyclodextrin-Based *O*-α-Mannoside (M-1B to M-3B, M-1C to M-3C and M-1D to M-3D).

Ru-series **Ru-1** to **Ru-3** were mixed in water with stoichiometric amounts of chiral and non-chiral mannose *β*-CD derivatives (**C-A** to **C-D**). Depending on the complex, different solubilities were observed. Using different mixing times and temperature, the supramolecular

inclusion complexes of the Ru-CDMan-series were obtained and were also found to be soluble in water.

M-1B: ^{1}H NMR (600 MHz, D_2O) δ_H: 8.95 (bs, 6H), 7.87 (bs, 6H), 7.73 (bs, 6H), 5.02 (bs, 42H), 4.42-3.37 (m, 657H), 2.87 (bs, 327H), 2.07 (bs, 54H), 1.76 (bs, 36H), 1.44 (bs, 18H).

M-2B: ^{1}H NMR (600 MHz, D_2O): δ_H: 8.96 (bs, 6H), 7.87 (bs, 6H), 7.71 (bs, 6H), 5.40-4.70 (m, 42H), 4.42-3.37 (m, 760H), 2.87 (bs, 224H), 2.36-2.26 (m, 18H), 2.06 (bs, 36H),1.65 (bs, 36H), 1.44 (bs, 18H).

M-3B: ^{1}H NMR (600 MHz, D_2O) δ_H: 8.96 (bs, 6H), 7.87 (bs, 6H), 7.71 (bs, 6H), 5.02 (bs, 42H), 4.42-3.44 (m, 806H), 2.87 (bs, 178H), 2.07 (bs, 54H), 1.76 (bs, 36H), 1.44 (bs, 18H).

M-1C: ^{1}H NMR (600 MHz, D_2O): δ_H: 8.95 (sb, 6H), 7.96 (bs, 6H), 7.86 (bs, 6H), 5.01 (bs, 42H), 4.11-3.07 (m, 582H), 2.81-2.51 (m, 352H), 2.20-2.04 (m, 92H), 1.98 (bs, 54H), 1.76 (bs, 36H), 1.43 (bs, 18H), 0.98 (bs, 126H).

M-2C: ^{1}H NMR (600 MHz, D_2O): δ_H: 8.95 (bs, 6H), 7.86 (bs, 6H), 7.65 (bs, 6H), 5.20 (bs, 42H), 3.85-3.69 (m, 611H), 3.59-3.38 (m, 341H), 2.83-2.54 (m, 74H), 2.26-1.81 (bs, 54H), 1.59 (bs, 54H), 0.95 (bs, 126H).

M-3C: ^{1}H NMR (600 MHz, D_2O): δ_H: 8.96 (bs, 6H), 7.87 (bs, 6H), 7.71 (bs, 6H), 5.02 (bs, 42H), 4.09-3.69 (m, 545H), 3.58-3.50 (m, 274H), 3.39-3.24 (m, 133H), 2.96-2.83 (m, 74H), 1.96 (bs, 54H), 1.82-1.63 (m, 36H), 1.43 (bs, 18H), 0.95 (bs, 126H).

M-1D: ^{1}H NMR (600 MHz, D_2O): δ_H: 8.92 (bs, 6H), 7.76 (bs, 6H), 7.52 (bs, 6H), 3.75-3.58 (m, 375H), 3.47-3.34 (m, 320H), 3.32-3.20 (m, 81H), 3.10-2.98 (m, 81H), 2.88-2.21 (m, 211H), 2.00-1.85 (m, 90H), 1.21 (bs, 18H), 0.94 (bs, 126H).

M-2D: ^{1}H NMR (600 MHz, D_2O): δ_H: 8.96 (bs, 6H), 7.87 (bs, 6H), 7.71 (bs, 6H), 5.02 (bs, 42H), 4.12-3.62 (m, 472H), 3.49-3.42 (m, 302H), 3.34-3.18 (m, 178H), 2.92-2.77 (m, 74H), 1.96 (bs, 54H), 1.79-1.45 (m, 54H), 0.95 (bs, 126H).

M-3D: ^{1}H NMR (600 MHz, D_2O): δ_H: 8.94 (bs, 6H), 7.87 (s, 6H), 7.69 (s, 6H), 5.01 (bs, 42H), 4.14-3.70 (m, 387), 3.59-3.50 (m, 240H), 3.44-3.37 (m, 112H), 2.96-2.73 (m, 93H), 2.62-2.47 (m, 71H), 2.21-2.07 (m, 123H), 1.98 (bs, 54H), 1.76 (bs, 36H), 1.42 (bs, 18H), 0.97 (bs, 126H).

2.5. References

1. C. R. Bertozzi, L. L. Kiessling, *Science* 2001, **291**, 2357.
2. L. L. Kiessling, J. E. Gestwicki, L. E. Strong, *Curr. Opin. Chem. Bio*l., 2000, **4**, 696.
3. J. R. Kramer, T. J. Deming, *J. Am. Chem. Soc.*, 2010, **132**, 15068-15071.
4. J. L. Jiménez Blanco, C. Ortiz Mellet, J. M. García Fernández, *Chem. Soc. Rev.*, 2013, **42**, 4518.
5. L. L. Kiessling, J. C. Grim, *Chem. Soc. Rev.*, 2013, **42**, 4476.
6. Y. Ruff, E. Buhler, S. J. Candau, E. Kesselman, Y. Talmon, J. M. Lehn, *J. Am. Chem. Soc.*, 2010, **132**, 2573.
7. S. Zhanq, R. O. Moussodia, S. Vertesy, S. Andre, M. L. Klein, H. J. Gabius, V. Percec, *Proc. Natl. Acad. Sci. U.S.A.*, 2015, **112**, 5585.
8. S. Zhanq, R. O. Moussodia, C. Murzeau, H. J. Sun, M. L. Klein, S. Vértesy, S. André R. Roy, H. J. Gabius, V. Percec, *Angew. Chem. Int. Ed.*, 2015, **54**, 4036.
9. Q. Xiao, S. S. Yadavalli, S. Zhang, S. E. Sherman, E. Fiorin, L. da Silva, D. A. Wilson, D. A. Hammer, S. André, H. J. Gabius, M. L. Klein, M. Goulian, V. Percec, *Proc. Natl. Acad. Sci. U.S.A.*, 2016, **113**, E1134.
10. S. Zhang, Q. Xiao, S. E. Sherman, A. Muncan, A. D. Ramos Vicente, Z. Wang, D. A. Hammer, D. Williams, Y. Chen, D. J. Pochan, S. Vértesy, S. André, M. L. Klein, H. J. Gabius, V. Percec, *J. Am. Chem. Soc.*, 2015, **137**, 13334.
11. R. Roy, T. C. Shiao, *Chem. Soc. Rev.*, 2015, **44**, 3924.
12. Y. M. Chabre, R. Roy, *Chem. Soc. Rev.*, 2013, **42**, 4657.
13. J. Luczkowiak, A. Muñoz, M. Sánchez-Navarro, R. Ribeiro-Viana, A. Ginieis, B. M. Illescas, N. Martín, R. Delgado, J. Rojo, *Biomacromolecules*, 2013, **14**, 431.
14. N. Varga, I. Sutkeviciute, R. Ribeiro-Viana, A. Berzi, R. Ramdasi, A. Daghetti, G. Vettoretti, A. Amara, M. Clerici, J. Rojo, F. Fieschi, A. Bernardi, *Biomaterials*, 2014, **35**, 4175.

15. A. Martinez, C. Ortiz Mellet, J. M. Garcia Fernandez, *Chem. Soc. Rev.*, 2013, **42**, 4746.

16. M. Delbianco, P. Bharate, S. Varela-Aramburu, P. H. Seeberger, *Chem. Rev.*, 2016, **116**, 1693.

17. Z. Qi, P. Bharate, C. H. Lai, B. Ziem, C. Böttcher, A. Schulz, F. Beckert, B. Hatting, R. Mülhaupt, P. H. Seeberger, R. Haag, *Nano Lett*., 2015, **15**, 6051.

18. H. Isobe, K. Cho, N. Solin, D. B. Werz, P. H. Seeberger, E. Nakamura, *Org. Lett.*, 2007, **9**, 4611.

19. T. Ohta, N. Miura, N. Fujitani, F. Nakajima, K. Nijkura, R. Sadamoto, C. T. Guo, T. Suzuki, Y. Suzuki, K. Monde, S. Nishimura, *Angew. Chem. Int. Ed.*, 2003, **42**, 5186.

20. P. M. Chaudhary, S. Sangabathuni, R. V. Murthy, A. Paul, H. V. Thulasiram, R. Kikkeri, *Chem. Commun.*, 2015, **51**, 15669.

21. S. Sangabathuni, R. V. Murthy, P. M. Chaudhary, M. Surve, A. Banerjee, R. Kikkeri, *Nanoscale*, 2016, **8**, 12729.

22. D. Ponader, P. Maffre, J. Aretz, D. Pussak, N. M. Ninnemann, S. Schmidt, P. H. Seeberger, C. Rademacher, G. U. Nienhaus, L. Hartmann, *J. Am. Chem. Soc.*, 2014, **136**, 2008.

23. V. Percec, P. Leowanawat, H. J. Sun, O. Kulikov, C. D. Nusbaum, T. M. Tran, A. Bertin, D. A. Wilson, M. Peterca, S. Zhang, N. P. Kamat, K. Vargo, D. Moock, E. D. Johnston, D. A. Hammer, D. J. Pochan, Y. Chen, Y. M. Chabre, T. C. Shiao, M. Bergeron-Brlek, S. André, R. Roy, H. J. Gabius, P. A. Heiney, *J. Am. Chem. Soc.*, 2013, **135**, 9055.

24. Q. Xiao, S. Zhang, Z. Wang, S. E. Sherman, R. O. Moussodia, M. Peterca, A. Muncan, D. R. Williams, D. A. Hammer, S. Vertesy, S. Andre, H. J. Gabius, M. L. Klein, V. Percec, *Proc. Natl. Acad. Sci. U.S.A.*, 2016, **113**,1162.

25. S. Zhanq, R. O. Moussodia, H. J. Sun, P. Leowanawat, A. Muncan, C. D. Nusbaum, K. M. Chelling, P. A. Heiney, M. L. Klein, S. Andre, R. Roy, H. J. Gabius, V. Percec, *Angew. Chem. Int. Ed.*, 2014, **53**, 10899.

26. Y. M. Chabre, R. Roy, *Chem. Soc. Rev.*, 2013, **42**, 4657.

27. D. Appelhans, B. Klajnert-Maculewicz, A. Janaszewska, J. Lazniewska, B. Voit, *Chem. Soc. Rev.*, 2015, **44**, 3968.

28. D. Seebach, P. B. Rheiner, G. Greiveldinger, T. Butz, H. Sellner, *Top. Curr. Chem.*, 1998, **197**, 125.

29. M. Liu, L. Zhang, T. Wang, *Chem. Rev.*, 2015, 115, 7304.

30. E. C. Constable, *Chem. Soc. Rev.*, 2013, 42, 1637.

31. N. S. Kehr, *Biomacromolecules*, 2016, **17**, 1117.

32. N. S. Kehr, H. –J. Galla, K. Riehemann, H. Fuchs, *RSC. Adv.*, 2015, **5**, 5704.

33. D. Schwefel, C. Maierhofer, J. G. Beck, S. Seeberger, K. Diederichs, H. M. Möller, W. Welte, V. Wittmann, *J. Am. Chem. Soc.*, 2010, **132**, 8704.

34. V. Wittmann, S. Seeberger, *Angew. Chem. Int. Ed.*, 2000, **39**, 4348.

35. D. Grünstein, M. Maglinao, R. Kikkeri, M. Collot, K. Barylyuk, B. Lepenies, F. Kamena, R. Zenobi, P. H. Seeberger, *J. Am. Chem. Soc.*, 2011, **133**, 13957.

36. R. Kikkeri, I. Garcia-Rubio, P. H. Seeberger, *Chem. Commun.*, 2009, **8**, 235.

37. R. Kikkeri, D. Grünstein, P. H. Seeberger, *J. Am. Chem. Soc.*, 2010, **132**, 10230.

38. N. Ousaka, Y. Takeyama, H. Iida, E. Yashima, *Nat. Chem.*, 2011, **3**, 856.

39. P. Sun, A. Krishnan, A. Yadav, S. Singh, F. M. MacDonnell, D. W. Armstrong, *Inorg. Chem.*, 2007, **46**, 10312.

40. C. Fu, M. Wenzel, E. Treutlein, K. Harms, E. Meggers, *Inorg. Chem.*, 2012, **51**, 10004.

41. K. Barylyuk, R. M. Balabin, D. Grünstein, R. Kikkeri, V. Frankevich, P. H. Seeberger, R. Zenobi, *J. Am. Soc. Mass. Spectrom.*, 2011, **22**, 1167.

42. I. Dolamic, B. Varnholt, T. Bürgi, *Nat. Commun.*, 2015, **6**, 7117.

43. M. Kodaka, *J. Am. Chem. Soc.*, 1993, **115**, 3702.

44. R. T. Lee, T. L. Hsu, S. K. Huang, S. L. Hsieh, C. H. Wong, Y. C. Lee, *Glycobiology*, 2011, **21**, 512.

45. B. Lepenies, J. Lee, S. Sonkaria, *Adv. Drug. Deliv. Rev.*, 2013, **65**, 1271.

46. S. K. Wang, P. H. Liang, R. D. Astronomo, T. L. Hsu, S. L. Hsieh, D. R. Burton, C. H. Wong, *Proc. Natl. Acad. Sci. U.S.A.*, 2008, **105**, 3690.

47. M. Maglinao, M. Eriksson, M. K. Schlegel, S. Zimmermann, T. Johannssen, S. Götze, P. H. Seeberger, B. Lepenies, *J. Control. Release.*, 2014, **175**, 36.

48. A. Cambi, M. Koopman, C. G. Figdor, *Cell. Microbiol.*, 2005, **7**, 481.

49. T. L. Hsu, S. C. Cheng, W. B. Yang, S. W. Chin, B. H. Chen, M. T. Huang, S. L. Hsieh, C. H. Wong, *J. Biol. Chem.*, 2009, **284**, 34479.

50. K. Neumann, M. Castineiras-Vilarino, U. Höckendorf, N. Hannesschläger, S. Lemeer, D. Kupka, S. Meyermann, M. Lech, H. J. Anders, B. Kuster, D. H. Busch, A. Gewies, R. Naumann, O. Groß, J. Ruland, *Immunity*, 2014, **40**, 389.

51. H. Schoenen, B. Bodendorfer, K. Hitchens, S. Manzanero, K. Werninghaus, F. Nimmerjahn, E. M. Agger, S. Stenger, P. Andersen, J. Ruland, G. D. Brown, C. Wells, R. Lang, *J. Immunol.*, 2010, **184**, 2756.

52. S. Menon, K. Rosenberg, S. A. Graham, E. M. Ward, M. E. Taylor, K. Drickamer, D. E. Leckband, *Proc. Natl. Acad. Sci. U.S.A.*,2009, **106**, 11524.

53. P. W. P. Hong, S. Nguyen, S. Young, S. V. Su, B. Lee, *J. Virology.*, 2007, **81**, 8325.

54. D. A. Mitchell, A. J. Fadden, K. Drickamer, *J. Bio. Chem*., 2001, **276**, 28939.

55. A. Kotar, T. Tomasic, M. Lenarcic Zivkovic, G. Jug, J. Plavec, M. Anderluh, *Org. Biomol. Chem.*, 2016, **14**, 862.

56. D. Suresh, A. Zambre, N. Chandra, T. J. Hoffman, C. J. Smith, J. D. Robertson, R. Kannan, *Bioconjugate Chem.*, 2014, **25**, 1565.

57. W. K. Lai, P. J. Sun, J. Zhang, A. Jennings, P. F. Lalor, S. Hubscher, J. A. McKeating, D. H. Adams, *Am. J. Pathol*. 2006, **169**, 200.

58. M. J. Frisch, G. W. Trucks, H. B. Schlegel, G. E. Scuseria, M. A. Robb, J. R. Cheeseman, G. Scalmani, V. Barone, B. Mennucci, G. A. Petersson, H. Nakatsuji, M. Caricato, X. Li, H. P. Hratchian, A. F. Izmaylov, J. Bloino, G. Zheng, J. L. Sonnenberg, M. Hada, M. Ehara, K. Toyota, R. Fukuda, J. Hasegawa, M. Ishida, T. Nakajima, Y. Honda, O. Kitao, H. Nakai, T. Vreven, J. A. Montgomery, J. E. Peralta, F. Ogliaro, M. Bearpark, J. J. Heyd, E. Brothers, K. N. Kudin, V. N. Staroverov, T. Keith, R. Kobayashi, J. Normand, K. Raghavachari, A. Rendell, J. C. Burant, S. S. Iyengar, J. Tomasi, M. Cossi, N. Rega, J. M. Millam, M. Klene, J.E. Knox, J. B. Cross, V. Bakken, C. Adamo, J. Jaramillo, R. Gomperts, R.E. Stratmann, O. Yazyev, A. J. Austin, R. Cammi, C. Pomelli, J. W. Ochterski, R. L. Martin, K. Morokuma, V. G. Zakrzewski, G. A. Voth, P. Salvador, J. J. Dannenberg, S. Dapprich, A. D. Daniels, O. Farkas, J. B. Foresman, J. V. Ortiz, J. Cioslowski, D. J. Fox, Gaussian Development Version, Revision H.12+ ed.; Gaussian Inc.: Wallingford, CT, 2010.

59. C. Lee, W. Yang, R. G. Parr, *Phys. Rev. B* 1988, **37**, 785.

60. A. D. Becke, *J. Chem. Phys*. 1993, **98**, 5648.

61. P. Fuentealba, H. Preuss, H. Stoll, L. Von Szentpály, *Chem. Phys. Lett.* 1982, **89**, 418.

62. A. D. Mclean, G. S. Chandler, *J. Chem. Phys.* 1980, **72**, 5639.

63. N. C. Fletcher, M. Nieuwenhuyzen, S. Rainey, *J. Chem. Soc. Dolton Trans.* 2001, 2641.

64. C. Garino, A. Ternzi, G. Barone, L. Salassa, *J. Chem. Edu.* 2016, **93**, 292.

65. G. Scalmani, M. J. Frisch, *J. Chem. Phys.* 2010, **132**, 114110.

66. M. Mayer, T. L. James, *J. Am. Chem. Soc.* 2004, **126**, 453.

2.6. Appendix I: Characterization Data of Synthesized Compounds…..

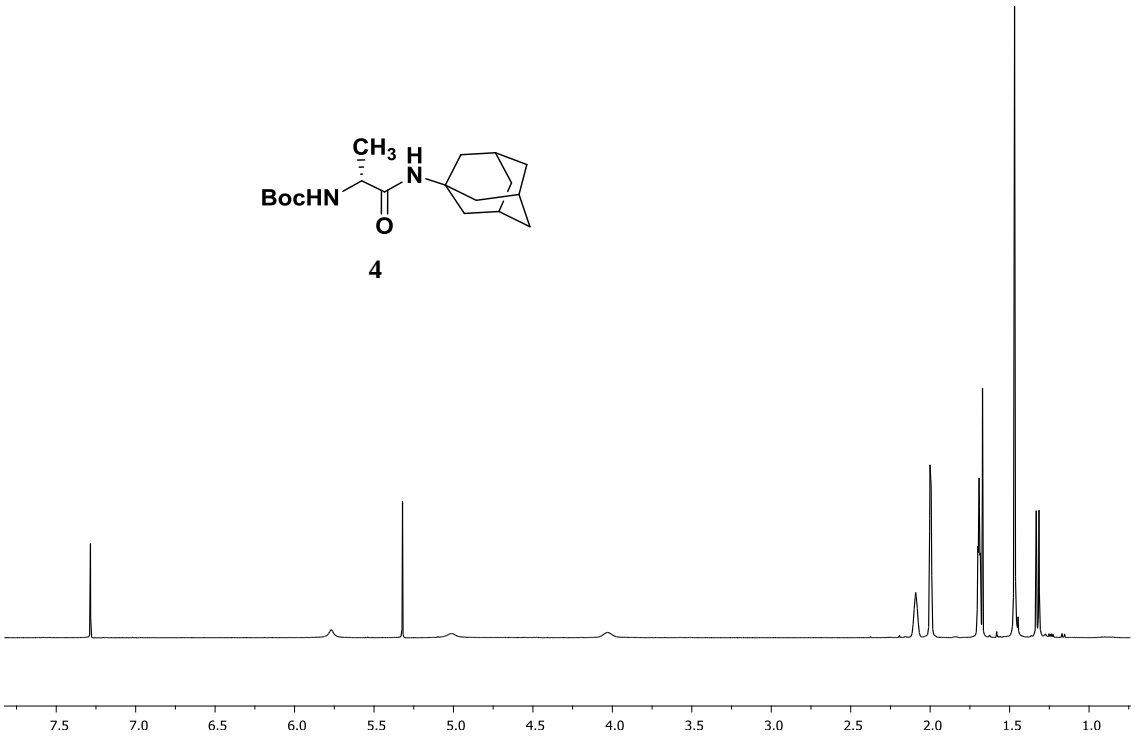

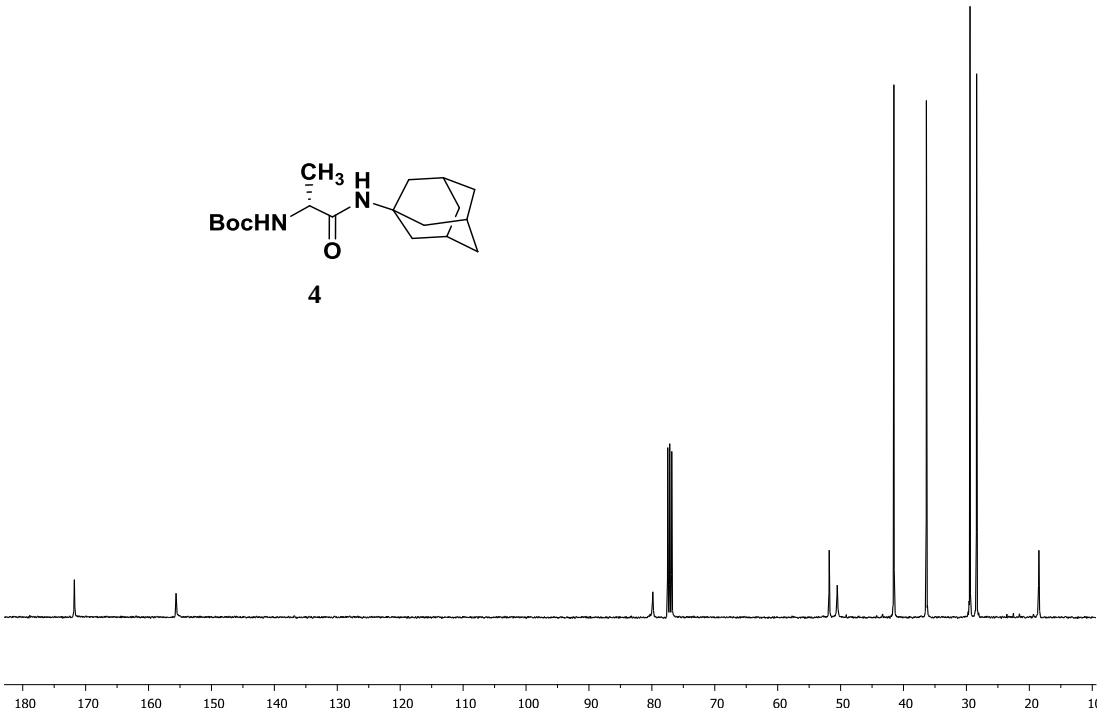

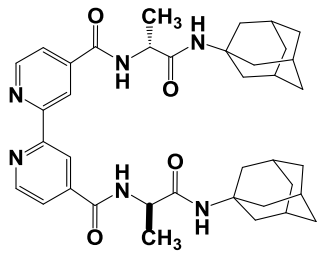

13

9.0
8.5
8.0
7.5
7.0
6.5
6.0
5.5
5.0
4.5
4.0
3.5
3.0
2.5
2.0
1.5

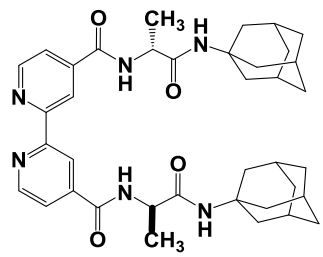

13

170
160
150
140
130
120
110
100
90
80
70
60
50
40
30
20
f1 (ppm)

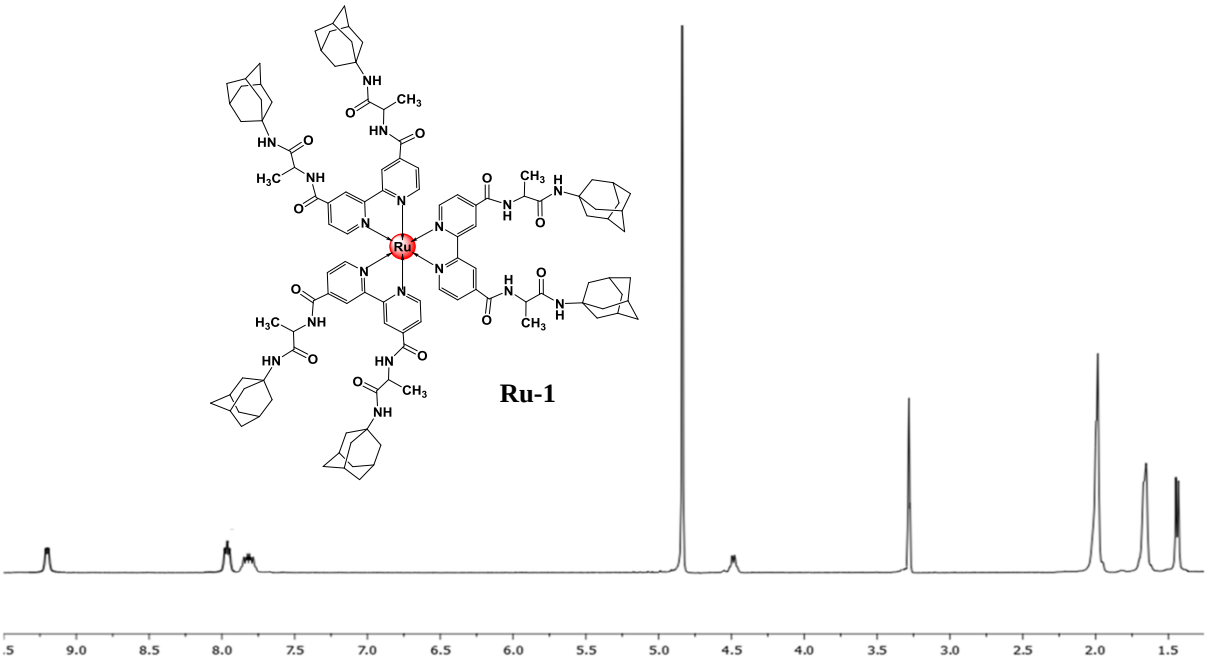
Ru-1
9.0
8.5
8.0
7.5
7.0
6.5
6.0
5.5
5.0
4.5
4.0
3.5
3.0
2.5
2.0
1.5

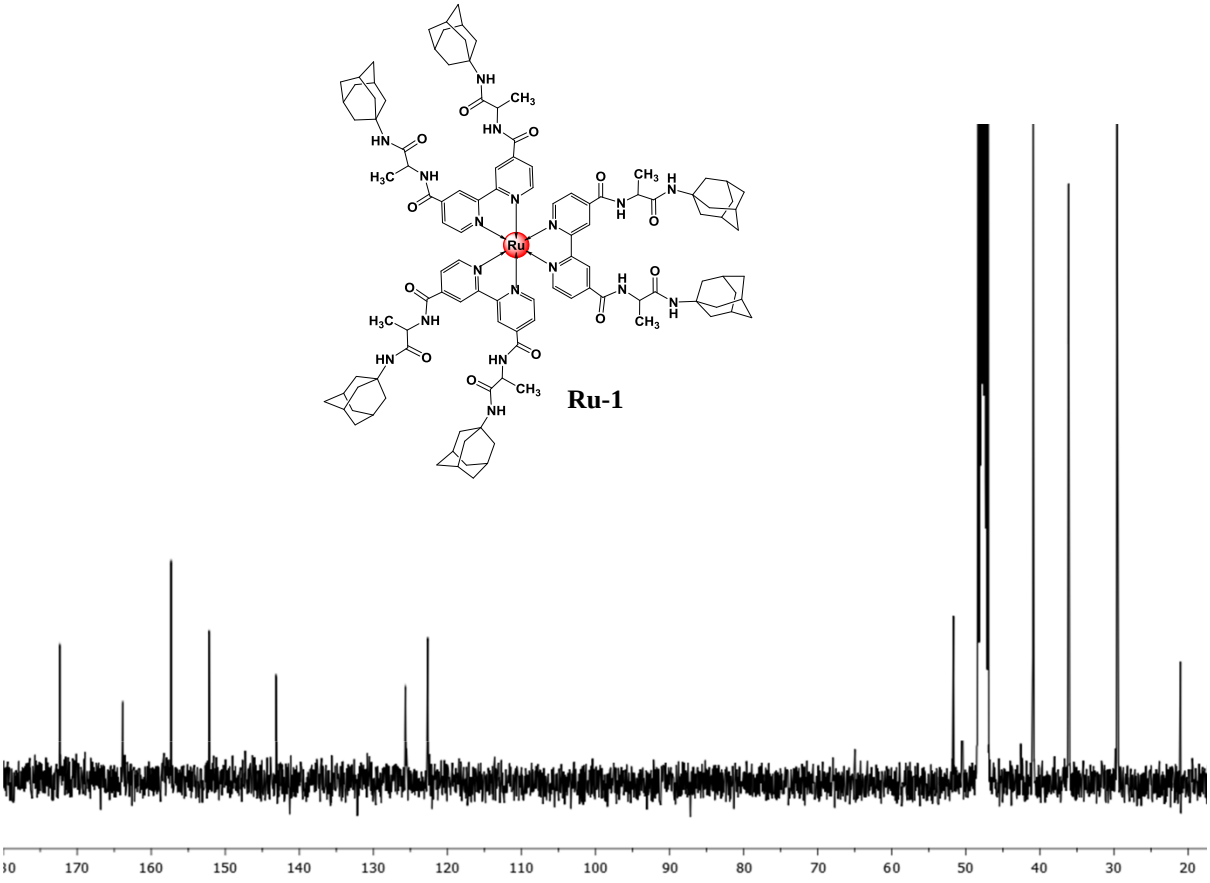
Ru-1
170
160
150
140
130
120
110
100
90
80
70
60
50
40
30
20

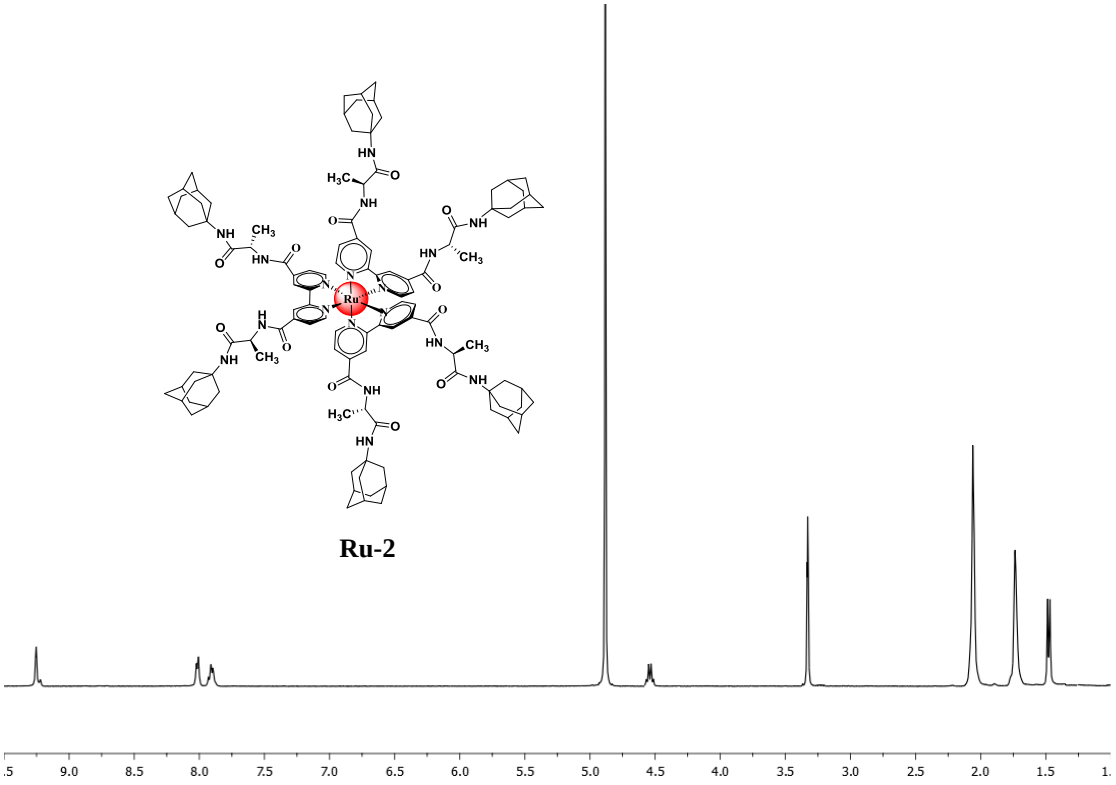
Ru
9.0
8.5
8.0
7.5
7.0
6.5
6.0
5.5
5.0
4.5
4.0
3.5
3.0
2.5
2.0
1.5

Ru-2

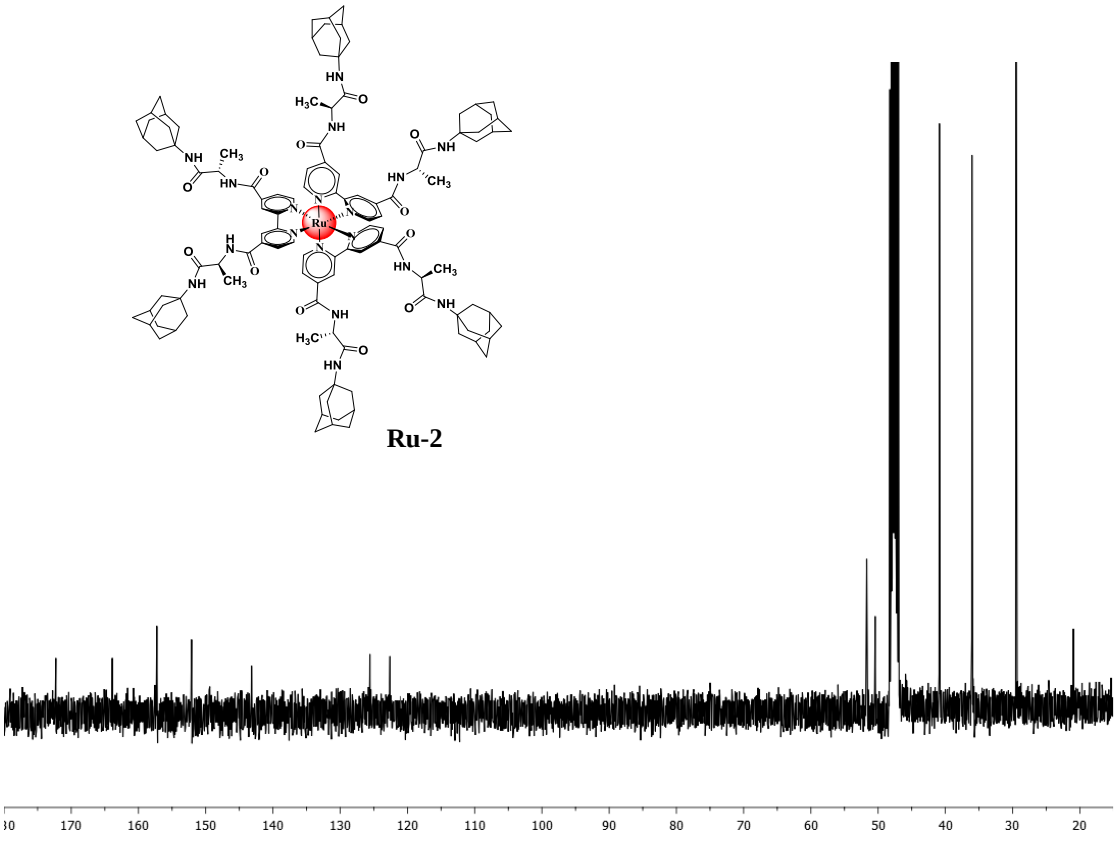
Ru
170
160
150
140
130
120
110
100
90
80
70
60
50
40
30
20

Ru-2

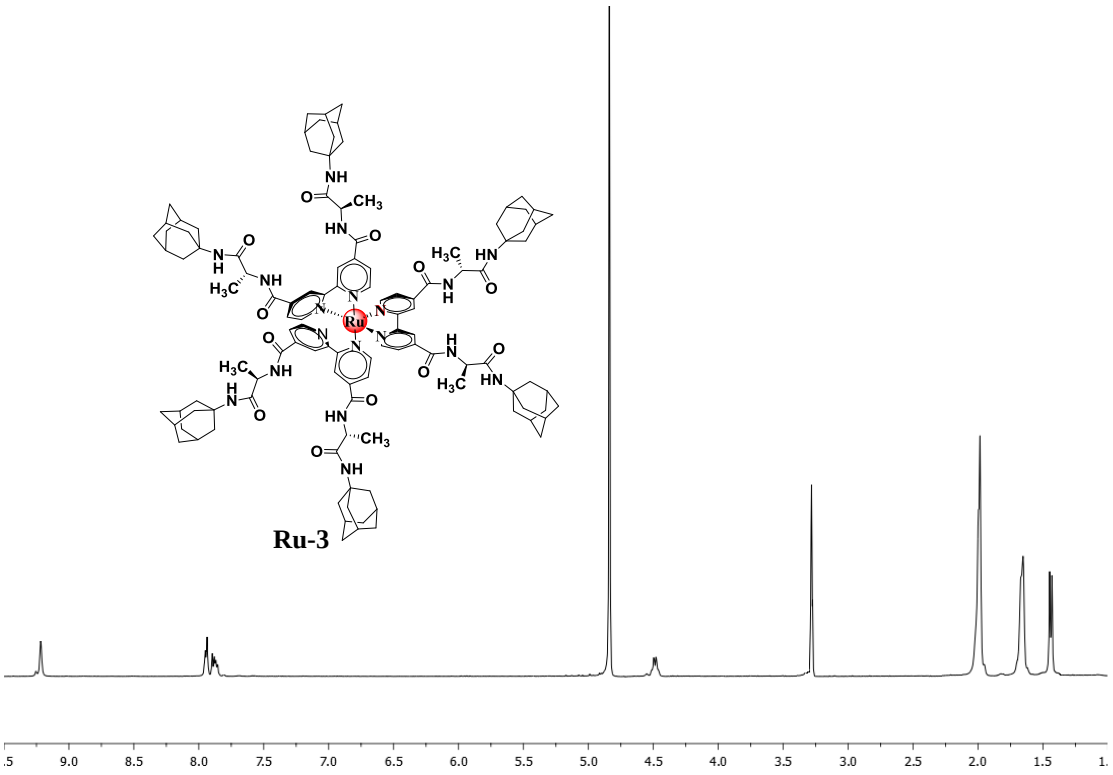
Ru-3
9.0
8.5
8.0
7.5
7.0
6.5
6.0
5.5
5.0
4.5
4.0
3.5
3.0
2.5
2.0
1.5

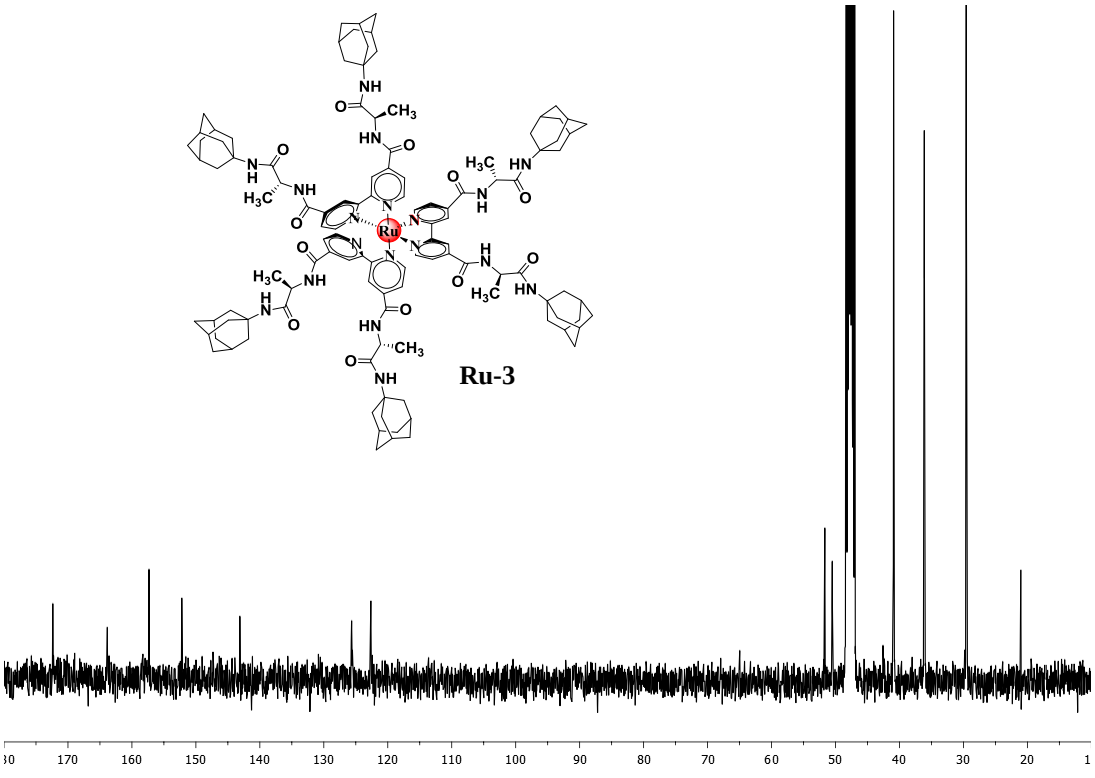
Ru-3
170
160
150
140
130
120
110
100
90
80
70
60
50
40
30
20

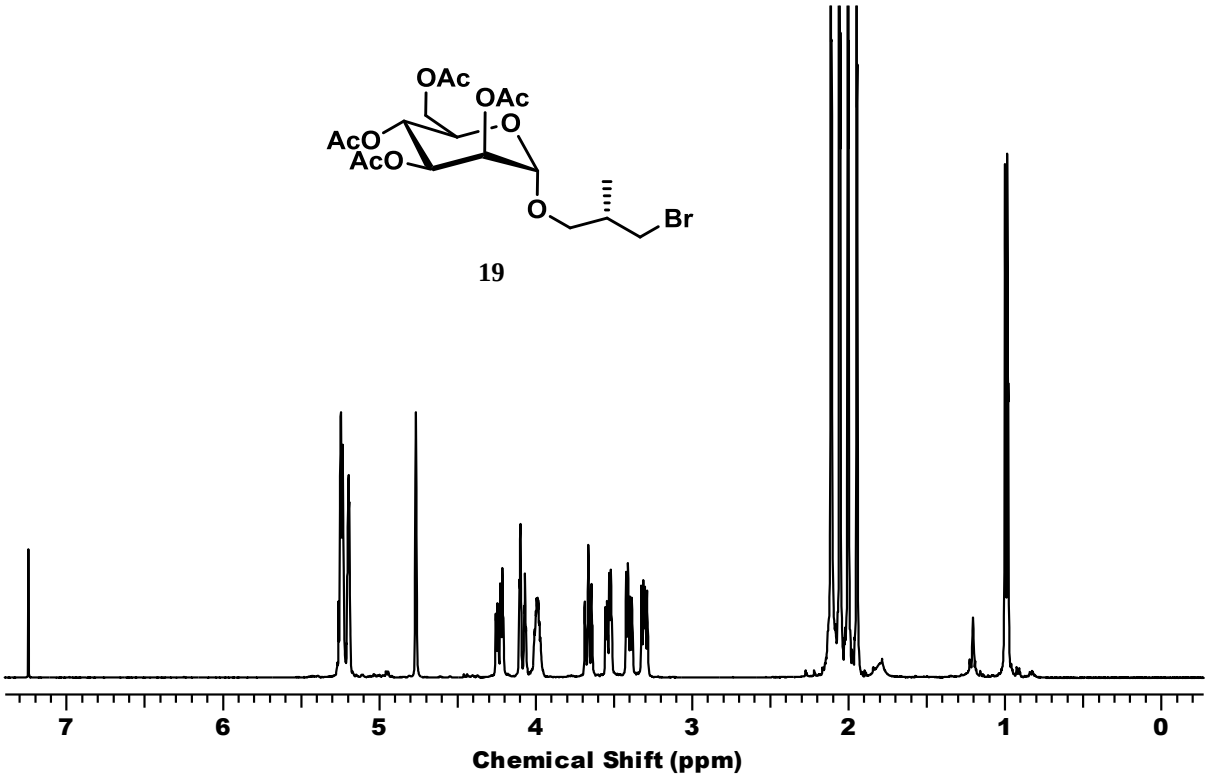
OAc
OAc
AcO
AcO
O
O
Br
7
6
5
4
3
2
1
0
Chemical Shift (ppm)

19

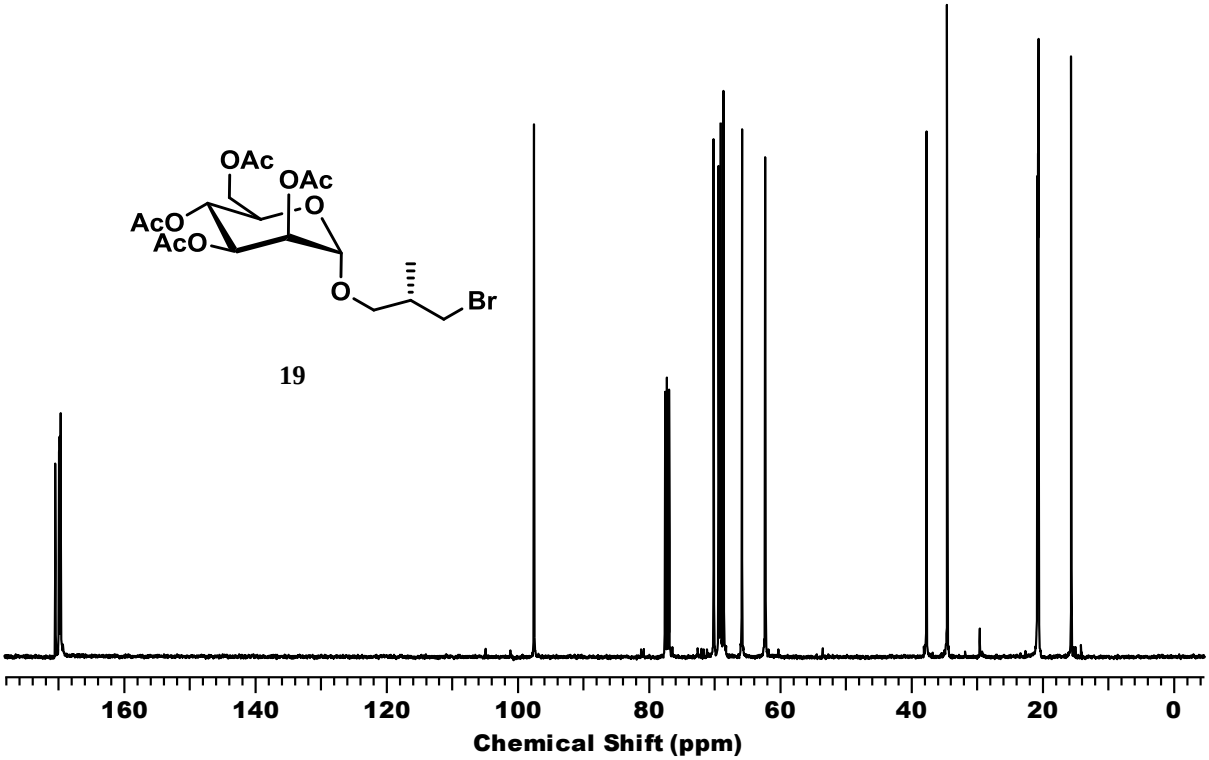
OAc
OAc
AcO
AcO
O
O
Br
160
140
120
100
80
60
40
20
0
Chemical Shift (ppm)

19

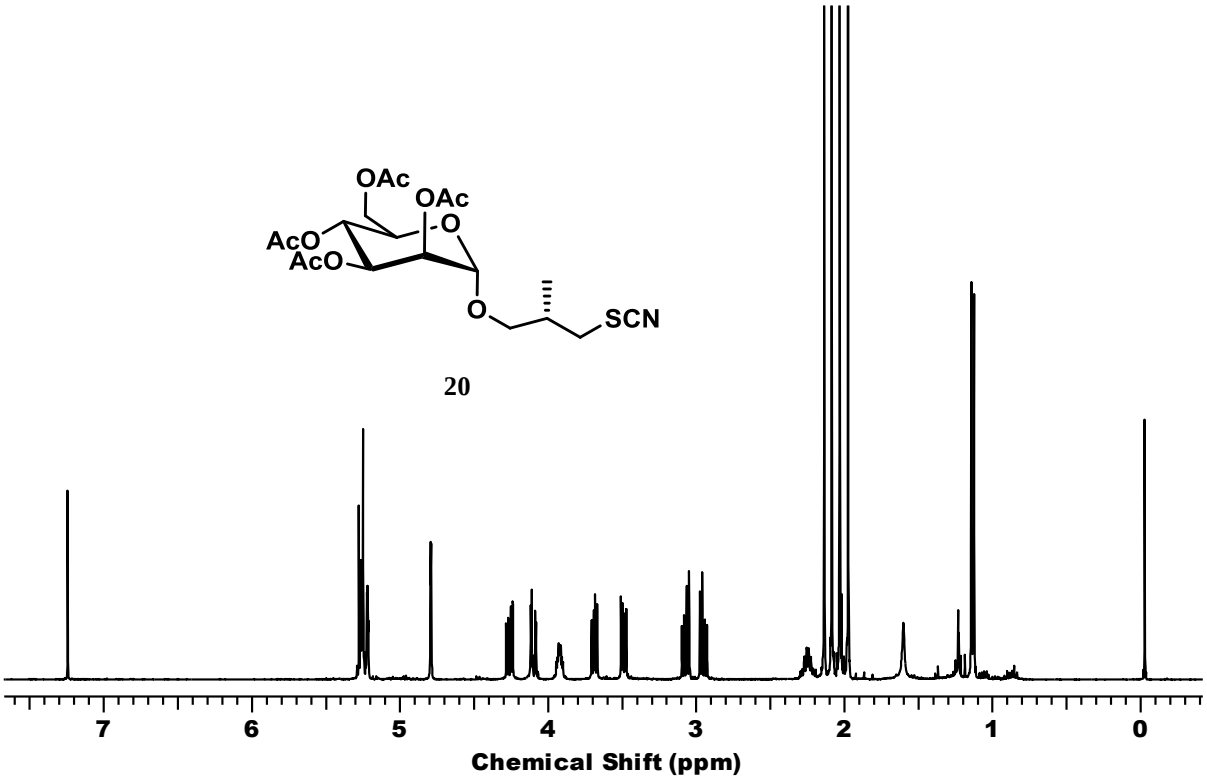
OAc
OAc
AcO
AcO
O
O
SCN
7
6
5
4
3
2
1
0
Chemical Shift (ppm)

20

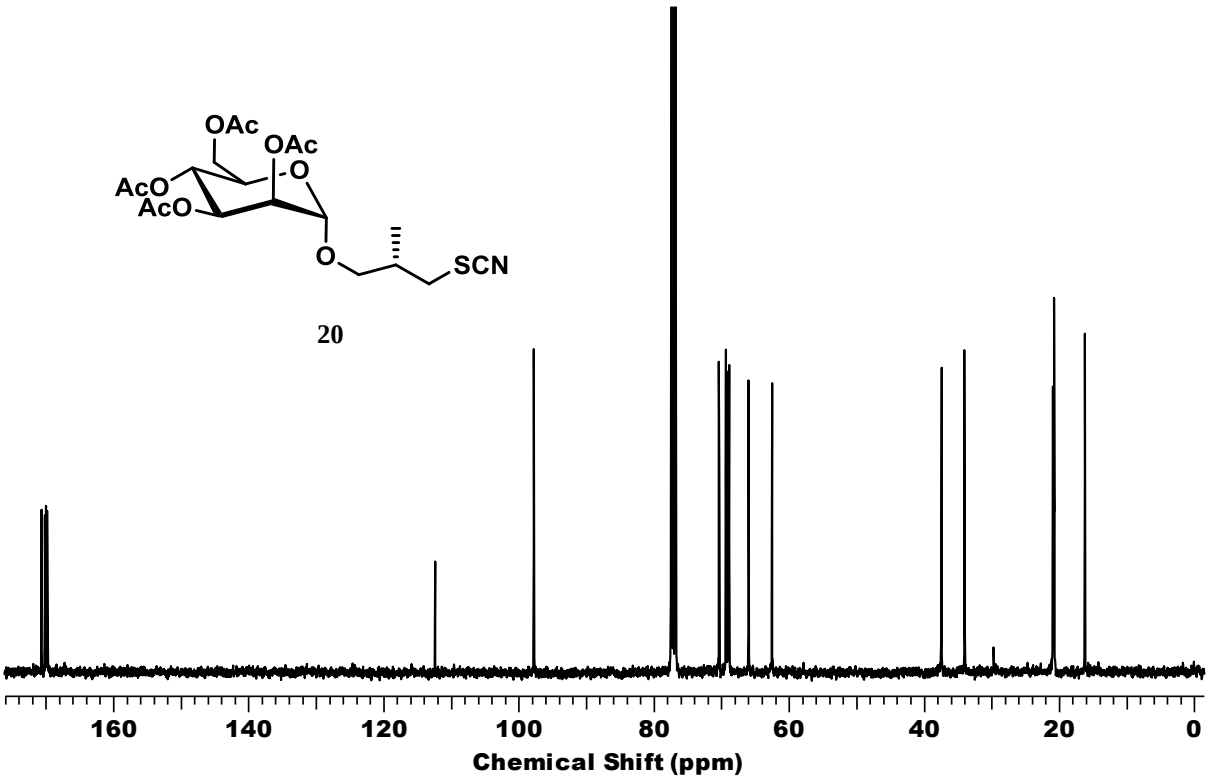
OAc
OAc
AcO
AcO
O
O
SCN
160
140
120
100
80
60
40
20
0
Chemical Shift (ppm)

20

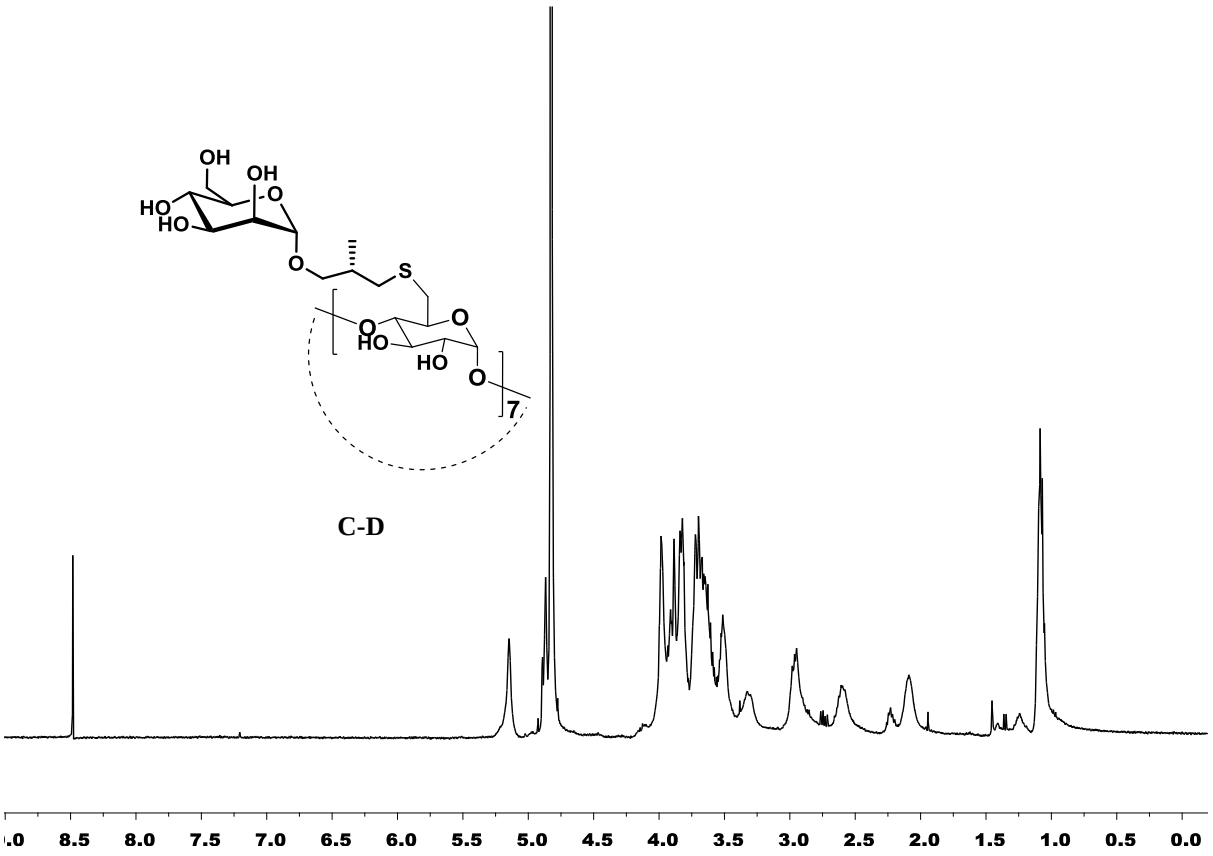
OH
OH
HO
HO
O
O
S
O
O
HO
HO
O
7
8.5
8.0
7.5
7.0
6.5
6.0
5.5
5.0
4.5
4.0
3.5
3.0
2.5
2.0
1.5
1.0
0.5
0.0

C-D

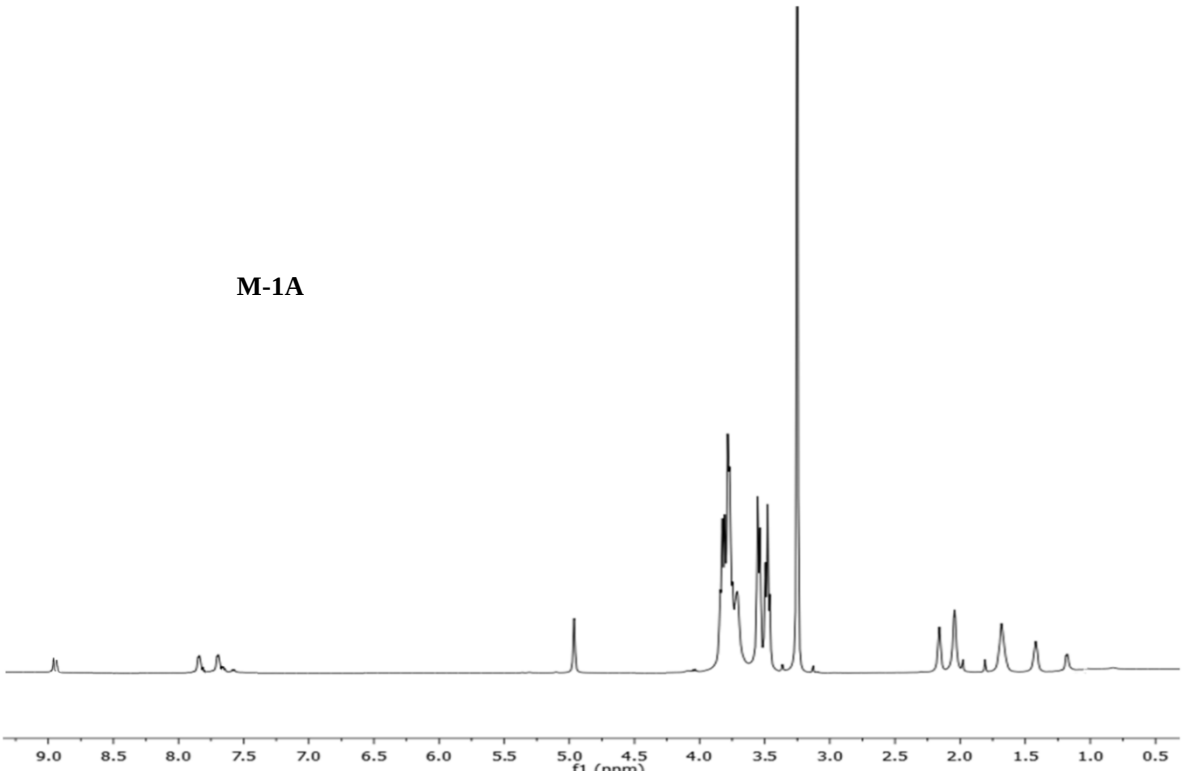
9.0
8.5
8.0
7.5
7.0
6.5
6.0
5.5
5.0
4.5
4.0
3.5
3.0
2.5
2.0
1.5
1.0
0.5

M-1A

M-2A

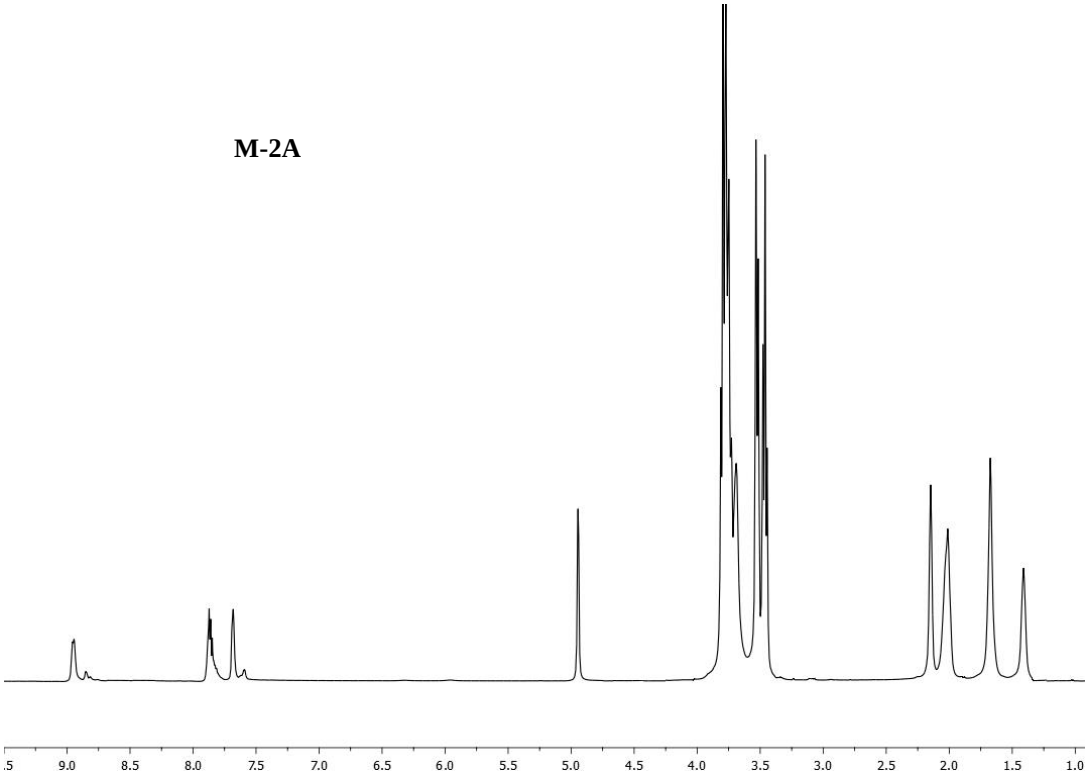
9.0
8.5
8.0
7.5
7.0
6.5
6.0
5.5
5.0
4.5
4.0
3.5
3.0
2.5
2.0
1.5
1.0

M-3A

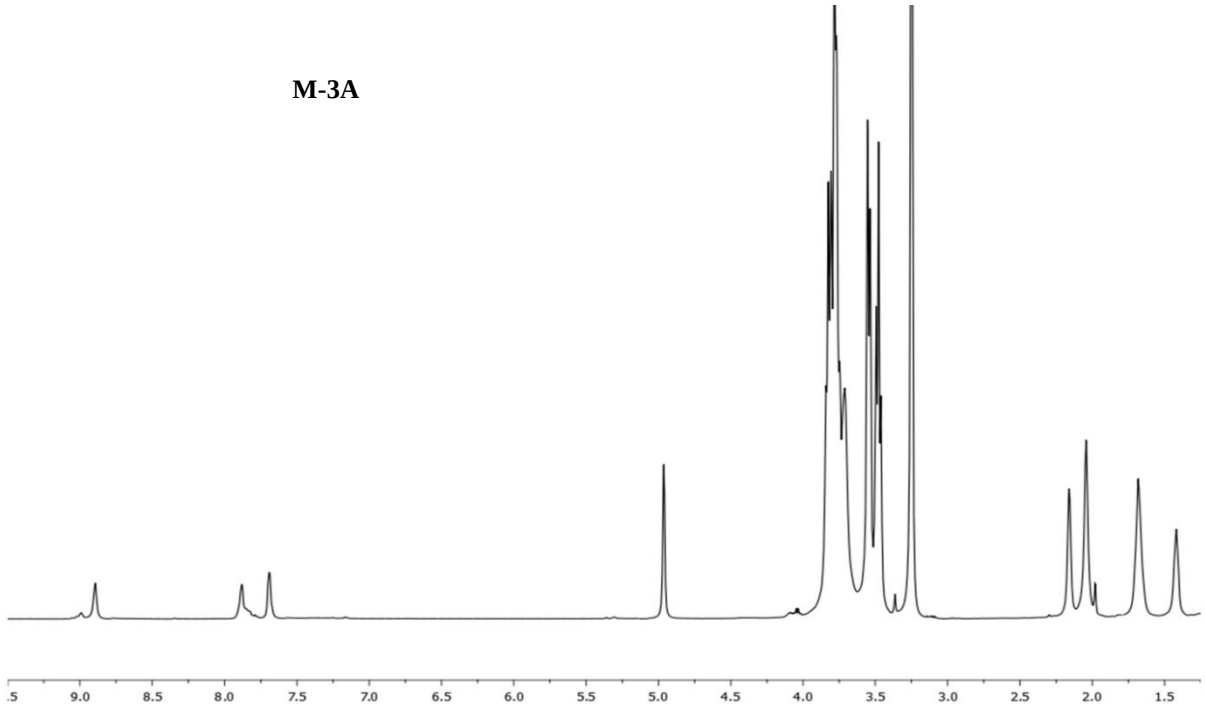
9.0
8.5
8.0
7.5
7.0
6.5
6.0
5.5
5.0
4.5
4.0
3.5
3.0
2.5
2.0
1.5

M-1B

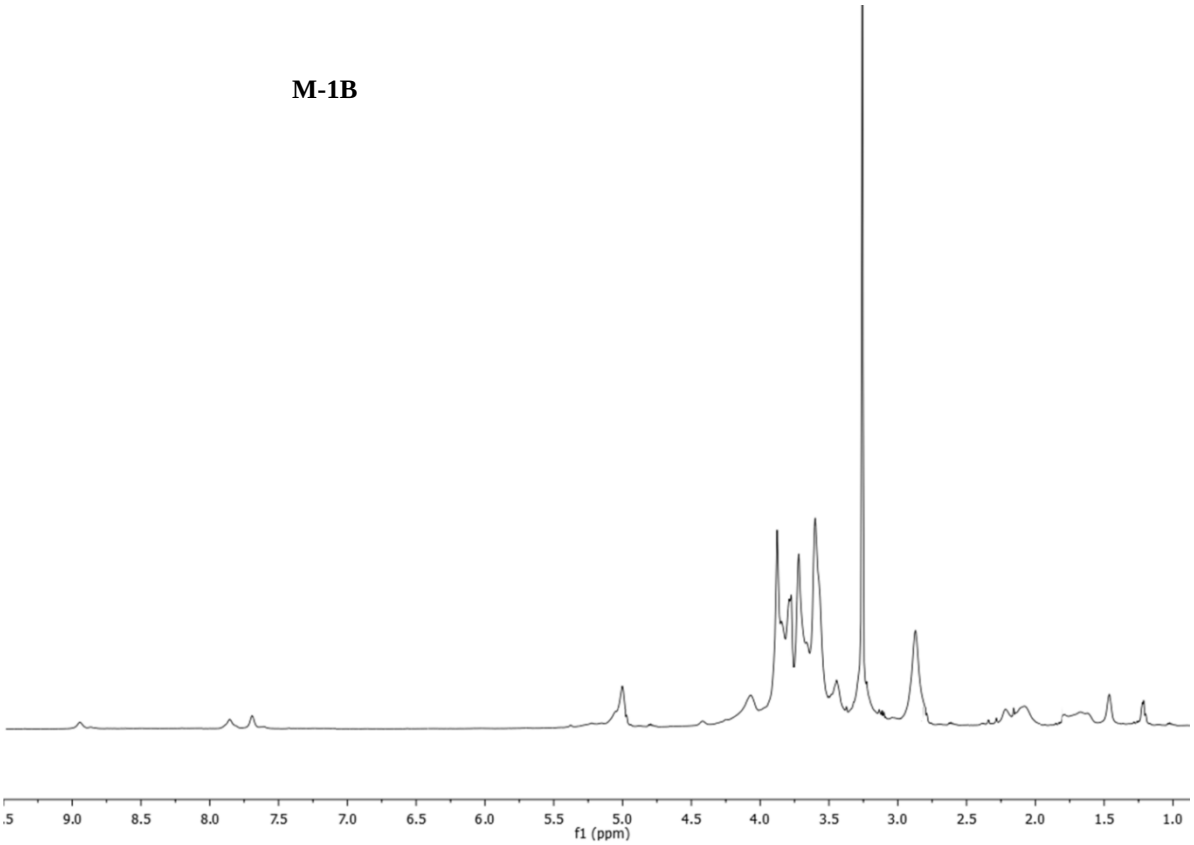
9.0
8.5
8.0
7.5
7.0
6.5
6.0
5.5
5.0
4.5
4.0
3.5
3.0
2.5
2.0
1.5
1.0
f1 (ppm)

M-2B

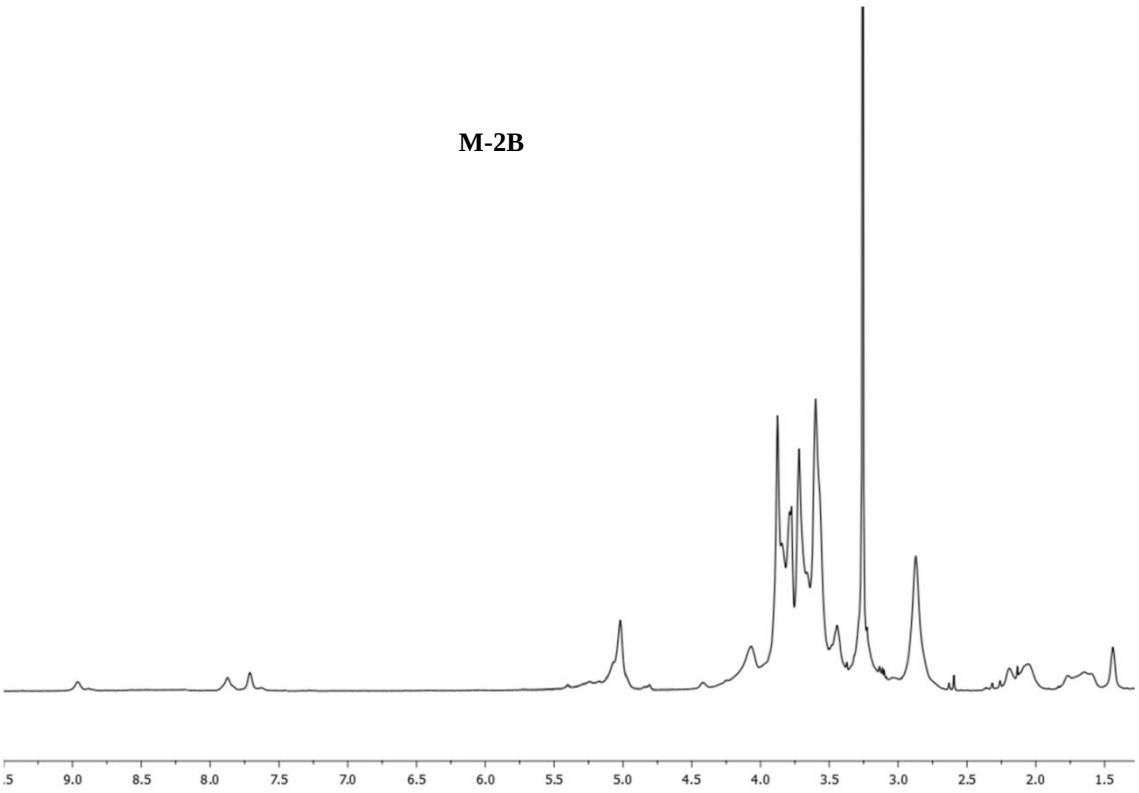
9.0
8.5
8.0
7.5
7.0
6.5
6.0
5.5
5.0
4.5
4.0
3.5
3.0
2.5
2.0
1.5

M-3B

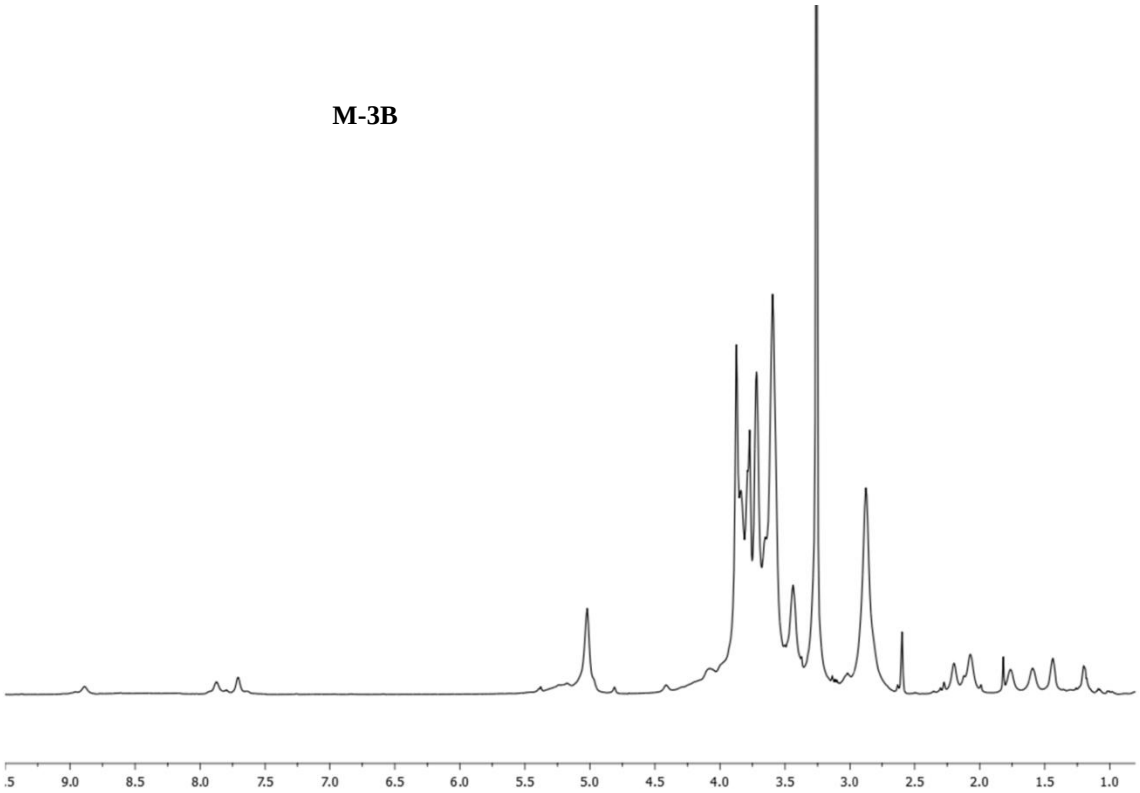
9.0
8.5
8.0
7.5
7.0
6.5
6.0
5.5
5.0
4.5
4.0
3.5
3.0
2.5
2.0
1.5
1.0

M-1C

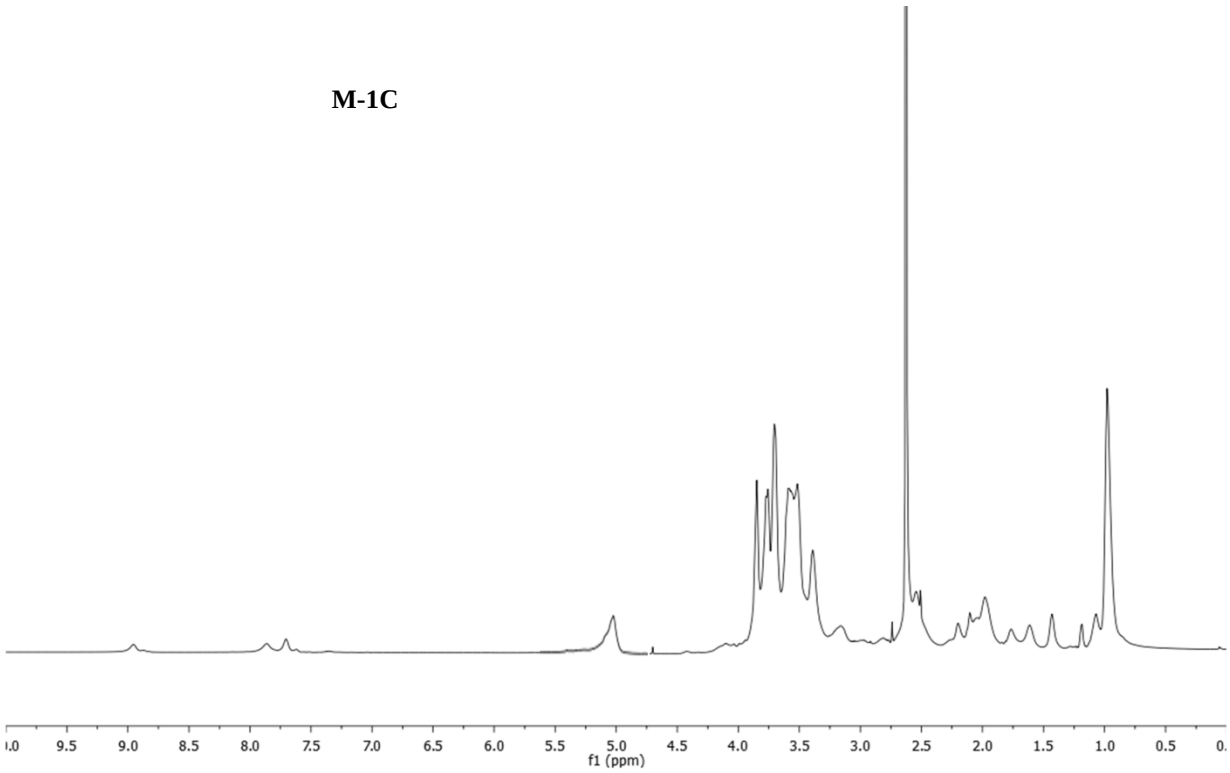
9.5
9.0
8.5
8.0
7.5
7.0
6.5
6.0
5.5
5.0
4.5
4.0
3.5
3.0
2.5
2.0
1.5
1.0
0.5
f1 (ppm)

M-2C

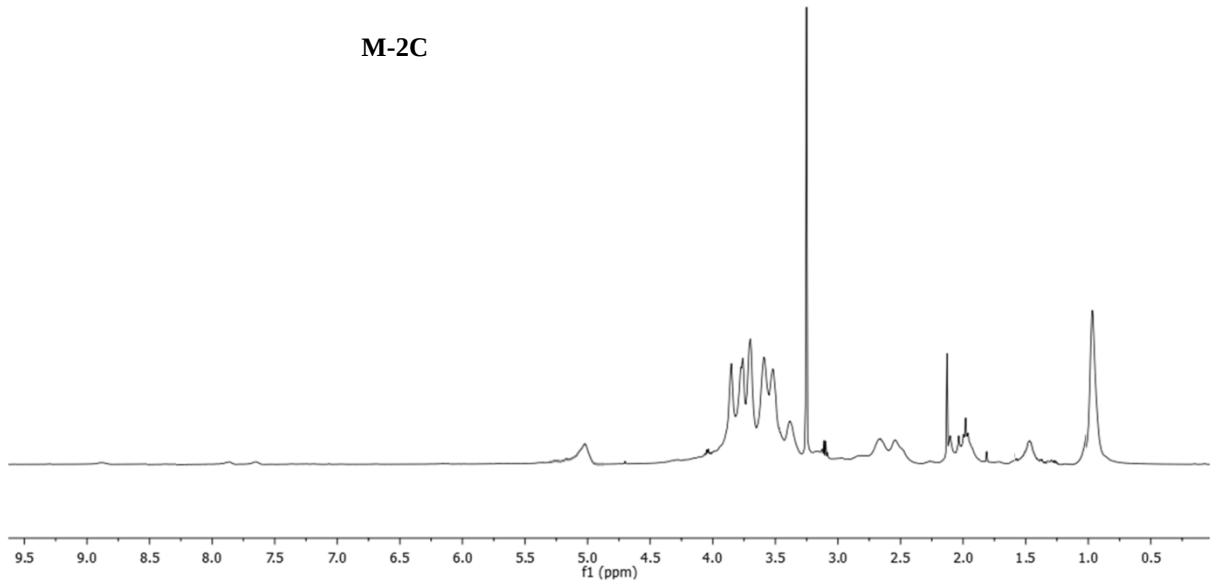
9.5 9.0 8.5 8.0 7.5 7.0 6.5 6.0 5.5 5.0 4.5 4.0 3.5 3.0 2.5 2.0 1.5 1.0 0.5
f1 (ppm)

M-3C

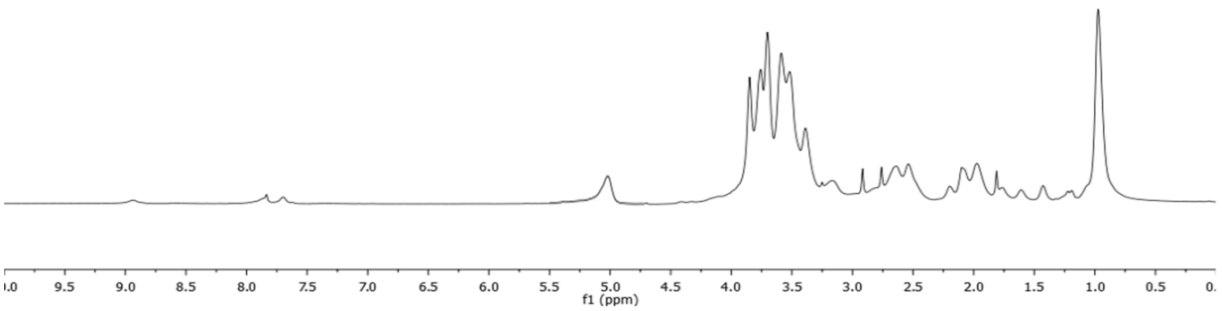
9.5 9.0 8.5 8.0 7.5 7.0 6.5 6.0 5.5 5.0 4.5 4.0 3.5 3.0 2.5 2.0 1.5 1.0 0.5
f1 (ppm)

CHAPTER 3

Supramolecular Metalloglycodendrimers Selectively Modulate Lectin Binding and Delivery of Ru(II) Complex into Mammalian Cells

Abstract

Host-guest interaction between Ru(II)-complex and sugar-capped β-cyclodextrin was employed to synthesize metalloglycodendrimers. These glycodendrimers demonstrated selective carbohydrate-protein interactions and control the delivery of Ru(II) complex into cancer cells, which may facilitate cell-specific apoptosis. Lectin binding assay revealed micromolar range IC_{50} values with different plant lectins. Cell viability assay and confocal imaging studies of Ru(II) complexes exhibited cytotoxic activities in cancer cells compared to normal cells with IC_{50} values close to other literature Ru(II) complexes. The cell death inducer was found to accumulate favorably to the endoplasmic reticulum (ER) and induced ER stress in cells. The upregulation of CHOP, caspase-3 and caspase-12 disturbed the ER morphology initiating apoptosis pathway.

3.1. Introduction

Bioinorganic chemistry is a rapidly developing field and there is enormous potential for applications in medicine. Metals have been used from long time as an important component in the clinic, for example, platinum compounds are extensively used in the treatment of cancer; silver compounds are useful as antimicrobial agents and gold compounds are used routinely in the treatment of rheumatoid arthritis.[1-5]

Still, the majority of current applications for metal complexes are for acute diseases such as cancer, for example, cisplatin a chemotherapy drug.[6,7] However, prolonged treatment with these drugs can lead to acquired resistance of the cells, resulting in decreased efficacy of the metal-based chemotherapy. These limitations have prompted research for more effective and less toxic metal based anti-cancer drugs. Among transition metal anticancer drugs, Ru(II) complexes are one of the attractive anticancer angents.[8-12] They have two accessible oxidation states, low toxicity and ability to mimic iron in binding to certain biological molecules, such as albumin and transferrin.[13]

Some ruthenium anticancer agents have recently entered the clinic research stage, demonstrating promising activity on tumors.[14-17] Barton's and Thomas's groups have shown that complexes such as $[Ru(DIP)_2dppz]^{2+}$, $[Ru(bpy)_2dppz]^{2+}$ and $[Ru(Phen)_2dppz]^{2+}$ {dppz = dipyrido[3,2-*a*:2′,3′-*c*]phenazine; bpy = bipyridine; phen = phenanthroline} induced cytotoxicity by non-covalent interaction with DNA/RNA or G-quadruples.[18-21] Other studies have shown that factors like cell membrane modification, cell adhesion properties or mitochondria-mediated apoptosis induced by Ru(II) complexes could be responsible for their cytotoxicity.[22-29] Still, all studies reveal a certain level of difficulty for these complexes to penetrate the cell membrane and cellular uptake of these complexes is often non-specific by passive diffusion.[30,31] We have decided to tackle and solve the cell penetration problem by using a new drug carrier vehicle, which is based on multivalent sugar scaffolds, which are expected to enhance carbohydrate-protein interactions and thereby cell-type specificity.[32-34]

We have prepared a series of Ru(II)-based metallo-glycodendrimers and studied their lecting binding, followed by anticancer activities with different cancer and normal cell lines and also elucidated the molecular mechanisms through which Ru(II) complexes cause cancer cell death.

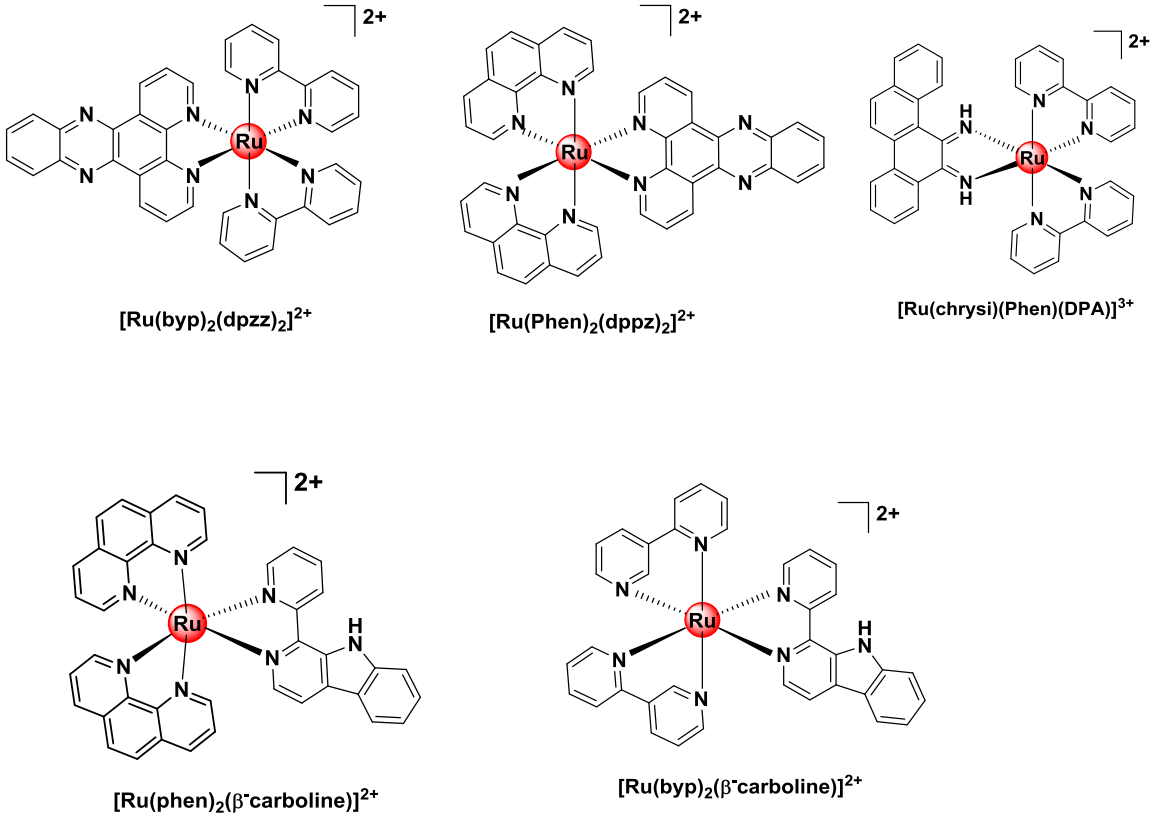

Figure 1: Ru(II) anticancer drugs.

3.2. Results and Discussion

3.2.1. Synthesis of Ru(II) Complex

Compound **2** was prepared according to a published protocol.[35] The Bipyridine ligand **L-1** was prepared via convergent synthesis by using Boc protected alanine and 4,4[1] Bipyridine dicarboxylic acid. **8** was synthesised by coupling of 1-admantylamine with Boc protected alanine in presence of water soluble coupling reagent *N*-ethyl-*N*'-(diethylaminopropyl)-carbodiimide (EDC) and triethyl amine (Et_3N), followed by deprotection of Boc protecting group by using trifluoro acetic acid (TFA). Parllely bipyridine carboxylic **10** acid was synthesised by oxidising the 4,4[1] dimethyl bipyridine with chromium trioxide (CrO_3) in presence of sulphuric acid (H_2SO_4) then carboxylic acids were converted into acid chlorides using thionyl chloride ($SOCl_2$) at refluxing temparature followed by coupling with **8** to afford lgand **L-1** (**Scheme 1**).

Di adamantyl complex was obtained by ligand complexation of **L-1** with $[Ru(bipy)_2]Cl_2$.

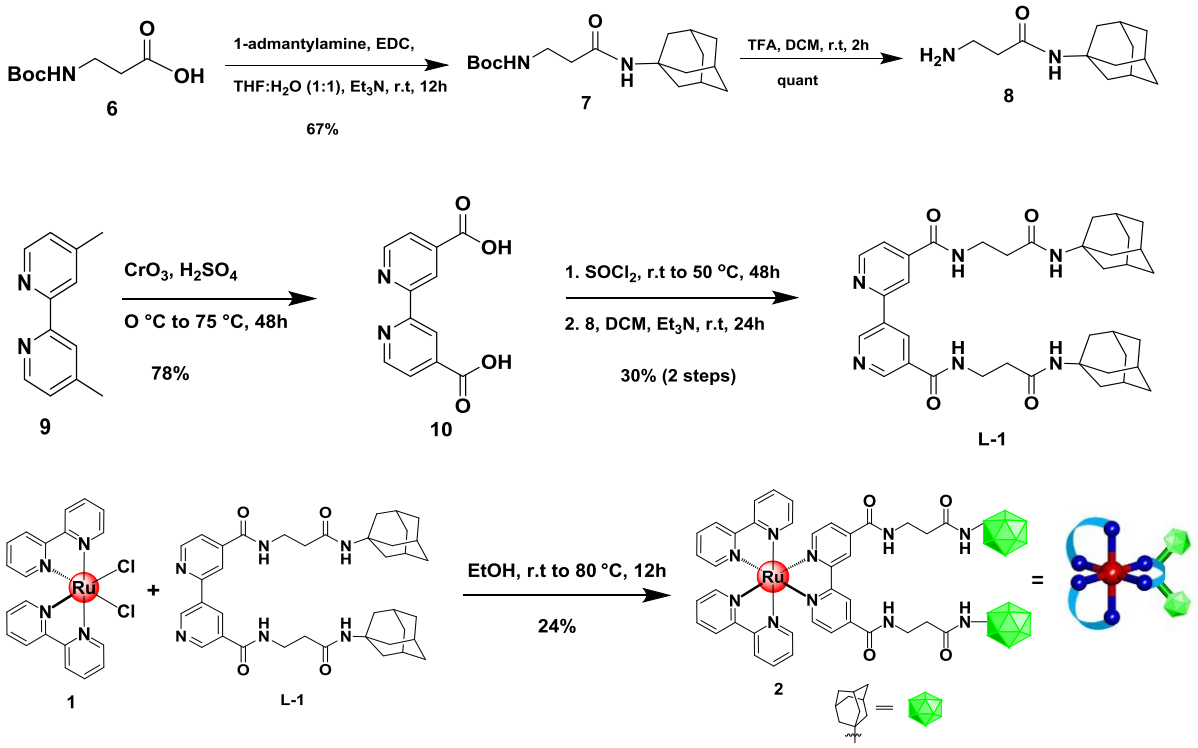

Scheme 1: Synthesis of di adamantyl Ru(II) complex.

Cyclodextrin derivatives have been synthesized according to the described procedure in the chapter 2 (Section 2.2.5).

3.2.2. Host-Guest Formation

Metallo-glycodendrimers (**3** to **5**) were prepared by mixing stoichiometric amounts of **2** with either *β*-CD or man-*β*-CD or gal-*β*-CD (**Scheme 2**).

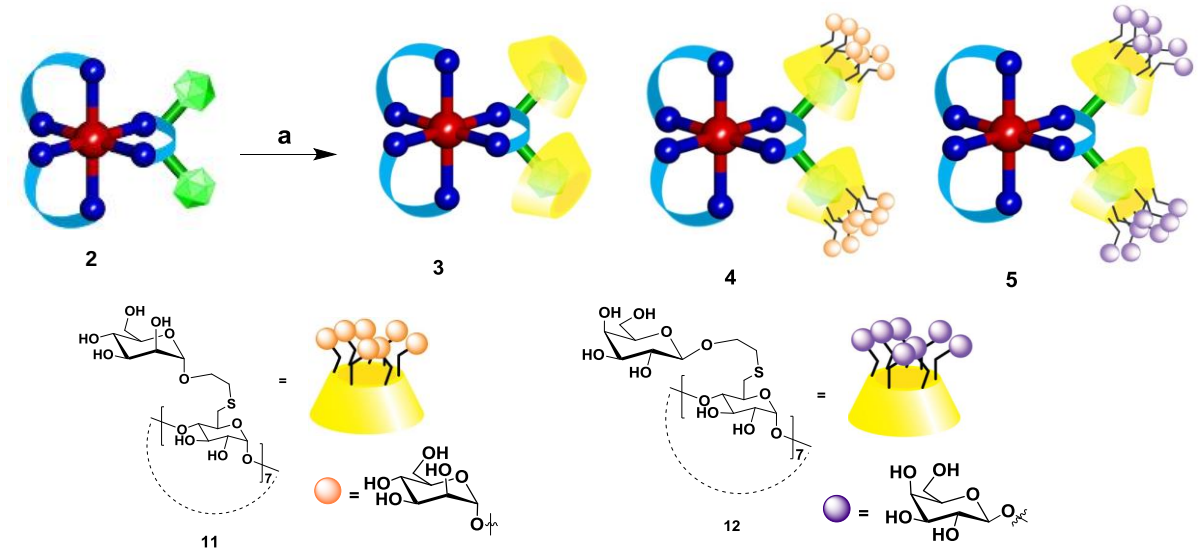

Scheme 2: Synthetic scheme of compounds **3** to **5**: **(a)** *β*-CD or man-*β*-CD or gal-*β*-CD/H_2O.

3.2.3. NMR study of supramolecular complexes

NMR was employed to confirm the supramolecular assemblies are anchored by adamantly groups are acting as hosts in the cyclodextrin guests. NOESY spectrum of **3** (**Fig 2**) displayed clear and strong nuclear Overhauser effect (NOE) from **H3** and **H5** of *β*-CD and the adamantyl skeleton indicating the encapsulation of adamantyl from **2** in the *β*-CD inner core as was reported by Grünstein et al.[35]

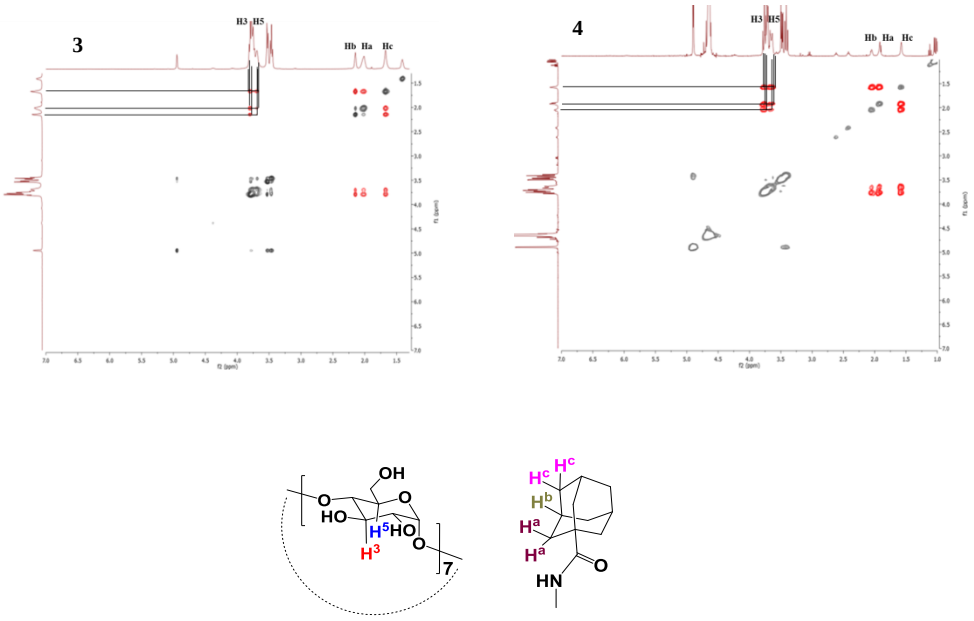

Figure 2: NOESY spectra of metallo-glycodendrimers.

3.2.4. Uv-visible spectra and fluorescence spectra

UV-visible spectra of the complexes **2** to **4** in water displayed identical spectra at MLCT region and slightly different spectral profile at LC region. MLCT and LC band of the complexes were observed at 475 nm and 350 nm respectively (**Fig. 3a**).

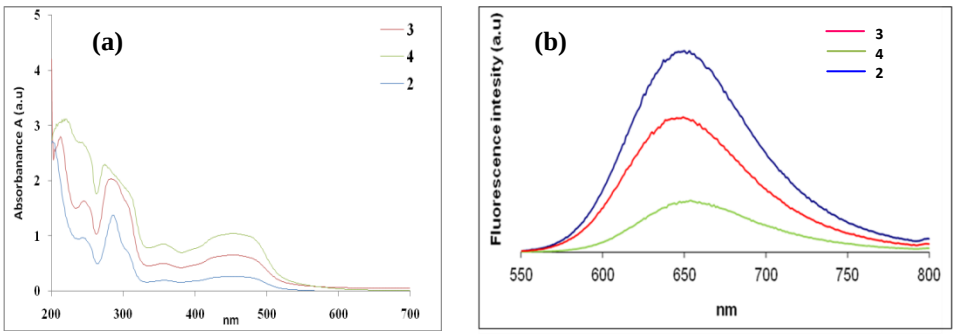

Figure 3: **(a)** Absorption spectra of Ru(II) complexes in water; **(b)** Fluorescent spectra of Ru(II) complexes; **2** (blue line), **3** (red line) and **4** (green line).

The emission spectra of the **Ru** series and the **Ru-CD** series exhibited an emission band at $\lambda_{max}^{em} \approx 650$ nm when excited at 450 nm. An increase in emission intensity and calculated quantum yield (Φ) directly correlates with the increasing complexity of the structures as more units of **2** and CD are assembled around the Ru(II) core (**Fig 3b**).

Table 1: Photophysical data of Ruthenium complexes

Complex	MLCT (nm)	ε (L. mol^{-1}. Cm^{-1})	Λmax	Φ
2 in H_2O	462	4730	648	0.09
3 in H_2O	471	5073	652	0.22
4 in H_2O	470	5345	655	0.28

3.2.5. ITC profile of MGDs

The number of incorporated molecules of *β*-CD complex in **3** and **4** was established by ITC analysis (**Fig. 4, Table 2**).

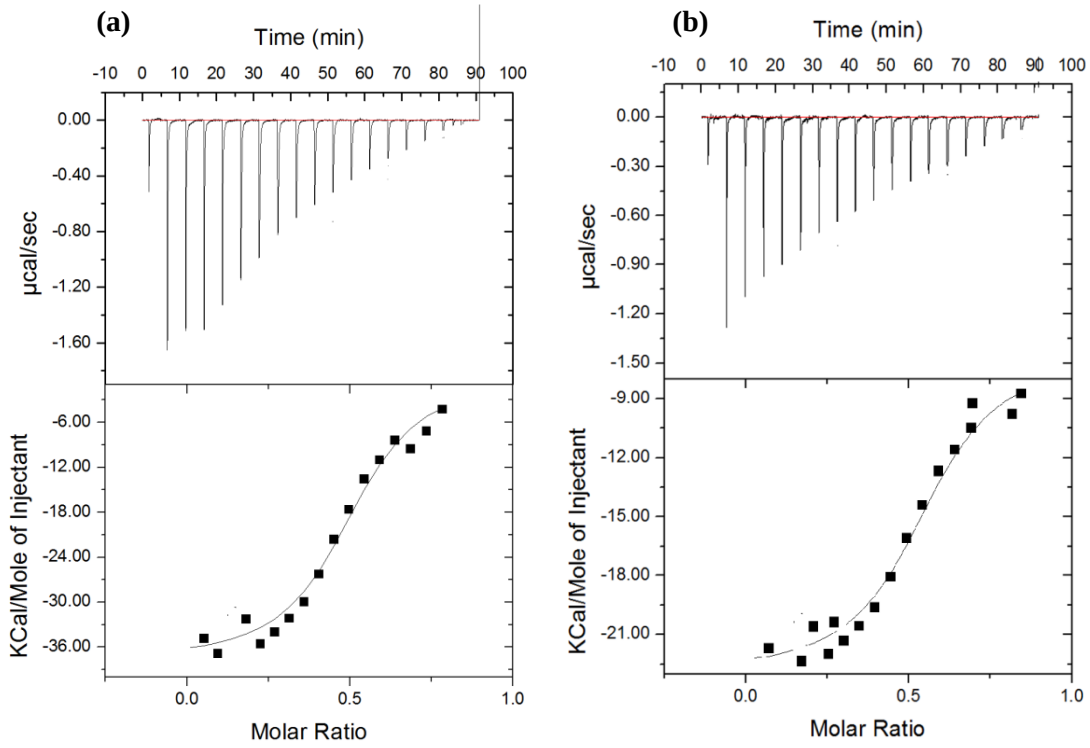

Figure 4: ITC profile for the reaction of man-*β*-CD **(a)** and gal-*β*-CD **(b)** with Ru-2.

Table 2: Binding parameters

Complex	n	Binding Constant (M^{-1})	ΔH(Kcal/mol)	ΔS(cal/mol/deg)
2 *vs* Gal-*β*-CD	0.41	5.64×10^3	-1.04 ± 0.12	-3.12×10^3
2 *vs* Man-*β*-CD	0.46	5.12×10^3	-2.01 ± 0.12	-4.33×10^3

3.2.6. Binding affinity of Ru(II) complexes

To address the selective and sensitive carbohydrate-protein interactions, we first investigated the ELISA plate lectin binding affinity. Mannose-BSA and galactose-BSA were immobilized on a 96-well plate and treated with different concentration of Ru(II) complexes (**3** to **5**) in the presence of HRP-conjugated Concanavalin A (ConA), peanut agglutinin (PNA) and galantus nivilis agglutinin (GNA) lectins respectively. The mannose-Ru(II) complexes could be seen selectively inhibiting the ConA and GNA lectins compared to PNA lectins on mannose-BSA conjugates (**Fig. 5**). The 2-fold difference between ConA and GNA lectins corresponds to tetrameric nature of the protein that contains one and three mannose binding sites per subunit respectively. On the other hand, the PNA lectins binding were selectively inhibited by complex **4**. These results confirmed the selective carbohydrate-protein interactions with IC_{50} values in the range of 10^{-5}-10^{-6}M (**Table 3**).

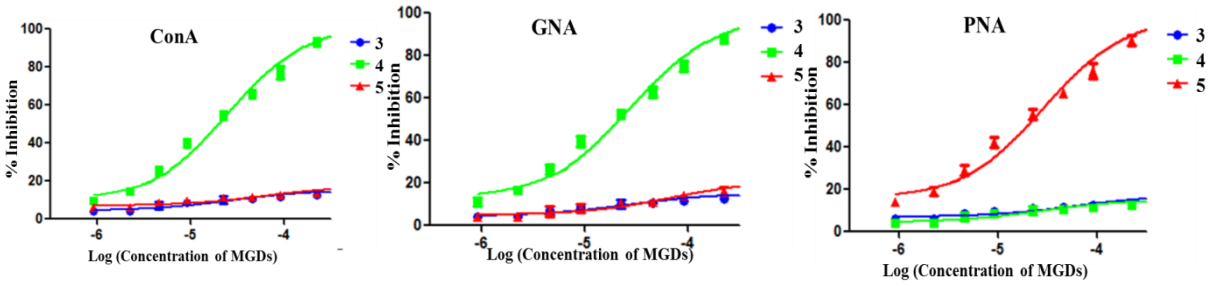

Figure 5: The binding affinity between different Ruthenium complexes **3** to **5** and ConA, GNA and PNA (each point represents the average of three independent experiments).

3.2.7. Cell viability assay

Next, we determined whether Ru(II) complexes can generate cytotoxicity in the mammalian cells. To this end, we performed MTT assay in DC-SIGN transfected-HeLa (D-HeLa) and liver carcinoma HepG2 cell lines with compound **3** to **5**.[36] Normal NIH-3T3 fibroblasts were used as a control. The survival of cells treated with different doses of Ru(II) complexes were compared to that of cells treated with cisplatin as a positive control and PBS as a negative control. The doses used for Ru(II) complexes were 10-100 μM, respectively and the results were very encouraging (**Table 3**). The Ru(II) complexes were less toxic to normal cells than to cancer cells, indicating a better therapeutic index than cisplatin. Another interesting finding was that complex **3**, when used in 25-100 μM concentration range revealed 78-92% cell viability in all cancer cells, indicating the absence of any receptor for CD on cell surfaces and decreased cell penetration of the Ru(II) complex (**Fig. 6 and Table 3**). At 24 and 48 h, **2** induced concentration-dependent cell death. This behavior indicates a passive diffusion mechanism for the cellular entry in a similar manner to that of other Ru(II) complexes.[22-24]

Table 3: Binding and cytotoxic effects (IC_{50} in μM) of Ru(II) complexes on cancer and normal cells after 48 h. Data represent mean ± SD, n = 3.

Comps	ConA	PNA	GNA	DC-SIGN Transfected HeLa	HepG2	NIH-3T3
2	ND	ND	ND	34 ± 2.1	48 ± 1.5	≥ 100
3	-	-	-	≥ 100	≥ 100	≥ 100
4	31 ± 2.7	-	19 ± 3.7	37 ± 1.2	> 100	≥ 100
5	-	60 ± 3.4	-	> 100	38 ± 1.1	≥ 100
cisplatin				17.8 ± 0.8	13.6 ± 2.0	18.7 ± 0.6[17]

When the man-*β*-CD derivative **4** was used, D-HeLa cell lines, which expresses mannose specificity,[37] revealed time-dependent cytotoxicity (**Fig. 6**) while **4** revealed less toxicity towards HepG2 cancer cell line, which lack mannose binding receptors.[38] At 48 h, **4** induced D-HeLa cell death with an IC_{50} value of 37 ± 1.2 μM and >100 μM with HepG2 cells. In contrast, **5** exhibited IC_{50} value around 38 ± 1.1 μM with HepG2 and > 100 μM with D-HeLa cells. After 72 h, **4** and **5** induced more cell death due to slow receptor mediated uptake,

whereas **2** displayed least effect. Overall, it is evident from the above data that **4** is more efficient in D-HeLa cells as compared to HepG2 or NIH-3T3 cells. In contrast, **5** is more effective in HepG2 cells.

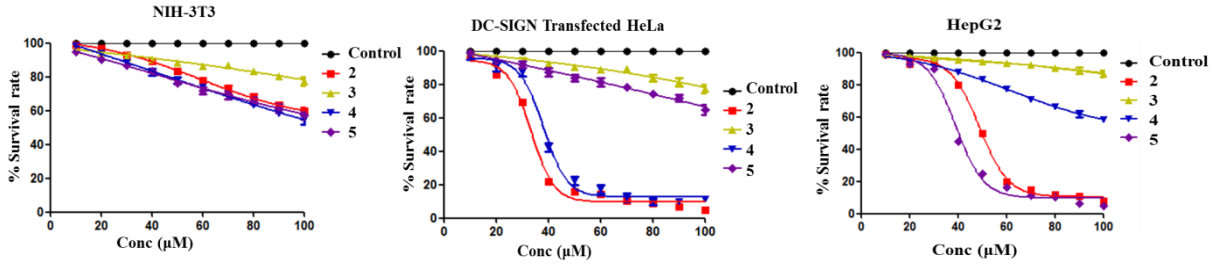

Figure 6: MTT assay with DC-SIGN HeLa, NIH-3T3 and HepG2 cells after treatment with **2** to **5** (10-100 µM) for 48 h. Cells were grown in 96-well plates and the compounds were added at 90% confluence. The results are presented as percentage compared to the control (PBS treated cells). Data represent mean ± SD, n = 3.

3.2.8. Confocal laser scanning microscopy images

The optical properties of Ru(II) bipyridine complex, an integral component of compounds **2** to **5**, were utilised for evaluating cellular uptake mechanism and cytotoxicity. In order to follow the internalization process, cells were incubated with **2** to **5** (50 µM) for 24 and 48 hours, followed by staining with Hoechst 33342, a membrane permeating molecule that binds to DNA of live cells causing blue fluorescence. As shown in Fig. 7, the red and blue fluorescence of the metal complexes and Hoechst 33342 respectively, emerge in the cells in a time dependent manner. After 24 hours, compound **2** homing close to the nuclei, while **3** and **4** revealed only faint fluorescence. With longer time periods, large accumulation of **4** in the nuclear vicinity was observed. Only traces of **3** was observed after 48 hours indicating a time-controlled delivery process, which is dependent on the structure of the Ru(II)-based complexes, with a major role to sugar encapsulation (**Fig. 7a**). Similar imaging studies with NIH-3T3 cells showed virtually equal level of fluorescence intensity at different time intervals and almost no significant difference between the fluorescence of **2**, **3** or **4** at different time intervals. Moreover, the fluorescence observed was not concentric around nuclei (**Fig. 7b**). A possible reason for this behavior, which is different to that obtained for

the D-HeLa cells might be attributed to the differences in cellular behavior between normal and cancer cells (**Fig. 7b**).

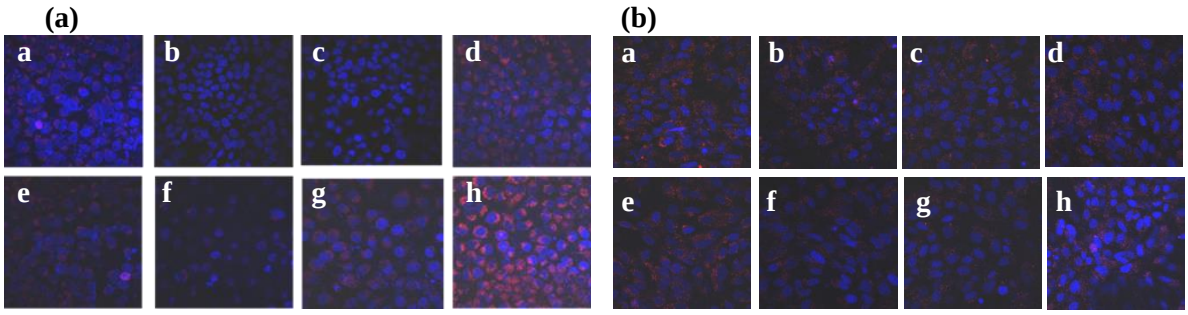

Figure 7: Fluorescence confocal microscopy images **(a)** D-HeLa cells treated with 50 μM solutions of **2** (a, e); **3** (b, f) and **4** (c, g); **5** (d, h) for different time periods: (a, b, c, d) 24 hours and (d, e, f, h) 48 hours; **(b)** NIH-3T3 cells treated with 50 μM of **2** (a, e); **3** (b, f); **4** (c, g) and **5** (d, h) after 24 (a, b, c, d) and 48 (e, f, g, h), staining with Hoechst 33342. Confocal fluorescence images were taken under identical conditions, magnification is 63×.

3.2.9. Co-localization

Further information on the location of **4** in the cells after 24 hours of incubation was obtained by two additional experiments using mitochondria (MT) specific green-MT tracker and endoplasmic reticulum specific green-ER tracker dyes within live cells.

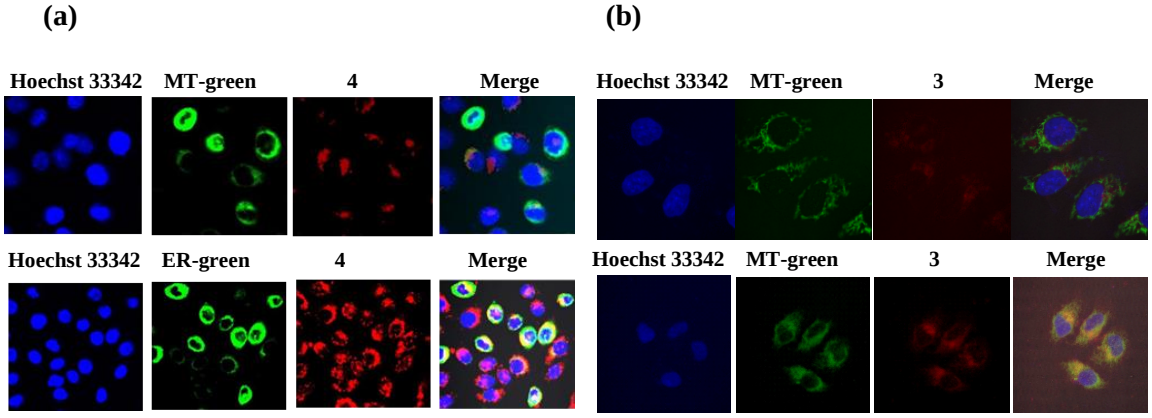

Figure 8: Fluorescence confocal microscopy images **(a)** D-HeLa cells incubated with **4** for 24 h. **(b)** D-HeLa cells incubated with **3** for 24 h. Images show Hoechst 33342, MT or ER, ruthenium complexes and the overlay.

As shown in figure 8, MT-tracker treated cells showed separated areas of red and green fluorescence, indicating **4** was not binding to MT within cells. Whereas, an

excellent superimposed pattern between ER dye and **4** was observed, which refers to the accumulation of the compound in the ER membrane (**Fig. 8a**). A similar experiment with **3** also revealed ER-specific binding (**Fig. 8b**), indicating that once the **3** and **4** were taken up by the cells, host-guest complex might get segregated and **2** might become active component, which may involve in cytotoxicity.[39]

3.2.10. Mechanistic studies

To examine the mechanism(s) by which **2, 3** and **4** induced apoptosis, the nuclear transcription factor C/EBP homologous protein (CHOP) and caspase pathways known to induce ER-stress mediated cell death were examined.[40-45] Elevated expression level of these proteins are considered as a general marker of ER stress. To test if the accumulation of **2** and **4** in the ER further induced ER stress, protein extracts of **2** and **4** treated cells at 48 h were analyzed for the expression level of CHOP (**Fig. 9**). Western blot analysis of CHOP showed that cells treated with **2** and **4** expressed high levels of CHOP (21-KDa). Overall, these results suggest the ER-induced apoptosis in cancer cells. These findings are correlated to other published results of ER-mediated apoptosis.[46-49]

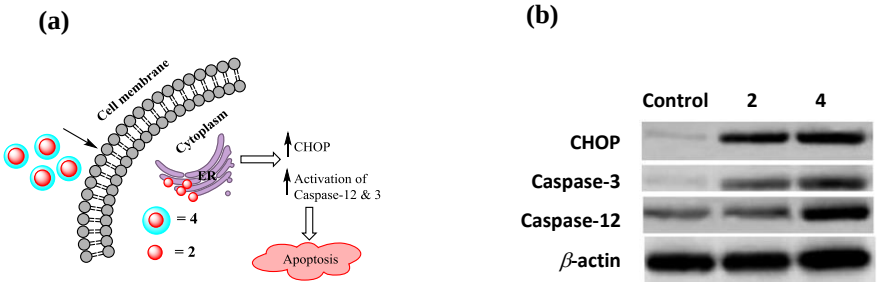

Figure 9: (a) Schematic presentation of ER stress triggered pathways in D-HeLa cells by **2** and **4**; **(b)** The expression of CHOP, caspase-3 and 12 were analyzed by western blot (35 µg whole-cell lysate of proteins) Protein loading was assessed by probing the blots with anti-*β*-actin mAb.

3.3. Conclusions

In conclusion, host-guest interaction to prepare metalloglycodendrimers was developed to understand the cell specific delivery of Ru(II) complexes. Validated through a series of imaging techniques and MTT assay, we have shown controlled

delivery of metal complexes over a period of 48 h in cancer cells. Our studies also documented the mechanism of cytotoxicity *via* ER-stress, triggering CHOP, caspase-3 and 12 activations. The simplicity and effectiveness of the system underscore its potential to accelerate metal complex or toxic metal delivery into cancer cells *via* specific receptors. Moreover, expanding the scope of this platform and the synthesis of new libraries of metallo-glycodenrimers opens up a new direction in exploring and understanding the role of sugar-metal complexes in various biological responses.

3.4. Experimental part

General Information

Commercial grade reagents and solvents were used without further purification except as indicated below. Deionized water was obtained from an in-house purification system. Analytical thin layer chromatography (TLC) was performed on Merck silica gel 60 F254 plates (0.25 mm) and visualized by UV or by dipping the plate in CAM solution followed by heating. Medium pressure column chromatography was carried out on Fluka Kieselgel 60 (230–400 mesh). ^{1}H and ^{13}C NMR spectra were recorded on Jeol 400 MHz and 100 MHz respectively using the residual solvents' signals as internal references (for $CDCl_3$: δ_H, 7.26 ppm, δ_c 77.3 ppm and for CD_3OH: δ_H 3.31 ppm, δ_c 49.0 ppm). Chemical shifts (δ) are reported in *ppm* and coupling constants (J) in Hz. DMEM media and 3-(4, 5-dimethylthiazol-2-yl)-2, 5-diphenyltetrazolium bromide (MTT) were purchased from Invitrogen and Sigma-Aldrich respectively. HeLa, HepG2 and NIH-3T3 cells were obtained from the National Centre for Cell Science (NCCS), Pune. High resolution mass spectra (HRMS) were recorded with an Agilent 6210 ESI-TOF mass spectrometer. UV/Vis spectra were recorded with an Ultrospec 6300 pro UV/Visible Spectrophotometer (GE Healthcare, Amersham Biosciences, Piscataway, NJ, USA). Fluorescence spectra were recorded with LS 55 fluorescence spectrometer (Perkin Elmer, MA, USA). All measurements were performed in ultra-pure water or in methanol HPLC grade (VWR, Darmstadt, Germany).

Binding affinity

96-well ELISA plates were treated with immobilized mannose-BSA and galactose-BSA (1 mg/ml) as reference ligands and incubated with horseradish peroxidase (HRP)-labeled ConA/PNA/GNA (0.5 mg/ml) in the presence of different Ruthenium complexes 2 to 5 (10^{-3} to 10^{-6} g) in varying concentrations in HEPES buffer (pH 7.2 containing 0.15 M NaCl and 20

mM $CaCl_2$). After incubation for 2 h, the plates were washed and remaining labeled lectin bound to the reference ligand was quantified by the HRP-catalysed color reaction using 2, 2'-azidobis(3-ethyl-benzo-thiazoline-6-sulfonic acid) diammonium salt (ABTS) as substrate. The logarithmic curve for inhibition of lectin binding to immobilized Mannose was shown in the Figure 5. From these curves the concentration that reduces the binding of labeled lectin to the microtiter plates by 50% (IC_{50} values) was determined as a means of potency of the synthesized inhibitors.

MTT Assay

Different types of cells (D-HeLa, NIH-3T3, or HepG2, approx. 5000) were seeded in DMEM (100 μL), placed in 96-well microtiter plates and left overnight in a 5% CO_2 incubator at 37 °C. At 90% confluence, different concentrations of Ruthenium complexes **2** to **5** (10-100 μM) were added to each well (100 μL) and the plates were incubated for different periods of time (24, 48 and 72 hours) in 5% CO_2 at 37 °C, followed by addition of MTT reagent (20 μL, 5 mg mL^{-1} in PBS solution) to each well to assess the number of viable cells. After incubation for 4 hours in the incubator, purple crystals of formazan that were formed were solubilized with DMSO (100 μl) and the absorbance was measured at λ = 570 nm. The amounts of purple formazan in different wells were calculated based on the absorption and comparison to the controls demonstrated the influence of different compounds on the cells.

Confocal laser scanning microscopi images

D-HeLa or NIH-3T3 ($5x10^4$) cells were seeded on a cover slip in a 24-well plate and incubated overnight at 37 °C in a CO_2 incubator. The cells were washed with PBS (pH = 7.4) and treated with compounds **2** to **5** (0.05 mM,100 μL) for 24 and 48 hours respectively. The cells were washed twice with PBS and fixed with paraformaldehyde (500 μL, 3.7% in PBS, pH = 7.4) by incubating for 10 minutes at 4 °C. The solvent was aspirated; the cells were washed with PBS and treated with Hoechst 33342 reagent (2 μg/mL) to stain the nuclei. The cells were washed three times with PBS buffer and mounted on a glass slide using Antifed-mounting medium (5 μL). Fluorescence measurements were done using excitation with an argon laser, I = 405 and 450 nm, with the emission collected through 403 - 452 nm and 600 - 650 nm filters, respectively. The cells were stained with two dyes, green fluorescent ER and MT-tracker (in two different experiments). Excitation λ_{ex} = 530 and λ_{em} = 550 nm.

Isolation of Total Cellular Protein

D-HeLa cells were grown on a 100 mm Petri-dish and treated with 50 µM solutions of **2** and **4** for 24 and 48 hours, respectively. Cells were pelleted, washed with PBS and treated with protease inhibitors before treating with lysis buffer containing 150 mM NaCl, 1% NP-40, 0.25% SDS, 1 mM EDTA, 1 mM PMSF and 1 mM sodium orthovanadate in 50 mM Tris-Cl (pH 7.4). After 1 hour, the supernatant was collected by centrifugation at 14,000 rpm for 15 min and stored in aliquots. Protein content was quantified using Lowry's method.

Immunoblot Analysis

Approximately 50 µg of protein was separated by SDS–polyacrylamide gel electrophoresis (10%) and electro-blotted onto a PVDF membrane. The membrane was incubated for 2 hours with specific antibodies corresponding to CHOP, caspase-3 and caspase-12. Thereafter, the membranes were incubated with an HRP-conjugated secondary antibody for 1 hour at room temperature. Band visualization was done using the Immobilon Western Chemiluminescent HRP substrate kit (Millipore Corporation, MA, USA). β-actin was used as an internal standard. Biorad Protein Ladder (Thermo, EU) was used to determine the molecular weights of the protein bands.

Synthesis of Ru(II) complex

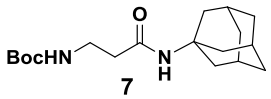

7

***tert-butyl (3-((3s,5s,7s)-adamantan-1-ylamino)-3-oxopropyl)carbamate* (7).**

1-Adamantylamine (1.0 g, 6.62 mmol) and Boc-alanine (1.4 g, 7.2 mmol) were dissolved in DCM (60 mL) at r.t. DIC (1.0 g, 7.94 mmol) was then added, followed by the addition of DIPEA (2.1 g, 16.5mmol). The reaction mixture was stirred at r.t for 12 h. The product was then extracted with EtOAc (70 mL) and the organic layer was washed with H_2O (2×50 mL). The resulting organic layer was then dried over $MgSO_4$, filtered, concentrated, and the crude was purified by flash column chromatography (silica gel, DCM:MeOH 19:1) and dried under *high vacuo* to give the final product (1.5 g, 71%) as a white foam.

R_f 0.72 (DCM:MeOH 19:1). ^{1}H NMR ($CDCl_3$, 400 MHz) δ_H: 5.29 (s, 1H), 5.21(s, 1H), 3.37 (q, *J*= 8 Hz, 2H), 2.32 (t, *J*= 8 Hz, 2H), 2.07 (s, 3H), 1.98 (d, *J*= 4Hz, 6H), 1.67 (t, *J*= 4Hz,

6H), 1.43 (s, 9H). ^{13}C NMR ($CDCl_3$, 100 MHz) δ_C: 170.42, 155.96, 79.00, 51.89, 41.46, 36.88, 36.62, 36.13, 29.21, 28.24; HRMS (ESI, positive mode) calc'd. for $C_{18}H_{30}N_2O_3[M+H]^+$: 323.2334; found: 323.2339.

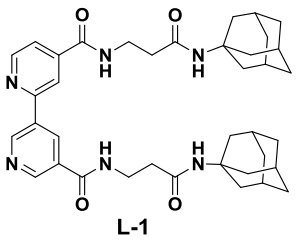

L-1

N^4,$N^{5'}$-bis(3-((3s,5s,7s)-adamantan-1-ylamino)-3-oxopropyl)-[2,3'-bipyridine]-4,5'-dicarboxamide (L-1).

Under an Ar atmosphere, 2,2'-bipyridine-4,4'-dicarboxylic acid (100 mg, 1.23 mmol) and $SOCl_2$ (5.0 mL, 42.6 mmol) were mixed together at r.t. to give a white suspension. The reaction mixture was then heated under reflux over 2 d at 60 °C to give a clear green solution. Excess of $SOCl_2$ was removed by vacuum distillation at 70 °C and the crude was dried under *high vacuo* to give 2,2'-bipyridine-4,4'-dicarbonyl dichloride as a green solid which was then dissolved in dry DCM (5 mL) under N_2 atmosphere, followed by the addition of adamantyl derivative **7** (340 mg, 4.6 mmol). The resulting mixture was then treated dropwise with Et_3N to reach pH 8. The solution was stirred over 1 d at r.t. The solvent was then removed under reduced pressure and the residue was then purified by flash column chromatography (silica gel, DCM:MeOH 19:1 to 9:1), and dried under *high vacuo* to give **L-1** (100 mg, 37%) as a white solid.

R_f 0.45 (DCM:MeOH (9 : 1)). ^{1}H NMR ($CDCl_3$, 400 MHz) δ_H: 8.98 (d, *J*= 8Hz, 2H), 8.91 (s, 2H), 7.94 (d, *J*= 4Hz, 2H), 3.83 (t, *J*= 8Hz, 4H), 2.65 (t, *J*= 8Hz, 4H), 2.22 (s, 6H), 2.17 (s, 12H), 1.85 (s, 12H). ^{13}C NMR ($CDCl_3$, 100 MHz) δ_C: 172.41, 164.87, 156.74, 150.30, 141.66, 121.74, 118.71, 52.37, 41.71, 36.51, 36.28, 29.41. HRMS (ESI, positive mode) calc'd. for $C_{38}H_{48}N_6O_4H$ $[M+H]^+$: 653.3815; found: 653.3812.

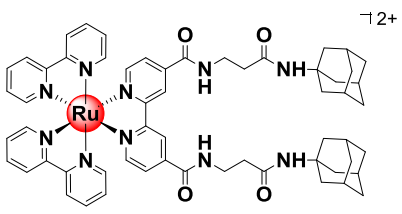

2

***cis-Bis(bipyridine){1,1'-(2,2'-bipyridine-4,4'-diyl)bis-3-β-ethane-(adamantane)ruthenium(II)* (2).**

Ligand **L-1** (52.0 mg, 79.7 μmol) was dissolved in EtOH (10 ml) at room temperature followed by *cis*-bis(2,2′-bipyridine)dichlororuthenium(II) hydrate (45.5 mg, 87.7 μmol) was added. The reaction mixture was then heated to 80 °C for 12h. The solvent was then removed under reduced pressure and the residue was then dissolved in CH_3CN. The crude product was then purified by flash column chromatography (silica gel, CH_3CN/sat. solution of KNO_3 8 : 2 to 7 : 3), and dried under *high vacuo* and dissolved in a minimum of CH_3CN and filtered to remove salts. The precipitation was repeated three times to ensure complete removal of salt and the filtrate was then dried under high *vacuo* to give the product **2** (21.4 mg, 19.6%) as a red solid; R_f 0.35 (CH_3CN/sat. solution of KNO_3 9 : 1). ^{1}H NMR ($CDCl_3$, 400 MHz) δ_H: 9.13 (s, 2H), 8.74 (d, *J*= 8Hz, 4H), 8.18 (dd, *J*= 8Hz, *J*= 8Hz, 4H), 8.02 (t, *J*= 4Hz, 2H), 7.85 (m, 6H), 7.54 (m, 4H), 3.70 (t, *J*= 8Hz, 4H), 2.53 (t, *J*= 8Hz, 4H), 2.02 (bs, 18H), 1.70 (bs, 12H). ^{13}C NMR ($CDCl_3$, 100 MHz) δ_C: 172.7, 165.5, 159.0, 157.6, 156.9, 152.0, 138.7, 127.7, 125.2, 124.3, 122.1, 51.4, 49.5, 40.8, 38.3, 37.5, 36.0, 30.9, 29.4. HRMS (ESI, positive mode) calc'd. for $C_{58}H_{64}N_{10}O_4Ru$ $[M]^{2+}$: 1066.4156; found: 533.2077 $[M/2]^{2+}$.

Synthesis of complexes 3-5

Synthesis of 3:

Cis-bis(bipyridine){1,1'-(2,2'-bipyridine-4,4'-diyl)bis-3-β-ethane-(adamantane)ruthenium(II)} **2** (1 eq) was dissolved in MeOH (3 mL). *β*-Cyclodextrin or *β*-cyclodextrin-based *O*-α-mannoside or *β*-cyclodextrin-based *O*- *β*-galactoside (2 eq) was added and the reaction mixture was kept at 22 °C for 12 h. The solvent was removed under reduced pressure and dried under high *vacuo*. The residue was dissolved in H_2O (3 mL) and lyophilized to afford **3** to **5** respectively as brown solids.

^{1}H NMR (D_2O, 400 MHz) δ_H: 8.77 (bs, 2H), 8.41 (m, 4H), 7.93 (m, 4H), 7.87 (m, 2H), 7.67 (m, 6H), 7.25 (m, 4H), 3.78 (m, 83H), 3.50 (29H), 2.44 (t, *J*= 8Hz 4H), 2.05 (bs, 12H), 1.92 (bs, 18H).

Theoretical Elemental Analysis: C (51.12), H (6.16), N (4.20), O (35.49), Ru (3.03).

Observed Elemental Analysis: C (49.98), H (5.91), N (4.01), O (34.07).

Theoretical Elemental Analysis for **4**: C (47.32), H (6.25), N (2.17), O (35.73), Ru (1.57) S (6.96).

Elemental Analysis for **4**: C (45.92), N (2.09), O (34.75).

Theoretical Elemental Analysis for **5**: C (47.32), H (6.25), N (2.17), O (35.73), Ru (1.57) S (6.96).

Elemental Analysis for **5**: C (46.07), N (2.13), O (34.62) S (6.77).

3.5. References

1. A. Castonguay, C. Doucet, M. Juhas, D. Maysinger, *J. Med. Chem.,* 2012, **55**, 8799.
2. J. M. Hearn, I. Romero-Canelon, B. Qamar, Z. Liu, I. Hands-Portman, P. J. Sadler, *ACS Chem. Biol*., 2013, **8**, 1335.
3. C. Santini, M. Pellei, V. Gandin, M. Porchia, F. Tisato, C. Marzano, *Chem. Rev*., 2014, **114**, 815.
4. L. Larry Tso-Lun, C. Wing-Kin, T. Chun-Yat, Y. Shek-Man, K. Chi-Chu, C. Sung-Kay, *Organometallics,* 2011, **30**, 5873.
5. M. Ahmed, S. Mamba, X. H. Yang, J. Darkwa, P. Kumar, R. Narain, *Bioconjugate Chem.,* 2013, **24**, 979.
6. J. S. Butler, J. A. Woods, N. J. Farrer, M. E. Newton, P. J. Sadler, *J. Am. Chem. Soc*., 2012, **134**, 16508.
7. T. H. Vien, P. Samuel, N. Janina-Miriam, A. Amanda, H. U. Robert, L. Hongxu, H. S. Martina, *ACS Macro Lett*., 2013, **2**, 246.
8. A. Bergamo, G. Sava, *Dalton Trans.*, 2011, **40**, 7817.
9. E. S. Antonarakis, A. Emadi, *Cancer Chemother. Pharmacol*., 2010, **66**, 1.
10. A. Amin, M. A. Buratovich, *Mini. Rev. Med. Chem*., 2009, **9**, 1489.
11. I. Kostova, *Curr. Med. Chem*., 2006, **13**, 1085.
12. Y. K. Yan, M. Melchart, A. Habtemariam, P. J. Sadler, *Chem. Commun*., 2005, **38**, 4764.
13. G. C. Smith, B. Therrien, *Dalton Trans.,* 2011, **40**, 10793.
14. G. Gasser, I. Ott, N. Metzler-Nolte, *J. Med. Chem.,* 2011, **54**, 3.
15. X. Meng, M. L. Leyva, M. Jenny, I. Gross, S. Benosman, B. Fricker, S. Harlepp, P. Hebraud, A. Boos, P. Wlosik, P. Bischoff, C. Sirlin, M. Pfeffer, J. P. Loeffler, C. Gaiddon, *Cancer. Res*., 2007, **69**, 5458.
16. C. G. Hartinger, S. Zorbas-Seifried, M. A. Jakupec, B. Kynast, H. Zorbas, B. K. Keppler, *J. Inorg. Biochem*., 2006, **100**, 891.
17. C. Qian, J. Q Wang, C. L. Song, L. L. Wang, L. N. Ji, H. Chao, *Metallomics*, 2013, **5**, 844.

18. M. Strasberg-Rieber, A. Anzellotti, R. A. Sanchez-Delgado, M. Rieber, *Int. J. Cancer.,* 2004, **112**, 376.

19. A. E. Friedman, J. C. Chambron, J. P. Sauvage, N. J. Turro, J. K. Barton, *J. Am. Chem. Soc*., 1990, **112**, 4960.

20. R. M. Hartshorn, J. K. Barton, *J. Am. Chem. Soc*., 1992, **114**, 5919.

21. T. Phillips, I. Haq, A. J. Meijer, H. Adams, I. Soutar, L. Swanson, M. J. Sykes, J. A. Thomas, *Biochemistry,* 2004, **43**, 13657.

22. B. M. Zeglis, V. C. Pierre, J. K. Barton, *Chem. Commun*., 2007, **44**, 4565.

23. A. C. Komor, C. J. Schneider, A. G. Weidmann, J. K. Barton, *J. Am. Chem. Soc*., 2012, **134**, 19223.

24. A. C. Komor, J. K. Barton, *Chem. Commun.,* 2013, **49**, 3617.

25. H. Song, J. T. Kaiser, J. K. Barton, *Nat. Chem*., 2012, **4**, 615.

26. A. J. McConnell, H. Song, J. K. Barton, *Inorg. Chem*., 2013, **52**, 10131.

27. X. Tian, M. R. Gill, I. Canton, J. A. Thomas, G. Battaglia, *ChemBioChem,* 2011, **12**, 548.

28. T. Wilson, P. J. Costa, V. Felix, M. P. Williamson, J. A. Thomas, *J. Med. Chem*., 2013, **56**, 8674.

29. C. Rajput, R. Rutkaite, L. Swanson, I. Haq, J. A. Thomas, *Chem. Eur. J*., 2006, **12**, 4611.

30. C. A. Puckett, J. K. Barton, *J. Am. Chem. Soc*., 2007, **129**, 46.

31. C. A. Puckett, J. K. Barton, *Biochemistry,* 2008, **47**, 11711.

32. A. Wild, K. Batiuch, M. Konig, A. Winter, M. D. Hager, M. Gottschaldt, A. Prokop U. S. Schubert, *Chem. Commun.,* 2012, **48**, 6357.

33. M. Gottschaldt, U. S. Schubert, S. Rau, S. Yano, J. G. Vos, T. Kroll, J. Clement, I. Hilger, *ChemBioChem,* 2010, **11**, 649.

34. K. Y. Zhang, K. K. Tso, M. Louie, H. Liu, K. K. Lo, *Organometallics,* 2013, **32**, 5098.

35. D. Grünstein, M. Maglinao, R. Kikkeri, M. Collot, K. Barylyuk, B. Lepenies, F. Kamena, R. Zenobi, P. H. Seeberger, *J. Am. Chem. Soc*., 2011, **133**, 13957.

36. F. U. Rahman, A. Ali, R. Guo, Y. C. Zhang, H. Wang, Z. T. Li, D. W. Zhang, *Dalton Trans*., 2015, 44, 2166.

37. S. Sivakoti, R. V. Murthy, P. M. Chaudhary, M. Surve, A. Banerjee, R. Kikkeri, *Nanoscale.,* 2016, **8**, 12729.

38. R. Kikkeri, B. lepenies, A. Adibekian, P. Laurino, P. H. Seeberger, *J. Am. Chem. Soc*., 2009, **131**, 2110.

39. M. Klajner, C. Licona, L. Fetzer, P. Hebraud, G. Mellitzer, M. Pfeffer, S. Harlepp, C. Gaiddon, *Inorg. Chem.*, 2014, **53**, 5150.

40. C. Xu, B. Bailly-Maitre, J. C. Reed, *J. Clin. Invest.*, 2005, **115**, 2656.

41. T. Momoi, *J. Chem. Neuroanat.*, 2004, **28**, 101.

42. M. Saleh, J. P. Vaillancourt, R. K. Graham, M. Huyck, S. M. Srinivasula, E. S. Alnemri, M. H. Steinberg, V. Nolan, C. T. Baldwin, R. S. Hotchkiss, T. G. Buchman, B. A. Zehnbauer, M. R. Hayden, L. A. Farrer, S. Roy, D. W. Nicholson, *Nature,* 2004, **429**, 75.

43. T. Nakagawa, J. Yuan, *J. Cell Biol.*, 2000, **150**, 887.

44. S. Oyadomari, M. Mori, *Cell Death Differ*., 2004, **11**, 381.

45. K. D. McCullough, J. L. Martindale, L. O. Klotz, T. Y. Aw, N. J. Holbrook, *Mol. Cell. Biol*., 2001, **21**, 1249.

46. E. Rosati, R. Sabatini, G. Rampino, F. De Falco, M. Di Ianni, F. Falzetti, K. Fettucciari, A. Bartoli, I. Screpanti, P. Marconi, *Blood*, 2010, **116**, 2713.

47. M. Strasberg-Rieber, A. Anzellotti, A. Roberto, S. Delgado, M. Rieber, *Int. J. Cancer.*, 2004, **112**, 376.

48. J. X. Ru, L. P. Guan, X. L. Tang, W. Dou, X. Yao, W. M. Chen, Y. M. Liu, G. L. Zhang, W. S. Liu, Y. Meng, C. M. Wang, *Inorg. Chem.*, 2014, **53**, 11498.

49. K. Raina, D. J. Noblin, Y. V. Serebrenik, A. Adams, C. Zhao, C. M. Crews, *Nat. Chem. Biol.*, 2014, **10**, 957.

3.6. Appendix I: Characterization Data of Synthesized Compounds…..

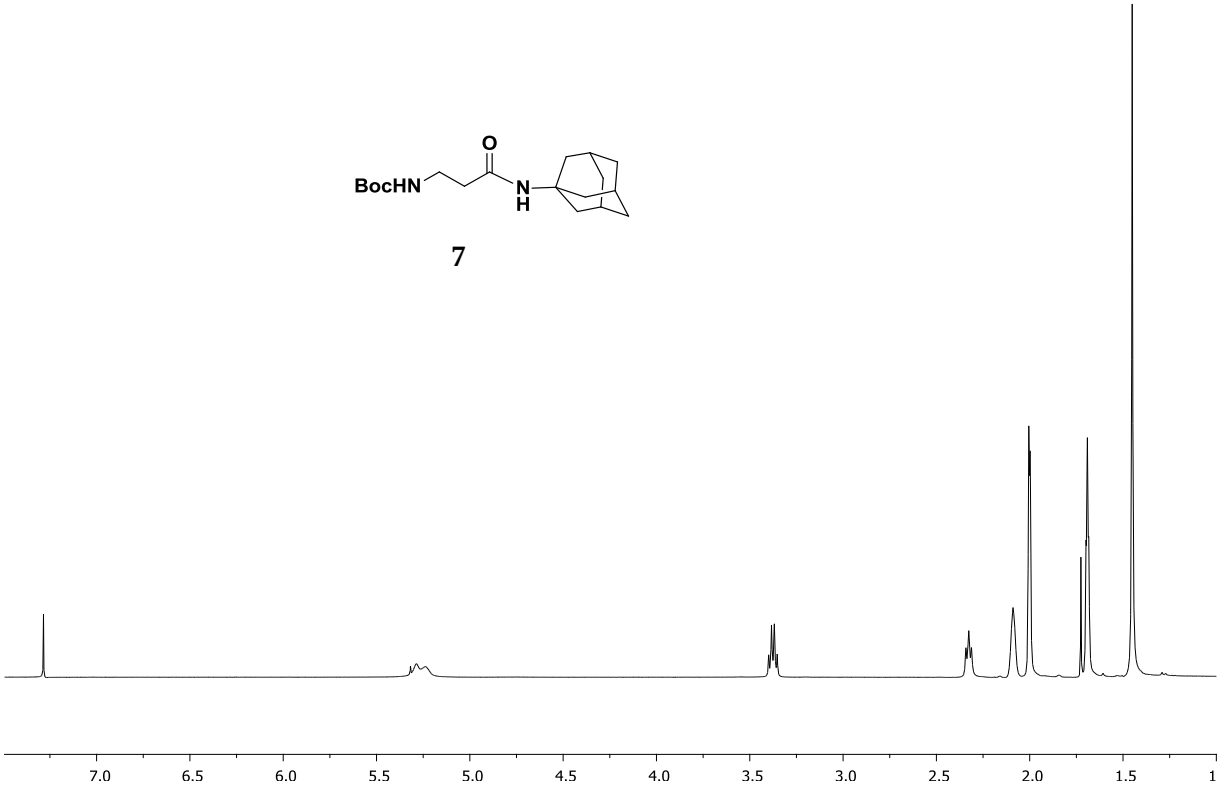
O
BocHN
N
H
7.0
6.5
6.0
5.5
5.0
4.5
4.0
3.5
3.0
2.5
2.0
1.5
1

7

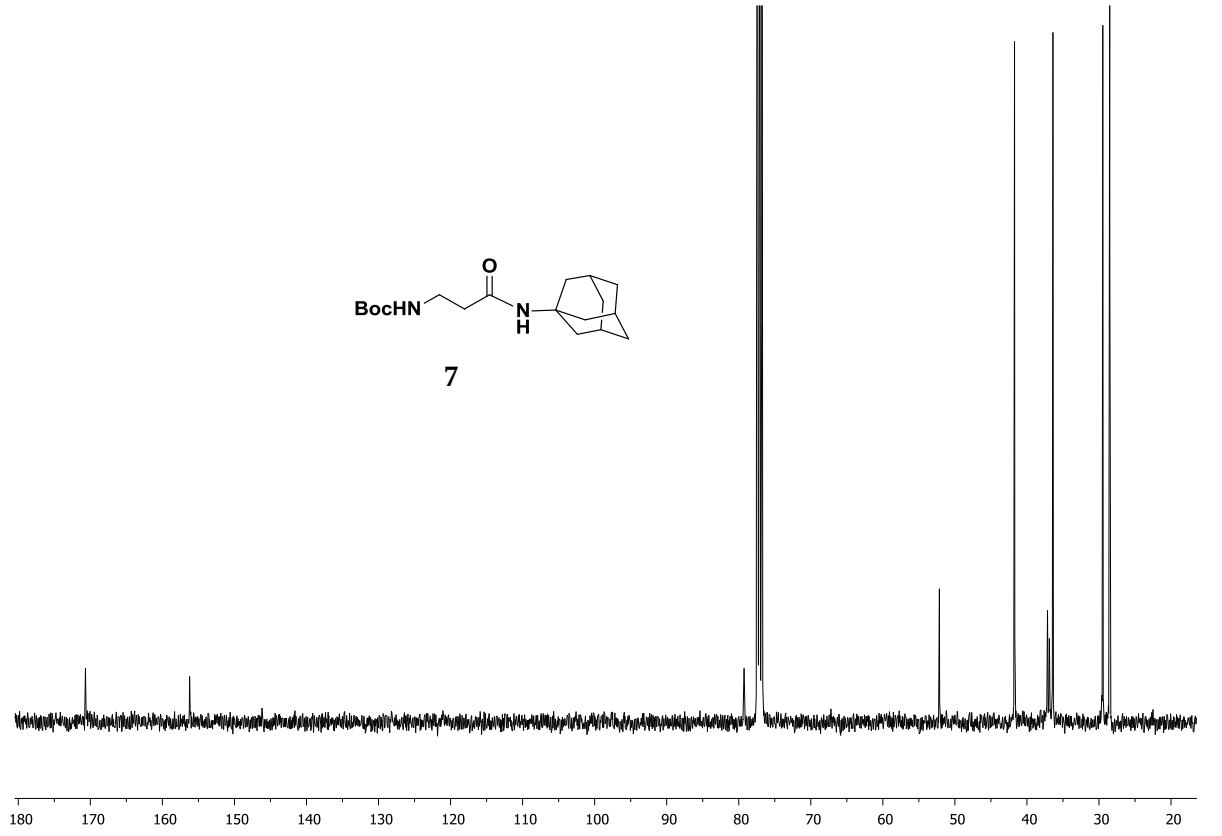
O
BocHN
N
H
180
170
160
150
140
130
120
110
100
90
80
70
60
50
40
30
20

7

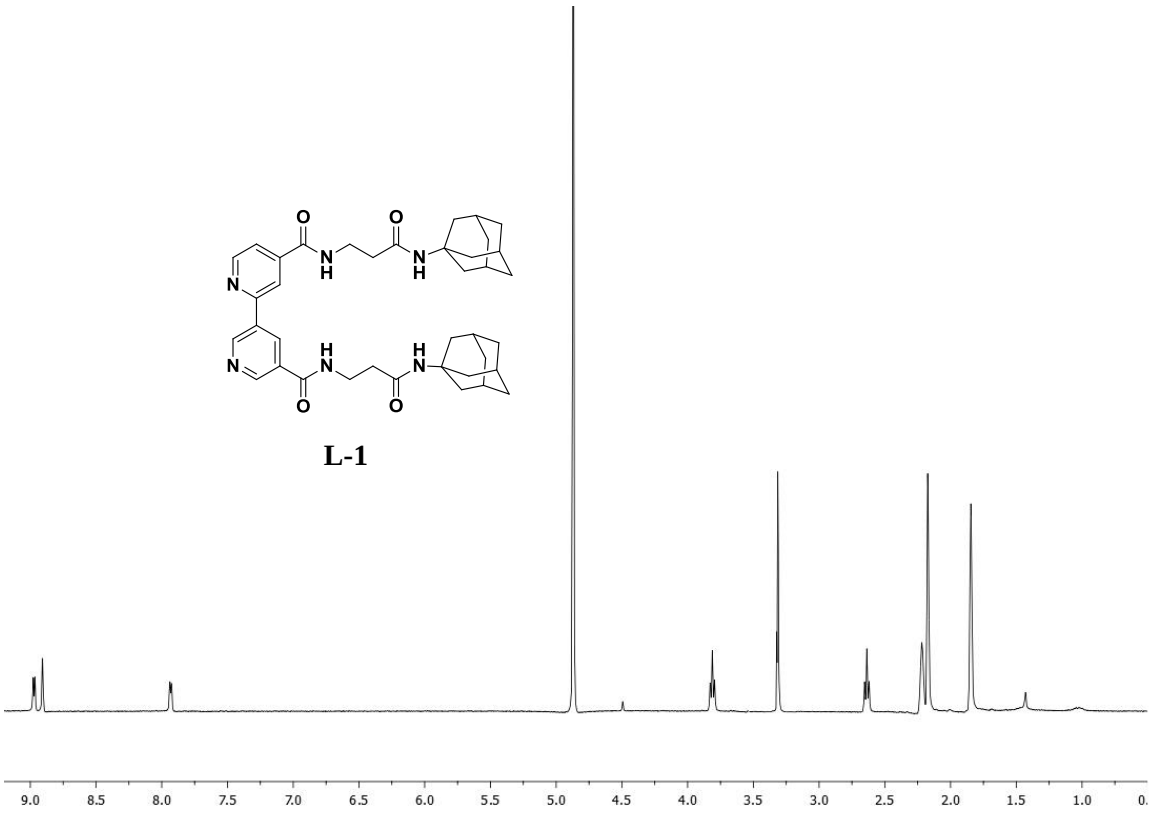

L-1

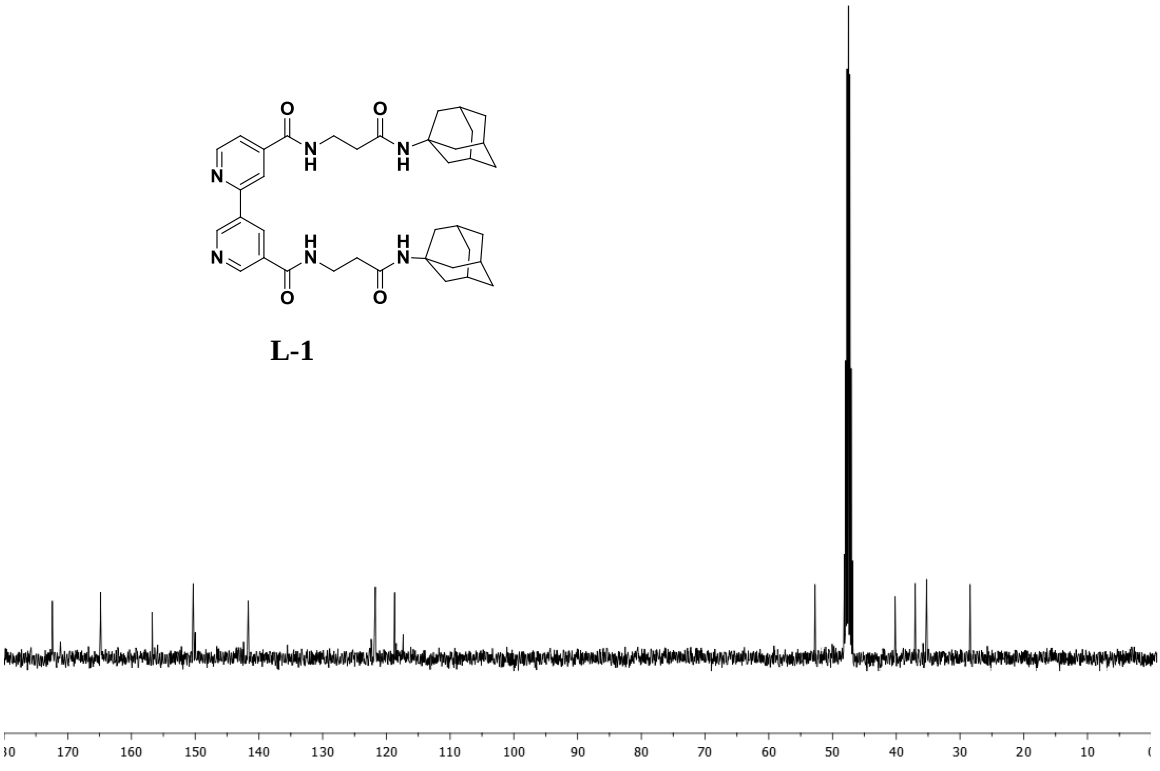

L-1

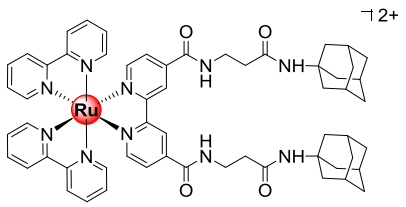
2+
Ru
N
O
NH
H

2

9.5
9.0
8.5
8.0
7.5
7.0
6.5
6.0
5.5
5.0
4.5
4.0
3.5
3.0
2.5
2.0
1.5

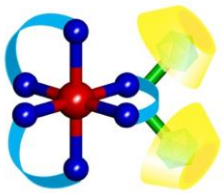

3

9.0
8.5
8.0
7.5
7.0
6.5
6.0
5.5
5.0
4.5
4.0
3.5
3.0
2.5
2.0
1.5
1.0
0.5

CHAPTER 4

Glyco-Cyclodextrin Capped Quantum Dots: Synthesis, Cytotoxicity and Optical Detection of Carbohydrate-Protein Interactions

Abstract

Highly fluorescent water soluble glyco-quantum dots were synthesized using sonochemical procedure. The synthetic approach is based on specific host-guest interaction between *β*-cyclodextrin (*β*-CD) and trioctylphospine oxide (TOPO) surfactants on quantum dots. The modified QDs were analyzed by a combination of FT-IR, ^{1}H-NOESY NMR spectroscopy and by TEM. The high sugar density on QDs resulted in selective colloidal aggregation with ConcanavalinA (ConA), Galanthus nivalis lectin (GNA) and Peanut agglutinin (PNA) lectins. Subsequently, *in-vitro* studies indicated that *β*-CD modification of QDs had good cell viability of human hepatocellular carcinoma cell line (HepG2) cells. Finally, flow cytometry and confocal imaging studies revealed that *β*-CDgal capped QDs undergo preferential binding with HepG2 cells compared to *β*-CD capped QDs. These results clearly demonstrate that *β*-CD capped QDs could be a promising candidate for further carbohydrate based biomedical applications.

4.1. Introduction

Quantum dots (QDs) are semiconductor nanocrystals, which display very interesting optical properties such as broad absorption band, size-dependent narrow emission, high luminescence, and low photo-bleaching.[1-3] These properties make quantum dots very attractive candidates for biomedical and electrical applications and more recently in analytical chemistry.

QDs adorned with DNA, protein and carbohydrates have been reported and a host of new therapeutic targets are being vigorously pursued.[4-7] However, major impediments to the rapidly growing field of glyco-nanotechnology include time-consuming synthesis of carbohydrates and the fact that cytotoxicity of the CdSe core demands an appropriate coating for *in-vitro* or *in-vivo* applications.

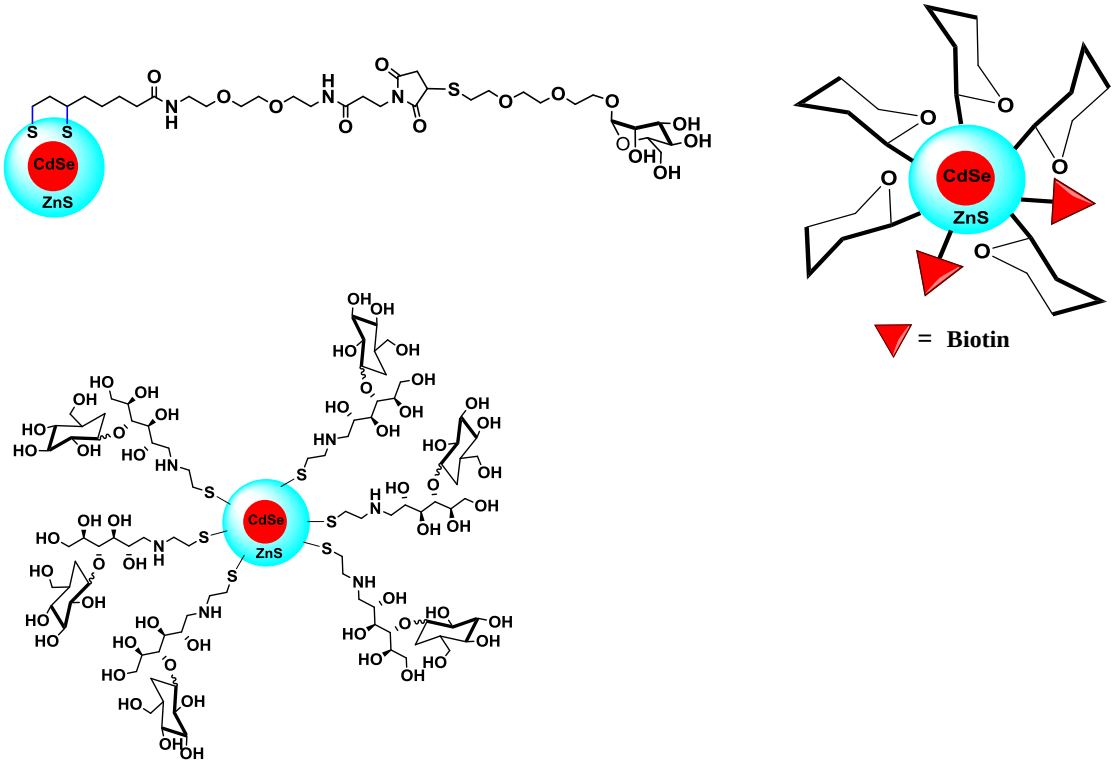

Figure 1: Different glyco-quantum dots.

Several strategies have been reported in literature for synthesis of glyco-QDs. Seeberger et al. reported sugar-capped PEGylated QDs for *in vitro* imaging and *in vivo* liver targeting.[8] Narain et al. reported biotinylated glyco-QDs for biomedical applications.[9] Meanwhile, Nishimura et al. reported an efficient method for the synthesis of glyco-QDs by phosphoryl choline self-assembled monolayer coated QDs to improve the life time of glyco-QDs for *in vivo* imaging.[10] However, we still need a versatile glyco-QDs synthesis platform displaying

multivalent sugars and a reduction in nonspecific interaction without loss of quantum yield of the original QDs.

Cyclodextrin capped QDs provide an efficient alternative to previous approaches in preventing cytotoxicity and a multivalent carbohydrate based tool to monitor specific carbohydrate-lectin interactions. Recently, enormous effort has been expended, by the group of Willner, Li, Pérez-Prieto, Vansco, and others to the development of *β*-cyclodextrin-capped QDs for molecular sensing of different analytes by fluorescence resonance energy transfer (FRET) and electron transfer (ET) process.[11-19] However, cellular viability and optical application of *β*-cyclodextrin-capped QDs during specific carbohydrate-protein interaction has not been reported.

Here, we report a host-guest strategy to synthesize sugar capped-QDs with distinct optical properties for the detection of specific carbohydrate-protein interactions in a biological system. In brief, the platform is based on hydrophilic-hydrophobic interaction between sugar embedded *β*-cyclodextrin (*β*-CD) and TOPO (*n*-trioctylphosphine) coated QDs. Self-assembly of TOPO and CD was assessed by a variety of spectroscopic means. To profile bioavailability of the QDs, agglutination assay[20] with lectins, cytotoxicity studies and *in-vitro* assays were performed.

4.2. Results and discussion

4.2.1. Host-guest assembly of glyco-QD complexes

Cyclodextrin derivatives have been synthesized according to the described procedure in the chapter 2 (Section 2.2.5).

.

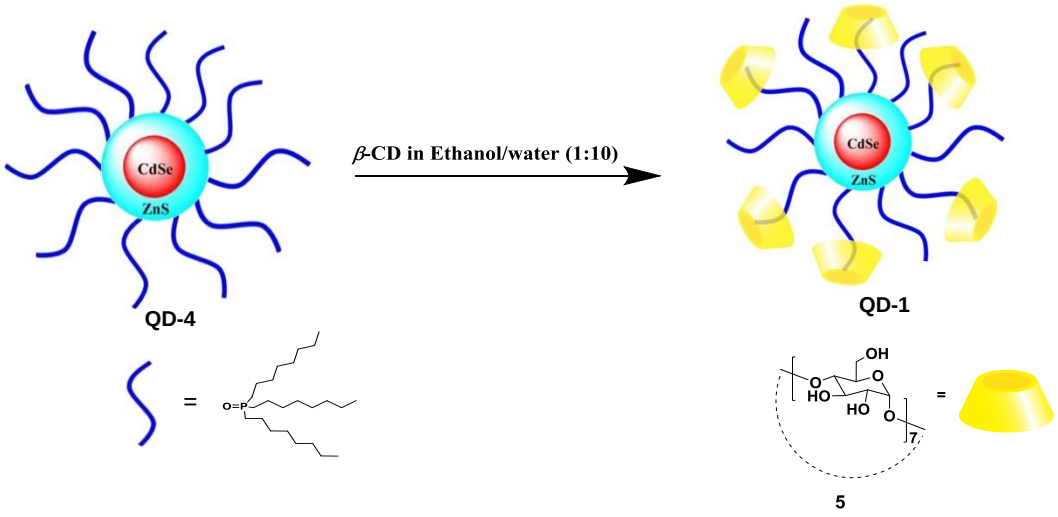

Scheme 1: Preparation of glycol-QDs.

Commercially available QD_{640}-TOPO (0.5 mg/ml) was sonicated with optimum concentration of β-CD (2-3 mM) for 30 mins, followed by centrifugation yielding **QD- 1.**

Similarly **QD-2** and **QD-3** have been synthesized with β-CDman and β-CDgal respectively.

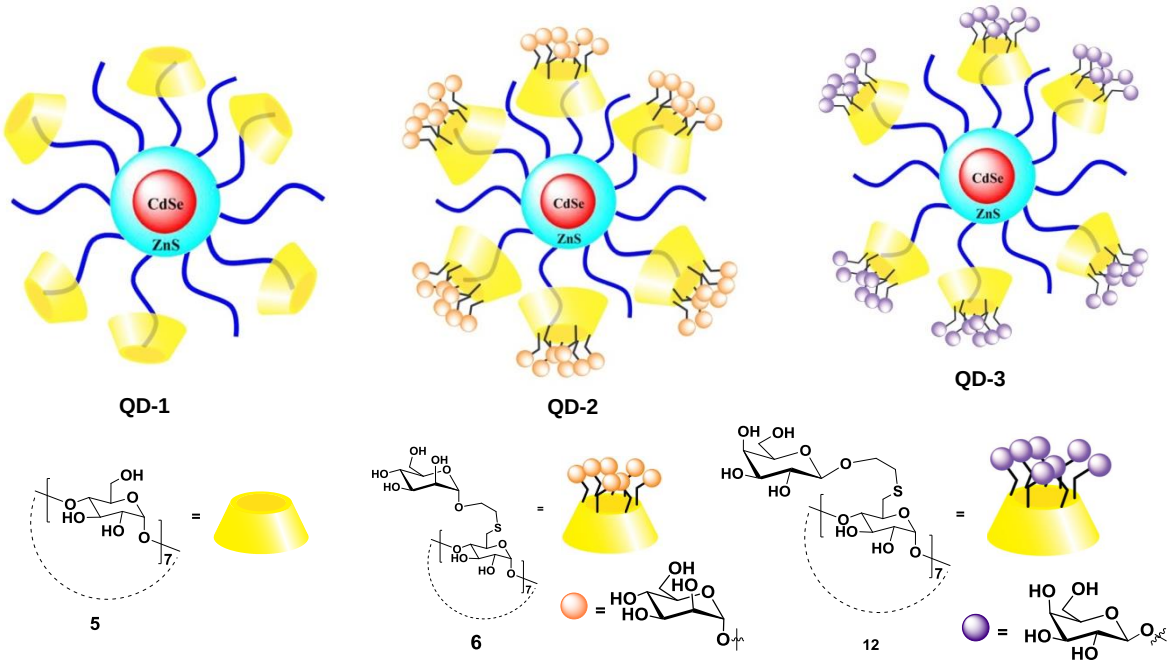

Figure 2: Systamatic representation of Glyco Quantum dots.

4.2.2. TEM images of glyco-QD complexes

The morphology of sugar functionalized QDs were observed in TEM. Figure **3** shows TEM images of the QD_{640}-TOPO and QD-1. The average diameter of the dispersed QD_{640}-TOPO is 3.5 ± 5 nm whereas that of the modified QDs size increased slightly to 3.8 ± 5 nm (**Fig. 3**).

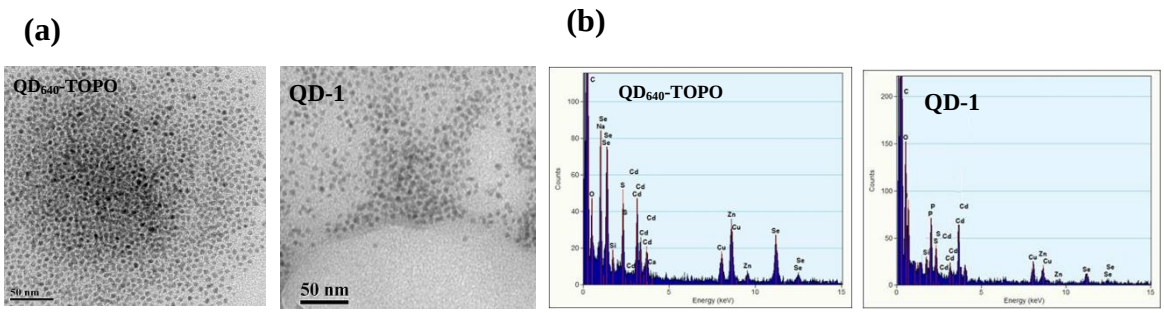

Figure 3. (a) TEM images of **QDs**; **(b)** EDX spectra of **QDs**.

4.2.3. UV-visible and fluorescence spectra

Uv-visible spectra of both modified and QD-TOPO showed a broad absorption band. Upon excitation at the 400 nm, a maximum emission at 640 nm was observed (**Fig. 4**). Quantum yields have been calculated using the equation.

$$\Phi_{comp}/\Phi_{ref} = A_{comp} \text{ X } [C]_{ref} / A_{ref} \text{ X } [C]_{comp}$$

where [C] refers to the concentration of the samples and A to the area of the emission spectra. Quantum yield was determined relative to that of fluorescein at 470 nm (0.093).[20]

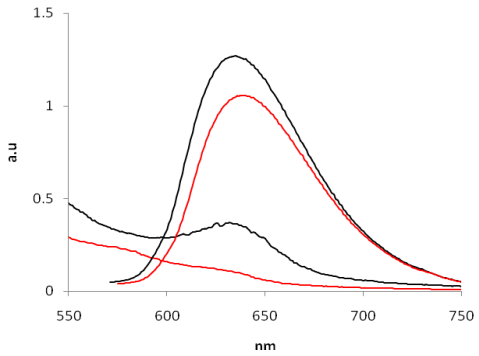

Figure 4. Normalized UV-visible and fluorescence spectra of QD-TOPO (black line) and **QD-1** (red line) of the compound.

Table 1: Photophysical properties of comp **1-3** and QD-TOPO. The quantum yields (QYs) of glycol-QDs in water were measured relative to the value of fluorescein.

Compound	λ_{max}	QY (Φ)
1	641	0.42
2	641	0.38
3	643	0.39
QD-TOPO	643	0.29

4.2.4. FT-IR spectroscopic studies

In Figure 5, IR spectrum of free QD_{640}-TOPO shows a peak corresponding to CH_2 stretching mode for TOPO at 2925 cm^{-1}. Whereas, *β*-CD-modified QDs (**Fig. 5b**) spectrum strongly

resembles that of free *β*-CDs with the broad band at ~3300 $cm^{-1}$from the O-H vibration and an intense stretching vibration band at 1086 and 1044cm^{-1} that corresponds to glycosidic bond, and slightly shifted CH_2 stretching mode at 2974 cm^{-1} from TOPO inclusion confirming that the surface of QDs has been modified by *β*-CDs (**Table 2**).

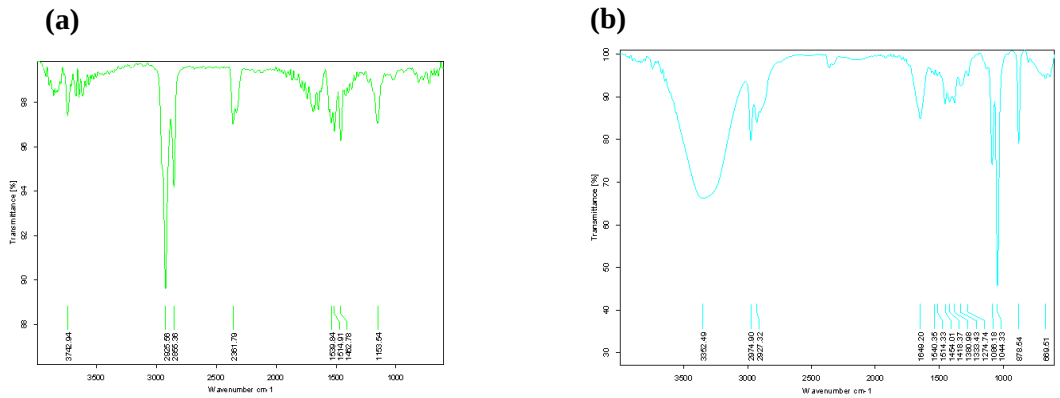

Figure 5: FTIR spectra of QD_{640}-TOPO (green color) and **1 (**bright turquoise color).

Table 2*:* Characteristic IR frequencies of glyco-QDs

Compound	**FT-IR frequency (cm^{-1})**
QD_{640}-TOPO	2925, 2855 (CH-stretch),
***β*-CDs**	3284 (OH- br stretch), 1031 (C-O-C stretch)
1	3352 (OH-br stretch), 2974, 2927 (CH-stretch), 1086, 1044 (C-O-C stretch)

4.2.5. ^{1}H-NOESY spectra

The formation of host-guest complexes was further characterized by ^{1}H-NOESY NMR spectroscopy. ^{1}H NMR of the complex showed a slightly different chemical shift compared to the native compound due to strong host-guest interactions. The 2D NOESY spectra (**Fig. 6**) prove intermolecular correlations between the TOPO and *β*-CD groups in D_2O. Figure 6a displayed the H-proton of the *β*-CD and TOPO and the cross peaks in 2D NOESY indicate strong nuclear overhauser effect (NOE) correction between the inner core proton **H3** and **H5** of *β*-CD with aliphatic chain of TOPO moiety at 1.22 and 0.87 ppm respectively. However, it was difficult to identify **H3** and **H5** of *β*-CDman and *β*-CDgal. Instead, our attention was drawn on to the protons of TOPO as we observed a strong NOE interaction with protons from

the *β*-CDman and *β*-CDgal region. It was observed that proton **1, 2, 3** of TOPO showed a strong overhauser effect with *β*-CD protons and a weak or no interaction with proton **4-8**, indicating the *β*-CD inner core is in close proximity to aliphatic part of TOPO moieties (**Fig. 6**).

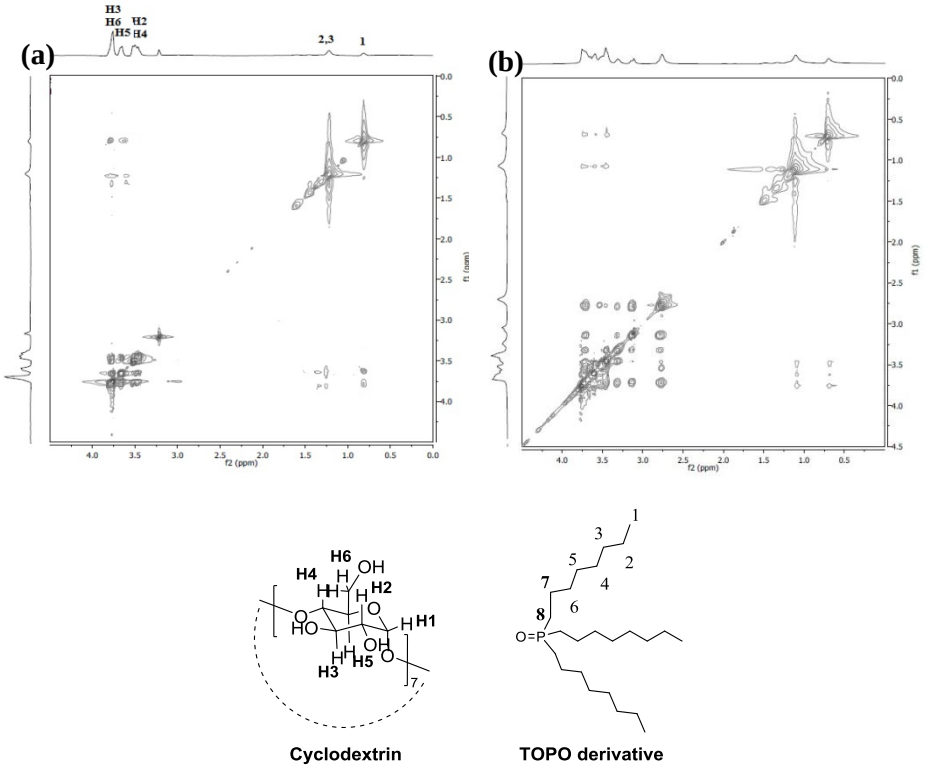

Figure 6: Proton designation of the relevant molecule moiety involved in host-guest complex.

4.2.6. Binding affinity of modified quantum dots

In order to assess the specific protein-carbohydrate interactions between **QD 1-3**, we studied their agglutination with concanavalinA (Con A) Galanthus nivalis lectin (GNA) and Peanut agglutinin (PNA) lectins. ConA has four sugar binding sites at above pH 7.0, can bind *O*-α-mannopyranoside by means of specific molecular recognition.[21] In addition, ConA has been shown to interact with many carbohydrates, such as dextran, glycodendrimer, *β*-CDs sugar moieties which contain α-D-glucopyranosyl subunits.[22,23] When aqueous solutions 50 µM of **QD 1-3** were added to solution of ConA (0.5 mg/mL) in HEPES buffer, **QD-1** and **2** showed an increase in turbidity of the mixture, indicative of binding (**Fig. 7**). In order to demonstrate that the turbidity increase observed is as a result of specific carbohydrate-protein interaction, mannose and galactose specific lectins, GNA and PNA lectins were added to **QD 1-3**. As

expected, **QD-2** and **QD-3** showed carbohydrate dependent agglutination with GNA and PNA lectin respectively (**Fig. 7**).

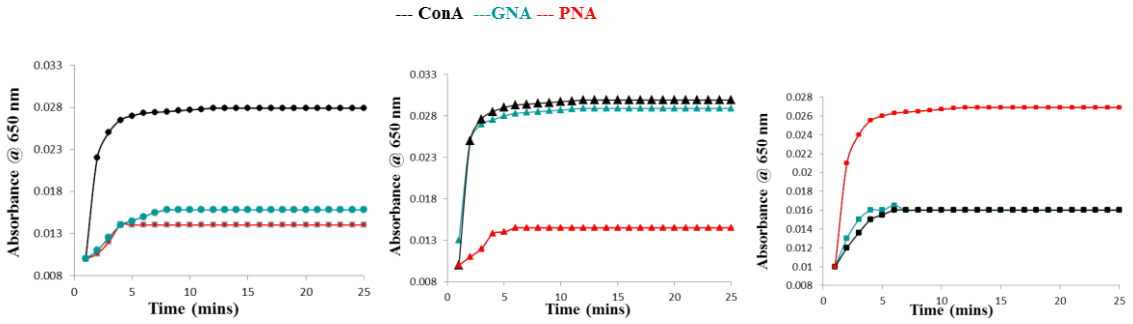

Figure 7: Turbidity analysis: Absorption change of compound QD-**1 (** ● , ● , ▲**),** QD-**2 (** ▲**,** ▲ **,** ▲ QD-**3 (**■**,**■**,**■**)** (50 µM) at 650 nm on addition of ConA (black), GNA (light blue) and PNA (red) (0.5 mg/mL) in HEPES buffer with 1 mM of $CaCl_2$ and 1 mM $MgCl_2$.

After gaining insight into how the specific carbohydrate-protein interactions are affected turbidity assay, we study how selective and sensitive these process processes can be by illustrating the capabilities of QD **1-3** as lectin biosensors. The sensor is based on specific and strong binding and subsequent agglutination of lectin. Upon addition of ConA to **QD 1-3** in HEPES buffer, a concentration dependent spontaneous agglutination was observed with **QD-1** and **QD-2**, indicating that mannose and glucose moieties on QDs successfully formed complex with ConA lectin and atleast <0.5 µM of ConA required for agglutination. Alternatively, when GNA was added to **QD 1-3** in HEPES buffer, an enhancement of **QD-2** agglutination was observed with <0.1 µM, A similar experiment with PNA resulted agglutination of **QD-3** with alteast <0.2 µM compared to **QD-1** and **QD-2**, indicating the specific carbohydrate protein interactions (**Fig 8**). Finally, carbohydrate-lectin interactions were also monitored by fluorescence mode. However, the data obtained were difficult to interpret. This could be because of simultaneous occurrence of various processes, such as agglutination, scatting and photo- induced energy and electron transfer between metals in the lectin medium. Importantly, all these results are comparable to the glyco-QD model explained by Babu et al.[22]

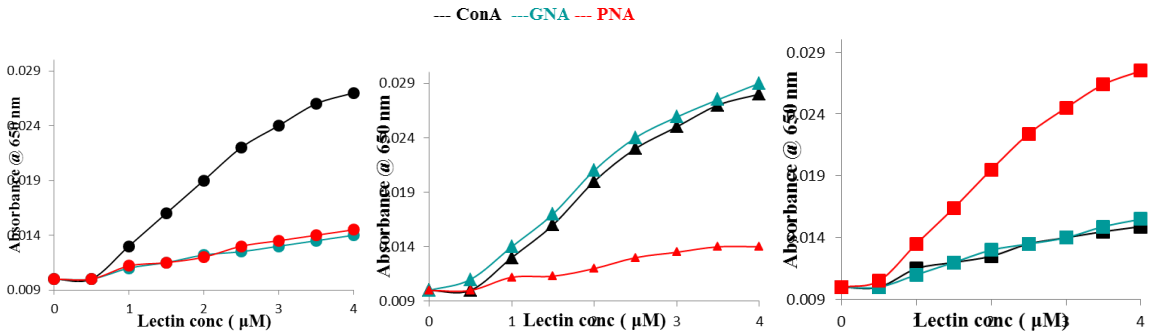

Figure 8: Turbidity formation by QD-**1** (●, ●, ●), QD-**2** (▲, ▲, ▲), QD-**3** (■, ■, ■) (50 µM) with varying concentration of ConA (black), GNA (light blue) and PNA (red) at 650 nm

After successfully studying the specific carbohydrate-protein interactions, we performed the deglutination experiment with different concentration of *O*-methyl α-D-mannose. Figure 9 displayed QD-2/ConA mixture behaviour at different concentration of methyl α-D-mannose. As expected, at 100 mM of mannose derivatives, deagglutination process was very fast compared to 0.1 mM of mannose derivatives (**Fig 9**).

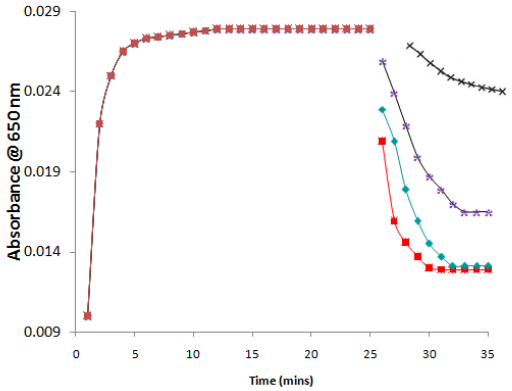

Figure 9: After 25 mins of agglutination assay of QD-2/ConA ((50 µM)/4.5 µM), de-aggregation kinetics with variable concentration of *O*-methyl α-D-mannose (100 mM (■), 10 mM (♦), 1 mM (*), 0.1mM (×). All these results are mean of three parallel experiments.

4.2.7. Cell viability assay

To demonstrate the cytotoxicity of **QD-1** to **3** in human hepatocellular liver carcinoma (HepG2) cell line. MTT (3-(4,5-dimethylthiazol-2-yl)-2,5- diphenyltetrazolium bromide) assay which is an *in vitro* colorimetric method of determining cell viability was used here to assess cell toxicity.[24,25] The MTT assay produces formazan crystals based on the mitochondrial activity and their absorbance at 570 nm indicates number of viable cells. The survival of cells carrying different doses of QDs was compared with cells treated with PBS as

a negative control and QD-PEG2000 was used as standard biomarker. The doses of QDs applied here are 1 nM, 10nM, 20 nM and 50 nM respectively. Upon addition of QDs to HepG2 medium, a concentration and time dependent cell viability was observed, indicating that *β*-CD moieties on QDs successfully prevented the interaction of CdSe core with proteins and DNA in the nucleus and the resultant cell viability is comparable to QD-PEG2000. After 4 h incubation of QDs, we found 93-77% cell viability between 1-50 nM concentrations. Importantly, this value is in close agreement to QD-PEG2000 (95-80%) (**Fig. 10a**). Alternatively, when QDs were incubated for 6 h, the cell viability drastically reduced and **QD-1** showed 79-40 % cell viability and **2** and **3** showed 79-45 % cell viability between 1-50 nM concentrations (**Fig. 10c, Table 3**). This shows that sugar substituted *β*-CD moieties improve the stability of CdSe core compared to *β*-CD alone. Importantly, all these values are in reasonably close agreement with other QDs substrated cytotoxicity values.[26-31]

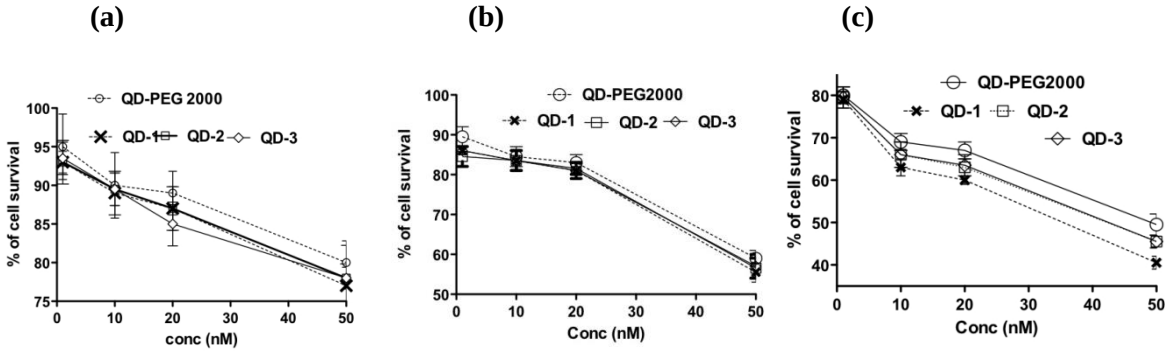

Figure 10: Time dependent cell survival/cytotoxicity at three different time intervals: 4 h **(a)**, 5 h **(b)**, 6 h **(c)**. The values represent the means ± standard deviations from three parallel cultures.

Table 3: HepG2 cells viability at different time intervals.

Compound	After 4 h	After 5 h	After 6 h
1	92-77%	84-55 %	79-40 %
2	93-78 %	86-57 %	79-45 %
3	93-77%	86-57%	79-45%
QD-PEG2000	95-80%	90-59%	80-49 %

4.2.8. FACS analysis

After establishing the cytotoxicity effect of **QD 1-3**, we wanted to establish that this system can also be utilized for optical detection of protein-carbohydrate interactions. The prototypical ASGPR (asialoglycoprotein receptor)-galactose interactions in HepG2 cells serve as a model to illustrate the *in-vitro* approach.[8] HepG2 cell line was incubated with **QD-1** to **3** at 10, 20 and 50 nM concentrations and after 1 h incubation at 4 ^{o}C and RT uptake was detected by flow cytometry. Upon addition of **QD 1-3** to HepG2 cells, a concentration dependent update of **QD-3** was observed at 4 ^{o}C, indicating that galactose residues on QDs resulted specific carbohydrate-protein interactions on cell surfaces. A similar experiment with **QD1-3** at RT resulted preferential update of **QD-3** compared to **QD-1** and **2**, indicating that flow cytometry measurement at RT is suboptimal compared to 4 ^{o}C.

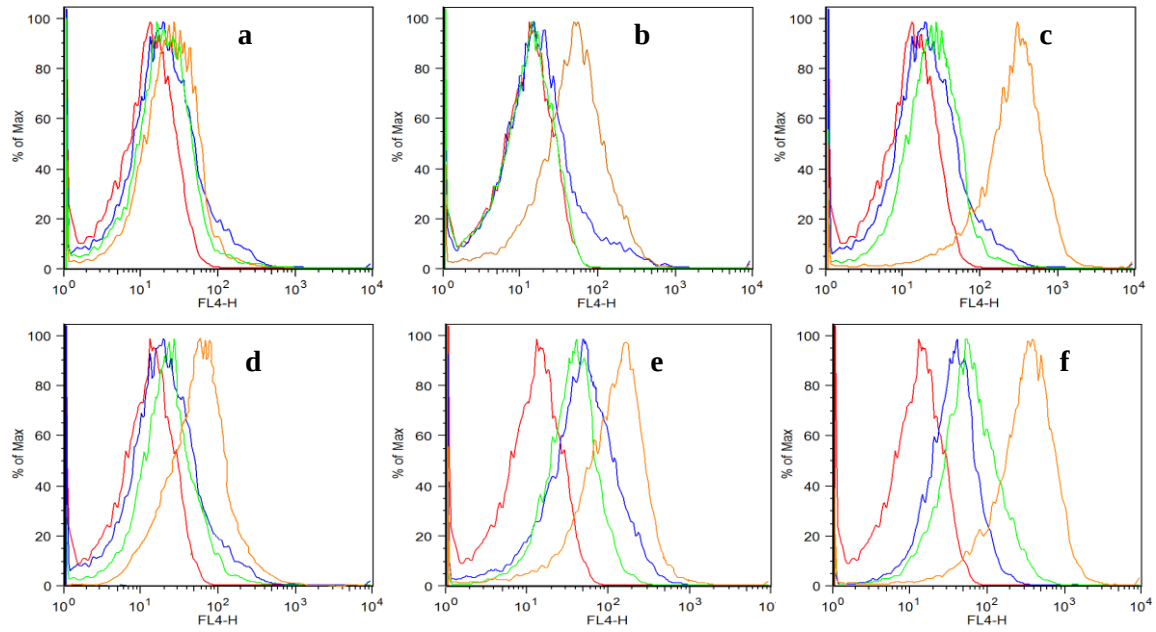

Figure 11: Flow cytometry graph of HepG2 cells with QD **1-3** (a) HepG2 cells were left untreated (red line), incubated with 10 nM (a, d), 20 nM (b, e) and 50 nm (c, f) of QD-1 (blue line), QD-2 (green line) and QD-3 (orange line) 50 nM at 4^{o}C (a, b, c) and room temperature (RT) (d, e, f).

4.2.9. Confocal laser scanning microscopy (CLSM) studies

Finally, to further support our observation we decided to image the specific uptake of **QD1-3** by confocal microscopy (**Fig. 12**). Cells were again incubated with 50 nM of comp **3** for 1h at

4 ^{o}C and then observed. As predicted, the picture confirmed the specificity of the interaction with galactose capped QD's.

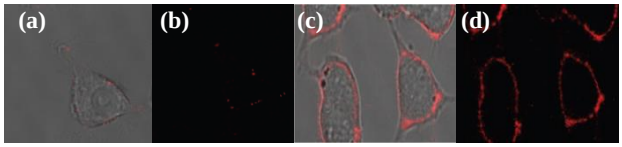

Figure 12. Confocal fluorescence of HepG2 cells treated with 50 nM of QD-1 (a, b) and QD-2 (c, d) (overlaid fluorescence and bright field images (a, c) fluorescence images scale 10 μm (b, d)

4.3. Conclusions

In conclusion, we have shown a host-guest approach to prepare water-soluble glyco-QDs by using *O*-α-manno and *O*-β-galactopyranoside capped *β*-CD as surface-coating agents. The resulting water-soluble QD nanoparticles are biologically compatible as PEGylated-QDs to study specific carbohydrate-protein interactions in *in–vitro* level. The use of the sugar-*β*-CD coated QDs in selective amplifications of *in vitro* carbohydrate-protein interactions and *in-vivo* cellular imaging is currently under investigation in our laboratory.

4.4. Experimental section

General information

All chemicals used were reagent grade and used as supplied except where noted. Analytical thin layer chromatography (TLC) was performed on Merck silica gel 60 F254 plates (0.25 mm). Compounds were visualized by UV irradiation or dipping the plate in CAN (ceric ammonium nitrate) solution followed by heating. Column chromatography was carried out using force flow of the indicated solvent on Fluka Kieselgel 60 (230–400 mesh). ^{1}H and ^{13}C NMR spectra were recorded on Jeol 400 MHz using residual solvents signals as an internal reference ($CDCl_3$ δH, 7.26 ppm, δc 77.3 ppm and CD_3OH δH 3.31 ppm, δc 49.0 ppm). The chemical shifts (δ) are reported in *ppm* and coupling constants (*J*) in Hz. IR spectra were recorded on a Perkin Elmer 1600 FTIR spectrometer.

Tubidimetric analysis

The solution of lectin (0.5 mg/ml) in HEPES buffer (10 mM Hepes pH 6.5, 1mM $MgCl_2$, 1mM $CaCl_2$, 1% BSA) and QDs **1-3** (50 μM) in water was added. The time dependent turbidity kinetics was recorded by measuring the absorption coefficient at 650 nm after every

one minutes. After 30 minutes the turbidity was disturbed by adding 100 mM of mannose to the solution.

Electron microscopy

A drop of the 0.5 μM concentration sample was deposited on a 400 mesh copper grids coated with nitrocellulose followed by carbon evaporation and dried overnight. The grids were observed in a Philips CM 120 at an accelerating voltage of 200 kV. Figure 1 shows typical TEM images of monodispersed QD-*β*-CD. The size of the QDs measured was about 5-6 nm, which fits well with the expected actual size.

Cell viability assay

Human hepatocytes (cell line: HepG2) cells were purchased from National Centre for Cell Science, Pune (India) and cultivated in D-MEM medium supplemented with 10% fetal calf serum (FCS) and 1% penicillin– streptomycin. Cells were harvested for use by removing culture media and adding trypsin (1mL) to the culture flask to release the cells from the wall of the dish. 10% fetal bovine serum (FBS) media (1mL) was added to quench the trypsin. The cells were suspended in solution, centrifuged (1000 rpm, 5 min), and diluted to a concentration of 10^4 cells per 100 μL media. Cells were allotted to the wells of a 96-well plate (10^4 cells or 100 μL per well) and incubated (37 °C, 24 h). QD **1-3** and **QD-PEG2000** were dissolved in 10% FBS media at different concentration ranging from 1 to 50 nM and incubated for 1-3 h. The well containing only medium was used as a positive control for cell death. After incubation 3-(4,5-dimethylthiazol-2-yl)-2,5-diphenyltetrazolium bromide (MTT; 50 μL of 2.5 g/L in PBS) was added and cells were incubated for an additional 3 h. Supernatant was removed and the cells were dissolved in PBS (150 μL). Absorbance was measured at 570 nm and referenced to the blank wells to find the relative cell viabilities for each assay condition.

Fluorescence-activated cell sorting assay

HepG2 were cultured as described above and different concentrations (10 nM, 20 nM and 50 nM) of compoundQD- **1**, 2 and **3** were added to the cells. After 1 h incubation at 4 °C and RT cells were washed with phosphate buffered saline (PBS). The cells were then collected with PBS containing 1% FCS by shearing force. Binding of nanoparticles and asialoglycoprotein receptor (ASGPR) on HepG2 cells were measured by flow cytometry using a FACSCantoTM II flow cytometer (Becton Dickinson and Co., Mountain View. CA). Excitation wavelength in the FACS experiments was 633 nm. Cells were gated on living cells and fluorescence

channel FL-4 was used to detect HepG2 cells that had QD-labeled molecules. All data were analyzed with the FlowJo software.

Confocal laser scanning microscopy (CLSM) studies

HepG2 cells were incubated with a solution of QD **2** and **3** (50 nM in PBS, pH 7.4) at 4^{o}C for 1 h and washed 2 times with PBS. For the control experiment, the cells were treated with PBS in culture media at at 4^{o}C for 1 h. The fluorescence images were taken using Olympus inverted fluorescence microscope CKX-41-TR equipped with ProgRes CT3 camera.

Chemical synthesis

CdSe/ZnS quantum dots and QD-PEG_{2000} Purchased from invitrozen

Synthesis of *β*-CD capped quantum dots (QD 1-3)

0.5 mg/ml of QD_{640}-TOPO and 3 mM of *β*-CD or *β*-CDman or *β*-CDgal in 0.5- 2 ml of ethanol/water mixture (1: 10) were mixed. The mixture was sonicated for 30 mins. Centrifugation at 10000 rpm for 3 min yielded a clear pellet-like suspension. This pellet was separated and dissolved in distilled water (1 mL) and stored at room temperature for further investigation. Concentration of the QDs was estimated using a previously published procedure.[2] Note: Aggregation of QDs can be controlled by effective sonication, varying the ethanol/water mixture.

4.5. Reference

1. R. Clapp, I. L. Medintz, H. T. Uyeda, B. R. Fisher, E. R. Goldman, M. G. Bawendi, H. Mattoussi, *J. Am. Chem. Soc.,* 2005, **127,** 18212.
2. W. Liu, H. S. Choi, J. P. Zimmer, E. Tanaka, J. V. Frangioni, M. G. Bawendi, *J. Am. Chem. Soc.*, 2007, **129,** 14530.
3. B. N. Giepmans, S. R. Adams, M. H. Ellisman, R. Tsien, *Science*, 2006, **312,** 217.
4. M. Howarth, W. Liu, S. Puthenveetil, Y. Zheng, L. F. Marshall, M. M. Schmidt, K. D. Wittrup, M. G. Bawendi, A. Y. Ting, *Nat. Methods.*, 2008, **5**, 397.
5. M. Stroh, J. P. Zimmer, D. G. Duda, T. S. Levchenko, K. S. Cohen, E. B. Brown, D. T. Scadden, V. P. Torchilin, M. G. Bawendi, D. Fukumura, R. K. Jain, R. K. *Nat. Med.,* 2005, **11,** 678.
6. R. C. Somers, M. G. Bawendi, D. G. Nocera, *Chem. Soc. Rev.,* 2007, **36,** 579.
7. J. M. Nam, C. S. Thaxton, C. A. Mirkin, *Science*, 2003, **301**, 1884.

8. R. Kikkeri, B. Lepenies, A. Adibekian, P. Laurino, P. H. Seeberger, *J. Am. Chem. Soc.*, 2009, **131,** 2110.

9. X. Jiang, M. Ahmed, Z. Deng, R. Narain, *Bioconjugate Chem.*, 2009, **20**, 994.

10. T. Ohyanagi, N. Nagahori, K. Shimawaki, H. Hinou, T. Yamashita, A. Sasaki, T. Jin, T. Iwanaga, M. Kinjo, S. Nishimura, *J. Am. Chem. Soc.*, 2011, **133**, 12507.

11. R. Freeman, T. Finder, L. Bahshi, I. Willner, *Nano Lett.*, 2009, **9**, 2073.

12. R. Tel-Vered, H. B. Yildiz, I. Willner, *Adv. Mat*., 2009, **21**, 716.

13. H. B. Yildiz, R. Tel-Vered, I. Willner, *Angew. Chem. Int. Ed*., 2008, **47**, 6629.

14. B. Basner, R. Elnathan, I. Willner, *Anal. Chem*., 2006, **78**, 3638.

15. H. Li, C. Han, *Chem. Mater*., 2008, **20**, 6053.

16. D. Dorokhin, S. H. Hsu, N. Tomczak, D. N. Reinhoudt, J. Huskens, A. H. Velders, G. J. Vancso, *ACS Nano*, 2010, **4**, 137.

17. L. Jia, J. P. Xu, D. Li, S. P. Pang, Y. Fang, Z. G. Song, J. Ji, *Chem. Commun*., 2010, **46**, 7166.

18. D. Dorokhin, S. H. Hsu, N. Tomczak, C. Blum, V. Subramaniam, J. Huskens, D. N. Reinhoudt, A. H. Velders, G. J. Vancso, *Small*, 2010, **6**, 2870.

19. Y. Wang, Y. Zheng, F. Yang, X. Yang, *Chem. Commun*., 2012, **48**, 2873.

20. M. M. Martin, *Chem. Phys. Lett*., 1975, **35**, 105.

21. R. Kikkeri, L. H. Hossain, P. H. Seeberger, *Chem Commun.*, 2008, 2127.

22. T. Hasegawa, S. Kondoh, K. Matsuura, K. Kobayashi, *Macromolecules*, 1999, **32**, 6595.

23. D. M. Willard, L. L. Carillo, J. Jung, A. Van Orden, *Nano Lett*., 2001, **1**, 469.

24. N. Lewinski, V. Colvin, R. Drezek, *Small*, 2008, **4**, 26.

25. B. Ballou, C. Langerholm, L. Ernst, M. Bruchez, A. Waggoner, *Bioconjugate Chem*., 2004, **15**, 79.

26. F. Chen, D. Gerion, *Nano Lett*., 2004, **4**, 1827.

27. M. Akerman, W. Chan, P. Laakkonen, S. Bhatia, E. Ruoslahti, *Proc. Natl. Acad. Sci. U.S.A.*, 2002, **99**, 12617.

28. J. Jaiswal, H. Mattoussi, J. Mauro, S. Simon, *Nat. Biotech*., 2003, **21**, 47.

29. K. Hanaki, A. Momo, T. Oku, A. Komoto, S. Maenosono, Y. Yamaguchi, K. Yamamoto, *Biochem. Biophys. Res. Commun*., 2003, **302**, 496.

30. E. Voura, J. Jaiswal, H. Mattoussi, S. Simon, *Nat. Med*., 2004, **10**, 993.

31. M. Green, E. Howman, *Chem. Commun*., 2005, 121.

4.6. Appendix I: Characterization Data of Synthesized Compounds…..

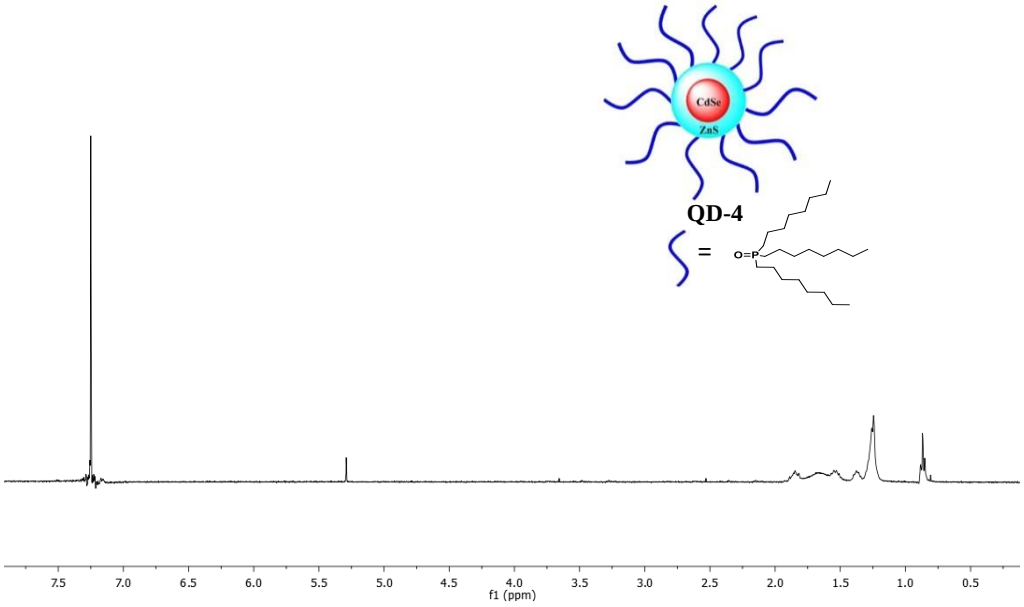

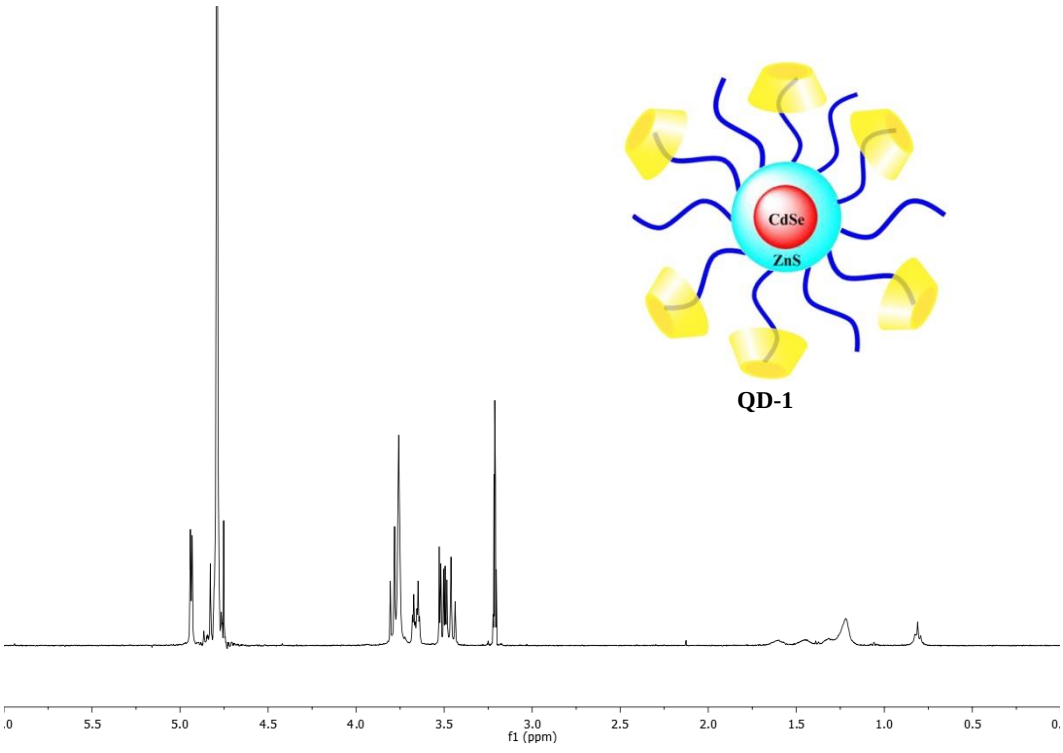

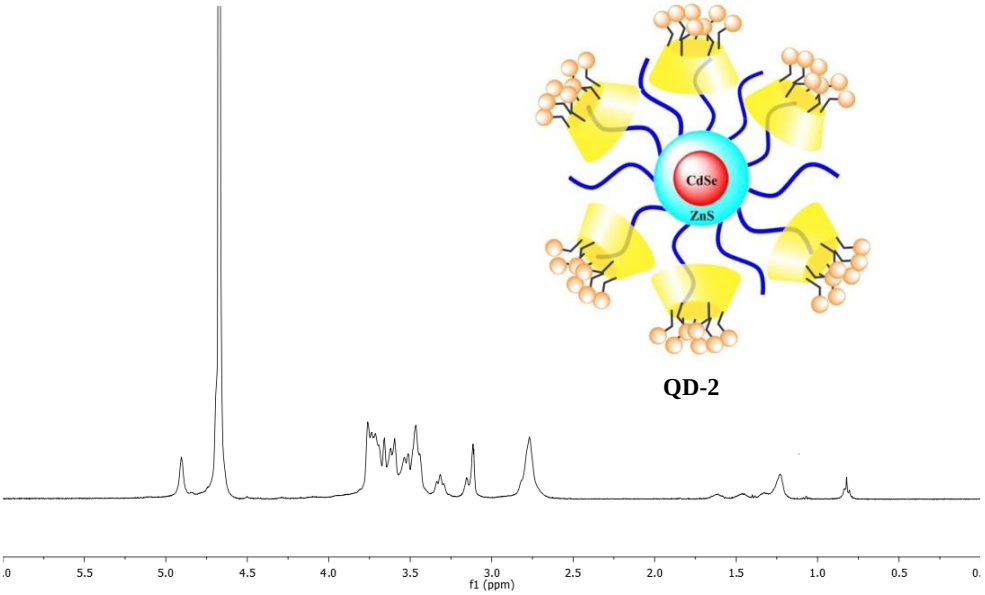
CdSe
ZnS
5.5
5.0
4.5
4.0
3.5
3.0
2.5
2.0
1.5
1.0
0.5
f1 (ppm)

QD-2

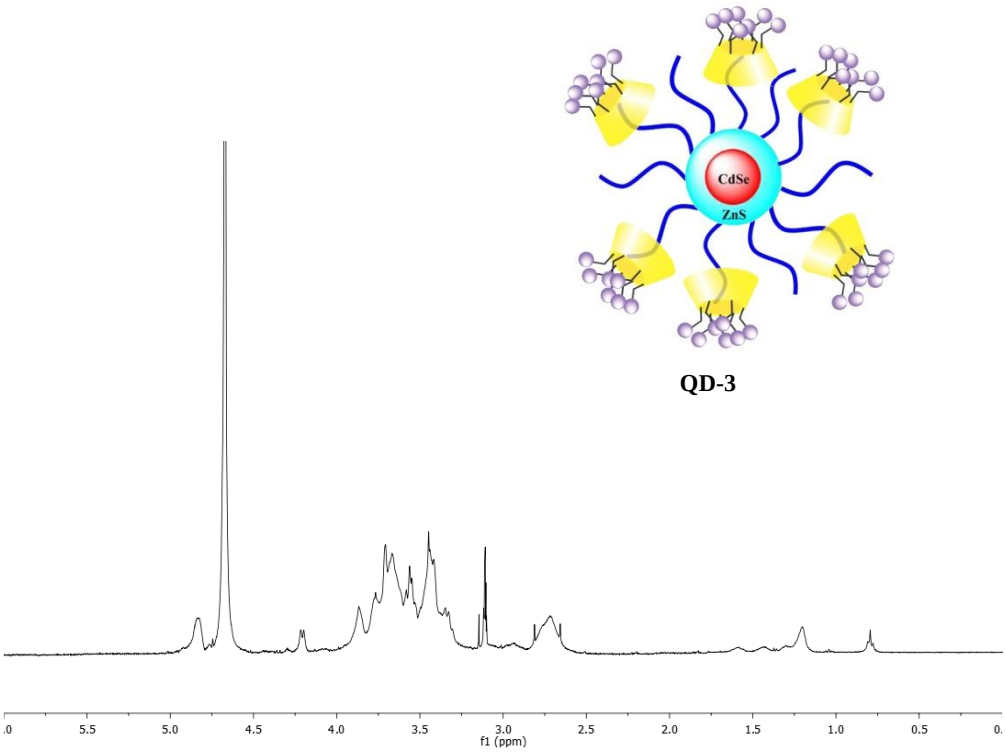
CdSe
ZnS
5.5
5.0
4.5
4.0
3.5
3.0
2.5
2.0
1.5
1.0
0.5
f1 (ppm)

QD-3